



**Universidad de Valladolid**

**PROGRAMA DE DOCTORADO EN QUÍMICA: QUÍMICA DE SÍNTESIS,  
CATÁLISIS Y MATERIALES AVANZADOS**

DOCTORAL THESIS/TESIS DOCTORAL:

**Gas-Phase Rotational Analysis of  
Non-Covalent Interactions in Thiol  
and Carbon Dioxide Aggregates**

Presented by / *Presentada por*

**Wenqin Li**

In fulfillment for the degree of / *para optar al grado de*

Doctor / *Doctora*

from the / *por la*

Universidad de Valladolid

Supervised by / *Dirigida por:*

Alberto Lesarri Gómez

Cristóbal Pérez Cuadrado



This Thesis was possible thanks to the funding of the following institutions:

*Esta Tesis ha sido posible gracias a la financiación de las instituciones siguientes:*

本论文的完成得益于以下机构的资助:

China Scholarship Council: Grant No. 202106050017



Research Project: PID2021-125015NB-I00,  
*Ministerio de Ciencia, Innovación y Universidades*



Research Project: INFRARED IR2021-UVa13,  
*Junta de Castilla y León*



FONDO EUROPEO DE  
DESARROLLO REGIONAL





# Contents

<b>Contents</b> .....	<b>V</b>
<b>Abstract</b> .....	<b>XI</b>
<b>Resumen</b> .....	<b>XIII</b>
<b>摘要</b> .....	<b>XV</b>
<b>Acknowledgements</b> .....	<b>XV</b>
<b>Chapter 1. Introduction</b> .....	<b>1</b>
1.1 Non-Covalent Interactions.....	1
1.1.1 Sulfur-centered Non-Covalent Interactions.....	1
1.1.1.1 Hydrogen Bonds involving Sulfur.....	3
1.1.1.2 $\pi$ - $\pi$ Stacking.....	4
1.1.2 Non-Covalent Interactions on Carbon Dioxide.....	5
1.2 Methods .....	8
1.2.1 Rotational Spectroscopy.....	8
1.2.1.1 Rigid rotor.....	11
1.2.1.2 Non-rigid rotor.....	15
1.2.2 Microwave spectroscopy techniques.....	17
1.2.2.1 Balle-Flygare FTMW spectrometer.....	18
1.2.2.2 Chirped-Pulse FTMW spectrometer.....	19
1.2.3 Computational methods.....	22
1.2.3.1 Classical and Semi-empirical molecular calculations .....	23
1.2.3.2 Quantum chemical calculations .....	24
1.2.3.3 Non-covalent interactions analysis .....	25

1.2.3.4 Natural bond orbitals (NBO) .....	26
1.2.3.5 Symmetry-adapted perturbation theory (SAPT).....	27
1.2.4 Spectral analysis.....	27
<b>Chapter 2. The Phenol - Thiophenol Heterodimer .....</b>	<b>29</b>
2.1 Introduction.....	29
2.2 Experimental and Theoretical Methods .....	30
2.2.1 Experimental Methods .....	30
2.2.2 Computational Methods .....	31
2.3 Results and Discussion .....	31
2.4 Conclusions.....	38
<b>Chapter 3. The 1-Naphthol - 1-Naphthalenethiol Heterodimer .....</b>	<b>39</b>
3.1 Introduction.....	39
3.2 Experimental and Theoretical Methods .....	40
3.2.1 Experimental Methods .....	40
3.2.2 Computational Methods .....	41
3.3 Results and Discussion .....	41
3.4 Conclusions.....	47
<b>Chapter 4. The 2-Naphthol - 2-Naphthalenethiol Heterodimer .....</b>	<b>49</b>
4.1 Introduction.....	49
4.2 Experimental and Theoretical Methods .....	50
4.2.1 Experimental Methods .....	50
4.2.2 Computational Methods .....	51
4.3 Results and Discussion .....	51

4.4 Conclusions.....	57
<b>Chapter 5. The <math>\beta</math>-Propiolactone - CO<sub>2</sub> Clusters.....</b>	<b>59</b>
5.1 Introduction.....	59
5.2 Experimental and Theoretical Methods.....	61
5.2.1 Experimental Methods .....	61
5.2.2 Computational Methods .....	61
5.3 Results and Discussion .....	62
5.4 Conclusions.....	68
<b>Chapter 6. The Cyclobutanone - CO<sub>2</sub> Clusters .....</b>	<b>71</b>
6.1 Introduction.....	71
6.2 Experimental and Theoretical Methods.....	72
6.2.1 Experimental Methods .....	72
6.2.2 Computational Methods .....	72
6.3 Results and Discussion .....	73
6.4 Conclusions.....	77
<b>Chapter 7. Conclusions.....</b>	<b>79</b>
<b>References .....</b>	<b>81</b>
<b>Contents of Appendixes .....</b>	<b>S1</b>
<b>Table S2.1.</b> Observed rotational transitions and residuals (in MHz) for phenol and thiophenol (dimer-I). .....	S1
<b>Table S2.2.</b> Observed rotational transitions and residuals (in MHz) for phenol and thiophenol (dimer-II). .....	S6

<b>Table S2.3</b> Theoretical spectroscopic parameters at B3LYP-D3(BJ)/def2-TZVP for phenol and thiophenol cluster in less than 5 kJ mol <sup>-1</sup> of the relative zero-point corrected energy.....	S8
<b>Table S3.1</b> Theoretical spectroscopic parameters at B3LYP-D3(BJ)/def2-TZVP for the first eleven isomers of 1-naphthol and 1-naphthalenethiol complex in less than 5 kJ mol <sup>-1</sup> of the relative zero-point corrected energy. S9	S9
<b>Table S3.2.</b> Observed rotational transitions and residuals (in MHz) for 1-naphthol and 1-naphthalenethiol. ....	S10
<b>Table S4.1</b> Theoretical spectroscopic parameters at B3LYP-D3(BJ)/def2-TZVP for the first ten isomers of 2-naphthol and 2-naphthalenethiol complex in less than 5 kJ mol <sup>-1</sup> of the relative zero-point corrected energy. ....	S14
<b>Table S4.2.</b> Observed rotational transitions and residuals (in MHz) for 2-naphthol and 2-naphthalenethiol. ....	S15
<b>Table S5.1.</b> Calculated geometries and spectroscopic parameters of the plausible isomers of BPL-CO <sub>2</sub> at the B3LYP-D3(BJ)/def2-TZVP level of theory.....	S19
<b>Table S5.2.</b> Calculated geometries and spectroscopic parameters of the plausible isomers of BPL-(CO <sub>2</sub> ) <sub>2</sub> at the B3LYP-D3(BJ)/def2-TZVP level of theory.....	S20
<b>Table S5.3.</b> Calculated geometries and spectroscopic parameters of the plausible isomers of BPL-(CO <sub>2</sub> ) <sub>3</sub> at the B3LYP-D3(BJ)/def2-TZVP level of theory.....	S21
<b>Table S5.4.</b> Calculated geometries and spectroscopic parameters of the plausible isomers of (BPL) <sub>2</sub> at the B3LYP-D3(BJ)/def2-TZVP level of theory. ....	S24
<b>Table S5.5.</b> Calculated geometries and spectroscopic parameters of the plausible isomers of (BPL) <sub>2</sub> -CO <sub>2</sub> at the B3LYP-D3(BJ)/def2-TZVP level of theory.....	S25

<b>Table S5.6.</b> Calculated geometries and spectroscopic parameters of the plausible isomers of $(\text{BPL})_2\text{-(CO}_2)_2$ at the B3LYP-D3(BJ)/def2-TZVP level of theory.....	S26
<b>Table S5.7.</b> Calculated geometries and spectroscopic parameters of the plausible isomers of $(\text{BPL})_2\text{-(CO}_2)_3$ at the B3LYP-D3(BJ)/def2-TZVP level of theory.....	S29
<b>Table S5.8.</b> Observed rotational transitions and residuals (in MHz) for BPL- $\text{CO}_2$ .....	S33
<b>Table S5.9.</b> Observed rotational transitions and residuals (in MHz) for BPL- $(\text{CO}_2)_2$ .....	S34
<b>Table S5.10.</b> Observed rotational transitions and residuals (in MHz) for BPL- $(\text{CO}_2)_3$ .....	S36
<b>Table S5.11.</b> Observed rotational transitions and residuals (in MHz) for $(\text{BPL})_2$ .....	S38
<b>Table S5.12.</b> Observed rotational transitions and residuals (in MHz) for $(\text{BPL})_2\text{-CO}_2$ .....	S41
<b>Table S5.13.</b> Observed rotational transitions and residuals (in MHz) for $(\text{BPL})_2\text{-(CO}_2)_2$ .....	S44
<b>Table S6.1.</b> Calculated geometries and spectroscopic parameters of the plausible isomers of CBN- $\text{CO}_2$ at the B3LYP-D3(BJ)/def2-TZVP level of theory.....	S46
<b>Table S6.2.</b> Calculated geometries and spectroscopic parameters of the plausible isomers of CBN- $(\text{CO}_2)_2$ at the B3LYP-D3(BJ)/def2-TZVP level of theory.....	S47
<b>Table S6.3.</b> Calculated geometries and spectroscopic parameters of the plausible isomers of CBN- $(\text{CO}_2)_3$ at the B3LYP-D3(BJ)/def2-TZVP level of theory.....	S48

<b>Table S6.4.</b> Calculated geometries and spectroscopic parameters of the plausible isomers of (CBN) <sub>2</sub> at the B3LYP-D3(BJ)/def2-TZVP level of theory. ....	S49
<b>Table S6.5.</b> Calculated geometries and spectroscopic parameters of the plausible isomers of (CBN) <sub>2</sub> -CO <sub>2</sub> at the B3LYP-D3(BJ)/def2-TZVP level of theory.....	S50
<b>Table S6.6.</b> Calculated geometries and spectroscopic parameters of the plausible isomers of (CBN) <sub>2</sub> -(CO <sub>2</sub> ) <sub>2</sub> at the B3LYP-D3(BJ)/def2-TZVP level of theory. ....	S51
<b>Table S6.7.</b> Calculated geometries and spectroscopic parameters of the plausible isomers of (CBN) <sub>2</sub> -(CO <sub>2</sub> ) <sub>3</sub> at the B3LYP-D3(BJ)/def2-TZVP level of theory. ....	S53
<b>Table S6.8.</b> Observed rotational transitions and residuals (in MHz) for CBN-CO <sub>2</sub> .....	S57
<b>Table S6.9.</b> Observed rotational transitions and residuals (in MHz) for CBN-(CO <sub>2</sub> ) <sub>2</sub> .....	S58
<b>Table S6.10.</b> Observed rotational transitions and residuals (in MHz) for (CBN) <sub>2</sub> -CO <sub>2</sub> . ....	S59
<b>Table S6.11.</b> Observed rotational transitions and residuals (in MHz) for (CBN) <sub>2</sub> -(CO <sub>2</sub> ) <sub>2</sub> . ....	S62

# Gas-Phase Rotational Analysis of Non-Covalent Interactions in Thiol and Carbon Dioxide Aggregates

## Abstract

Non-covalent interactions play a crucial role in various chemical fields like supramolecular, atmospheric or biological Chemistry. For this reason, the investigation of non-covalent interactions at the molecular level is a crucial step for understanding their nature and physical properties. In this Thesis we have examined non-covalent interactions using weakly-bound intermolecular aggregates generated in jet-cooled supersonic expansions, with the triple objective of discerning their electronic, structural and aggregation properties. The methodology used in the Thesis combined high-resolution broadband Microwave Spectroscopy and quantum mechanical calculations. The molecular targets included two different chemical classes: 1) Heteroaggregates containing mono- and bi-arenes functionalized with thiols and alcohols, and 2) Heteroaggregates containing four-membered cyclic ketones and carbon dioxide. The thiol adducts reported in the Thesis include the heterodimers of phenol-thiophenol, (1-naphthol)-(1-naphthalenethiol) and (2-naphthol)-(2-naphthalenethiol). The aggregates of carbon dioxide included the substrates of  $\beta$ -propiolactone and cyclobutanone, for which we studied the adducts made of up to three carbon dioxide molecules and two substrate molecules. The experiments included the spectral analysis of the rotational spectra, the quantum mechanical prediction of electronic, structural and conformational properties and the investigation of the noncovalent interactions using post-calculation tools based on the electronic density gradients, molecular orbital populations and energy decomposition analysis. The combined experimental and theoretical work provides a detailed molecular description of the intermolecular forces stabilizing the adducts, including specifically the hydrogen bond,  $\pi$ - $\pi$  stacking and tetrel bond interactions.



# **Análisis de Rotación en Fase Gas de Interacciones No-Covalentes en Agregados de Tioles y Dióxido de Carbono**

## **Resumen**

Las interacciones no-covalentes juegan un papel crucial en varias áreas químicas, como la Química supramolecular, atmosférica o biológica. Por este motivo, la investigación de las interacciones intermoleculares a nivel molecular representa un paso crucial para entender su naturaleza y propiedades físicas. En esta Tesis se han examinado las interacciones no-covalentes utilizando agregados intermoleculares débilmente enlazados generados en expansiones supersónicas sobreenfriadas, con el triple objetivo de discernir sus propiedades electrónicas, estructurales y de agregación. La metodología usada en la Tesis ha combinado la Espectroscopía de Microondas de banda ancha de alta resolución y cálculos mecanocuánticos. Los objetivos moleculares incluyeron dos tipos de clases químicas: 1) Heteroagregados conteniendo mono- y bi-arenos funcionalizados con tioles y alcoholes, y 2) Heteroagregados conteniendo cetonas cíclicas con anillos de cuatro miembros y dióxido de carbono. Los aductos con tioles presentados en la Tesis incluyen los heterodímeros de fenoltiofenol, (1-naftol)-(1-naftalenotiol) y (2-naftol)-(2-naftalenotiol). Los agregados de dióxido de carbono incluyen los substratos de  $\beta$ -propiolactona y ciclobutanona, para los cuales se estudiaron los aductos compuestos de hasta tres moléculas de dióxido de carbono y dos moléculas de substrato. Los experimentos incluyeron el análisis espectral de los espectros de rotación, la predicción mecano cuántica de las propiedades electrónicas, estructurales y de conformación, y la investigación de las interacciones no covalentes utilizando herramientas post-cálculo basadas en los gradientes de densidad electrónica, las poblaciones de orbitales moleculares y el análisis de descomposición de energía. El trabajo combinado experimental y teórico proporciona una descripción molecular detallada de las fuerzas intermoleculares que estabilizan los aductos, incluyendo específicamente el enlace de hidrógeno, el apilamiento  $\pi$ - $\pi$  y las interacciones de enlaces de tetrel.



# 含硫醇非共价相互作用及二氧化碳非共价聚集的微波光谱研究

## 摘要

非共价相互作用在超分子化学、大气化学和生物化学等多个化学领域中发挥着至关重要的作用。因此，从分子层面研究非共价相互作用是理解其本质及物理性质的重要步骤。本论文通过在冷却射流超音速膨胀条件下生成的弱束缚分子间复合物，研究了其包含的非共价相互作用，旨在揭示其电子结构和聚集特性。本论文采用了的研究方法结合了高分辨率宽带微波光谱技术和量子化学计算。研究对象包括了两类不同的化学体系：1) 由功能性硫醇和醇的单或双环芳烃组成的异源二聚体；2) 四元环酮和二氧化碳的异源多聚体。硫醇复合物的研究对象包括苯酚-苯硫酚异源二聚体、(1-萘酚)-(1-萘硫酚)异源二聚体和(2-萘酚)-(2-萘硫酚)异源二聚体。二氧化碳的非共价聚集研究中二氧化碳的作用对象包括了 $\beta$ -丙内酯和环丁酮，实验上观测到了多达三个二氧化碳分子及两个 $\beta$ -丙内酯或环丁酮分子形成的复合物。实验内容包括：转动光谱的谱线分析；电子结构及构象性质的量子化学预测；以及基于电子密度梯度、分子轨道占据和能量分解分析等手段来探究这些体系包含的非共价相互作用。通过实验与理论相结合的方法，本论文详细揭示了稳定这些复合物的分子间非共价相互作用，包括了氢键、 $\pi$ - $\pi$ 堆积和 tetrel 键。



## Acknowledgements

As we know, completing this PhD dissertation has been a journey marked by invaluable guidance, encouragement, and support from numerous people, without whom this work would not have been possible.

Firstly, I was honored to get the scholarship from *China Scholarship Council* in 2021 to pursue my doctoral degree in Spain. I am profoundly grateful to the *China Scholarship Council* to support my whole PhD life at *Universidad de Valladolid*. This opportunity has allowed me to immerse myself in an inspiring academic environment and broaden my research perspectives.

Besides, the first person I would like to express my deepest gratitude to is my supervisor Alberto Lesarri, who always tried his best to give me help when I was helpless during my PhD period. For me, Alberto Lesarri always took care of and supported me like my parents. I am deeply grateful to Cristóbal Pérez for his guidance and advice. I also want to thank Jens-Uwe Grabow who accepted me to visit his laboratory at *Leibniz Universität Hannover* for his insightful guidance, patience, and unwavering support throughout my stay. Their expertise and encouragement have been instrumental in helping me navigate the challenges of my PhD life, pushing me to refine my ideas and strive for excellence. My sincere thanks go to my friend, Meng Li studying at *Leibniz Universität Hannover* who always gave me encouragement and shares your ideas with me. You made me stronger and helped me grow. I am especially thankful to Isabel, Camilla, Celina, Amanda, Marcos, Rizalina, Ricardo, Farha, Zhen, Megan, Domingo, whose insights and feedback have contributed significantly to this dissertation during my PhD period.

Finally, I really would like to thank my family for their unconditional love, patience, and support, especially my parents and my younger sister. Thank you very much for always being my greatest support and giving me the courage to pursue my dreams. Your love and encouragement have been my greatest motivation, guiding me through every challenge and helping me grow.

Last but not least, to all who have been part of my whole PhD period, I am deeply thankful.



## Chapter 1. Introduction

This Thesis is focused on the characterization of intermolecular non-covalent interactions in the gas phase using rotational spectroscopy and quantum chemical calculations. We present in the Thesis the results concerning weakly bound heterodimers involving sulfur atoms and carbon dioxide complexes. Other complementary investigations conducted during the doctoral period are summarized in Chapter 8. The doctoral work included also a three-month visit in 2024 to the *Leibniz Universität Hannover*, to obtain the mention of International Doctorate.

This chapter introduces the research objectives and methodology of the Thesis, as well as the theoretical background of the experimental and computational methods. The chapter is divided into two parts: the first part discusses non-covalent interactions, specifically sulfur-centered non-covalent interactions and non-covalent interactions involving carbon dioxide. The second part provides an overview of the methods and theories employed in the Thesis. The theoretical section will discuss rotational spectroscopy and quantum chemical calculations relevant to this work, while the experimental section will describe two different types of microwave spectrometers and the analysis of the molecular spectra.

### 1.1 Non-Covalent Interactions

Non-covalent interactions (NCIs) are widely used in materials science, drug design, Biology and Chemistry, since they are essential forces that affect molecular structure, chemical reactions, biological properties and biochemical functions.<sup>1-5</sup> NCIs are defined as intermolecular interactions that do not involve the formation of chemical bonds, including van der Waals forces, hydrogen bonding, ion- $\pi$  interactions,  $\pi$ - $\pi$  interactions, and others. NCIs are the result of electromagnetic forces operating at molecular level between different charge distributions, like microscopic dipoles, quadrupoles or transiently induced dipolar dispersion forces. These diverse varieties of NCIs act between molecules to attract or repel each other, significantly influencing the molecular conformation, thermodynamic stability, and reactivity.<sup>6-10</sup> Thus, NCIs have always been a research hotspot in different fields for decades.

#### 1.1.1 Sulfur-centered Non-Covalent Interactions

Sulfur-centered NCIs play a vital role in many biological and organic molecules, extending its influence to the secondary structure of proteins and the stability of DNA.<sup>11-16</sup> Sulfur-centered NCIs include hydrogen bonds, chalcogen bonds and other weak interactions.<sup>17-20</sup> Most analysis on protein and crystal structures typically define

sulfur hydrogen bonds as weak considering its small electronegativity, polarizability and diffused electron density. In contrast to conventional hydrogen bonds sulfur hydrogen bonds are longer and have substantial deviations from linearity. However, sulfur has larger polarizabilities compared with oxygen, which may compensate for some of these factors. For example, in molecules containing thiol groups, the S-H $\cdots$ S interactions stabilize the most stable structures and is the underlying mechanism of molecular recognition and the aggregations of some biological molecules.<sup>21</sup> The S $\cdots$  $\pi$  interactions typically appear between sulfur atoms and aromatic rings, influencing the folding and stability of biological molecules.<sup>22,23</sup> Other sulfur-centered interactions include S $\cdots$ O<sup>24</sup> and S $\cdots$ N contacts.<sup>25</sup> While most of previous studies on sulfur interactions have used vibrational spectroscopy, rotational studies permit an efficient study of NCIs, simultaneously providing insights into the molecular properties and internal large amplitude motions of molecules and intermolecular complexes. So far, various molecular probes have been employed to explore sulfur-centered NCIs using rotational spectroscopy,<sup>21,26-33</sup> including sulfides, thiols, and sulfonamides. These studies include numerous intramolecular<sup>34-36</sup> and intermolecular interactions, such as O-H $\cdots$ S,<sup>37</sup> F-H $\cdots$ S,<sup>38</sup> C-H $\cdots$ S,<sup>39</sup> S-H $\cdots$ S,<sup>40</sup> S-H $\cdots$ N,<sup>41</sup>  $\pi\cdots\pi$ ,<sup>33,42</sup> and S-H $\cdots\pi$ <sup>43-45</sup> interactions. The gas-phase data can supplement earlier molecular studies that were solely based on crystallographic data and theoretical calculations.<sup>18,46-50</sup> Additionally, valuable insights into sulfur-centered NCIs can be also obtained, revealing molecular structures, electronic properties and the nature of the intermolecular forces. Recently, rotational spectroscopy focused on the interactions between several molecules containing thiol groups, providing important information for in depth understanding of their structure and function. In our laboratory, a few systems, for instance, 1,2-butanedithiol,<sup>36</sup> thienyl mercaptan,<sup>27</sup> benzyl mercaptan,<sup>51</sup> 2-phenylethanethiol,<sup>52</sup> the thiophenol dimer and trimer,<sup>33</sup> and the homodimers of benzyl mercaptan<sup>21</sup> and 2-naphthalenethiol,<sup>42</sup> have been investigated recently. Those studies showed that molecules containing thiol groups exhibit unique properties concerning hydrogen bonds and other NCIs interactions.

Some of the molecular studies involving sulfur NCIs include aromatic compounds, because of their importance in various chemical fields, particularly in molecular recognition,<sup>53-55</sup> catalysis,<sup>54,56</sup> crystal engineering,<sup>57</sup> drug delivery<sup>58</sup> and DNA.<sup>59</sup> The versatility of aromatic compounds is demonstrated by the variety of NCIs they can form. For instance, the stacked arrangement of nucleobases in DNA depends on a subtle balance of electrostatic and dispersive attractive forces. However, when it comes to aromatic compounds, side chains including functional groups cannot be neglected. The side chains of amino acids can provide hydroxyl or thiol groups to engage in intermolecular interactions,<sup>60</sup> significantly influencing protein structure and function.<sup>61-63</sup> In addition, many aromatic drug feature hydroxyl or thiol groups as side chains, and their NCIs formed with target proteins can influence the activity and selectivity of drugs, making these interactions critical in drug research and

development.<sup>64,65</sup> Currently, studies investigating the NCIs of aromatic compounds containing hydroxyl and thiol groups at the molecular level using high-resolution spectroscopic methods have primarily been limited to aromatic self-aggregates. Known examples include the thiophenol dimer and trimer,<sup>33</sup> and the homodimers of benzyl mercaptan,<sup>21</sup> 2-naphthalenethiol,<sup>42</sup> 1-naphthol,<sup>66</sup> and the phenol dimer and trimer.<sup>67</sup> Conversely, the number of high-resolution gas-phase spectroscopic studies of aggregation between thiol and hydroxyl aromatic compounds is almost zero. While research has long focused on NCIs involving aromatic compounds with hydroxyl and thiol groups, it remains challenging to control, observe, and predict these interactions at the physical level in larger molecules.

In this Thesis, some of the chapters aim at investigating the NCIs between aromatic compounds containing hydroxyl and thiol groups. By exploring the NCIs between these such molecules and the effect of extended the number of aromatic and effect of the position substituent, we can explain their intrinsic properties, offering new insights and methods for drug design, biomedicine, and other fields, enhancing our understanding of the structure and function of biological molecules.

### 1.1.1.1 Hydrogen Bonds involving Sulfur

The hydrogen bond (HB) is a chemically specific, directional attractive interaction involving a hydrogen atom in a donor-acceptor bridging role. According to the empirical concept developed by Pauling in *The Nature of the Chemical Bond*<sup>68</sup> and Pimentel and McClellan in *The Hydrogen bond*,<sup>69</sup> an  $A-H \cdots B$  HB exists between a functional group  $A-H$  and a  $B$  atom or group involving  $B$  atoms within the same molecule or between different molecules when two conditions are met: (a) there is evidence of bond formation (such as association or chelation), and (b) it can be confirmed that this bond links  $A-H$  and  $B$ , specifically involving the hydrogen atom in  $A-H$ . Typically  $A$  represents an electronegative atom, such as the O, N, S atoms, halogens (F, Cl, Br, I), or C, while the acceptor is an atom with lone pair electrons or the  $\pi$  electrons of an unsaturated system. In 1971, Vinogradov and Linnell<sup>70</sup> in *Hydrogen bonding* extended the classical definition of HB, making direct reference to the valence bond theory of chemical bonding. In brief, the underlying of the formation of HB can be seen as proton sharing between two lone electron pairs. This chemical definition highlights the presence of electron density at the acceptor group  $B$  and defines the conventional HB as a three-center four-electron interaction ( $A-H \cdots :B$ ). This definition also identifies the bond polarity as  $A^{\delta-} - H^{\delta+} \cdots B^{\delta-}$ . In 1997, the IUPAC formally defined the HB as an interaction between an electronegative atom and a hydrogen atom bonded to a relatively electronegative atom, typically with energies below 21-25 kJ mol<sup>-1</sup>. This interaction is considered predominantly electrostatic and favored by the small size of the hydrogen atom, which permits a proximity of interaction between molecular charges. At that time HBs were limited to very electronegative atoms, mostly from the first row of the periodic table

like N, O or F. The understanding on HBs was later led by advances in experimental and theoretical research, encompassing much weaker, broader, and more diverse interactions (ranging from 2 to 170 kJ mol<sup>-1</sup>), including atoms beyond the first row. IUPAC redefined the HB in 2011<sup>71</sup> as an attractive interaction between a hydrogen atom in a molecule or a molecular fragment X–H (X being more electronegative than H) and an atom or a group in the same molecule or different molecules where “*there is evidence of formation of a bond*”. The general properties of the HB have been recently reviewed by Gili in the book *The Nature of the Hydrogen Bond*.<sup>72</sup>

Pimentel first discussed the possibility of sulfur-centered HBs associated to the broadening of the S-H stretching mode.<sup>69</sup> The observed shift towards lower vibrational frequencies and an enhancement in intensity suggested that the S-H group may become a potential HB proton donor. Sulfur-centered HBs were later confirmed to influence the structure and function of many proteins and organic crystals using crystal diffraction. Sulfur-centered HBs are traditionally considered weak forces, with a lower interaction strength compared to HBs involving the O atom, such as the O–H···O, O–H···N, or N–H···O HBs.<sup>68,73,74</sup> However, Biswal<sup>18</sup> and Wategaonkar<sup>75</sup> have recently reevaluated sulfur-centered HBs, viewing them as multifaceted interactions with several key aspects worth noting: (1) sulfur can form both  $\sigma$  and  $\pi$  HBs as donors (S–H···O, S–H···S, S–H··· $\pi$ , etc.) and acceptors (O–H···S, N–H···S, etc.); (2) sulfur-centered HBs can be as strong as traditional HBs, unlike previous understanding; (3) sulfur-centered HBs may exhibit significant electrostatic characteristics. Nevertheless, the number of studies on sulfur HBs remains scarce compared to more electronegative atoms, such as oxygen (O) and nitrogen (N). This is also the reason for an increased interest in the study of sulfur NCIs in recent years.

To date, vibrational evidence for sulfur-centered HBs mostly comes from infrared spectroscopy (IR),<sup>76,77</sup> and double resonance (UV-UV or UV-IR) laser spectroscopy,<sup>18,37,40,78–86</sup> which are normally limited in resolution and do not permit rotational discrimination. Based on the advantages of rotational spectroscopy, this technique has also been used to investigate several intramolecular and intermolecular NCIs containing sulfur.<sup>26,33–36,51,52,87</sup> The investigations so far proved that sulfur most normally behaves as proton acceptor, such as in the O–H···S,<sup>37,75,78,80,82,85,86,88–90</sup> N–H···S,<sup>81</sup> F–H···S,<sup>38</sup> and C–H···S<sup>39</sup> HBs. Research on S–H acting as proton donor, such as the S–H···S<sup>40,79,84</sup> and other weak sulfur interactions (like S–H···O,<sup>86</sup> S–H···N<sup>41</sup>, and S–H··· $\pi$ <sup>43,91</sup> HBs) is relatively rare, which makes interesting to examine a larger set of intermolecular interactions.

### 1.1.1.2 $\pi$ - $\pi$ Stacking

$\pi$ - $\pi$  Stacking interactions are crucial NCIs in the assembly and engineering of molecules,<sup>92,93</sup> affecting molecular aggregation in several chemical fields, including polycyclic systems in synthetic organic and organometallic molecules,<sup>94,95</sup> protein and

crystal design,<sup>96</sup> functional material design,<sup>97</sup> supramolecular systems,<sup>98</sup> as well as organic catalytic activity and selectivity.<sup>99</sup>  $\pi$ - $\pi$  Stacking interactions can also participate in defining the structure of biomacromolecules such as DNA and RNA.<sup>59,100,101</sup> The stacking stability of aromatics has been discussed by several authors. It should be noted that stacking is not attributed to the mutual attraction between  $\pi$  clouds, so this term can only be used as a positional descriptor. Initially, Hunter and Sanders<sup>102</sup> explained  $\pi$ - $\pi$  stacking interactions using a polar electrostatic model, where aromatic rings were considered as a collection of locally centered quadrupole moments. An intuitive physical description concerning the influence of substituent effects in  $\pi$ - $\pi$  stacking interactions evolved from this model, where aromatic rings are treated as positively charged  $\sigma$  frameworks and negatively charged  $\pi$  clouds. Sinnokrot and Sherill<sup>103</sup> later found that substituent effects can be driven by electrostatic effects or other forces, such as dispersion, induction, etc. Wheeler and Houk studied substituted and unsubstituted aromatic rings, concluding that dispersion interactions are the primarily force maintaining the stacking conformation, while electrostatic interactions are secondary forces to stabilize the whole structure.<sup>104</sup> The physical origins of  $\pi$ - $\pi$  stacking stabilization are thus primarily attributed to dispersion forces ( $1/r^6$  dependence).<sup>92,93</sup> Recently, the balance between dispersion and electrostatic effects, as well as the connection between dispersion and DNA helicity, has also been discussed by some computational studies.<sup>104-106</sup>

Most of the gas-phase  $\pi$ - $\pi$  stacking experiments have been conducted with double resonance infrared-ultraviolet spectroscopy.<sup>107-111</sup> Currently, there is a small number of studies on using rotational spectroscopy (most notably the benzene dimer), demanding additional studies to improve our understanding of this important NCIs.

### 1.1.2 Non-Covalent Interactions on Carbon Dioxide

Carbon dioxide (CO<sub>2</sub>) is a colorless, odorless gas that is essential to life on Earth and is also a greenhouse gas that plays a crucial role in regulating the temperature on Earth by trapping heat in the atmosphere.<sup>112,113</sup> In addition to its role in climate change, CO<sub>2</sub> is also important in various industrial processes, such as in the production of carbonated beverages and as a refrigerant.<sup>114</sup> Recently, there has been a growing interest in studying the NCIs originated by CO<sub>2</sub> molecules. One of the reasons is the potential applications of CO<sub>2</sub>, such as carbon capture and storage, where the interactions between CO<sub>2</sub> and other molecules can affect the efficiency of the process.<sup>115-117</sup> CO<sub>2</sub> capture aims at reducing greenhouse gas emissions in the atmosphere. NCIs play a critical role in CO<sub>2</sub> capture, referring to the attractive or repulsive forces between molecules caused by its charge distribution. These interactions occur both between CO<sub>2</sub> and the adsorbent and among the adsorbent molecules themselves and influence the adsorption and desorption behavior of CO<sub>2</sub>, even directly affecting the capture efficiency. Commonly used adsorbents include

activated carbon, metal-organic frameworks (MOFs), and porous organic polymers.<sup>116</sup> These adsorbents have large surface areas and pore structures, allowing them to interact with CO<sub>2</sub> through different types of van der Waals forces, thereby adsorbing CO<sub>2</sub> from the gas phase to the solid phase. There are also NCIs which occur between adsorbents. For example, in MOFs, organic groups can form HBs and  $\pi$ - $\pi$  stacking interactions, enhancing the structural stability and CO<sub>2</sub> adsorption performance of the adsorbent.<sup>117</sup> Research has demonstrated that  $\pi$ - $\pi$  stacking interactions between cations in functionalized ionic liquids and CO<sub>2</sub> can increase the solubility of CO<sub>2</sub> and reduce volatility of CO<sub>2</sub>, thereby improving capture efficiency.<sup>117</sup> Another reason for studying the NCIs of CO<sub>2</sub> is to gain insight into the fundamental properties of CO<sub>2</sub>. By investigating how CO<sub>2</sub> interacts with other molecules, we can gain a better understanding of its behavior in different environments and its role in various chemical processes.

Currently, there is some evidence suggesting that some molecules can enhance capture efficiency through HBs to CO<sub>2</sub>.<sup>118</sup> Research on NCIs involving CO<sub>2</sub> capture focuses both on gas and condensed phases, but only the gas phase can eliminate possible solvent effects. As we mentioned before, one of the most common techniques for studying NCIs is through rotational spectroscopy, which can provide detailed information about the structure and properties of isolated molecules.<sup>119–124</sup> Rotational spectroscopy studies can thus explore the interactions between CO<sub>2</sub> and other interaction partners, as well as the effects of these interactions on the adsorption and desorption behavior of CO<sub>2</sub>. In recent years, several molecular complexes have been studied using rotational spectroscopy to investigate the NCIs originated by CO<sub>2</sub>. Some simple examples include CO<sub>2</sub>⋯Ar<sup>125</sup> and (CO<sub>2</sub>)<sub>1-2</sub>⋯H<sub>2</sub>O, where the C atom of CO<sub>2</sub> interacts with the O atom of the water molecule.<sup>126,127</sup> The last clusters are important for discovering the interactions involved in the solubility and reactivity of CO<sub>2</sub> in water. Rotational spectroscopy has also been used to investigate complexes of CO<sub>2</sub> with linear molecules<sup>128</sup> (i.e., HCN, OCS, N<sub>2</sub>O, and CS<sub>2</sub>) as well as several non-linear molecules such as vinyl fluoride,<sup>129</sup> trifluoromethane,<sup>130</sup> 1,1-difluoroethylene,<sup>131</sup> trifluoroethylene,<sup>132</sup> propylene oxide<sup>133</sup> or acetophenone.<sup>134</sup> Recently, Xie *et al.*<sup>135</sup> investigated the aggregation phenomenon of CO<sub>2</sub> in monoethanolamine, revealing that as the aggregation progresses, the self-aggregation interactions between CO<sub>2</sub> molecules become more readily observable.

From a fundamental point of view, the study of CO<sub>2</sub> clusters has permitted the study of a specific NCI called tetrel or carbon bond, introduced around 2013. The tetrel bond (TB) is analog to the halogen and chalcogen bonds, and describes the attractive NCIs formed when a group 14 element in a molecule (C, Si, etc) acts as an electrophilic site instead of a nucleophilic. TBs may appear in the solid, liquid or gas phases, resulting in the formation of weakly bound adducts. A tetrel bond in carbon arises when the carbon atom is covalently bonded to highly electronegative elements (such as oxygen and nitrogen), creating a localized electrophilic region ( $\sigma$  or  $\pi$  hole)

around the carbon atom, as described by Varadwaj *et al.*<sup>136</sup> In this cases, the carbon atom can donate  $\pi^*$  orbitals to accept lone pairs of electrons from a nucleophile, thereby forming tetrel bonds.<sup>136</sup> The TB has been observed in CO<sub>2</sub> clusters detected in the gas phase, though this interaction was recognized only recently.<sup>137</sup> In this cases the two C=O bonds create an electrophilic region in the carbon atom that can provide a  $\pi^*$  orbital for lone pairs of electrons from electron donors. Structurally representative examples of CO<sub>2</sub> clusters include early studies such as the HBr $\cdots$ CO<sub>2</sub>,<sup>138</sup> CO<sub>2</sub> $\cdots$ C<sub>2</sub>H<sub>2</sub>,<sup>139</sup> and CO<sub>2</sub> $\cdots$ H<sub>2</sub>O<sup>127</sup> complexes, as well as more recent studies like acetophenone $\cdots$ CO<sub>2</sub>,<sup>134</sup> CH<sub>3</sub>CN $\cdots$ CO<sub>2</sub>,<sup>140</sup> pyridine $\cdots$ CO<sub>2</sub>,<sup>141</sup> ether $\cdots$ CO<sub>2</sub><sup>142</sup> and formamide $\cdots$ CO<sub>2</sub>,<sup>143</sup> among others. These studies suggest that the formation of carbon bonds tends to build T-shaped structures. The T-shaped carbon bond permits maximizing the interaction between the electrophilic region of CO<sub>2</sub> and the nucleophilic region (lone pair electrons) in another molecule. The carbon bond may coexist with HBs in the same cluster to maximize cooperatively the attractive effects, as in monoethanolamine-(CO<sub>2</sub>)<sub>1-4</sub><sup>135</sup> and cyclopentene-(CO<sub>2</sub>)<sub>1-3</sub>.<sup>144</sup> In addition to complexes of CO<sub>2</sub>, carbon bonds may appear in other clusters containing the carbonyl group, like the acrolein dimer.<sup>145</sup>

For these reasons, the study of NCIs of carbon dioxide is important for understanding the electronic properties and chemical roles of CO<sub>2</sub> and mechanisms of interactions between CO<sub>2</sub> and other molecules. Since rotational spectroscopy is a powerful technique for studying intermolecular interactions, several molecular clusters have been studied in this Thesis to advance the investigations of NCIs in CO<sub>2</sub>.

## 1.2 Methods

Currently, there are numerous structural techniques for studying molecular clusters. Depending on the different phase of the molecules or molecular clusters, these techniques can be classified as solid, liquid, or gas-phase spectroscopy. Condensed-phase structural methods include X-Ray Single-Crystal Diffraction,<sup>146–148</sup> Matrix-Isolation Infrared Spectroscopy,<sup>149–153</sup> Matrix-Isolation Raman Spectroscopy,<sup>154</sup> Laser Spectroscopy,<sup>155,156</sup> Terahertz Spectroscopy,<sup>157,158</sup> and Nuclear Magnetic Resonance spectroscopy.<sup>159,160</sup> The most important gas-phase spectroscopic technologies include Photoelectron Spectroscopy,<sup>161,162</sup> Resonant two-photon Ionization Spectroscopy,<sup>163</sup> Ultraviolet Spectroscopy,<sup>164–166</sup> Infrared Photodissociation Spectroscopy,<sup>167–169</sup> and Fourier Transform Microwave Spectroscopy<sup>170–175</sup>. Condensed-phase Spectroscopy studies the structure of molecular clusters and the interactions between molecules in presence of crystal or solvation effects, while gas-phase spectroscopy can effectively avoid the interference of the external matrix and permits a free molecular rotation. Most of gas-phase experiments do not provide rotational resolution, so the structural information they provide is generally indirect.

Rotational spectroscopy, normally conducted in the cm-wave microwave region (3–30 GHz), uses different experimental techniques. Following the introduction of adiabatic cooling by supersonic expansions, the dominant rotational techniques are resonator-based Pulsed-Jet Fourier Transform Microwave Spectroscopy,<sup>176–178</sup> conceived by Balle and Flygare, and Broad-Band Chirped-Pulsed Fourier Transform Microwave Spectroscopy,<sup>179</sup> invented by Pate. Spectroscopy in the mm-wave and sub-mm-wave regions uses additional techniques not discussed here. A bunch of studies have demonstrated that microwave spectroscopy is one of the most sensitive and accurate gas-phase spectroscopic techniques for obtaining structural and internal dynamic information about molecules and clusters. Microwave spectroscopy is highly effective for studying molecular interactions, as it can precisely identify different isotopologues and conformers of the same molecule or cluster with small energy differences and determine their relative abundance in a pulsed jet expansion. When combined with quantum chemical calculations, it can accurately obtain spectroscopic parameters of molecular clusters, such as rotational constants, nuclear quadrupole coupling constants, and centrifugal distortion constants. This information leads to a deeper understanding of molecular properties and intermolecular interactions.

### 1.2.1 Rotational Spectroscopy

Spectroscopy is a type of structural method based on the interaction between the electromagnetic radiation and matter. This method measures the wavelength and intensity of radiation emitted, absorbed, or scattered by transitions between quantum

energy levels that occur within the substance, enabling the determination of its chemical composition, structure, and electronic properties. According to the nature of electromagnetic radiation, spectroscopy can be divided into atomic and molecular spectroscopy. Atomic spectroscopy is generated by changes in the energy levels of outer or inner electrons of atoms. Molecular spectroscopy is generated by changes in the electronic, vibrational, and rotational energy levels within molecules. Transitions or interactions between different molecular energy levels result in absorption or emission of energy corresponding to different regions of the electromagnetic radiation. As shown in Figure 1.1, the transition energies between the outer electronic levels of a molecule correspond to the absorption of ultraviolet-visible light. The energy levels of molecular vibrations are found in the infrared region. Transitions between electronic and vibrational energy levels are accompanied by transitions of rotational energy levels, which can be detected depending on the resolution of the experiment.

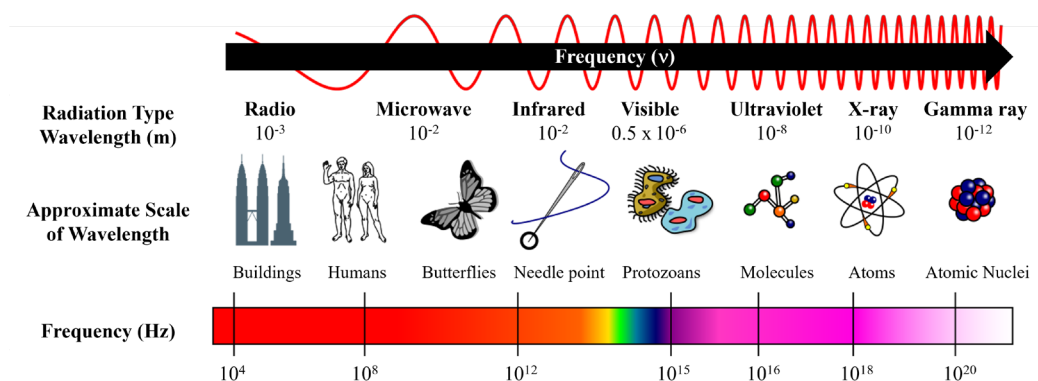


**Figure 1.1** Regions of electromagnetic radiation spectrum (Source: Wikipedia).

Microwave spectroscopy is caused by transitions between rotational levels of molecules or molecular clusters, generally in the same ground vibrational level. The energy of rotational transitions is much lower than that of electronic and vibrational transitions. The rotational transition energies correspond to the microwave region of the electromagnetic radiation, located between the infrared and radio regions. The microwave region can be further subdivided into cm-, mm-, and sub-mm-wave regions based on wavelength ranges<sup>180</sup> (See Table 1.1). The full range of microwave radiation covers between 0.01 cm to 100.0 cm, corresponding to frequencies of 0.3 GHz to 3000 GHz. Generally, the rotational transitions of heavier molecules and molecular clusters locate within the cm-wave range, while those of lighter molecules show up in the mm and sub-mm wave ranges. Microwave spectroscopy is characterized by a very high resolution and small linewidths (even sub-Doppler), so it is capable to accurately identify different isomers or isotopologues of the same

molecule or molecular cluster with very small energy differences, as well as to calculate the relative abundance of these species. Quantum chemical theory plays a crucial role in understanding spectra obtained from various spectroscopic techniques. A deeper understanding of the theory of this technique enables to assist the determination of molecules, such as rotational constants, centrifugal distortion constants, nuclear quadrupole coupling constants, internal rotation, electric dipole moments, and molecular structure. The theoretical principles of microwave spectroscopy have been extensively detailed in several authoritative books.<sup>180–183</sup> Therefore, in this chapter we will only briefly introduce some relevant theoretical knowledge of microwave spectroscopy.

**Table 1.1** The division of microwave region and its corresponding wavelength and frequency range.

Range	Wavelength (cm)	Frequency (GHz)	Energy / kJ mol <sup>-1</sup>
cm wave	~ 1.0 - 100.0	~ 30.0 - 0.3	~ 10 <sup>-3</sup> -10 <sup>-2</sup>
mm wave	~ 0.1 - 1.0	~ 300.0 - 30.0	~ 10 <sup>-2</sup> -10 <sup>-1</sup>
sub-mm wave	~ 0.01 - 0.1	~ 3000.0 - 300.0	~ 10 <sup>-1</sup> -10

In general, the quantized energy of the individual states of a molecule can be obtained by solving a time-independent Schrodinger equation:

$$\hat{H}\Psi_n = E_n\Psi_n \quad (1.1)$$

where  $\Psi_n$  represents the eigenfunctions of the Hamiltonian operator, and  $E_n$  represents the corresponding eigenvalues.

In the Born-Oppenheimer approximation, the electron and nuclear motions can be separated because of their different masses.<sup>184</sup> Therefore, the total eigenfunction of the molecule can be expressed as the product of the electronic ( $\Psi_{elec}$ ) and nuclear motions ( $\Psi_{nuclear}$ ). Solving the electronic Hamiltonian for different nuclear configurations produces the potential energy surface (PES). The internal motions can in turn be divided into rotational ( $\Psi_{rot}$ ) and vibrational motions ( $\Psi_{vib}$ ) if translation is ignored. Assuming a total factorization of the eigenfunctions:

$$\Psi_n = \Psi_{elec} \times \Psi_{vib} \times \Psi_{rot} \quad (1.2)$$

Thus, the total Hamiltonian operator representing the total energy of the molecular system can be expressed as the sum of the electronic, vibrational and rotational parts:<sup>185</sup>

$$\hat{H}_{total} = \hat{H}_{elec} + \hat{H}_{vib} + \hat{H}_{rot} \quad (1.3)$$

so

$$E_{total} = E_{elec} + E_{vib} + E_{rot} \quad (1.4)$$

In this work we will assume the total separation of vibrational and rotational motions, and microwave spectroscopy will be used to evaluate the rotational energy of a system in the ground electronic and vibrational states, so only the rotational Schrodinger equation is discussed next:

$$\hat{H}_{rot}\Psi_n = E_n\Psi_n \quad (1.5)$$

### 1.2.1.1 Rigid rotor

The derivation of the quantum mechanical properties of molecular rotors, including their rotational spectra, can begin with classical expressions of the angular momentum and rotational energy. Similarly, the ultimate derivation of molecular structures from experimentally determined spectral constants requires the knowledge of the classical moment of inertia.

The classical angular momentum of a rigid system is:

$$\mathbf{P} = I\boldsymbol{\omega} \quad (1.6)$$

where  $I$  represents the moment of inertia and  $\boldsymbol{\omega}$  represents angular velocity. For a rotational system consisting of  $N$  atoms, each with a mass of  $m_i$  and space coordinates  $x_i, y_i, z_i$  in a cartesian coordinate system, the moment of inertia tensor can be expressed as:

$$I = \sum_{n=0}^N m_i \begin{pmatrix} y_i^2 + z_i^2 & -x_i y_i & -x_i z_i \\ -y_i x_i & x_i^2 + z_i^2 & -y_i z_i \\ -z_i x_i & -z_i y_i & x_i^2 + y_i^2 \end{pmatrix} = \begin{pmatrix} I_{xx} & I_{xy} & I_{xz} \\ I_{yx} & I_{yy} & I_{yz} \\ I_{zx} & I_{zy} & I_{zz} \end{pmatrix} \quad (1.7)$$

Because the inertial tensor is real and symmetric it can be diagonalized, leading to the principal inertial axes system, with origin at the center of mass of the rotating body. This eliminates the off-diagonal elements, which can be visualized with the ellipsoid of inertia. This coordinate system is unique to every rotating molecule. The inertial axes are labeled  $a, b,$  and  $c,$  and the corresponding moment of inertia are  $I_a, I_b,$  and  $I_c$  (Figure 1.2), customarily selected according to  $I_a \leq I_b \leq I_c$ . The magnitude of the moment of inertia is then simply related to the molecular mass distribution:

$$I = \sum_i m_i r_i^2 \quad (1.8)$$

where  $m_i$  represents the atomic mass and  $r_i$  represents the vertical distance between atom  $i$  and the axis of rotation. There are six different ways to associate the Cartesian coordinate system with the principal axis system or representations, shown in Table 1.2.

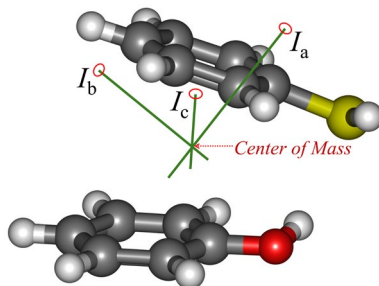


**Figure 1.2** The three-principal moment of inertia in an asymmetric-top rotor.

**Table 1.2** Six different representations between principal axes  $a, b, c$  and reference axes  $x, y, z$ .

	$I^r$	$I^l$	$II^r$	$II^l$	$III^r$	$III^l$
$x$	$b$	$c$	$c$	$a$	$a$	$b$
$y$	$c$	$b$	$a$	$c$	$b$	$a$
$z$	$a$	$a$	$b$	$b$	$c$	$c$

Molecules can be classified according to the values of the principal moments of inertia into different structural types:<sup>182</sup>

- Linear rotors,  $I_c = I_b > I_a = 0$
- Spherical rotors,  $I_c = I_b = I_a \neq 0$
- Symmetric-top rotors, those with triple or higher symmetry axis, further divided into prolate ( $I_c = I_b > I_a \neq 0$ ) or oblate symmetric-top rotors ( $I_c < I_b = I_a \neq 0$ )
- Asymmetric-top rotors,  $I_c \neq I_b \neq I_a \neq 0$

In the principal axes system, the classical expression for the rotational energy is:

$$H_{rot} = T + V = \frac{1}{2} \times (I_a \omega_a^2 + I_b \omega_b^2 + I_c \omega_c^2) = \frac{P_a^2}{2I_a} + \frac{P_b^2}{2I_b} + \frac{P_c^2}{2I_c} \quad (1.9)$$

where  $P$  represents the angular momentum along the principal axes  $a, b, c$  directions:

$$P_a = I_a \omega_a, P_b = I_b \omega_b, P_c = I_c \omega_c \quad (1.10)$$

The conversion of the classical Hamiltonian  $H$  to the quantum mechanical Hamiltonian  $\hat{H}$  gives:

$$\hat{H}_{rot} = A\hat{P}_a^2 + B\hat{P}_b^2 + C\hat{P}_c^2 \quad (1.11)$$

where  $A, B, C$  represent rotational constants, reciprocal to the rotational moments of inertia:

$$A = h/(8\pi^2 I_a), B = h/(8\pi^2 I_b), C = h/(8\pi^2 I_c) \quad (1.12)$$

According to the relationship between the values of the principal moments of inertia,  $A \geq B \geq C$ .

Using the rotational constants, the planar moment of inertia of each molecule can also be calculated. The planar moment of inertia is also related to the mass distribution of the molecule:

$$P_{aa} = \sum_i m_i a_i^2 \quad (1.13)$$

The planar moment gives the mass distribution along each axis:

$$P_{aa} = \frac{1}{2} \times (I_b + I_c - I_a) = \frac{h}{16\pi^2} \times \left( \frac{1}{B} + \frac{1}{C} - \frac{1}{A} \right) \quad (1.14)$$

$$P_{bb} = \frac{1}{2} \times (I_a + I_c - I_b) = \frac{h}{16\pi^2} \times \left( \frac{1}{A} + \frac{1}{C} - \frac{1}{B} \right) \quad (1.15)$$

$$P_{cc} = \frac{1}{2} \times (I_a + I_b - I_c) = \frac{h}{16\pi^2} \times \left( \frac{1}{A} + \frac{1}{B} - \frac{1}{C} \right) \quad (1.16)$$

By solving the rigid-rotor Schrödinger equation, the rotational energy levels of the molecule can be obtained. However, an analytical solution is only possible for linear and symmetrical rotors. In the first case the eigenvalues of the total angular momentum  $\hat{\mathbf{P}}^2 \psi_{JM} = \hbar^2 J(J+1) \psi_{JM}$  can be substituted into equation 1.11, where the eigenfunctions  $\psi_{JM}$  are coincident with the spherical harmonics  $Y_J^M$ . The quantum numbers  $J$  ( $= 0, 1, 2, \dots$ ) and  $M$  ( $= 0, \pm 1, \dots, \pm J$ ) represent the total angular momentum and its laboratory projection. The energy values do not depend on  $M$ , but this degeneracy is lifted in presence of external fields:

$$E_J = \frac{\hbar^2}{2I} J(J+1) = BhJ(J+1) \quad (1.17)$$

For a prolate or oblate symmetric-top rotor the Hamiltonian commutes with the total angular momentum  $J$  and the component on the molecular symmetry axis  $K$ , with common wavefunctions  $\psi_{JKM}$ . Using the eigenvalues  $\hat{\mathbf{P}}^2 \psi_{JKM} = \hbar^2 J(J+1) \psi_{JKM}$  and  $\hat{\mathbf{P}}_z \psi_{JKM} = \hbar K \psi_{JKM}$  the rotational energies depend only on  $J$  and  $K$  for the rigid rotor model:

$$E_{J,K} = h[BJ(J+1) + (A-B)K^2] \quad (1.18)$$

$$E_{J,K} = h[BJ(J+1) + (C-B)K^2] \quad (1.19)$$

where  $K$  ( $= 0, \pm 1, \dots, \pm J$ ) introduces a degeneracy of  $(2J+1)$  for each level. In presence of non-zero permanent dipole moments, both linear rotor and symmetric-top rotor obey the same selection rule:

$$\Delta J = 0, \pm 1; \Delta K = 0 \quad (1.20)$$

The frequencies  $\nu_{rot}$  corresponding to transitions between adjacent levels in linear and symmetric-top rigid rotors then correspond to

$$\nu_{rot} = \frac{(E_{J+1} - E_J)}{h} = 2B(J + 1) \quad (1.21)$$

The degeneracy in  $K$  is broken in symmetric rotors when the centrifugal distortion is considered. Spherical rotors do not exhibit pure rotational transitions.

The vast majority of molecules are asymmetric and can be described by Ray's asymmetry parameter  $\kappa$ , which quantifies the degree of asymmetry in a molecule:

$$\kappa = (2B - A - C)/(A - C) \quad (1.22)$$

The limits for  $\kappa$  are -1 and +1, corresponding to prolate ( $B = C$ ) and oblate ( $A = B$ ) symmetric-top rotors. When  $\kappa = 0$ , the molecule is maximally asymmetric. In the asymmetric rotor the Hamiltonian does not commute with the projection of the angular momentum along an internal axis. In consequence these quantities cannot be determined simultaneously and only  $J$  and  $M$  are good quantum numbers. For these reason pseudo-quantum numbers are used, following the double subscript notation of King-Hainer-Cross,  $J_{K_{-1}, K_{+1}}$ . The two subscripts represent the limiting prolate ( $K_{-1}$  or  $K_a$ ) and oblate ( $K_{+1}$  or  $K_c$ ) cases of the symmetric top. The double subscript also provides the symmetry of the wavefunctions. Figure 1.3 illustrates the energy levels of the asymmetric-top rotor.

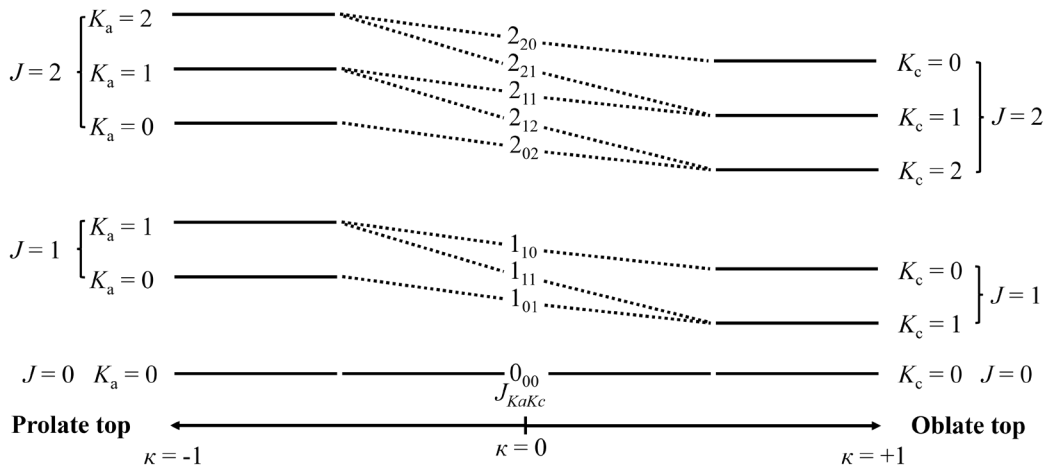


**Figure 1.3** Correlation diagram on the partial energy levels for the prolate and oblate limiting cases of an asymmetric-top rotor.

To obtain a numerical solution to the energies of the asymmetric rotor the wavefunctions  $\psi_{J\tau M}$  are expressed as linear combinations of the orthonormal wavefunctions of the symmetric rotor  $\psi_{JKM}$ :

$$\psi_{J\tau M} = \sum_{JKM} a_{JKM} \psi_{JKM} \quad (1.23)$$

where  $a_{JKM}$  are numerical constants and  $\tau = K_{-1} - K_{+1}$ . The expansion of the wavefunctions permits the construction of a secular determinant, which is diagonal in  $J$ . For this reason, each quantum level (with dimensions  $2J + 1$ ) can be solved independently. As discussed in the bibliography, the solutions of the determinant can be simplified using the symmetry of the Hamiltonian, which (similarly to the ellipsoid of inertia) belongs to the  $D_2 (= V)$  point group. For this purpose, the expansion of the symmetric rotor functions must be symmetrized (Wave functions), so that they can be classified according to the four symmetry species of the  $D_2$  group ( $A, B_a, B_b, B_c$ ). This process leads to four blocks in the secular determinant, which can be diagonalized independently.

The selection rules for the principal quantum number of an asymmetric top are again:

$$\Delta J = 0, \pm 1 \quad (1.24)$$

The transitions are conventionally denoted as  $P$  ( $\Delta J = -1$ ),  $Q$  ( $\Delta J = 0$ ) or  $R$  ( $\Delta J = +1$ ) branches.

The selection rules for the pseudo-quantum numbers are obtained using the symmetry properties of the rotational levels, as different combinations of the  $K_{-1}$  and  $K_{+1}$  values belong to different representations of the  $D_2$  group of the Hamiltonian. Three different selection rules can then be obtained based on the variations in  $K_{-1}$  and  $K_{+1}$ , as shown in Table 1.3.

**Table 1.3** Selection rules of an asymmetric-top rotor relative to changes in  $K_{-1}$  and  $K_{+1}$ .

Dipole moment	Transition type	$\Delta K_{-1}$	$\Delta K_{+1}$
$\mu_a \neq 0$	<i>a type</i>	$0, \pm 2, \dots$	$\pm 1, \pm 3, \dots$
$\mu_b \neq 0$	<i>b type</i>	$\pm 1, \pm 3, \dots$	$\pm 1, \pm 3, \dots$
$\mu_c \neq 0$	<i>c type</i>	$\pm 1, \pm 3, \dots$	$0, \pm 2, \dots$

### 1.2.1.2 Non-rigid rotor

Although the rigid rotor model is a good initial approximation, the covalent bonds between atoms are not absolutely rigid, but have a certain force constant for stretching. Consequently, as the molecule rotates, centrifugal forces can cause deformations in bond lengths, bond angles, and other parameters, leading to shifts in the rotational spectrum away from the positions predicted by the rigid model.

Generally, the centrifugal distortion effect is more pronounced in lighter molecules. The deviations caused by the centrifugal distortion are typically small, usually within a few MHz. In some cases, however, this effect can be significant even for lower rotational energy levels. To accurately predict the transition frequencies, it is necessary to introduce higher-order Hamiltonian operators:

$$\hat{H}_{rot} = \hat{H}_r + \hat{H}_d \quad (1.25)$$

where  $\hat{H}_r$  is the Hamiltonian operator of the rigid rotor, and  $\hat{H}_d$  represents the Hamiltonian operator of centrifugal distortion, which can be expressed as:

$$\psi_{J\tau M} = -\frac{\hbar^4}{4} \sum_{\alpha\beta\gamma\delta} \hat{P}_\alpha \hat{P}_\beta \hat{P}_\gamma \hat{P}_\delta + \hbar^6 \sum_{\alpha\beta\gamma\delta\epsilon\eta} \hat{P}_\alpha \hat{P}_\beta \hat{P}_\gamma \hat{P}_\delta \hat{P}_\epsilon \hat{P}_\eta \quad (1.26)$$

where  $\tau_{\alpha\beta\gamma\delta}$  and  $\tau_{\alpha\beta\gamma\delta\epsilon\eta}$  are the fourth-order and sixth-order centrifugal distortion constants, with  $\alpha, \beta, \gamma, \delta, \epsilon, \eta = x, y, z$ .

To derive the measurable centrifugal distortion constants for an asymmetric-top rotor, Watson<sup>186</sup> completed a series of transformations of the Hamiltonian operators. He successfully reduced the fourth- and sixth-order centrifugal distortion constants into five and seven independent parameters, respectively, using first-order perturbation theory. For the representation  $I$  and  $A$ -reduction type, the Hamiltonian operators containing fourth-order distortion constants are expressed as:

$$\begin{aligned} \hat{H}_d^{(A)} = & -\Delta_J \hat{P}^4 - \Delta_{JK} \hat{P}^2 \hat{P}_z^2 - \Delta_K \hat{P}_z^4 - 2\delta_J \hat{P}^2 (\hat{P}_x^2 - \hat{P}_y^2) \\ & - \delta_K [\hat{P}_z^2 (\hat{P}_x^2 - \hat{P}_y^2) + (\hat{P}_x^2 - \hat{P}_y^2) \hat{P}_z^2] \end{aligned} \quad (1.27)$$

where  $\Delta_J, \Delta_{JK}, \Delta_K, \delta_J$  and  $\delta_K$  are the fourth-order centrifugal distortion constants. Sixth-order centrifugal terms have not been used in this thesis. The Hamiltonian operator for the  $S$ -reduction representation of centrifugal distortion on rotational energy levels is similar to that of the  $A$ -reduction. Watson derived the Hamiltonian operator for  $S$ -reduction for the fourth-order centrifugal distortion as:

$$\hat{H}_d^{(S)} = -D_J \hat{P}^4 - D_{JK} \hat{P}^2 \hat{P}_z^2 - D_K \hat{P}_z^4 + d_1 \hat{P}^2 (\hat{P}_+^2 - \hat{P}_-^2) + d_2 (\hat{P}_+^4 - \hat{P}_-^4) \quad (1.28)$$

Where  $\hat{P}_+ = (\hat{P}_x + i\hat{P}_y)$ ,  $\hat{P}_- = (\hat{P}_x - i\hat{P}_y)$ . More details about the  $S$ -reduction Hamiltonian operators can be found in the book by Gordy and Cook.<sup>182</sup>

Based on the previously defined rotational constants and centrifugal distortion constants, least squares fitting can be performed to determine the rotational parameters for most asymmetric rotors. In practical applications, the  $A$ -reduction and  $S$ -reduction Hamiltonians can often be used interchangeably. The  $A$ -reduction is generally more suitable for molecules in the class of asymmetric rotor, while molecules with very low asymmetry require the use of the  $S$ -reduction Hamiltonian.

## 1.2.2 Microwave spectroscopy techniques

Fourier Transform Microwave (FTMW) spectroscopy,<sup>176,187</sup> proceeds by transient excitation of the rotational energy levels of molecules or clusters in the microwave frequency range, followed by the time detection of the rotation relaxation signal or free induction decay (FID). The FID is analyzed with a Fourier transform to generate the frequency-domain spectra, containing the transitions between rotational levels. The combination of supersonic jet technology<sup>188</sup> with FTMW spectroscopy greatly improves the efficiency and speed of rotational transitions, producing strong rovibrational cooling, small linewidths and cluster production *in situ*.<sup>189</sup> At the start of this doctoral work our *Group of Supersonic Jets and Plasma Spectroscopies* (GEPCS) at the *Universidad de Valladolid* (UVa) was equipped with two FTMW spectrometers: a Balle-Flygare cavity FTMW spectrometer operating in the 8-18 GHz range and a Chirped-Pulse FTMW spectrometer covering the 2-8 GHz range. Both spectrometers use supersonic jet expansions for preparation of the sample.

All the spectra collected in this Thesis were recorded in the microwave spectrometers at UVa. The two present set-ups at UVa first require the formation of a pulsed supersonic jet, by injection of a pressurized gas mixture containing the sample into a high-vacuum chamber through a circular nozzle (diameters between 0.5 and 1.5 mm). The expansion requires a large pressure difference between the high-vacuum chamber ( $10^{-5}$ - $10^{-7}$  mbar) and the gas reservoir (1-10 bar).<sup>190</sup> The sample then suddenly goes from the high-pressure random thermal motion to a directed motion in the expansion chamber. This rapid change of the kinetic conditions changes the broad velocity distribution into a narrow velocity distribution centered around the terminal speed in the jet. As a result, the internal molecular energies are converted to kinetic energy, leading to considerable molecular freezing. However, the different internal motions cannot equilibrate, so that rotational and vibrational temperatures are different. Typically, the effective rotational temperatures are 2-3 K, while vibrational temperatures are found at 100-150 K. Supersonic jet techniques can simplify the spectrum by moving the molecular population to the lower rotational levels of the vibronic ground-state. In addition, supersonic jet methods effectively reduce intermolecular collisions in the silence zone of the jet, preventing chemical reactions or decomposition and making it an ideal tool for investigating the molecular clusters generated at the first stages of the jet.<sup>191</sup> This reduction of intermolecular collisions contributes to reducing spectral line widths, which may achieve sub-Doppler resolution for coaxial expansions (spectral resolutions below 5 kHz). For perpendicular expansion the resolution is slightly larger. These advantages make the jet expansion a crucial method for the spectroscopic studies of gas-phase molecular clusters, using either rotational, vibrational or electronic spectroscopy.

### 1.2.2.1 Balle-Flygare FTMW spectrometer

The resonator-based FTMW spectrometer located in our group is a non-commercial instrument based on the Balle-Flygare design,<sup>192</sup> featuring a Fabry-Perot multi-pass cavity composed of two spherical mirrors.



**Figure 1.4** The high-resolution Balle-Flygare Fourier transform microwave spectrometer in our group with the front and side views.

Figures 1.4 and 1.5 present the physical image and functional diagram of the Balle-Flygare FTMW spectrometer. Gas samples are prepared as gas mixtures (typically 0.5-1.0%) with a carrier gas. Liquid or solid samples can be placed in a reservoir nozzle and vaporized under heating or at room temperature. The spectrometer uses a circular nozzle with diameters of 0.5-1.5 mm and can be heated to a maximum temperature of approximately 473 K, depending on the molecular properties such as melting point, boiling point and vapor pressure. Samples are flowed with an inert carrier gas (He, Ne, Ar or a 1:1 mixture of Ar + He) at a pressure of approximately 1-5 bar. The jet expansion is created by opening a solenoid pulsed valve located near the center of a Fabry-Perot MW resonator. The resonator installed in the vacuum chamber is composed of two spherical mirrors in a nearly confocal position (diameter = 33 cm), which enhances the detection sensitivity by multipass averaging. Two dipole antennas ( $\sim\lambda/4$  wavelengths) are located at the center of the mirrors. Because of the co-linear orientation of the jet and resonator axes each transition is split into two Doppler components.<sup>177,193</sup> The gas pulse lasts for 500-1000  $\mu\text{s}$ , then a brief microwave pulse of fixed frequency ( $\sim 1 \mu\text{s}$ ,  $< 100 \text{ mW}$ ) excites the molecules. The radiation interacts with the polar molecules in the expansion inducing a molecular polarization. Generally, up to four microwave pulses can be used for each gas pulse. The resulting free induction decay (FID) is later recorded in the time

domain (400-900  $\mu$ s), amplified and recorded by a heterodyne receiver centered at 30 MHz. Finally, the FTMW++ control software written by Grabow,<sup>194</sup> permits the automatic operation of the instrument, averaging the molecular signal and real-time Fourier transform and presentation of results. The accuracy of rotational transition frequencies is below 5 kHz. All frequency oscillators in the system are fixed to a 10 MHz rubidium standard. The main limitation of this instrument is the narrow bandwidth (typ. 1 MHz) and reduced speed (typically 10 Hz).

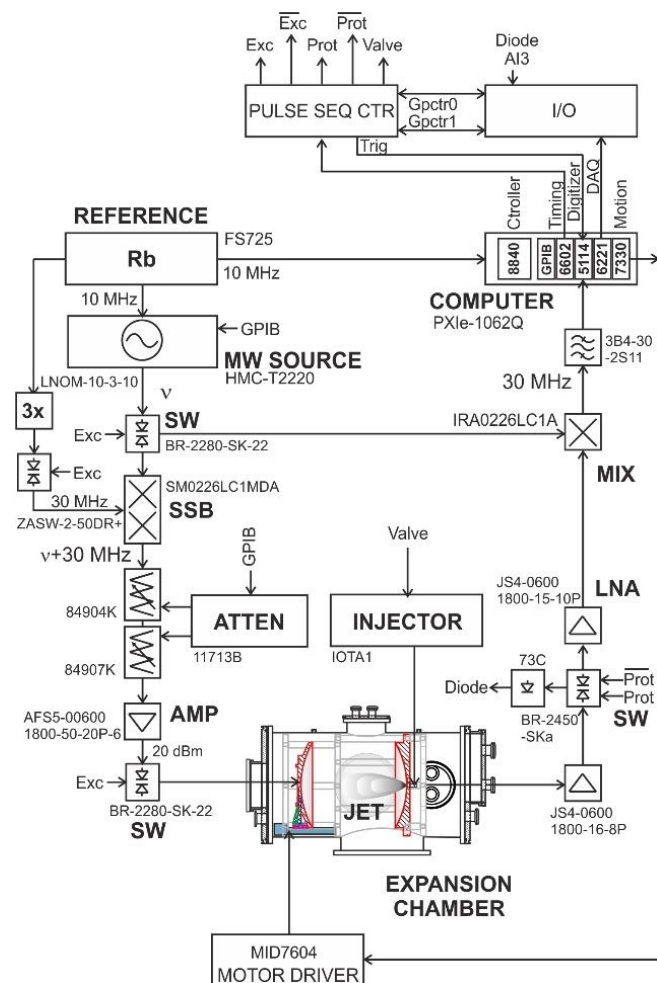


**Figure 1.5** The functional diagram of high-resolution Balle-Flygare Fourier transform microwave spectrometer.

### 1.2.2.2 Chirped-Pulse FTMW spectrometer

The broadband experiments done in this Thesis were conducted using a pulsed jet Chirped-Pulse Fourier Transform Microwave (CP-FTMW) spectrometer at the GEPCS group originally purchased in 2015 (BrightSpec Inc) and recently updated.

The instrument uses a direct-digital design introduced by Pate, avoiding frequency mixing or multiplication. The electronics of the spectrometer permits operation in the frequency range of 2-8 GHz.<sup>195</sup> The CP-FTMW spectrometer is seen in Figure 1.6, with its functional diagram shown in Figure 1.7. In this setup, an arbitrary waveform generator (AWG, 25 GS/s) digitally produces a linearly modulated (or chirped) pulse, covering a bandwidth of 6 GHz in very short times ( $\sim\mu\text{s}$ ). This excitation technique is called fast-passage and is required to obtain an excitation rate significantly faster than the dephasing time of the molecular coherence.<sup>196</sup> In the configuration used, the chirped pulse covers all molecular transitions within the 2-8 GHz range, but the recent instrumental developments permit an extension to 18 GHz. The pulsed sample injection is similar to that of the Balle-Flygare FTMW spectrometer. However, the larger expansion chamber permits using up to three solenoid valves. Since this instrument lacks a resonator, the interaction between the radiation and the jet uses two collinear excitation and detection horn antennas. Because of the size of the horn antennas the injection valves are perpendicular to the propagation of radiation. The interaction volume is smaller than in a coaxial expansion and is affected by a larger velocity distribution, resulting in larger Doppler broadening (FWHM ca. 100 kHz). The power requirements to obtain large operation bandwidths are much larger than in the narrow-band resonator spectrometer. In our set-up the chirped pulses are amplified by a traveling-wave tube (TWT) or a solid-state (SSA) amplifier, with pulsed powers up to 300 W. The detection system includes a diode limiter, a PIN-diode switch (closed during excitation), and a low-noise microwave amplifier. Finally, the high-speed digital oscilloscope (25 GS/s) records the time-domain within 40  $\mu\text{s}$  time. The molecular time-domain signal is converted to the frequency domain through a fast Fourier transform process. Signal averaging is accumulated at a repetition rate of 5 Hz. All frequencies locked at a 10 MHz rubidium standard.



**Figure 1.6** Broadband CP-FTMW spectrometer at Universidad de Valladolid, showing the electronic rack and the expansion chamber. The arrow shows the gas inlet.



spectroscopic procedure. The excitation is followed by a very short (ns) delay before detection.

3) FID acquisition. The FID signal from the molecular emission is recorded for a maximum of 40  $\mu$ s. The molecular signal is amplified before detection with the digital oscilloscope.

4) Averaging. The experimental measurements require averaging (typically  $10^3$  to  $10^6$  cycles). Figure 1.6 shows an image of the CP-FTMW. The functional diagram of the set-up using a SSA is detailed in Figure 1.7, where components highlighted in red are employed for perpendicular double-resonance.

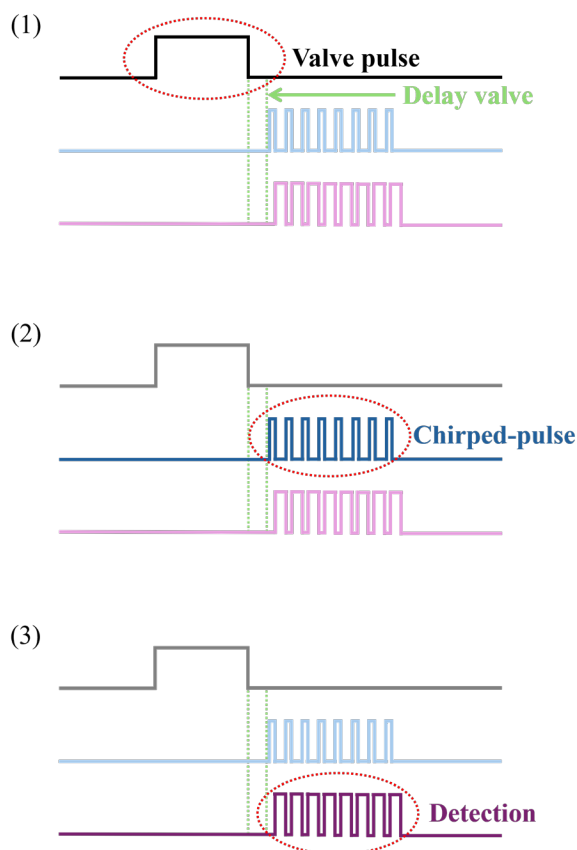


**Figure 1.8** Scheme of the operation sequence in the CP-FTMW spectrometer, (1) Valve pulse and supersonic expansion. (2) Chirped pulse that causes polarization and molecular excitation. (3) FID detection, then followed by a Fourier transform.

### 1.2.3 Computational methods

Several computational calculations complemented the experimental measurements of the Thesis, using different theoretical methods. Low-level molecular

mechanics (MM) or semi-empirical (SE) methods were used only for the initial conformational search and screening of molecular geometries. Further quantum mechanical calculations were conducted with high-level density-functional theory (DFT) or *ab initio* methods. Complementary techniques required for analyzing molecular properties or NCIs analyzed the electronic density with the Non-Covalent (NCI) or Natural-Bond Orbital (NBO) methods. The energy decomposition was conducted with the Symmetry-Adapted Perturbation Theory (SAPT).

### 1.2.3.1 Classical and Semi-empirical molecular calculations

The SE and MM methods were used in this Thesis only for the initial exploration of the PES and for obtaining starting molecular geometries for a molecule or molecular cluster. MM methods are based on classical molecular force methods, which ignore the electronic structure of matter. The SE are more advanced and include some quantum mechanical calculations. Both methods have a low accuracy for calculating molecular energies, but they permit a fast screening of the conformational landscape. In particular, we used in this study the recently developed Conformer-Rotamer Ensemble Sampling Tool (CREST)<sup>197</sup> to search for initial structures of all systems. CREST employs a novel approach to generate a conformational ensemble based on SE direct sampling, rather than using knowledge-based algorithms. Although this method inherently cannot compete with quantum chemical calculations in terms of computational precision, it possesses significant advantages in providing reasonable conformational energies for virtually any chemical species.

The main application of CREST is to generate conformations using an algorithm suite called iMTD-GC.<sup>198</sup> In the iMTD-GC workflow, conformational configurations are generated at the GFNn-XTB level. The SE methods generally produce acceptable initial molecular geometries. This is particularly true for the GFNn-XTB family of methods, which are parameterized specifically to yield relatively accurate structures.<sup>199–201</sup> However, the calculation of conformational energies at the SE level is not sufficiently accurate for spectroscopic applications, which require precise descriptions of small energy differences. For these systems with very dense conformational spaces (i.e.,  $\Delta E \ll 0.5 \text{ kJ}\cdot\text{mol}^{-1}$  and conformers with very similar rotational constants), it is crucial to examine the impact of different sorting thresholds on the final CREST results.

In terms of the operation principle, CREST involves the following steps: (1) Generation of the initial structures: based on the given molecular structure, molecular modeling software is used to generate a set of initial conformers or isomers. (2) Energy evaluation: each conformer or isomer is calculated through energy evaluation to determine its stability and optimized structure. (3) Sampling and optimization: based on the result of energy evaluation, the most stable conformers or isomers are sampled and optimized to generate additional potential conformers or isomers. (4)

Results output: all sampled isomers are consolidated and provided to the user for further analysis and research.

### 1.2.3.2 Quantum chemical calculations

Quantum chemical calculations have become an indispensable tool for assisting the study of NCIs and molecular structures. There are various programs to carry out quantum chemical calculations. In this Thesis we used mostly Gaussian16<sup>202</sup> and ORCA<sup>203</sup> for geometry optimization, frequency calculations, large-amplitude motions, Natural Bond Orbitals (NBO),<sup>204</sup> and Natural Energy Decomposition Analysis (NEDA)<sup>205</sup> of molecules or molecular clusters. Further analyses can be performed using other programs such as Multiwfn,<sup>206</sup> Quantum Theory of Atoms in Molecules (QTAIM)<sup>207</sup>, and Non-Covalent Interactions analysis<sup>208,209</sup>, which can be used to quantify and visualize various intra- and inter-molecular NCIs. PSI4<sup>210</sup> was used for computing the Symmetry Adapted Perturbation Theory (SAPT)<sup>211,212</sup> and quantifying the binding energy of molecular complexes. Several visualization tools were also used to present the results, like Visual Molecular Dynamic (VMD)<sup>213</sup> or Chemcraft.

Most of the quantum mechanical calculations, in particular geometry optimizations and vibrational frequency calculations used Density Functional Theory (DFT),<sup>214</sup> mostly with hybrid (B3LYP<sup>215,216</sup>) or double-hybrid functionals<sup>217</sup> (such as B2PLYP, revDSD-PBEP-86), which were typically combined with triple- $\zeta$  basis sets. The basis set most commonly used was Ahlrich's def2-TZVP.<sup>218,219</sup> For DFT calculations D3(BJ)<sup>220,221</sup> empirical dispersion corrections were also included. Other *ab initio* calculation levels were sometimes used, like Møller–Plesset second-order perturbation theory (MP2)<sup>222</sup> or DLPNO-CCSD(T). A description of these methods is found in the bibliography.

In this work we were mainly concerned with weakly-bound intermolecular molecular clusters. For these systems the computational work proceeds through the following flow diagram:

- 1) The first step includes determining all possible initial geometrical structures using MM or CREST software, together with a revision of the structures of the monomers or isomers, which sometimes may present different low-energy conformations. Since the energy calculations at this level are not accurate it is necessary to obtain a large dataset of initial geometries to ensure a good scan of the conformational landscape. The conformational search can be started from different guess structures and different methods to improve the number of initial structures.
- 2) The second step involves optimizing the initial set of molecular structures. It is convenient to repeat these calculations at different computational levels to check the consistency of the chemical models. For spectroscopic purposes, a

reasonably good result is generally obtained at the B3LYP-D3(BJ)/def2-TZVP<sup>215,216,218–221</sup> level, which may be complemented with more advanced theoretical methods. This step provides electronic structures, electric properties (i.e, electric dipole moment and nuclear quadrupole moments) and geometric parameters.

- 3) Once a first energy ordering has been obtained it is necessary to conduct harmonic frequency calculations on the optimized structures (using the same theoretical methods) to verify whether the obtained geometries correspond to real energy minimum or saddle points. This process yields crucial information for the spectroscopic measurements and conformer assignments, such as vibrational zero-point corrections, thermal corrections such as Gibbs energies and the molecular force field. The molecular force field permits determining the centrifugal distortion constants. This step is normally carried out within the harmonic approximation. However, if necessary anharmonic calculations can also be carried out.
- 4) The fourth step involves determining the complexation energy or the binding energy. The complexation energy is easier to calculate, as it only requires the energy of the dimer and the monomers at the geometry of the complex. The calculation of the binding energy needs to evaluate the deformation energy between the isolated monomers and the monomers in the complex. In this process it is necessary to consider the basis set superposition errors (BSSE), which are accounted for using the counterpoise correction methods.<sup>223</sup>
- 5) Finally, other methods can be used to enhance our understanding of molecular clusters, mostly based on examining the properties of molecular electron density or conducting an energy decomposition analysis. The primary methods used in the Thesis were Johnson's NCI analysis,<sup>208</sup> implemented with the Multiwfn program<sup>206</sup>, and the Symmetry-adapted perturbation theory (SAPT) energy decomposition,<sup>211,212</sup> computed with PSI4.<sup>210</sup>

### 1.2.3.3 Non-covalent interactions analysis

The Non-covalent Interaction (NCI) analysis is a computational tool specifically designed to quantify and map the NCIs between molecules or within a single molecule, enabling the discrimination of various types of NCIs. The NCI analysis employs a topological approach based on the reduced electron density to characterize these intermolecular interactions. The NCIs regions are identified through the isosurfaces of the reduced density gradient  $s(r)$ :<sup>208,224,225</sup>

$$s(r) = \frac{1}{2(3\pi^2)^{1/3}} \frac{|\nabla\rho(r)|}{\rho(r)^{4/3}} \quad (1.29)$$

Attractive and repulsive interactions are defined by the product of electron density and the second Hessian eigenvalue  $\text{sign}(\lambda_2)\rho$ , (normally within a range of -0.05 to

0.05 a.u). Here,  $\lambda_2$  represents the second eigenvalue of the electron density Hessian, and  $\rho$  is the electron density. The NCIPLOT can also represent the strength and type of these interactions through colors, symbols, or intensity. Typically, blue indicates stable (attractive) interactions, green represents weak interactions, and red denotes unstable (repulsive) interactions. The sign of  $\text{sign}(\lambda_2)\rho$  and the intensity of the color represent the strength of the interactions. For instance, a negative value of  $\text{sign}(\lambda_2)\rho$  indicates attractive interactions, while a positive value signifies repulsive interactions. A deep blue color denotes a stronger HB compared to a lighter blue, indicating the relative strength of the HBs.

### 1.2.3.4 Natural bond orbitals (NBO)

The Natural Bond Orbitals (NBO) model is a powerful tool for visualizing chemical bonds between various molecules by deriving localized orbitals from the overall molecular density, similar to Lewis structures. The concept of natural orbitals was first introduced by Löwdin in 1955. Natural (localized) orbitals are used to calculate the distribution of electron density across bonds within molecules and atoms. These orbitals are distinguished by their "maximum occupation number" within corresponding single-atom or double-atom regions. Specifically, when represented by natural orbitals in the matrix of the first-order reduced density operator, the diagonal elements are maximized, typically reaching or approaching 2. As a result, NBOs explain the most significant natural Lewis structures associated with the wave functions. In a natural Lewis structure, the occupation numbers of natural bond orbitals typically encompass the majority of the electron density, often exceeding 99% for common organic molecules.

Each bonding NBO (donor)  $\sigma_{AB}$  can be expressed in terms of two directed valence hybrids (NHO, Nuclear Hybrid Orbitals)  $h_A$  and  $h_B$  on atoms A and B, respectively, with corresponding polarization coefficients  $c_A$  and  $c_B$ :

$$\sigma_{AB} = c_A h_A + c_B h_B \quad (1.30)$$

These bonds transition smoothly from a fully covalent state ( $c_A = c_B$ ) to a fully ionic state ( $c_A \gg c_B$ ). Each valence bonding NBO  $\sigma$  must be paired with a corresponding valence antibonding NBO  $\sigma^*$  (acceptor) to span the valence space:

$$\sigma_{AB}^* = c_A h_A - c_B h_B \quad (1.31)$$

Valence covalent NBOs are classified as "Lewis orbitals", characterized by occupation numbers close to 2, whereas valence antibonding NBOs are termed "non-Lewis orbitals", with occupation numbers close to 0. In an idealized Lewis structure, complete Lewis orbitals (each containing two electrons) are complemented by formally empty non-Lewis orbitals. The weak occupancy of valence antibonds presents an irreversible deviation from an idealized localized Lewis structure, indicating genuine "delocalization effects".<sup>226</sup> NBOs can be computed using

Gaussian16 to identify the optimal Lewis structure, defined as the one with the highest electron charge in the Lewis orbitals (referred to as Lewis charge). A low electron charge in the Lewis orbitals suggests a strong influence of electron delocalization. Importantly, in NBO calculations, there is no need to consider "covalent ion resonance," as the resonant structure already incorporates bond polarity effects.<sup>227</sup>

### 1.2.3.5 Symmetry-adapted perturbation theory (SAPT)

SAPT is a theoretical approach used to calculate intermolecular interaction energies for clusters. According to the introduction of Mazziotti in 1992, SAPT was developed to overcome the limitations of traditional molecular orbital theory in computing weak intermolecular interactions. SAPT decomposes the intermolecular interaction energy into several components, providing a more precise and intuitive description of intermolecular interactions. The core concept of SAPT decomposes the intermolecular interaction energy into independent contribution terms, which can be computed using quantum chemical methods. These contributions include:

1. Exchange energy ( $E_{ex}$ ): Describing the energy change due to electron exchange when electron clouds overlap between molecules.
2. Dispersive energy ( $E_d$ ): Reflecting the energy change due to instantaneous dipole interactions, which are particularly significant at larger intermolecular distances.
3. Inductive energy ( $E_i$ ): Capturing the energy change due to a molecule inducing a dipole moment in another molecule.
4. Electrostatic energy ( $E_{elst}$ ): Representing the energy change due to the interaction of charge distributions between molecules.

In SAPT, the Hamiltonian of dimer is partitioned into contributions of each monomer and the interaction. The simplest truncation in SAPT, known as SAPT0, as defined in Equation (1.32), captures the first-order contributions from two charge densities and exchange, with the second-order contributions including electrostatic induction and dispersion, along with their exchange counterparts.

$$E_{int}^{SAPT0} = E_{elst}^{(1)} + E_{ex}^{(1)} + E_i^{(2)} + E_{ex-i}^{(2)} + E_d^{(2)} + E_{ex-d}^{(2)} \quad (1.32)$$

### 1.2.4 Spectral analysis

The spectral analysis has benefited in recent years from the introduction of calculation programs and other graphical simulation tools. Some of these programs include only numerical predictions and fitting, while others combine fitting routines with graphical simulations with different Hamiltonian models. The most powerful

spectral fitting program is CALPGM<sup>228</sup> by Pickett. CALPGM is made of two main programs (SPCAT/SPFIT) which permit the introduction of generic Hamiltonians and fitting terms, which are solved by direct diagonalization. While most of spectroscopic problems can be solved with SPCAT/SPFIT, some other programs have been designed for more specific situations. For example, the program XIAM<sup>229</sup> is commonly used for spectra with internal rotors. Graphical simulation tools include JB95<sup>33</sup>, AABS<sup>230,231</sup> and PGOPHER<sup>232</sup>, which permit a fast presentation of predicted results and the assignment of new spectra. Graphical simulations are especially useful for the analysis of dense broadband spectra. Some of these programs implement routines for automatic assignments, like AUTOFIT.<sup>233</sup> Detailed descriptions of these programs can be found in the relevant literature. Additional programs for rotational spectroscopy are freely available in the PROSPE repository from Kisiel.

## Chapter 2. The Phenol - Thiophenol Heterodimer

This chapter explores the non-covalent interactions responsible for the formation of heterodimers between phenol and thiophenol ( $C_6H_6O \cdots C_6H_6S$ ), using both experimental and computational methods. Experimentally, broadband chirped-pulse Fourier transform microwave (CP-FTMW) spectroscopy was employed. Two heterodimers were detected, which correspond to the first two energy minima identified through density functional theory (DFT) predictions. The two heterodimers are stabilized by a combination of O-H $\cdots$ S hydrogen bonds and  $\pi$ - $\pi$  stacking interactions. The findings presented in this chapter provide new insight into the complex interactions between aromatic compounds functionalized with alcohol or thiol groups, offering a benchmark for quantum chemical calculations and eventually practical guidance for the design of novel functional materials based on these compounds.

### 2.1 Introduction

In Chemistry, aromatic compounds have long been a focus of research due to their unique electronic structures and potential NCI characteristics, which create intricate molecular frameworks.<sup>234,235</sup> These compounds often self-aggregate using  $\pi$ - $\pi$  stacking geometries, a stable intermolecular structure formed by the dispersion-based interaction between the  $\pi$ -electron clouds.<sup>234</sup>  $\pi$ - $\pi$  Stacking is also the key to their mutual recognition in organisms and the presence of unique properties in material chemistry.<sup>59,100,101</sup> The  $\pi$ - $\pi$  stacking self-aggregation process can affect significantly the physicochemical properties of compounds such as solubility, melting point, and crystallinity, but also holds broad potential for applications in biochemistry, drug design, and organic synthesis.<sup>53,94,96,236</sup> However, most current gas-phase investigations on  $\pi$ - $\pi$  stacking in aromatic compounds only focused on homo-aggregated complexes, with no examples published of  $\pi$ - $\pi$  stacking in heterodimers.

In this chapter, rotational spectroscopy will be employed for studying the NCIs and intermolecular forces between the monosubstituted aromatic compounds of phenol and thiophenol.<sup>170-175</sup> The rotational motion of these molecular systems can offer insight about the molecular structure and underlying dynamics of the formed NCIs.<sup>170-175</sup> Previous studies have analyzed the rotational signatures of several homodimers and homotrimers involving only alcohols or thiols.

For alcohol-substituted mono-arene clusters, like the phenol dimer and trimer<sup>67</sup> or the benzyl alcohol<sup>237</sup> and 2-phenylethanol dimers,<sup>238</sup> the aggregates are stabilized by hydrogen bonds. This situation is observed also for some thiol clusters, like the benzyl mercaptan<sup>21</sup> and 2-phenylethanethiol<sup>52</sup> dimers or the thiophenol trimer.<sup>33</sup> The

thiophenol dimer<sup>33</sup> represents an exceptional case, since it is stabilized both by  $\pi$ - $\pi$  stacking and a hydrogen bond. Regarding the larger bi-arenes, the presence of two phenyl rings is expected to promote the  $\pi$ - $\pi$  stacking geometries. This is the case for the naphthyl derivatives like the 1-naphthol dimer<sup>66</sup> and the 2-naphthalenethiol dimer,<sup>42</sup> which are controlled only by  $\pi$ - $\pi$  stacking interactions. In consequence, the aromatic clusters show different NCIs depending on the ring size and substituent groups. For the experiments done so far, we thus observe that when the ring size is increased from a mono- to a bi-arene, the aromatic thiols are stabilized by  $\pi$ - $\pi$  stacking instead of a hydrogen bond and only in thiophenol both interactions coexist.

This chapter investigates the NCIs involved in the formation of the heterodimer formed by two aromatic compounds, phenol and thiophenol. We aim to uncover how NCIs between alcohols and thiols influence the structure, properties, and chemical functions of these compounds during the formation of heterodimer, and how the aggregation patterns differ from the homodimers. This study offers new insights into the complex behavior of aromatic compounds and provides a theoretical foundation and practical guidance for the design of new functional materials and compounds involving these compounds.

## 2.2 Experimental and Theoretical Methods

### 2.2.1 Experimental Methods

The samples of phenol (99% purity, boiling point 181.9°C) and thiophenol (>98% purity, boiling point 168.3°C) were obtained commercially and did not require further purification. The samples were mixed inside two heating reservoirs and vaporized at 80°C. The vapors were expanded through two 1.0 mm diameter nozzles (separated ca. 25 cm) into the vacuum chamber, forming a supersonic jet. In this experiment we used either a 1:1 mixture of Helium and Argon or pure Helium as carrier gases, maintained at backing pressures of ~0.3 MPa. The mixed sample of phenol and thiophenol was flowed for typical molecular pulses ranging from 350 (He) to 500  $\mu$ s (He:Ar). The rotational spectrum of the heterodimer within the 2-8 GHz frequency range was analyzed using a direct-digital chirped-pulse Fourier transform microwave (CP-FTMW) spectrometer,<sup>196</sup> described in Chapter 1. During the measurement, we used chirped pulses of 4  $\mu$ s duration emitted perpendicularly to the jet, which were later amplified by a 300 W Traveling-Wave Tube (TWT) amplifier. The microwave radiation induces a rapid broadband transient excitation, covering the entire spectral bandwidth. Following the excitation, the heterodimer emits a free-induction decay, which was detected in the time domain (40  $\mu$ s) and recorded by a digital oscilloscope (25 GSamples/s sampling rate). In the present experiment approximately 2 million averages were accumulated at a 5 Hz repetition rate, with an estimated uncertainty in

frequency measurements of less than 20 kHz. Full lists of assigned transitions are provided in Tables S2.1 and S2.2 of the Appendix.

## 2.2.2 Computational Methods

An initial conformational search of the phenol-thiophenol (PN-TPN) was performed using CREST.<sup>197</sup> All the starting isomers were later reoptimized employing DFT. The hybrid B3LYP<sup>215</sup> method with D3<sup>220</sup> empirical dispersion corrections and Becke-Johnson damping functions was used in conjunction with Ahlrichs' polarized triple-zeta basis set (def2-TZVP).<sup>218</sup> This calculation level has proved appropriate for spectroscopic purposes in previous studies. The harmonic approximation was employed to perform frequency computations at the same level of theory. During the computation of complexation energies the basis set superposition error (BSSE) was accounted for using the counterpoise correction method.<sup>223</sup> All the computations were conducted using Gaussian 16.<sup>202</sup> An energy decomposition analysis was carried out with second-order symmetry-adapted perturbation theory (SAPT),<sup>73,211</sup> implemented in the PSI4 program,<sup>210</sup> to estimate the physical contributions to the binding energy of clusters. Finally, the NCIs were analyzed using the NCI analysis, based on the reduced electron density gradient of Johnson and Contreras.<sup>208</sup>

## 2.3 Results and Discussion

At the B3LYP-D3(BJ)/def2-TZVP level of theory, the eight most stable geometries of the heterodimer of PN-TPN are predicted within relative energies of 5 kJ mol<sup>-1</sup>. The most stable isomers are shown in Figure 2.1, together with their corresponding relative electronic energies. The theoretical spectroscopic parameters are listed in Table S2.3 in the Appendix. The B3LYP-D3(BJ)/def2-TZVP calculation level proved to have accuracies below 3% for the rotational constants of similar clusters.

As observed in Figure 2.1, the most stable PN-TPN isomers can be categorized in two groups. The first group is characterized by a O-H $\cdots$ S hydrogen bond and  $\pi$ - $\pi$  stacking, while the second group contains only O-H $\cdots$  $\pi$  or S-H $\cdots$   $\pi$  hydrogen bonds. Top and side views are presented for the eight more stable isomers. In comparison, the structures stabilized by O/S-H $\cdots$  $\pi$  bonds exhibit higher energies than those stabilized by the O-H $\cdots$ S hydrogen bond and  $\pi$ - $\pi$  stacking. In terms of isomers belonging to the first group, torsional isomerism emerges. More specifically, the only difference between isomers I and II is the ( $\pi$  radians) opposite orientation of the S-H group in thiophenol. As in the monomers, the alcohol and thiol group are nearly coplanar with the aromatic ring in the two isomers. However, isomers I and II differ because the thiol group can adopt two different synperiplanar conformations, with the two polar groups either in near parallel (*cis*) or antiparallel (*trans*) configurations. This

inversion motion is not expected to produce torsional doubling because the two isomers are not equivalent. Regarding isomers III and IV a similar situation arises, as the two species again differ in the *cis/trans* orientation of the thiol group in thiophenol. Each isomer is chiral, so they exhibit a pair of mirror-image structures. However, a mirror reflection maintains the *cis* or *trans* orientations. For the four higher-energy isomers shown in Figure 2.1, the phenyl groups of the two molecules are positioned farther away from each other, which results in the absence of any  $\pi$ - $\pi$  stacking. Isomer V features both an O-H $\cdots$  $\pi$  bond and a S-H $\cdots$  $\pi$  bond, while a dominant O-H $\cdots$  $\pi$  bond is present in isomer VI. For isomer VII, the phenyl groups in the two molecules unexpectedly present a situation close to a T shape, which is similar to the benzene dimer.<sup>239</sup> However, it can be seen that the C-H $\cdots$  $\pi$  bond seems weaker than the O-H $\cdots$  $\pi$  bond attending to the longer interaction distance. In isomer VIII, the C-H $\cdots$  $\pi$  interaction appears slightly shorter than the S-H $\cdots$  $\pi$  hydrogen bond.

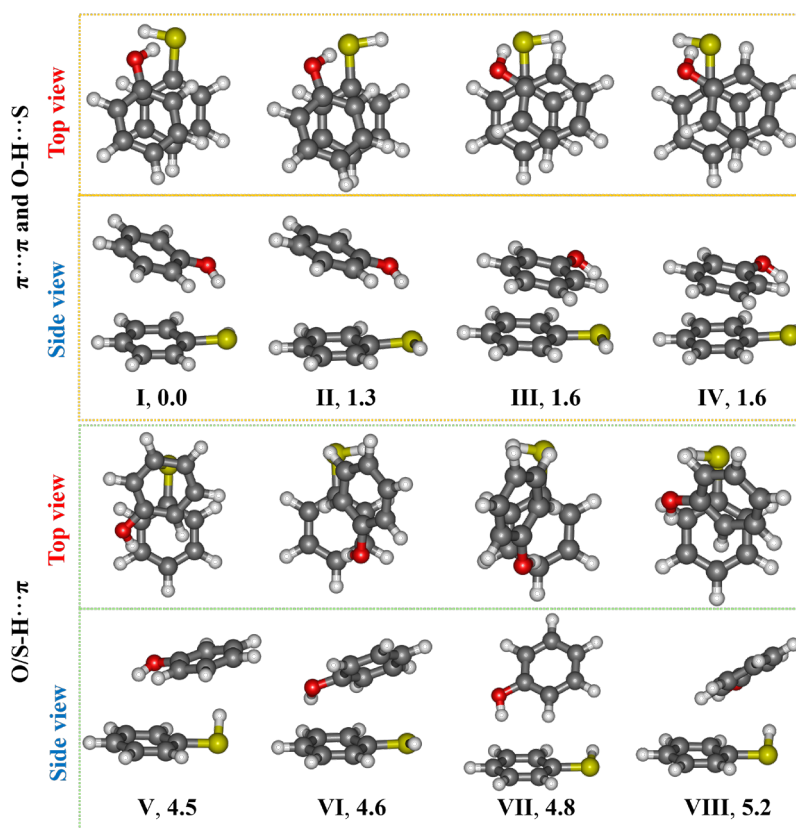


**Figure 2.1** The structures of the eight most stable PN-TPN heterodimers at the B3LYP-D3(BJ)/def2-TZVP level of theory. Relative electronic energies in  $\text{kJ mol}^{-1}$ .

In our experiment, only the isomer *I-trans* was successfully assigned in the spectrum recorded using the mixed carrier gas of Helium (He) and Argon (Ar) (1:1). However, when using pure Helium as the carrier gas, isomer *II-cis* was also successfully detected. This fact confirmed that isomer *I-trans* is the global minimum. The spectroscopic parameters of two isomers, obtained by fitting the experimental rotational transitions, are presented in Table 2.1. Additionally, their corresponding theoretical spectroscopic parameters calculated at the B3LYP-D3(BJ)/def2-TZVP level of theory are also provided in the same table. Based on the comparison, the experimental parameters match the theoretical parameters very well. Figure 2.2 illustrates four sets of transitions with a quartet made of two pairs of equally distanced  $\mu_a$ - $\mu_b$  transitions for both isomers *I-trans* and *II-cis*. The upper traces represent the experimental spectra collected in pure helium (in black) and the 1:1 Ar+He mixture (in red), respectively. The lower traces show simulated spectra of the phenol-thiophenol dimers based on the experimental spectroscopic parameters, with isomer *I-trans* in green and isomer *II-cis* in blue. In the weaker experimental spectra obtained in the 1:1 Ar+He mixture, no transition corresponding to isomer II was observed, further confirming the energy ordering.

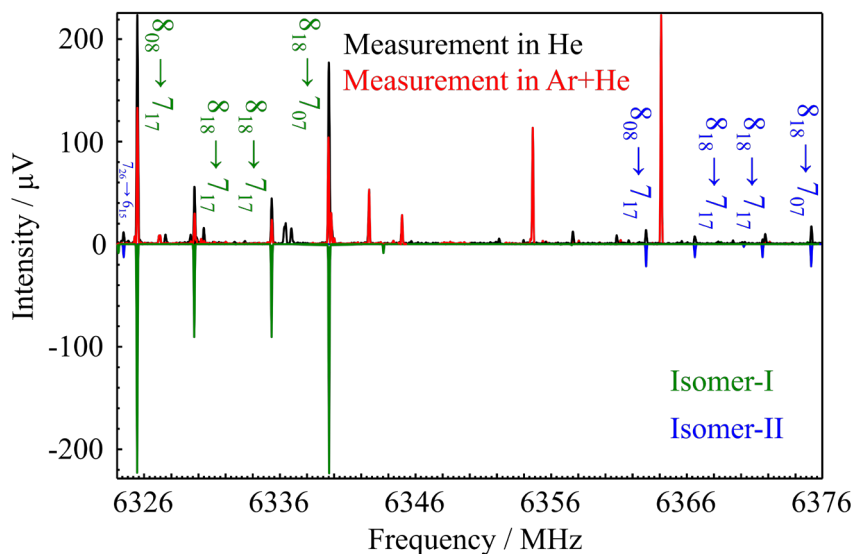


**Figure 2.2** The rotational spectra of PN-TPN heterodimer in the frequency range of 6324 MHz - 6376 MHz (upper panel). The positive traces show the experimental spectra using as carrier gas either pure He (black trace) or 1:1 Ar+He (red trace). The negative traces are the simulations based on the fitted rotational constants of the two isomers of phenol-thiophenol heterodimer (Isomer *I-trans* is in green, Isomer *II-cis* is in blue). Isomer I is visible for He and Ar+He, while Isomer II is visible only with He). Lines present only with Ar+He could be due to argon or helium clusters, but are not assigned.

The experiment confirms the prevalence of the alcohol-to-thiol O-H $\cdots$ S hydrogen bond and  $\pi$ - $\pi$  stacking interactions over the thiol-to-alcohol S-H $\cdots$ O hydrogen bond or the O/S-H $\cdots$  $\pi$  and C-H $\cdots$  $\pi$  interactions for the heterodimers of PN-TPN. This trend is similar to most of previous observations in the gas phase involving alcohols and thiols, where the existence of the O-H $\cdots$ S hydrogen bond is also found dominant. Some examples include intramolecular HBs (2-mercaptoethanol monomer,<sup>240</sup> etc), monohydrates (thienyl mercaptan $\cdots$ H<sub>2</sub>O,<sup>27</sup> etc), hydrogen sulfide adducts (*p*-cresol $\cdots$ H<sub>2</sub>S,<sup>75</sup> methanol $\cdots$ H<sub>2</sub>S,<sup>79</sup> etc) and tioether dimers (methanol $\cdots$ dimethyl sulfide,<sup>241</sup> *p*-cresol $\cdots$ diethyl sulfide,<sup>242</sup> phenol $\cdots$ dimethyl sulfide,<sup>90</sup> tetrahydrofuran $\cdots$ thioether,<sup>78</sup> etc). These examples seem to indicate that in the presence of both S-H and O-H groups, the alcohol group preferentially acts as a proton donor, while the sulfur atom more readily serves as a proton acceptor.

**Table 2.1** Experimental rotational parameters compared with computational predictions at the B3LYP-D3(BJ)/def2-TZVP level of theory for the observed isomers of the PN-TPN heterodimer.

Parameter <sup>a</sup>	Experimental		Theoretical	
	I- <i>trans</i>	II- <i>cis</i>	I- <i>trans</i>	II- <i>cis</i>
<i>A</i> / MHz	858.69257(21) <sup>b</sup>	849.45588(70)	862.3	856.8
<i>B</i> / MHz	494.63494(16)	497.66411(85)	516.4	517.4
<i>C</i> / MHz	381.20128(15)	383.62870(63)	394.2	395.3
<i>D</i> <sub>J</sub> / kHz	0.3081(10)	0.2992(56)	0.183	0.199
<i>D</i> <sub>K</sub> / kHz	0.1352(24)	[-0.00722] <sup>c</sup>	0.0717	-0.00722
<i>D</i> <sub>JK</sub> / kHz	-0.0762(22)	[0.108]	0.0429	0.108
<i>d</i> <sub>1</sub> / kHz	-0.06940(47)	-0.0663(30)	-0.0459	-0.0526
<i>d</i> <sub>2</sub> / kHz	-0.01295(15)	[-0.0122]	-0.0104	-0.0122
<i>N</i>	218	102	-	-
$\sigma$ / kHz	7.2	9.2	-	-
$ \mu_a ,  \mu_b ,  \mu_c $ / D	yes, yes, yes	yes, yes, yes	0.9, 1.5, 0.3	1.3, 1.8, 1.1
$\Delta E_0$ / kJ mol <sup>-1</sup>	-	-	0.0	1.1

<sup>a</sup>Rotational constants (*A*, *B*, *C*), Watson's *S*-reduction centrifugal distortion constants (*D*<sub>J</sub>, *D*<sub>JK</sub>, *D*<sub>K</sub>, *d*<sub>1</sub>, *d*<sub>2</sub>), electric dipole moments ( $\mu_\alpha$ ,  $\alpha = a, b, c$ ), number of transitions (*N*) to be used in the fits, root-mean-square deviation of the fits ( $\sigma$ ) and electronic relative energies with the zero-point relative energies ( $\Delta E_0$ ). <sup>b</sup>Values in parentheses are standard errors in units of the last digit. <sup>c</sup>Values in brackets are fixed to their theoretical ones.

The experimentally observed conformations of the two dimers of PN-TPN permit a structural comparison with the homodimers of phenol<sup>67</sup> (PN-PN) and thiophenol<sup>33</sup> (TPN-TPN) in Figure 2.3. For the PN-PN cluster the dimer adopts a so

called “hinged” configuration controlled by the alcohol-to-alcohol O-H $\cdots$ O hydrogen bond and other weaker interactions between the rings. This interaction resembles the prototype water dimer but with additional complexity caused by the delicate balance between the two rings. In any case,  $\pi$ - $\pi$  stacking is not observed for the PN-PN. Conversely, the thiophenol dimer presents a prototypic  $\pi$ - $\pi$  stacking near-parallel arrangement. Interestingly, the two possible orientations of the thiol group give rise to tunnelling splitting in the spectrum, which permitted the determination of the torsional barrier in the dimer. For the PN-TPN cluster, the strength of the hydrogen bond interaction is increased, as suggested by the shorter hydrogen bond distance. At the same time the two rings become slightly tilted, suggesting that  $\pi$ - $\pi$  stacking interactions play a less important role compared to TPN-TPN.

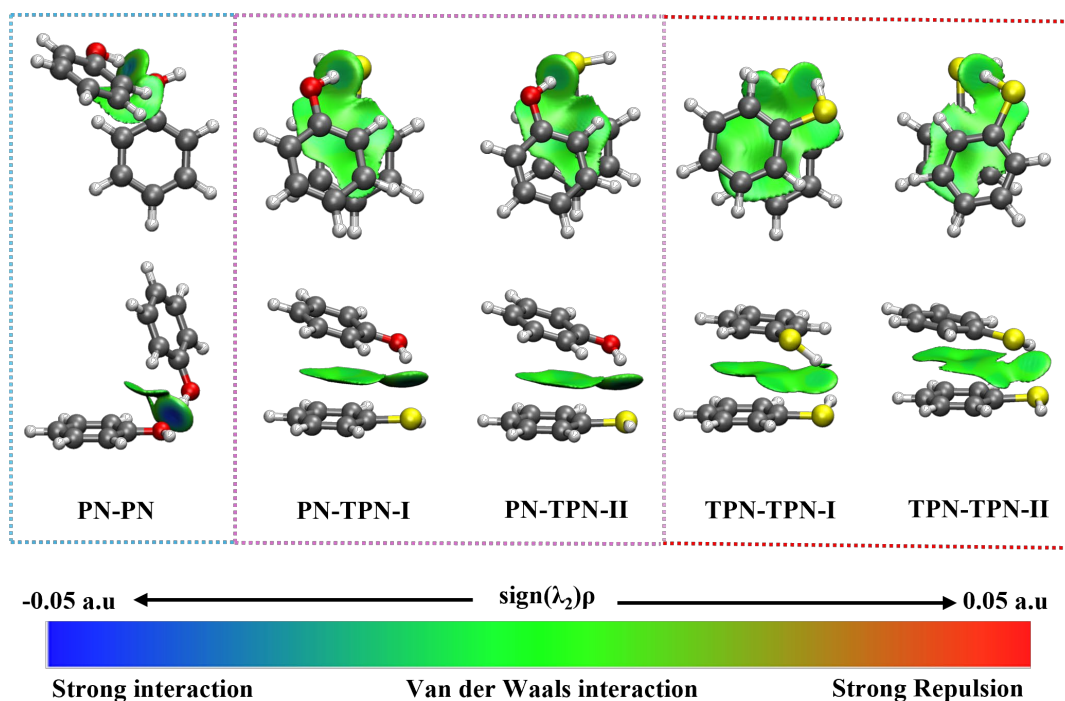


**Figure 2.3** Non-covalent interaction plots (NCIPlots) for the all experimentally assigned isomers of the phenol dimer (PN-PN), thiophenol dimer (TPN-TPN) and the phenol-thiophenol heterodimer (PN-TPN). The cut-off value for the isosurface is set at 0.5. Attractive and repulsive interactions are defined by the product of electron density and the second Hessian eigenvalue [ $\text{sign}(\lambda_2)\rho$ ] with the range of -0.05 to 0.05 a.u. Here,  $\lambda_2$  represents the second eigenvalue of the electron density Hessian, and  $\rho$  is the electron density. In the color bar at the bottom, deep blue indicates strong attractive interactions, green represents weaker van der Waals interactions, and red means strong repulsive interactions.

Despite no isotopic species were observed in this work, some structural comparisons between the isomers of PN-TPN and other dimers are possible using the computational results. The hydrogen bond distance in the two isomers is practically the same (isomer I-*trans*: B3LYP:  $r(\text{O-H}\cdots\text{S}) = 2.55 \text{ \AA}$ ; isomer II-*cis*:  $r(\text{O-H}\cdots\text{S}) = 2.54 \text{ \AA}$ , see Table 2.2). The bond distances in these two isomers are slightly shorter than those of the prototype  $\text{H}_2\text{S-H}_2\text{O}$  dimer in Table 2.2, suggesting that the aromatic ring affects the  $\text{O-H}\cdots\text{S}$  hydrogen bond to a small extent. However, a more accurate comparison would require isotopic measurements. The intermolecular hydrogen bonds in both isomers are non-linear (isomer I-*trans*:  $\angle(\text{O-H}\cdots\text{S}) = 142.9^\circ$ ; isomer II-*cis*:  $\angle(\text{O-H}\cdots\text{S}) = 143.2^\circ$ ), as required to maintain the  $\pi$ - $\pi$  stacking alignment.

**Table 2.2** Hydrogen bond structural parameters in the dimers of  $\text{H}_2\text{S-H}_2\text{O}$  and PN-TPN.

Molecules	Method	$r(\text{O-H}\cdots\text{S}) / \text{\AA}$	$\angle(\text{O-H}\cdots\text{S}) / ^\circ$
$\text{H}_2\text{S-H}_2\text{O}^{\text{a}}$	MW <sup>b</sup>	2.597(4)	193.4(4)
	MW <sup>c</sup>	2.590(6)	185.2(63)
PN-TPN	I B3LYP <sup>d</sup>	2.55	142.9
	II B3LYP	2.54	143.2

<sup>a</sup> MW: microwave spectroscopy. <sup>b</sup>  $\text{A}_2$  state: F. Lovas, private communication, 2020. <sup>c</sup>  $\text{B}_2$  state: F. Lovas, private communication, 2020. <sup>d</sup> B3LYP/def2-TZVP, calculated in this work.

Table 2.3 and Figure 2.4 report the results of the binding energy decomposition for the observed isomers of  $\text{H}_2\text{S-H}_2\text{O}$ , PN-PN, TPN-TPN, and PN-TPN, which were carried out based on SAPT using the SAPT2+3(CCD)/aug-cc-pVDZ level of theory. The analysis reveals that the electrostatic contribution to the total attractive energy is larger in  $\text{H}_2\text{S-H}_2\text{O}$  (59.2%), while the dispersion energy is the most significant contribution in the two isomers of TPN-TPN (isomer I-*trans*: 62.2%, isomer II-*cis*: 59.7%). In comparison to  $\text{H}_2\text{S-H}_2\text{O}$ , the introduction of the phenyl group in PN-TPN increases the dispersion contribution from 20.7% to 48.3% or 49.1%. Regarding the comparison between TPN-TPN and PN-TPN, the electrostatic contribution increases, while the dispersion contribution decreases. Compared to PN-PN, the electrostatic contribution in PN-TPN decreases by around 15%, while the dispersion contribution of PN-TPN increases by about 10%. In terms of the electrostatic and dispersion contributions for PN-PN, TPN-TPN, and PN-TPN, it shows that PN-TPN lies at an intermediate level. These suggest that aromatic component can dramatically dominate the dispersion contribution, while S-H group will reduce the electrostatic contribution at some extent.

**Table 2.3** The results of binding energy decomposition for the dimers of H<sub>2</sub>S-H<sub>2</sub>O, PN-PN, TPN-TPN and PN-TPN, comparing the magnitude of the electrostatic, dispersion and induction contributions (all values in kJ mol<sup>-1</sup>). The calculations are based on SAPT energy decomposition at SAPT2+3(CCD)/aug-cc-pVDZ level.

Dimer	SAPT energy decomposition					
	$\Delta\vec{E}_{\text{Electrostatic}}$	$\Delta\vec{E}_{\text{Dispersion}}$	$\Delta\vec{E}_{\text{Induction}}$	$\Delta\vec{E}_{\text{Exchange}}$	$\Delta\vec{E}_{\text{Total}}$	
H <sub>2</sub> S-H <sub>2</sub> O	-20.0(59.2%)	-7.0(20.7%)	-6.8(20.1%)	24.0	-9.8	
PN-PN	-39.4(50.1%)	-23.5(29.9%)	-15.7(20.0%)	50.5	-28.1	
TPN-TPN	I	-23.1(29.9%)	-48.1(62.2%)	-6.1(7.9%)	48.4	-28.8
	II	-22.8(31.5%)	-43.3(59.7%)	-6.4(8.8%)	44.3	-28.1
PN-TPN	I	-29.6(36.2%)	-39.5(48.3%)	-12.6(15.4%)	50.3	-31.5
	II	-28.1(35.3%)	-39.0(49.1%)	-12.4(15.6%)	49.5	-30.0

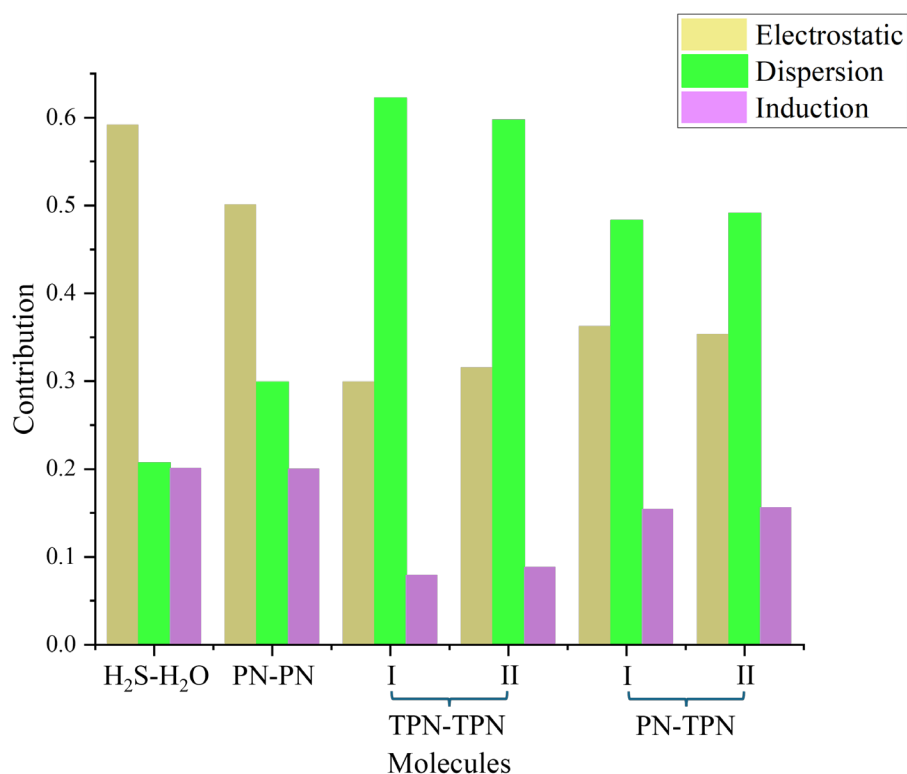


**Figure 2.4** The bar chart illustrates the decomposition of binding energy (considering only the attractive components) for interactions between H<sub>2</sub>S-H<sub>2</sub>O, PN-PN, TPN-TPN, and PN-TPN. The detailed results are given in **Table 2.3**.

## 2.4 Conclusions

In this chapter, high-resolution chirped pulse FTMW spectroscopy was employed to record the rotational spectrum of the PN-TPN heterodimer. Two distinct isomers have been observed, only differing in the orientation of the thiol group, but maintaining a similar parallel-displaced near-planar arrangement of the two rings. This kind of torsional thiol isomerism has been observed only in a few cases, most notably in the TPN-TPN and would be undetectable using other spectroscopic techniques. This work thus illustrates the capabilities of rotational spectroscopy to discriminate the structural properties of weakly bound complexes with minor structural differences. The spectroscopic parameters obtained from the experimental fits closely matched those predicted by calculations (B3LYP-D3(BJ)/def2-TZVP level of theory). NCI analysis reveals that both isomers were stabilized by a combination of O-H $\cdots$ S hydrogen bond and  $\pi$ - $\pi$  stacking. The SAPT analysis indicates that the dispersion contribution significantly increases by nearly 30% due to the introduction of the phenyl group, in comparison to the H<sub>2</sub>S-H<sub>2</sub>O. Interestingly, replacing an O atom with an S atom, e.g., from the PN-PN to the PN-TPN, notably changes both the electrostatic and dispersion contributions: the electrostatic contribution decreases by approximately 15%, while the dispersion contribution increases by nearly 10%. Dispersion contributions were found to be the dominant interaction in both PN-TPN and TPN-TPN. This chapter thus satisfactorily explored the extent to which the phenyl group contributes to NCIs in PN-PN, TPN-TPN, and PN-TPN, and highlights the effect of different substituents (S-H or O-H groups) on the phenyl group role in establishing NCIs.

## Chapter 3. The 1-Naphthol - 1-Naphthalenethiol Heterodimer

In Chapter 2, we investigated the intermolecular interactions between the simplest monosubstituted aromatic alcohol and thiol molecules, namely the phenol-thiophenol dimer, observing the simultaneous presence of a O-H $\cdots$ S hydrogen bond and  $\pi$ - $\pi$  stacking interactions. In this chapter, we enlarged the size of the aromatic ring by going from a mono- to a bi-arene and studied the heterodimer formed between two naphthyl moieties substituted with an alcohol and thiol group, i. e., the 1-naphthol - 1-naphthalenethiol heterodimer. The experiment was conducted with high-resolution broadband rotational spectroscopy, supplemented with DFT computations. This study provides a comparative analysis with both the mono-arene heterodimers and the previously observed homodimers of naphthalene, 1-naphthol and 2-naphthalenethiol. We observed that the heterodimer of 1-naphthol and 1-naphthalenethiol is stabilized by a O-H $\cdots$ S hydrogen bond and  $\pi$ - $\pi$  stacking, unlike the dimers of 2-naphthalenethiol and 1-naphthol. We also observed that the dispersion contributions are significantly enhanced compared to the prototype non-aromatic mixed heterodimer of H<sub>2</sub>S-H<sub>2</sub>O.

### 3.1 Introduction

NCIs are essential forces in chemistry, and they play a critical role in molecular recognition, protein folding, biological activity, and material properties.<sup>1-4</sup>  $\pi$ - $\pi$  Stacking, denotes the intermolecular interactions when the  $\pi$  electron clouds are located in near-parallel arrangements, enhancing molecular stability.<sup>99,236,243</sup>  $\pi$ - $\pi$  Stacking interactions are not associated to an overlap of  $\pi$  electrons, but to dispersion forces established between the two rings.  $\pi$ - $\pi$  Stacking can affect the shape and structure of molecular systems, thereby altering their properties and functions.  $\pi$ - $\pi$  Stacking can compete or cooperate with other molecular interactions, particularly the hydrogen bond. The hydrogen bond is a special type of donor-acceptor NCI, formed when a proton acceptor atom (e.g. O, S, N, and F atoms, but also less electronegative atoms or  $\pi$  systems) and a proton donor (e.g. a H atom connected to a electronegative atom) are present.<sup>244</sup> Typically, hydrogen bonds are stronger than  $\pi$ - $\pi$  stacking, and govern the stability of molecules or molecular clusters by formation of intra or interatomic interactions.<sup>245,246</sup> When a cluster is formed between molecules containing aromatic rings or similar  $\pi$  electron systems, it is possible to modulate the strength of the hydrogen bonds challenging to examine when  $\pi$ - $\pi$  stacking or hydrogen bond plays the dominant role.

Rotational spectroscopy<sup>122-124,247</sup> is a technique enabling deep insight into NCIs and the role of these interactions in different molecular clusters. The presence and

strength of NCIs can be inferred by the structure of the targeted clusters and rationalized with the aid of quantum chemical calculations. Besides, rotational spectroscopy offers several advantages.<sup>119–121,247</sup> First, it allows for direct measurement of gas-phase molecules without the need for extensive sample preparation. Second, it enables precise detection due to its high sensitivity, frequency resolution and structural selectivity. However, the number of thiol-containing aromatic clusters is still small compared to alcohols, and most of them are stabilized by hydrogen bonding in a non-parallel ring configuration.<sup>21</sup> The only dimer showing coexistence of  $\pi$ - $\pi$  stacking and hydrogen bond interactions is the thiophenol dimer.<sup>33</sup> A few aromatic clusters are stabilized by  $\pi$ - $\pi$  stacking but they do not show hydrogen bonding. For example, the homodimer of 1-naphthol<sup>66</sup> and the two isomers of 2-naphthalenethiol dimer<sup>42</sup> all adopt a V-shaped configuration with a partially overlapping  $\pi$ - $\pi$  stacked arrangement, lacking hydrogen bonds between the subunits. For the naphthalene dimer there are no rotational data,<sup>248,249</sup> but its symmetric geometry is similar to the most stable isomer of the 2-naphthalenethiol dimer.<sup>42</sup> For this reason, an interesting point to us was to know whether it is possible to observe the coexistence of  $\pi$ - $\pi$  stacking and hydrogen bond on the compounds containing naphthyl groups combining an alcohol and a thiol.

Therefore, in this chapter we chose 1-naphthol (1NA) and 1-naphthalenethiol (1NT) as target molecules to investigate their potential intermolecular NCIs. Based on the presence and strength of NCIs in the heterodimer of 1NA - 1NT, the roles and effect of  $\pi$ - $\pi$  stacking and hydrogen bond in molecular structures will be better understood.

## 3.2 Experimental and Theoretical Methods

### 3.2.1 Experimental Methods

The samples of 1NA (99%) and 1NT (99%) were obtained commercially and did not require further purification. Equal amounts of 1NA and 1NT samples were mixed in two heating reservoirs with circular nozzles (diameter of 1.0 mm), where they were vaporized at 90 °C. The vapor samples were injected into the vacuum chamber by dilution with a carrier gas (Neon at 3 bar pressure). A broadband chirped-pulse FTMW spectrometer detailed in Chapter 1 was employed to probe the supersonic jet, covering the frequency range 2-8 GHz.<sup>195</sup> In this experiment, a 4  $\mu$ s chirped pulse generated by an Arbitrary Waveform Generator (AWG), was amplified to ca. 300 W by a Traveling-Wave Tube (TWT) amplifier, and radiated perpendicularly to the direction of jet expansion through a horn antenna. Subsequently, the transient molecular emission spanning 40  $\mu$ s was detected using a second horn antenna, recorded by a digital oscilloscope, and transformed into the frequency domain. The frequency measurement accuracy was better than 20 kHz.

### 3.2.2 Computational Methods

The experimental study required quantum chemical calculations to support the spectral assignment. Initially, the structures of the 1NA-1NT heterodimer were explored using semi-empirical calculations implemented in Grimme's CREST program.<sup>197</sup> All the initial structures were later optimized using the B3LYP<sup>215,216</sup> density functional method. The D3 empirical dispersion corrections and the Becke-Johnson (D3(BJ))<sup>220,221</sup> damping function were applied with the B3LYP functional. Then the vibrational frequency calculations (harmonic approximation) and basis set superposition errors corrections were calculated. All the calculations used the Ahlrichs' def2-TZVP basis set<sup>218,219</sup> and were implemented in the Gaussian 16<sup>202</sup> program. Energy decomposition was conducted with second-order symmetry-adapted perturbation theory (SAPT)<sup>211,212</sup> implemented in PSI4 software<sup>210</sup> at the SAPT2+(3)/aug-cc-pVDZ level.<sup>211,250,251</sup> The derived molecular wavefunctions were analysed with the Multiwfn program<sup>206</sup> to create NCIPlots which were visualized using the Visual Molecular Dynamic (VMD)<sup>213</sup> program.<sup>224,225</sup>

### 3.3 Results and Discussion

The B3LYP-D3(BJ)/def2-TZVP level of theory was employed to optimize all the 107 initial structures of the 1NA-1NT dimer initially obtained from CREST. Figure 3.1 illustrates the three most stable conformations along with their relative zero-point corrected energies. Table S3.1 of Appendix provides the top eleven stable structures with their corresponding rotational constants, dipole moments, relative energies, and binding energies. It is evident that all the heterodimers exhibit near-parallel structures. Furthermore, the first eleven most stable structures are stabilized through the cooperation of the O-H $\cdots$ S hydrogen bond and  $\pi$ - $\pi$  stacking. This observation not only highlights the importance of cooperative effects in the formation of these heterodimers but also the compatibility of hydrogen bonds and  $\pi$ - $\pi$  stacking in monosubstituted bi-arenes, in contrast with previous observations.

Despite the eleven lowest-lying structures possess the same type of NCIs, there are notorious differences in the orientation of the S-H and O-H groups, as well as in the relative positions between the two naphthyl rings. The relative positions of the dimer subunits can be summarized as follows: 1) The hydrogen atoms in the S-H and O-H groups may adopt either *cis* or *trans* monomer conformations, as observed in the dimer of 2-naphthalenethiol, giving rise to four different (*cis-cis*, *cis-trans*, etc) combinations in the dimer. 2) The two naphthyl rings are arranged in a parallel-displaced or, occasionally, in a T-shape configuration. In the global minimum (isomer I) the two naphthyl rings overlap over the central ring, and the dimer adopts a configuration similar to the  $C_2$  symmetric geometry observed in the dimers of 2-naphthalenethiol<sup>42</sup> and naphthalene.<sup>248,249</sup> Obviously in this case the different

substituents prevent any symmetry in the dimer, unlike in naphthlanethiol and naphthalene. In isomer I both the alcohol and thiol are *trans*, with an antiparallel orientation of the two polar groups. Isomers II and III are only 0.3 kJ mol<sup>-1</sup> and 0.5 kJ mol<sup>-1</sup> higher than isomer I, respectively, and show larger overlap between the two rings. However, none of these geometries are similar to those previously observed in the 2-naphthlanethiol and naphthalene dimers. In isomers II and III, the hydrogen atoms in the S-H and O-H groups are always *trans*, but with a collinear orientation of the two polar groups. In isomer II the naphthol ring essentially overlaps with one of the rings of 2-naphthlanethiol. Conversely, isomer III presents a parallel displaced shape between the two naphthyl rings, maximizing ring overlap. In terms of binding energy, isomer VIII has the largest binding energy, but its relative energy is only 1.6 kJ mol<sup>-1</sup> larger than the global minimum isomer I. Additionally, some conformations present a set of very close rotational constants, as found between isomer I and isomer V. Fortunately, there is a significant difference in their dipole moments and centrifugal distortion constants, which aids in distinguishing the assigned isomer.

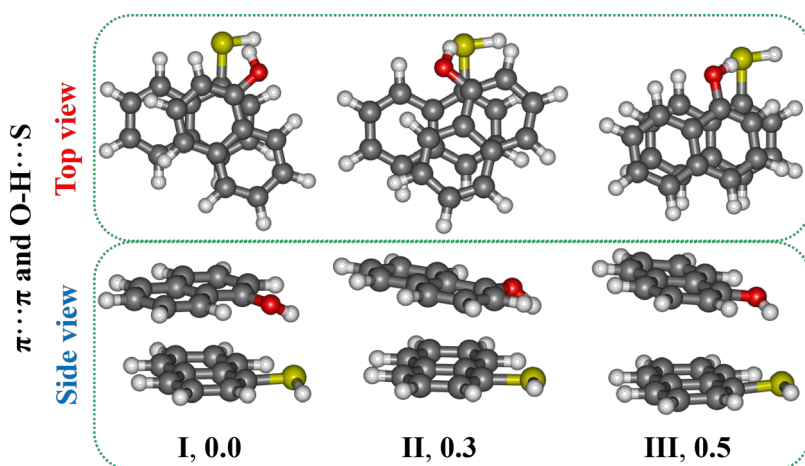


**Figure 3.1** The structures of the three most stable isomers of the 1NA-1NT heterodimer at the B3LYP-D3(BJ)/def2-TZVP level of theory, with top and side views. The three most stable isomers share a O-H $\cdots$ S hydrogen bond. 1NT is presented at the bottom for all structures. The relative zero-point corrected energies are provided in black (kJ mol<sup>-1</sup>).

The experiment on the 1NA-1NT heterodimer was conducted using only Neon as carrier gas. In these conditions only one isomer was identified in the spectrum. A section of the rotational spectrum in Figure 3.2 displays a  $\mu_b$ - $\mu_c$  quartet and a typical  $\mu_a$  transition, which are accompanied by the rotational spectra of the homodimers of 1NA and 1NT. The spectral assignment started with the fitting of experimental rotational constants, followed by iterative fitting of centrifugal distortion constants.

The rotational transitions were fitted using the Watson ( $S$ -reduced) semirigid rotor Hamiltonian<sup>186</sup> in its  $F$  representation, and the spectral parameters are listed in Table 3.1. The experimental parameters match the predictions for isomer I, confirming the detection of the global minimum. The theoretical centrifugal distortion constants are in good agreement with the experimental values. The measured transition lines are presented in Table S3.2 (see Appendix).

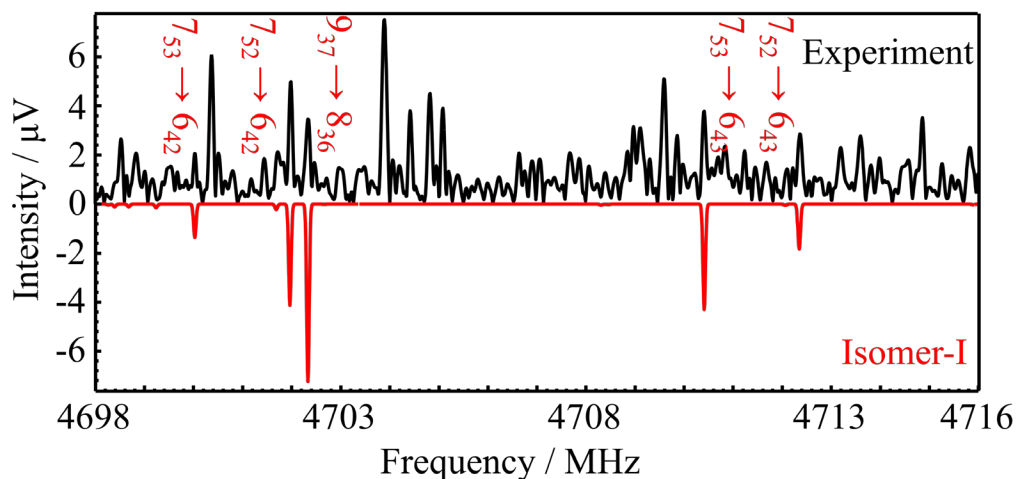


**Figure 3.2** A section of the rotational spectra of the 1NA-1NT cluster in the range of 4698-4716 MHz (upper panel). The upper trace shows the experimental spectrum in pure Ne (in black). The lower trace (in red) is the spectral simulation using the experimental rotational constants of isomer I of the 1NA-1NT cluster in Table 3.1. This spectral section includes a  $\mu_b$ - $\mu_c$  quartet suggesting a larger dipole moment component for  $\mu_c$ , as predicted.

The NCIs stabilizing the observed isomer of isomer I-*trans-trans* of the 1NA-1NT cluster were studied by employing the NCI analysis, based on Johnson's reduced electronic density gradient (RDG). The NCIs in the observed isomer of the 1NA-1NT cluster are shown in Figure 3.3 and exhibit some differences but also similarities with those observed in the PN-TPN heterodimer in Chapter 2 and the dimers of 2-naphthalenethiol.<sup>42</sup> As the color code indicates, there are no areas of strong attractive interactions (represented by blue regions), while wide green regions denote extended weak interactions between the two rings. It should be noted that the regions around the alcohol and thiol groups also appear associated to weak interactions and not apparently different from  $\pi$ - $\pi$  stacking. The plot of the RDG in Figure 3.3 further supports the presence of weak interactions including the O-H $\cdots$ S hydrogen bond and

the  $\pi$ - $\pi$  stacking in isomer I. Comparative representations for the dimers of naphthalene, 1-naphthol and 2-naphthalenethiol are found in references.<sup>42,66,248,249</sup>

**Table 3.1** Experimental rotational parameters for the observed isomer of 1NA-1NT heterodimer, and comparison with the theoretical values at the B3LYP-D3(BJ)/def2-TZVP level of theory.

Parameter <sup>a</sup>	Experimental	Theoretical		
		I- <i>trans-trans</i>	II- <i>trans-trans</i>	III- <i>trans-trans</i>
$A$ / MHz	376.55617(51) <sup>b</sup>	381.7	359.0	441.1
$B$ / MHz	282.51480(27)	288.7	318.4	247.0
$C$ / MHz	241.94596(32)	245.3	238.2	239.0
$D_J$ / kHz	0.0276(13)	0.0216	0.0303	0.0159
$D_K$ / kHz	0.0412(68)	0.0304	0.0268	0.0268
$D_{JK}$ / kHz	-0.0344(63)	-0.0268	-0.0311	-0.00303
$d_1$ / kHz	[-0.00147] <sup>c</sup>	-0.00147	0.00309	0.00116
$d_2$ / kHz	[0.000119]	0.000119	-0.00296	0.000796
$N$	205	-	-	-
$\sigma$ / kHz	12.7	-	-	-
$ \mu_a $ / D	yes	0.8	0.0	1.4
$ \mu_b $ / D	yes	0.4	0.5	1.3
$ \mu_c $ / D	yes	0.7	1.4	0.2
$\Delta E_0$ / kJ mol <sup>-1</sup>	-	0.0	0.3	0.5

<sup>a</sup>Rotational constants ( $A$ ,  $B$ ,  $C$ ), Watson's  $S$ -reduction centrifugal distortion constants ( $D_J$ ,  $D_{JK}$ ,  $D_K$ ,  $d_1$ ,  $d_2$ ), electric dipole moments ( $\mu_\alpha$ ,  $\alpha = a, b, c$ ), number of transitions ( $N$ ) included in the fits, root-mean-square deviation of the fit ( $\sigma$ ), relative electronic energies with the zero-point energy correction ( $\Delta E_0$ ). <sup>b</sup>Values in parentheses are standard errors in units of the last digit. <sup>c</sup>Values in brackets were fixed to their theoretical values.

Table 3.2 shows the result of the SAPT-based binding energy decomposition for the H<sub>2</sub>S-H<sub>2</sub>O, PN-TPN, 1NA-1NA, 2NT-2NT and 1NA-1NT dimers. Figure 3.4 illustrates the variation in the attractive contributions for each observed isomer. The results show that the total binding energy of 1NA-1NT is the largest (-50.3 kJ mol<sup>-1</sup>) among these isomers, and very close to that of the 1NA-1NA (-50.1 kJ mol<sup>-1</sup>) and the 2NT-2NT (-49.3 kJ mol<sup>-1</sup>) dimers. The additional O-H $\cdots$ S hydrogen bond in 1NA-1NT increases the electrostatic contribution to 29.4%, while decreases the dispersion contribution to 60.9%, and the induction contribution rises to 9.7%. Compared to the two isomers of PN-TPN, the electrostatic contribution in 1NA-1NT decreases, while the dispersion contribution increases. Moreover, this enhancement in dispersion leads to an increase in the total binding energy by approximately 20 kJ mol<sup>-1</sup> in 1NA-1NT. Considering H<sub>2</sub>S-H<sub>2</sub>O, the total binding energy and the dispersion contribution in 1NA-1NT are significantly larger due to the larger molecular size and  $\pi$ - $\pi$  stacking interactions.

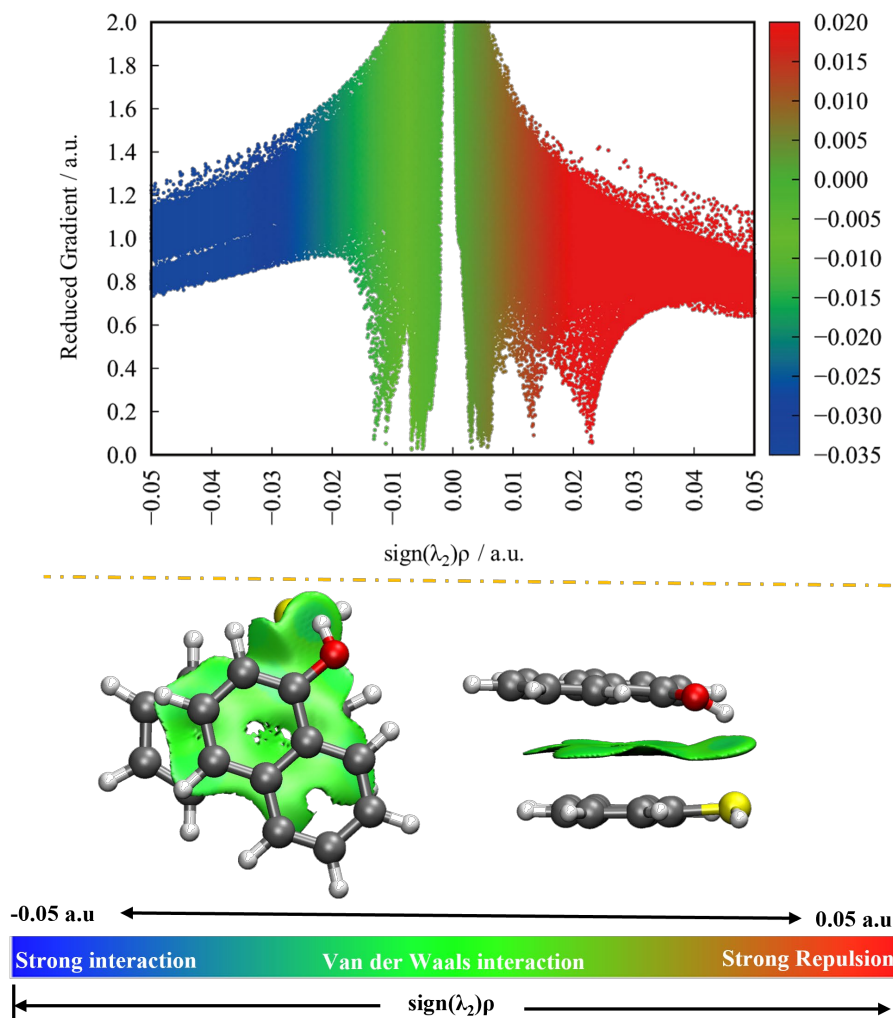


**Figure 3.3** Upper panel: Reduced electronic density gradient (RDG) Plot for isomer I of 1NA-1NT cluster. Below panel: Non-covalent interaction (NCI) Plot for isomer I of 1NA-1NT cluster. The cut-off value for the isosurface was established at 0.5 a.u. The interactions characterized as attractive or repulsive are determined by the product of electron density and the second Hessian eigenvalue [ $\text{sign}(\lambda_2)\rho$ ], within a range of -0.05 to 0.05 a.u. In this context,  $\lambda_2$  denotes the second eigenvalue of the electron density Hessian, and  $\rho$  represents the electron density. On the color scale below, deep blue shows strong attractive interactions, green indicates weaker van der Waals interactions, and red highlights strong repulsive interactions.

The overall trend for the energy decomposition shows that from H<sub>2</sub>S-H<sub>2</sub>O to PN-TPN and then to 1NA-1NT, the total binding energy increases significantly (413.2%). However, the dispersion contribution increases by only 27.6% (PN-TPN-I compared to H<sub>2</sub>S-H<sub>2</sub>O)/28.4% (PN-TPN-II compared to H<sub>2</sub>S-H<sub>2</sub>O), and by 12.6% (1NA-1NT compared to PN-TPN-I)/11.8% (1NA-1NT compared to PN-TPN-II), respectively.

These indicate that the  $\pi$ - $\pi$  stacking plays a vital role in the stability of aromatic dimer or similar dimer and contributes more to the dimer of naphthyl-based molecular clusters than to the dimer of phenyl-based molecular clusters. Additionally, the electrostatic contribution in 1NA-1NT decreases by only 6.8% and 5.9%, compared to PN-TPN-I, and PN-TPN-II, respectively.

**Table 3.2** The results of the SAPT (SAPT2+3(CCD)/aug-cc-pVDZ) binding energy decomposition for H<sub>2</sub>S-H<sub>2</sub>O, PN-TPN, 1NA-1NA, 2NT-2NT and 1NA-1NT dimers comparing the magnitude of the electrostatic, dispersion and induction contributions (all values in kJ mol<sup>-1</sup>).

Molecules	SAPT energy decomposition				
	$\Delta E_{\text{Electrostatic}}$	$\Delta E_{\text{Dispersion}}$	$\Delta E_{\text{Induction}}$	$\Delta E_{\text{Exchange}}$	$\Delta E_{\text{Total}}$
H <sub>2</sub> S-H <sub>2</sub> O	-20.0(59.2%)	-7.0(20.7%)	-6.8(20.1%)	24.0	-9.8
PN-TPN	I -29.6(36.2%)	-39.5(48.3%)	-12.6(15.4%)	50.3	-31.5
	II -28.1(35.3%)	-39.0(49.1%)	-12.4(15.6%)	49.5	-30.0
1NA-1NA	-30.4(27.8%)	-68.5(62.8%)	-10.3(9.4%)	73.1	-36.1
2NT-2NT	I -29.6(26.6%)	-74.2(66.7%)	-7.4(6.7%)	61.1	-50.1
	II -29.0(26.0%)	-75.6(67.7%)	-7.1(6.3%)	62.4	-49.3
1NA-1NT	-35.9 (29.4%)	-74.4 (60.9%)	-11.8 (9.7%)	71.8	-50.3

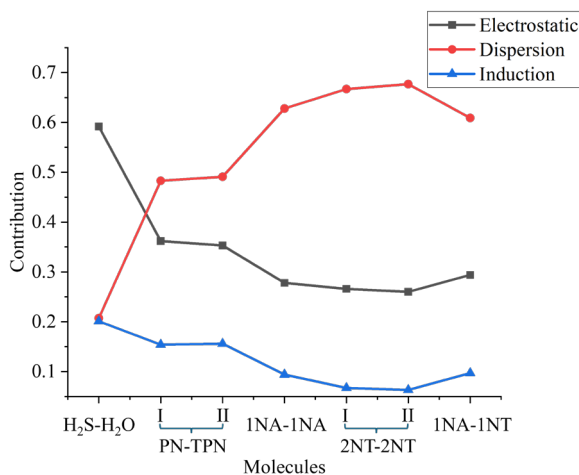


**Figure 3.4** The line chart illustrates the decomposition of binding energy (including only the attractive components) for the interactions in H<sub>2</sub>S-H<sub>2</sub>O, PN-TPN, 1NA-1NA, 2NT-2NT and 1NA-1NT dimers. The detailed results are given in **Table 3.2**.

### 3.4 Conclusions

In this chapter we employed high-resolution broadband CP-FTMW spectroscopy to characterize the conformational landscape of the 1NA-1NT heterodimer in a supersonic jet expansion. Based on the experimental observation of a single isomer for this dimer, we further conducted NCI analysis and SAPT energy decomposition calculations. These data offered an accurate description of the electronic and structural properties of the observed isomer of 1NA-1NT cluster. Unlike the observed isomer of 1NA-1NA and 2NT-2NT clusters, which are stabilized solely by  $\pi$ - $\pi$  stacking, the O-H $\cdots$ S hydrogen bond and  $\pi$ - $\pi$  stacking synergically stabilizes the 1NA-1NT dimer. The non-observation of a hydrogen bond in the 1NA-1NA homodimer is however surprising, considering the larger interaction strength of this hydrogen bond. A plausible explanation could be related to a failed observation of a second dimer in the 1NA-1NA homodimer, which should require further experimental work on that system. This study contributes to a deeper understanding of the balance between the O-H $\cdots$ S hydrogen bond and  $\pi$ - $\pi$  stacking. Although both the 1NA-1NT and PN-TPN dimers are stabilized by the synergic effect of O-H $\cdots$ S hydrogen bond and  $\pi$ - $\pi$  stacking, the SAPT analysis reveals significant differences. In the 1NA-1NT, the contribution of dispersion is 11.8% higher than in PN-TPN, while the contribution of electrostatic is correspondingly reduced by 4.1%, proving the dominant role of  $\pi$ - $\pi$  stacking is larger in 1NA-1NT than in aromatic-based dimer. Additionally, compared PN-TPN to H<sub>2</sub>S-H<sub>2</sub>O or 1NA-1NT to H<sub>2</sub>S-H<sub>2</sub>O,  $\pi$ - $\pi$  stacking in 1NA-1NT involving naphthyl ring contributes more to the stability of system contained phenyl ring.



## Chapter 4. The 2-Naphthol - 2-Naphthalenethiol Heterodimer

In chapter 2, we investigated the intermolecular interactions between the simplest monoarenes substituted with an alcohol and a thiol group, observing the coexistence of an O-H $\cdots$ S hydrogen bond and  $\pi$ - $\pi$  stacking, previously observed only for the thiophenol dimer. In chapter 3, with the introduction of a second phenyl ring in the  $\pi$ -system, we explored the possible changes affecting the balance of NCIs in the 1-naphthol - 1-naphthalenethiol complex, which *a priori* should favor the  $\pi$ - $\pi$  stacking interactions and might reduce the role of the hydrogen bond. Following the observation that this heterodimer is similarly stabilized by a combination of O-H $\cdots$ S and  $\pi$ - $\pi$  stacking interactions, we further study in this chapter the NCIs in the heterodimer formed by 2-naphthol and 2-naphthalenethiol, changing the position of the substituents with respect to Chapter 3. Supported by quantum chemical calculations and high-resolution rotational spectroscopy, we thus examined the balance between the O-H $\cdots$ S hydrogen bond and  $\pi$ - $\pi$  stacking interactions as the functional substitution is placed in a different position. The results indicate that the dimer adopts a different geometry, but the total binding energy and attractive contributions of the system do not exhibit significant changes compared to the 1-naphthol - 1-naphthalenethiol complex.

### 4.1 Introduction

Due to its high frequency resolution and sensitivity, microwave spectroscopy is considered one of the most powerful tools for studying weak intermolecular interactions in the gas phase.<sup>30,247</sup> This structural sensitivity is particularly useful in presence of weak competing interactions, as those involving  $\pi$ - $\pi$  stacking. Moreover, the aggregation process is normally accompanied by cooperative arrangements of different interactions to maximize molecular stability, as observed in the coexistence of the  $\pi$ - $\pi$  stacking and hydrogen bonds in chapters 2 and 3. In these systems,  $\pi$ - $\pi$  stacking has proven to be a dominant interaction unaffected by the presence of the hydrogen bond, which usually acts as the primary interaction in intermolecular clusters. The study of additional intermolecular systems not only adds empirical data to the scarce set of gas phase investigations on sulfur-containing  $\pi$ - $\pi$  stacking interactions (i.e., the dimers of thiophenol,<sup>33</sup> 1-naphthol<sup>66</sup> and 2-naphthalenethiol<sup>42</sup>), but offers also the possibility of exploring the influence of the substitution positions of the different functional groups. In the case of the weak  $\pi$ - $\pi$  stacking between biarenes we may ask if the rings adopt preferred conformations or whether the ring alignment is affected by a change in the substituents position. We will prove that the appearance of the hydrogen bond depends on the orientations of the aromatic rings

and functional groups<sup>67</sup>, while the formation of  $\pi$ - $\pi$  stacking mainly affects the arrangement of rings, e.g. influences the position and distance between the rings.<sup>33,42,66</sup>

As it is well known, molecular properties depend on the internal and external chemical environments. For internal chemical environments, the position of substituents is the key factor affecting electron distributions, and it may influence the binding behavior of molecules, the molecular structure or the internal large amplitude movements. Currently, the rotational studies exploring the influence of the substituents position have mainly focused on structural aspects or the variation of the internal rotation barriers of simple prototype molecules like furan, thiophene, pyrrole, thiazole, benzene and toluene.<sup>252,253</sup> The effect of the substituent position on  $\pi$ - $\pi$  stacking intermolecular interactions of aromatic clusters remains practically unexplored, justifying additional investigations involving polycyclic aromatic molecules.

In this study we extend the investigations of previous chapters using the heterodimer of 2-naphthol and 2-naphthalenethiol as molecular target. The experiment will prove whether the synergic effect between the O-H $\cdots$ S and  $\pi$ - $\pi$  stacking is maintained and what changes are induced by new substituent positions. The experiment was carried out using broadband chirped-pulse Fourier transform microwave (CP-FTMW) spectroscopy, aided by quantum chemical calculations. This work advances the understanding of the effect of the position of substituents on NCIs, offering valuable insights for the design of molecular materials and catalysts of sulfur-containing molecules, where precise control of these interactions is crucial.

## 4.2 Experimental and Theoretical Methods

### 4.2.1 Experimental Methods

An equal amount of 2-naphthol (2NA) and 2-naphthalenethiol (2NT) was mixed and placed in two separated heating injectors, both including circular exit nozzles (diameter of 1.0 mm). The samples are commercially available and did not require purification. The injectors were heated to 115°C to facilitate vaporization, using a flow of Ne as carrier gas to produce a jet expansion in the vacuum chamber. The carrier gas pressure was maintained at ca. 3 bar. The rotational spectrum of the supersonic jet containing 2NA and 2NT was collected using a CP-FTMW spectrometer<sup>196</sup> in the 2-8 GHz frequency range, described before.<sup>195</sup> This experiment involved generating chirped pulses (4  $\mu$ s duration) with a digital arbitrary wave generator, which were then amplified by a TWT amplifier (300 W) and emitted perpendicularly to the jet. The chirped pulse induces a rapid 2-8 GHz transient excitation of the polar compounds in the cooled supersonic jet. After transient

excitation, the molecules or clusters emit a free induction decay (FID), which is finally detected in the time domain ( $\sim 40 \mu\text{s}$ ) and recorded using a digital oscilloscope (sampling rate of 25 GSamples/s). A Fourier transformation yields linewidths of approximately 100 kHz. For this experiment, around 3.6 million averages were accumulated at a 5 Hz repetition rate, with an estimated frequency measurement uncertainty of less than 20 kHz. All radiation sources are locked to a Rb crystal standard.

## 4.2.2 Computational Methods

To help the assignment of the possible isomer species and obtain their experimental spectroscopic parameters, we first performed a conformational search for all possible structures of the 2NA-2NT heterodimer using the Grimme's CREST program.<sup>197</sup> Subsequently, all potential initial structures were optimized with the B3LYP-D3(BJ)/def2-TZVP level of theory,<sup>215,216,220,221</sup> implemented in Gaussian 16. Vibrational frequency calculations (harmonic approximation) and complexation energies were later carried out. The theoretical results for the first ten isomers are listed in Table S4.1 in the Appendix. To get a molecular insights on the NCIs in the 2NP-2NT cluster, we conducted a NCI analysis based on Johnson's reduced density gradient, using the Multiwfn program.<sup>206</sup> The results were visualized with the Visual Molecular Dynamics (VMD)<sup>213</sup> software.<sup>224,225</sup> Additionally, an energy decomposition analysis of the 2NA-2NT cluster was conducted to investigate the nature of the interactions and estimate their relative contributions, based on second-order symmetry-adapted perturbation theory (SAPT)<sup>211,212</sup> at the SAPT2+(3)/aug-cc-pVDZ level.<sup>211,250,251</sup> SAPT was implemented in the PSI4 software<sup>210</sup>.

## 4.3 Results and Discussion

In this chapter, 90 initial structures of the 2NA-2NT cluster obtained from the CREST conformational search were reoptimized at the B3LYP-D3(BJ)/def2-TZVP level of theory. Figure 4.1 presents the first three most stable isomers with their zero-point energy (ZPE)-corrected relative energies. Besides, Table S4.1 in the Appendix provides the detailed information on all optimized stable structures, particularly the first ten most stable isomers, including their rotational constants, dipole moments, relative energies (with ZPE corrections), and binding energies. All the lowest-lying structures of the 2NA-2NT cluster exhibit near-parallel arrangements. The stability of the first five most stable isomers is controlled by both an O-H $\cdots$ S hydrogen bond and  $\pi$ - $\pi$  stacking interactions. However, in the subsequent five higher energy isomers the O-H $\cdots$ S hydrogen bond is absent (except for isomer VII) with the stability primarily relying on independent  $\pi$ - $\pi$  stacking. In summary, the NCIs in these isomers can be classified into two categories: those involving a synergic effect of the O-H $\cdots$ S hydrogen bond and  $\pi$ - $\pi$  stacking, and those solely governed by  $\pi$ - $\pi$  stacking.

Furthermore, even among isomers stabilized by the same type of NCIs, there are differences in the orientations of the S-H and O-H groups (*cis-cis*, *cis-trans*, etc) and the relative positions of the two naphthyl rings, similarly to 1NA-1NT (See chapter 3 section 3.3). In the global minimum the polar groups are *cis-cis* and present an antiparallel orientation, with the two naphthyl groups rotated ca.  $60^\circ$ . In isomer II-*cis-trans* the two naphthyl groups are aligned near-parallel and the ring overlap is reduced. Finally, the structure of isomer III-*cis-cis* presents ring overlapping over one of the rings in each monomer, somehow resembling the most stable structure of the homodimer of 2-naphthalenethiol. Regarding binding energy, isomers I, II, III are relatively similar, implying that the intermolecular interaction strengths associated with isomers I, II, and III are highly comparable. However, concerning the electronic energies isomers II and III are still ca.  $1.2 \text{ kJ mol}^{-1}$  and  $1.3 \text{ kJ mol}^{-1}$ , respectively, less stable than isomer I.

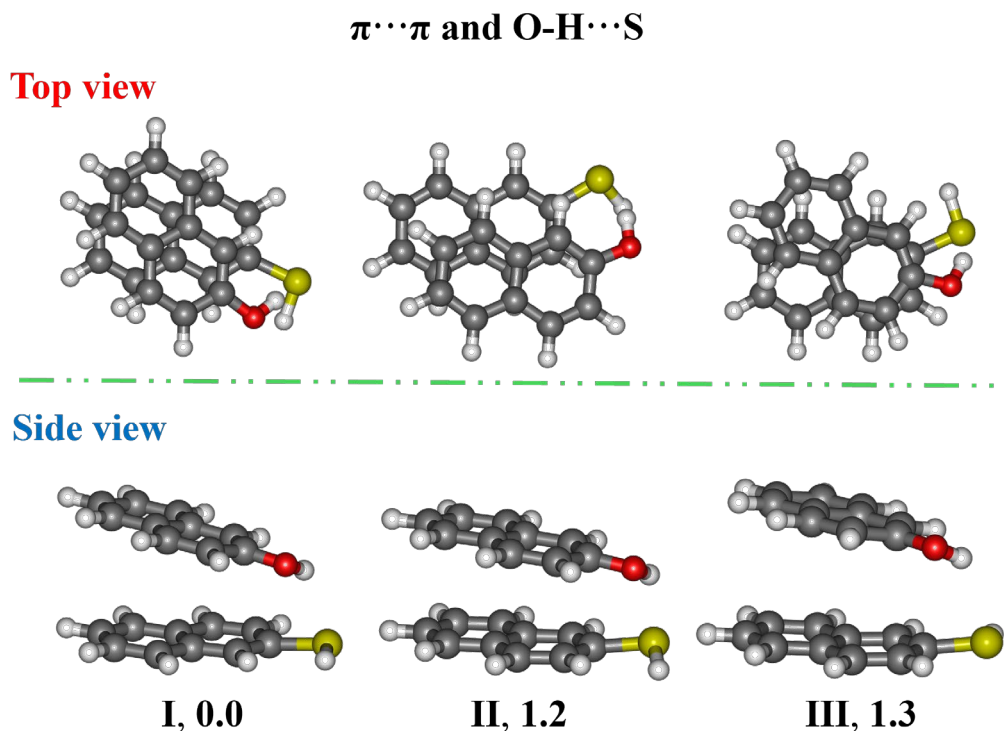


**Figure 4.1** The top and side views of the first three most stable isomers of the 2NA-2NT cluster, optimized at the B3LYP-D3(BJ)/def2-TZVP level of theory. In all structures, 2NT is positioned at the bottom. The relative zero-point corrected energy values, displayed in black, are given in  $\text{kJ mol}^{-1}$ .

In terms of the predicted spectroscopic parameters, the rotational constants of isomers I, III, and IV are very similar, making it challenging to distinguish between these isomers based only on their rotational constants. However, by further comparing their dipole moments and centrifugal distortion constants, we were able to provide an accurate isomer identification. We assigned in the spectrum a single isomer. Figure 4.2 shows a quartet with the rotational transitions first assigned to isomer I, including both the  $a$ -type and  $b$ -type transitions. The spectral assignment was performed by initially fitting the experimental rotational constants based on several rotational transitions with lower  $K_a$ , then progressively introducing centrifugal distortion constants after adding more transitions with higher  $K_a$ . The Watson ( $S$ -reduced) semi-rigid rotor Hamiltonian was employed, and the experimental spectroscopic parameters of isomer I are listed in Table 4.1, where also given the theoretical parameters of isomers I, II and III for comparison. The comparison with the predictions undoubtedly identified the experimentally observed spectrum to the global minimum isomer I. Apart from the good agreement between the experiment and the predicted rotational constants, the centrifugal distortion parameters correctly match with theoretical values of isomer I. All the observed transitions corresponding to isomer I are presented in Table S4.2 (see Appendix).

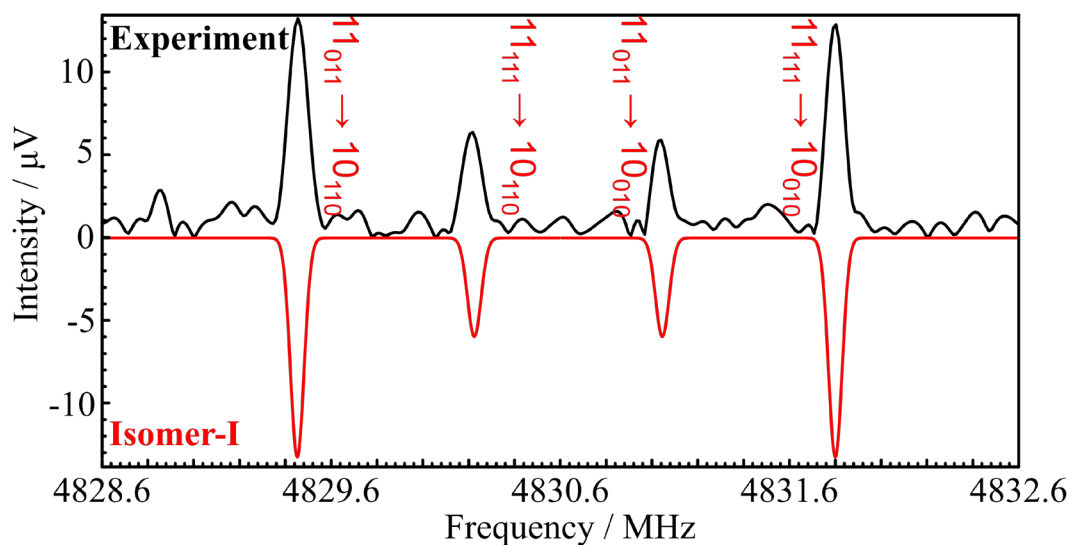


**Figure 4.2.** A section of the rotational spectrum for the 2NA-2NT heterodimer, covering the range from 4828.6 MHz to 4832.6 MHz, is displayed in the upper panel. The top trace (in black) presents the experimental spectra recorded in pure Ne, while the bottom trace (in red) shows the simulated spectrum based on the experimental rotational constants of isomer I. This region of the spectrum includes both  $a$ -type and  $b$ -type transitions, suggesting a larger value of  $\mu_b$  compared to  $\mu_a$ , as predicted.

**Table 4.1** The experimental spectroscopic parameters for the observed isomer of the 2NA-2NT heterodimer, compared with the theoretical values predicted at the B3LYP-D3(BJ)/def2-TZVP level of theory.

Parameter <sup>a</sup>	Experimental	Theoretical		
		I- <i>cis-cis</i>	II- <i>cis-trans</i>	III- <i>cis-cis</i>
<i>A</i> / MHz	404.32218(56) <sup>b</sup>	413.8	363.0	403.9
<i>B</i> / MHz	247.60144(19)	250.9	292.7	258.2
<i>C</i> / MHz	216.06427(21)	221.0	196.7	220.2
<i>D</i> <sub>J</sub> / kHz	0.02070(73)	0.0176	0.0951	0.0182
<i>D</i> <sub>K</sub> / kHz	-0.0409(38)	0.112	0.0754	0.141
<i>D</i> <sub>JK</sub> / kHz	0.1517(60)	-0.0283	-0.164	-0.0352
<i>d</i> <sub>1</sub> / kHz	[0.000657]	0.000657	-0.0149	-0.00440
<i>d</i> <sub>2</sub> / kHz	[0.000239]	0.000239	0.0284	-0.000203
<i>N</i>	187	-	-	-
$\sigma$ / kHz	7.0	-	-	-
$ \mu_a $ / D	yes	0.5	1.2	0.7
$ \mu_b $ / D	yes	1.1	0.9	0.7
$ \mu_c $ / D	no	0.1	0.7	1.1
$\Delta E_0$ / kJ mol <sup>-1</sup>	-	0.0	1.2	1.3

<sup>a</sup>Rotational constants (*A*, *B*, *C*), Watson's *S*-reduction centrifugal distortion constants (*D*<sub>J</sub>, *D*<sub>JK</sub>, *D*<sub>K</sub>, *d*<sub>1</sub>, *d*<sub>2</sub>), electric dipole moments ( $\mu_\alpha$ ,  $\alpha = a, b, c$ ), number of transitions (*N*) to in the fits, root-mean-square deviation of the fits ( $\sigma$ ), the relative electronic energies including the zero-point relative energies ( $\Delta E_0$ ). <sup>b</sup>Values in parentheses are standard errors in units of the last digit. <sup>c</sup>Values in brackets are fixed to their theoretical ones.

Subsequently, to confirm and visually represent the NCIs in isomer I, a NCI analysis was performed, as shown in Figure 4.3. The NCIPlot shows both a top-down view along with a side view, presented below. Evidently, the NCIs in the 2NA-2NT cluster resemble those in the PN-TPN and 1NA-1NT clusters, indicating the formation of the same types of weak extended interactions between the two rings. The color scale represents the interaction strengths, with no blue regions which could represent strong attractive interactions, a large green area indicating weak interactions, and red regions corresponding to repulsive interactions. The results are qualitatively in agreement with the presence of the weak O-H $\cdots$ S hydrogen bond and supporting  $\pi$ - $\pi$  stacking interactions. In the Reduced Electronic Density Gradient (RDG) Plot shown in the same Figure, the green regions correspond to the NCIs displayed in the NCIPlot, proving that the stability of isomer I primarily arises from very weak interactions. A minimum signal located around -0.01 a.u could imply the presence of the O-H $\cdots$ S hydrogen bond, while other signals in between -0.01 a.u and 0.00 a.u, suggest  $\pi$ - $\pi$  stacking.

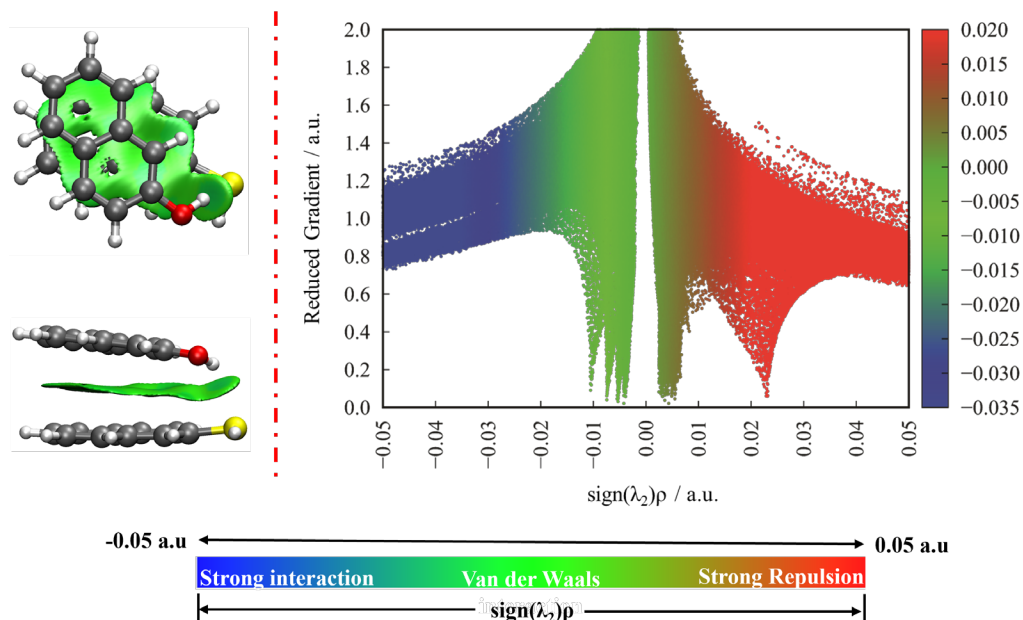


**Figure 4.3** Left panel: The Non-Covalent Interaction (NCI) Plot with different views for the same isomer I of the 2NA-2NT cluster. The isosurface cutoff value was set at 0.5. The classification of interactions as either attractive or repulsive is based on the product of the electron density ( $\rho$ ) and the second Hessian eigenvalue [ $\text{sign}(\lambda_2)\rho$ ], within the range of -0.05 to 0.05 a.u. Here,  $\lambda_2$  represents the second eigenvalue of the electron density Hessian, and  $\rho$  represents the electron density.

Table 4.2 includes the binding energy decomposition results for the dimers of  $\text{H}_2\text{S}-\text{H}_2\text{O}$ , PN-TPN, 1NA-1NA, 2NT-2NT, 1NA-1NT, and 2NA-2NT, based on SAPT. Figure 4.4 displays a radar plot focusing on the attractive energetic contributions of these systems. Compared with  $\text{H}_2\text{S}-\text{H}_2\text{O}$ , the  $\pi$ - $\pi$  stacking in 2NA-2NT significantly enhances the dispersion contribution (Table 4.2), confirming that the introduction of a phenyl group and associated  $\pi$ - $\pi$  stacking will provide more dispersion contribution. Similarly, compared to PN-TPN, the introduction of a phenyl group in 2NA-2NT increases the dispersion contribution, leading to an overall increase in the total binding energy. These phenomena are similar to the trend of the changes in 1NA-1NT. Besides, it can be discovered that the electrostatic contribution in 2NA-2NT is increased by  $\sim 2\%$ , while the dispersion contribution is reduced by  $\sim 5\%$  compared to 2NT-2NT, further indicating that O-H group is easier to involve in the formation of electrostatic force. Additionally, the results show that the total binding energy and attractive contributions of 1NA-1NT and 2NA-2NT are very similar, suggesting that the position of the substituent does not significantly affect the nature of O-H $\cdots$ S hydrogen bond and  $\pi$ - $\pi$  stacking: the contribution of dispersion increases by  $\sim 2\%$  only, the electrostatic contribution even decreases by solely  $\sim 1\%$ .

**Table 4.2** The binding energy decomposition results using Symmetry Adapted Perturbation Theory (SAPT2+3(CCD)/aug-cc-pVDZ) for H<sub>2</sub>S-H<sub>2</sub>O, PN-TPN, 1NA-1NA, 2NT-2NT dimer, 1NA-1NT, and 2NA-2NT (all values in kJ mol<sup>-1</sup>).

Molecules	SAPT energy decomposition					
	$\Delta E_{\text{Electrostatic}}$	$\Delta E_{\text{Dispersion}}$	$\Delta E_{\text{Induction}}$	$\Delta E_{\text{Exchange}}$	$\Delta E_{\text{Total}}$	
H <sub>2</sub> S-H <sub>2</sub> O	-20.0(59.2%)	-7.0(20.7%)	-6.8(20.1%)	24.0	-9.8	
PN-TPN	I	-29.6(36.2%)	-39.5(48.3%)	-12.6(15.4%)	50.3	-31.5
	II	-28.1(35.3%)	-39.0(49.1%)	-12.4(15.6%)	49.5	-30.0
1NA-1NA	-30.4(27.8%)	-68.5(62.8%)	-10.3(9.4%)	73.1	-36.1	
2NT-2NT	I	-29.6(26.6%)	-74.2(66.7%)	-7.4(6.7%)	61.1	-50.1
	II	-29.0(26.0%)	-75.6(67.7%)	-7.1(6.3%)	62.4	-49.3
1NA-1NT	-35.9 (29.4%)	-74.4 (60.9%)	-11.8 (9.7%)	71.8	-50.3	
2NA-2NT	-32.5(28.5%)	-70.9(62.1%)	-10.8(9.4%)	64.1	-50.1	

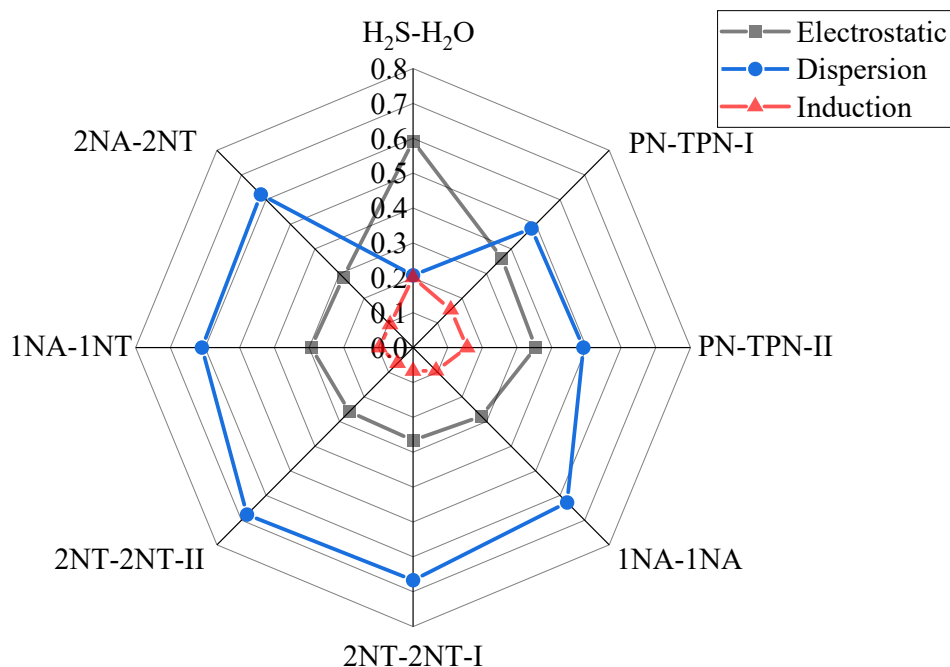


**Figure 4.4** The decomposition of binding energies (here, only the attractive components were taken into account) for the interactions between H<sub>2</sub>S-H<sub>2</sub>O, PN-TPN, 1NA-1NA, 2NT-2NT, 1NA-1NT, and 2NA-2NT, are presented in the radar chart. See **Table 4.3** for the detailed data.

## 4.4 Conclusions

In this chapter, high-resolution broadband FTMW spectroscopy was employed to characterize the conformational landscape in a cooled supersonic jet expansion of the heterodimers containing 2NA and 2NT. With the aid of quantum chemical calculation, we successfully identified and assigned the global minimum of 2NA-2NT cluster (namely isomer I). We further conducted an NCI analysis and SAPT energy decomposition calculations. The findings indicate that the dispersion contribution is significantly increased with the addition of more phenyl groups, thereby leading to an enhancement of the total binding energy. Nonetheless, the total binding energy and attractive contributions of 2NA-2NT are comparable to those of 1NA-1NT, suggesting that substituent position changes have little impact on the attractive contributions or total binding energy for structures stabilized through the synergic effect of O-H $\cdots$ S hydrogen bond and  $\pi$ - $\pi$  stacking.



## Chapter 5. The $\beta$ -Propiolactone - CO<sub>2</sub> Clusters

Chapters 5 and 6 will study the intermolecular interactions between aliphatic ketones and carbon dioxide. In chapter 5 we will first consider the interactions between  $\beta$ -propiolactone and carbon dioxide. The motivations for this study are both fundamental and applicative. From a fundamental point of view this study will contribute to establish the preferred aggregation patterns of carbon dioxide with this lactone, including up to three simultaneous carbon dioxide molecules. Specifically, we investigated the non-covalent interactions between  $\beta$ -propiolactone and (CO<sub>2</sub>)<sub>1-3</sub>, as well as those between the  $\beta$ -propiolactone dimer and (CO<sub>2</sub>)<sub>1-2</sub>. From an applicative point of view the intermolecular interactions of carbon dioxide may provide insight into the carbon dioxide capture processes and its association with organic compounds. Our study will include high resolution rotational spectroscopic results and computational calculations.

### 5.1 Introduction

The interest for molecular studies of CO<sub>2</sub> has expanded by rising concerns over global warming, which have encouraged extensive research focused on reducing CO<sub>2</sub> emissions and accumulation.<sup>254,255</sup> Among the various strategies being explored, CO<sub>2</sub> capture techniques have gained significant attention due to their potential to reduce atmospheric CO<sub>2</sub> levels.<sup>256-258</sup>

In fact, the underlying mechanisms of most CO<sub>2</sub> capture methods relate to its NCIs and chemical reactivity. The chemistry of CO<sub>2</sub> is characterized by its two oxygen atoms double bonded to a central carbon atom, resulting in locally anisotropic distributions of electronic density. In particular, an electrophilic region can be found at the C atom. For this reason, the formation of CO<sub>2</sub> clusters may proceed either by formation of hydrogen bonds or tetrel bonds. The tetrel or carbon bond<sup>136</sup> describes an attractive localized NCI occurring when an element from Group 14 (T = C, Si, Ge, etc) covalently bonded to a molecule behaves as electrophilic site for nucleophilic groups, leading to the formation of a bridged donor-acceptor R - T <sup>$\delta^+$</sup>  ... A <sup>$\delta^-$</sup>  interaction in the solid, liquid or gas phase. The nucleophilic groups may include electron lone pairs, pi-electron systems or anions in charged species. The definition of the tetrel bond is relatively recent<sup>259</sup> and followed that of the hydrogen bond<sup>71</sup> the chalcogen bond<sup>260</sup> and the pnictogen bond<sup>261</sup>. An illustration of the tetrel bond is shown in Figure 5.1.

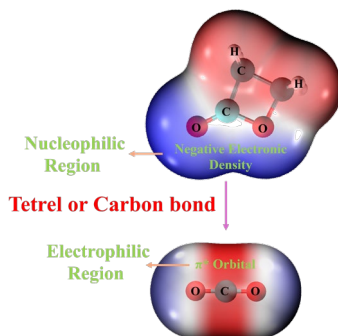


**Figure 5.1** An illustration of a tetrel NCI interaction in BPL $\cdots$ CO<sub>2</sub>.

The tetrel bonds may play a crucial role in the interaction between CO<sub>2</sub> and various partner molecules, including amines<sup>135,262</sup>, aldehydes,<sup>263</sup> ketones,<sup>134</sup> acids,<sup>264</sup> alcohols,<sup>265</sup> ethers,<sup>266</sup> and epoxides.<sup>133</sup> The optimal binding sites for tetrel bond formation between CO<sub>2</sub> and these molecules are determined by the electronegativity of the binding atom, leading to competitive interactions within a single molecule. For instance, in 2023, Xie *et al.*<sup>135</sup> found that as the number of CO<sub>2</sub> molecules increases, the interaction with the hydroxyl group in monoethanolamine is preferred with respect to the amino group, in sharp contrast to the results observed in the solution phase. Similarly, Gao *et al.*<sup>267</sup> observed that in two distinct isomers of the formamide-CO<sub>2</sub> cluster the C $\cdots$ O tetrel bond plays a dominant role in both isomers, accompanied by the formation of secondary bonds such as the N-H $\cdots$ O or C-H $\cdots$ O hydrogen bonds. In consequence the CO<sub>2</sub> clusters present the opportunity not only to observe the tetrel bond, but also to gauge the strength of the tetrel bond in comparison with other intermolecular interactions for specific numbers of aggregation patterns.

$\beta$ -Propiolactone (BPL), is a small four-membered cyclic carboxylic ester. BPL is involved in the reaction used to reduce the CO<sub>2</sub> emissions of the blast furnaces, suggesting a potential use in CO<sub>2</sub> capture.<sup>268</sup> Based on this, our study focuses on the investigation of the NCIs between BPL and CO<sub>2</sub> using rotational spectroscopy. The present study explored the binding preferences of BPL and the BPL dimer considering up to three CO<sub>2</sub> units, thus revealing the binding preferences and competition between the C $\cdots$ O and C $\cdots$ O=C tetrel bonds. The experiment was supported with quantum chemical calculations to gain insight into the binding process, the observed NCIs and the cluster structures. This research may provide new knowledge concerning CO<sub>2</sub> intermolecular interactions and eventually rationalizing the use of organic capture agents for CO<sub>2</sub>. This study is the first of several works initiated in our laboratory to explore the intermolecular interactions of CO<sub>2</sub>.

## 5.2 Experimental and Theoretical Methods

### 5.2.1 Experimental Methods

The commercial samples of BPL (purity 97%, boiling point 181.9°C) and CO<sub>2</sub> (purity ≥ 99%) were used without further purification. The rotational spectra were collected using a CP-FTMW spectrometer previously described in Chapter 1,<sup>195</sup> operating in the frequency range of 2-8 GHz. The clusters were prepared from gaseous CO<sub>2</sub> and a vaporized sample of liquid BPL. The CO<sub>2</sub> sample was prepared as a gas solution of CO<sub>2</sub>, diluted to a concentration of approximately 1% in a 1:1 Helium-Argon mixture (total pressure of 1 MPa). A pressure regulator was set to maintain the CO<sub>2</sub> backing pressure at 0.3 MPa. The liquid BPL samples were located in two separated heating injectors with circular exit nozzles ( $\phi = 1.0$  mm), where it was vaporized at a temperature of 40°C. The target molecules underwent supersonic expansion inside a high-vacuum chamber (with an ultimate pressure of 10<sup>-7</sup> mbar), forming a pulsed molecular jet. The time-domain transient excitation experiments recorded the free induction decay following the application of short (~ 40 μs) broadband chirped pulse excitation. Fourier transform processing then yielded the frequency-domain spectra. All frequency sources were referenced to a Rb crystal standard. The estimated uncertainty on the frequency measurements is less than 20 kHz.

### 5.2.2 Computational Methods

We employed several quantum chemistry methods to assist the spectral analysis. The conformational search was extended to the clusters of BPL-(CO<sub>2</sub>)<sub>1-3</sub> and (BPL)<sub>2</sub>-(CO<sub>2</sub>)<sub>0-3</sub>, using the CREST<sup>198</sup> software for automated exploration of the low-energy section of the Potential Energy Surface (PES). Comprehensive geometry optimizations and harmonic frequency calculations were then performed at the B3LYP-D3(BJ)/def2-TZVP level of theory to ensure an accurate description of the structural stability and NCIs. The Basis Set Superposition Error (BSSE)<sup>223</sup> was removed with the counterpoise method, and the interaction energies were calculated to examine the intermolecular interaction models. All computations were carried out employing Gaussian 16,<sup>202</sup> ensuring the accuracy and reliability of the results. The NCIs were analyzed in detail using the reduced gradient of the electron density,<sup>208,224</sup> providing a spatial understanding of the nature of NCIs. Further details are provided in Appendix (Tables S5.1-S5.7).

### 5.3 Results and Discussion

The spectral analysis was based on the structural predictions for the  $\text{BPL}-(\text{CO}_2)_{1-3}$  and  $(\text{BPL})_2-(\text{CO}_2)_{0-3}$  clusters, conducted at the B3LYP-D3(BJ)/def2-TZVP level of theory. The resulting molecular structures within an energy window of  $5 \text{ kJ mol}^{-1}$  are listed in Tables S5.1-S5.7 in the Appendix. The rotational spectrum was first processed by the BBA software to remove the transitions from the BPL monomer. The remaining spectrum in Figure 5.2 predominantly features transitions from the  $\text{BPL}-\text{CO}_2$  dimer, as expected. Based on the theoretical predictions, other species were successively investigated. For the  $\text{BPL}-(\text{CO}_2)_2$  trimer *a*-type rotational transitions were first assigned, followed by the addition of *c*-type transitions. Subsequently, some additional intense spectral signals were attributed to *c*-type transitions of the second stable isomer of  $(\text{BPL})_2$  cluster after further calculations and theoretical predictions. However, one of the BPL homodimers, denoted  $(\text{BPL})_2\text{-I}$ , was shown to contain a center of symmetry, so the electric dipole components in all three directions are zero and its observation by rotational spectroscopy is prevented.

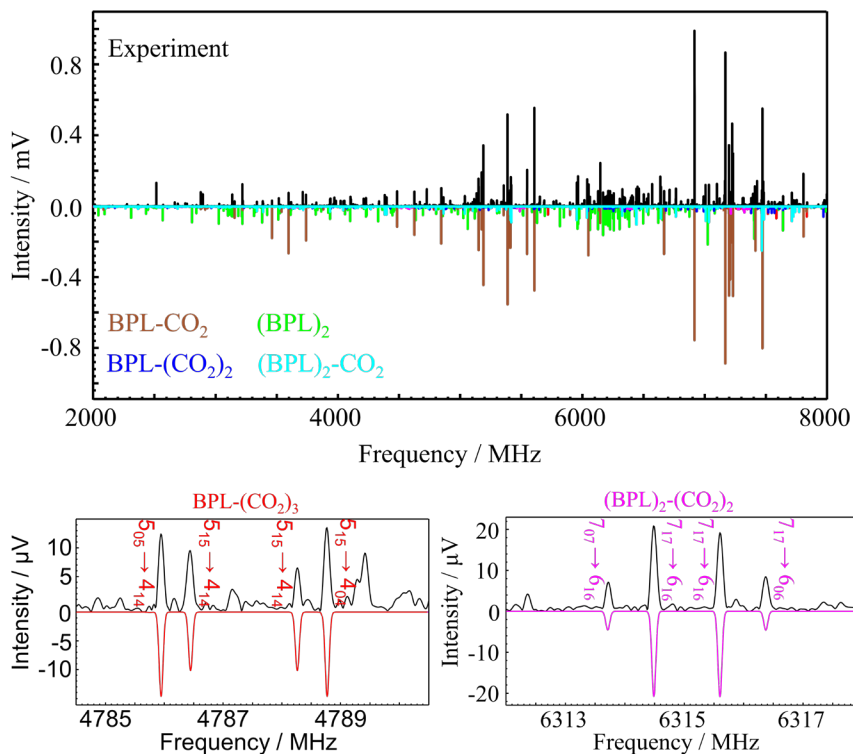


**Figure 5.2** The broadband rotational spectra of  $\text{BPL}-(\text{CO}_2)_{1-3}$  and  $(\text{BPL})_2-(\text{CO}_2)_{0-2}$  clusters. The black trace corresponds to the experimental spectra (1.6 million FID) after removing the transitions of the BPL monomer. The traces of different colors below represent the simulated spectra based on the experimental spectroscopic parameters.

After removing the transitions of BPL-CO<sub>2</sub>, BPL-(CO<sub>2</sub>)<sub>2</sub>, and (BPL)<sub>2</sub> clusters from the spectrum, the transitions of the (BPL)<sub>2</sub>-CO<sub>2</sub> cluster were assigned, including both *a*-type and *b*-type transitions. However, it was found that the spectra still contained numerous low-intensity spectral transitions. Among these transitions, some notable spectral patterns could be identified, characterized by quartets with two pairs of equally spaced spectral transitions. Examples of such transitions, which were first recognized and assigned, are displayed in the lower part of Figure 5.2. These spectral patterns are consistent with the transitions in a system composed of four quantum energy levels, including two *a*-type and two *b*-type transitions. Based on these spectral patterns, we initially fitted the three independent rotational constants, leading further to the determination of more centrifugal distortion constants by adding more rotational transitions. By comparing the experimental spectroscopic parameters to those of quantum chemical calculations, these spectral transitions were ultimately attributed to the BPL-(CO<sub>2</sub>)<sub>3</sub> and (BPL)<sub>2</sub>-(CO<sub>2</sub>)<sub>2</sub> clusters. It is apparent that the experimental parameters assigned to the isomers of the BPL-(CO<sub>2</sub>)<sub>1-3</sub> and (BPL)<sub>2</sub>-(CO<sub>2</sub>)<sub>0-2</sub> clusters are in good agreement with the parameters obtained from theoretical calculations. All the determined parameters are provided in Tables 5.1 and 5.2, while all the transitions for each isomer are listed in Tables S5.8-S5.13 of Appendix.

**Table 5.1** Experimental spectroscopic parameters for the observed isomers of the BPL-(CO<sub>2</sub>)<sub>1-3</sub> clusters.

Parameters	BPL-CO <sub>2</sub>	BPL-(CO <sub>2</sub> ) <sub>2</sub>	BPL-(CO <sub>2</sub> ) <sub>3</sub>
<i>A</i> / MHz <sup>a</sup>	5314.8240(49) <sup>c</sup>	1376.43791(108)	636.0025(16)
<i>B</i> / MHz	969.61221(87)	753.42115(74)	557.90249(68)
<i>C</i> / MHz	830.59251(85)	594.77818(64)	466.24220(77)
<i>D</i> <sub>J</sub> / kHz	0.5569(96)	0.3169(67)	0.1620(81)
<i>D</i> <sub>JK</sub> / kHz	[-0.4972] <sup>d</sup>	2.098(16)	0.606(33)
<i>D</i> <sub>K</sub> / kHz	0.01352(53)	1.318(34)	-0.300(43)
<i>d</i> <sub>1</sub> / kHz	[-0.0797]	-0.0852(27)	[-0.0207]
<i>d</i> <sub>2</sub> / Hz	[-5.0060]	-0.03502(73)	-0.0295(33)
<i>μ</i>   / D	<i>μ</i> <sub>b</sub> > <i>μ</i> <sub>a</sub> , no <i>μ</i> <sub>c</sub>	<i>μ</i> <sub>c</sub> > <i>μ</i> <sub>a</sub> , no <i>μ</i> <sub>b</sub>	<i>μ</i> <sub>b</sub> > <i>μ</i> <sub>a</sub> , no <i>μ</i> <sub>c</sub>
<i>N</i>	36	96	88
<i>σ</i> / kHz <sup>b</sup>	7.5	5.1	9.0

<sup>a</sup>Rotational constants (*A*, *B*, *C*), Watson's *S*-reduction centrifugal distortion constants (*D*<sub>J</sub>, *D*<sub>JK</sub>, *D*<sub>K</sub>, *d*<sub>1</sub>, *d*<sub>2</sub>), electric dipole moments (*μ*<sub>α</sub>, α = *a*, *b*, *c*) and number of transitions (*N*) be used in the fits. <sup>b</sup>Root-mean-square deviation of the fit. <sup>c</sup>Values in parentheses are standard errors in units of the last digit. <sup>d</sup>Values in squared brackets were fixed to their theoretical values.

**Table 5.2** Experimental spectroscopic parameters for the observed isomers of the (BPL)<sub>2</sub>-(CO<sub>2</sub>)<sub>0-2</sub> clusters.

Parameters	(BPL) <sub>2</sub>	(BPL) <sub>2</sub> -CO <sub>2</sub>	(BPL) <sub>2</sub> -(CO <sub>2</sub> ) <sub>2</sub>
<i>A</i> / MHz <sup>a</sup>	2170.9307(15) <sup>c</sup>	898.2791(11)	507.25933(83)
<i>B</i> / MHz	964.87811(53)	726.26690(82)	464.41859(70)
<i>C</i> / MHz	896.95602(47)	512.81878(81)	448.92531(66)
<i>D</i> <sub>J</sub> / kHz	[0.5320] <sup>d</sup>	0.139(14)	0.0864(58)
<i>D</i> <sub>JK</sub> / kHz	0.280(18)	0.277(42)	[-3.3080]
<i>D</i> <sub>K</sub> / kHz	0.824(89)	-0.232(82)	[5.0540]
<i>d</i> <sub>1</sub> / kHz	0.02060(23)	[-0.0480]	[6.7330]
<i>d</i> <sub>2</sub> / Hz	-2.40(68)	-0.0150(13)	[-2.7980]
$ \mu $ / D	$\mu_c > \mu_b > \mu_a$	$\mu_a > \mu_b$ , no $\mu_c$	$\mu_a > \mu_b$ , no $\mu_c$
<i>N</i>	120	120	83
$\sigma$ / kHz <sup>b</sup>	10.9	9.7	11.2

<sup>a</sup>Rotational constants (*A*, *B*, *C*), Watson's *S*-reduction centrifugal distortion constants (*D*<sub>J</sub>, *D*<sub>JK</sub>, *D*<sub>K</sub>, *d*<sub>1</sub>, *d*<sub>2</sub>), electric dipole moments ( $\mu_\alpha$ ,  $\alpha = a, b, c$ ) and number of transitions (*N*) be used in the fits. <sup>b</sup>Root-mean-square deviation of the fit. <sup>c</sup>Values in parentheses are standard errors in units of the last digit. <sup>d</sup>Values in squared brackets were fixed to their theoretical values.

For the BPL-CO<sub>2</sub> cluster, all predicted isomers are stabilized by C $\cdots$ O=C tetrel bonds (Figure 5.3). Four isomers are found within 5 kJ mol<sup>-1</sup>, differing in the position of the CO<sub>2</sub> moiety. The most stable structure involves a second CH<sub>2</sub> $\cdots$ O=C bifurcated hydrogen bond between CO<sub>2</sub> and the adjacent methylene group of BPL. In the structures of the second and third stable isomers, the CO<sub>2</sub> molecules bind to the two oxygen atoms in BPL simultaneously, while the structure of the higher isomer is stabilized by an interaction between the (-CH<sub>2</sub>)C-O and CO<sub>2</sub>. For the BPL-(CO<sub>2</sub>)<sub>2</sub> cluster there are eight isomers below 5 kJ mol<sup>-1</sup>. In all cases at least one CO<sub>2</sub> molecule is positioned above the four-membered ring, forming a C $\cdots$ O tetrel bond with another CO<sub>2</sub> molecule. Each CO<sub>2</sub> then interacts individually with the BPL molecule, leading to a stable structure. In terms of the BPL-(CO<sub>2</sub>)<sub>3</sub> tetramer, the number of isomers within 5 kJ mol<sup>-1</sup> is doubled compared to the BPL-(CO<sub>2</sub>)<sub>2</sub> trimer. A notable common feature among these isomers is the network formed among the three CO<sub>2</sub> molecules.

For the pure homodimer of (BPL)<sub>2</sub> there are only three low-energy isomers below 5 kJ mol<sup>-1</sup>. The most stable (antiparallel carbonyl) isomer I exhibits zero electric dipole moment components along all three coordinates. In the second lowest-energy isomer II, the two BPL molecules are parallel but with orthogonal carbonyl groups, while the third isomer is assembled in a "T" shape. When a single CO<sub>2</sub> molecule is introduced into the (BPL)<sub>2</sub> cluster, it acts as a bridge, linking the two BPL molecules in a configuration with orthogonal carbonyl groups. When one more CO<sub>2</sub> is added to the (BPL)<sub>2</sub>-CO<sub>2</sub> cluster, the second CO<sub>2</sub> leads to a shift from the C $\cdots$ O tetrel bond found in (BPL)<sub>2</sub>-(CO<sub>2</sub>)<sub>2</sub> cluster, with some structures separating the two CO<sub>2</sub> molecules across the BPL units. When three CO<sub>2</sub> molecules are introduced into the

(BPL)<sub>2</sub> cluster, a distinct pattern emerges: in all isomers, at least two of the three CO<sub>2</sub> molecules interact with both BPL units, stabilizing the overall structure.

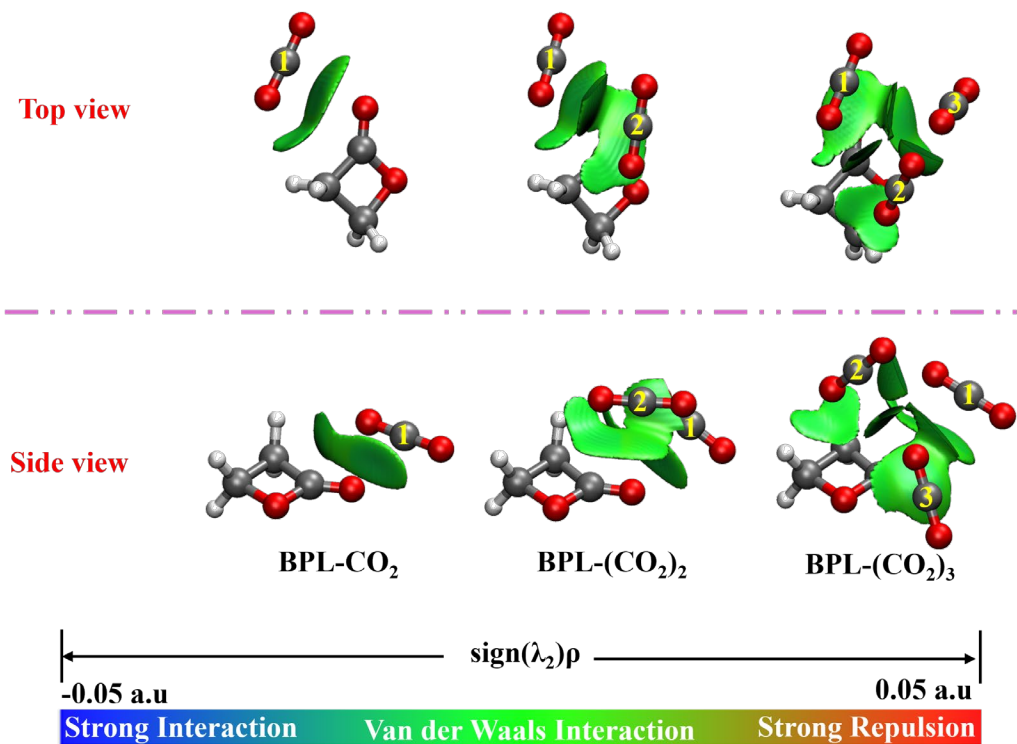


**Figure 5.3.** Non-covalent interaction plots (NCIPlots) for all the experimentally assigned isomers of the BPL-(CO<sub>2</sub>)<sub>1-3</sub> clusters. The upper panel depicts a top view, while the lower panel provides a side view. The cut-off value for the isosurface is set at 0.5 a.u. Attractive and repulsive interactions are defined by the product of electron density and the second Hessian eigenvalue [ $\text{sign}(\lambda_2)\rho$ ] with the range of -0.05 to 0.05 a.u. Here,  $\lambda_2$  represents the second eigenvalue of the electron density Hessian, and  $\rho$  is the electron density. In the color bar to the right, deep blue indicates strong attractive interactions, green represents weaker van der Waals interactions, and red signifies strong repulsive interactions.

The experimentally assigned isomers of the BPL-(CO<sub>2</sub>)<sub>1-3</sub> and (BPL)<sub>2</sub>-(CO<sub>2</sub>)<sub>0-2</sub> clusters are compared in Figures 5.3 and 5.4, where each isomer represents the structure corresponding to the predicted lowest-energy geometry from quantum chemical calculations (except for the pure (BPL)<sub>2</sub> homodimer). Figure 5.4 also includes the predicted structure of the global minimum of the (BPL)<sub>2</sub>-(CO<sub>2</sub>)<sub>3</sub> cluster, which was not detected. As can be observed, the heavy atom skeleton of the CO<sub>2</sub> and BPL molecules are co-planar in the BPL-CO<sub>2</sub> cluster, as expected from the C $\cdots$ O=C tetrel bond and the secondary CH<sub>2</sub> $\cdots$ O=C bifurcated hydrogen bond. When two CO<sub>2</sub>

molecules are introduced into the BPL molecule, both CO<sub>2</sub>(C1) and CO<sub>2</sub>(C2) participate in the formation of NCIs through the C=O groups, forming C $\cdots$ O=C tetrel bonds and C-H $\cdots$ O=C hydrogen bonds. Although CO<sub>2</sub>(C1) creates the type of NCIs found in the BPL-CO<sub>2</sub> cluster, it is no longer coplanar with the heavy atom skeleton of the BPL molecule. Additionally, there are two C $\cdots$ O tetrel bonds between CO<sub>2</sub>(C1) and CO<sub>2</sub>(C2), resulting in a slipped-barrel arrangement of the three carbonyl groups, one of them above the BPL plane and the second one located laterally and simultaneously establishing interaction with the other two carbonyl groups. This structure is similar to the second non-planar isomer of the pure CO<sub>2</sub> homotrimer of Figure 5.5.<sup>269</sup> In the BPL-(CO<sub>2</sub>)<sub>3</sub> cluster, the NCIs of CO<sub>2</sub>(C1) with the BPL molecule are similar to the BPL-(CO<sub>2</sub>)<sub>2</sub> cluster. However, with the addition of CO<sub>2</sub>(C3), the C $\cdots$ O(C2) tetrel bond between CO<sub>2</sub>(C1) and CO<sub>2</sub>(C2) is missing in the BPL-(CO<sub>2</sub>)<sub>3</sub> cluster. The newly introduced CO<sub>2</sub>(C3) molecule disrupts the C $\cdots$ O tetrel bond between CO<sub>2</sub>(C2) and BPL, resulting in the formation of four C $\cdots$ O tetrel bonds to keep stability between three CO<sub>2</sub> molecules. This situation produces a structure related to the pure CO<sub>2</sub> tetramer of Figure 5.5, with no parallel arrangements between the four carbonyl groups.<sup>270</sup> In brief, for the BPL-(CO<sub>2</sub>)<sub>1-3</sub> series, the alkyl O participates in the formation of only one tetrel bond in BPL-(CO<sub>2</sub>)<sub>3</sub> cluster, suggesting that the carbonyl O preferentially interacts with the C atom of CO<sub>2</sub> in the BPL-(CO<sub>2</sub>)<sub>1-3</sub> series.

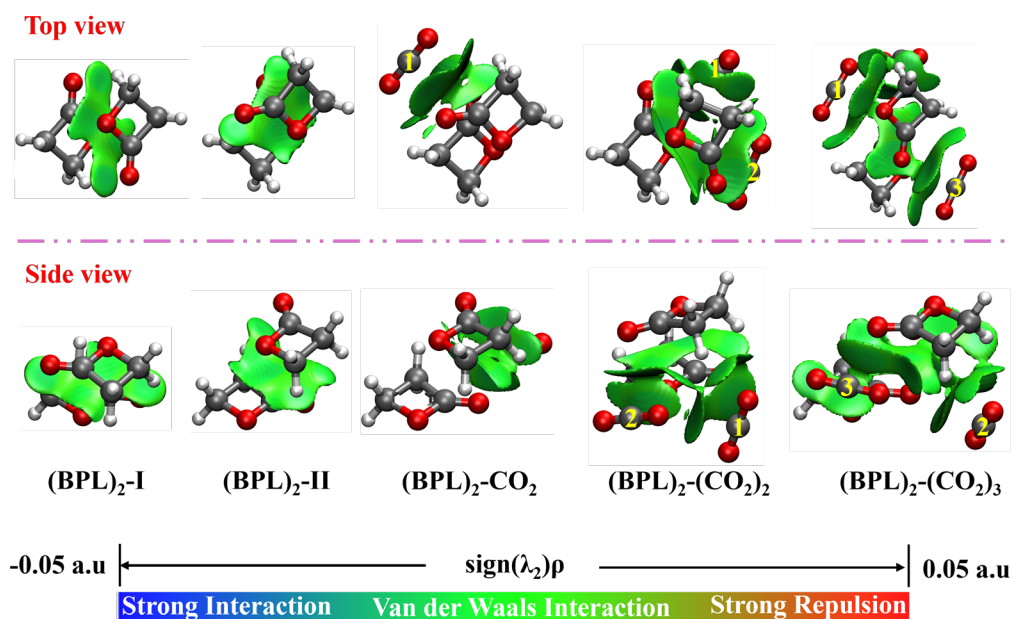


**Figure 5.4.** Non-covalent interaction plots (NCIPlots) for all the experimentally assigned isomers of the (BPL)<sub>2</sub>-(CO<sub>2</sub>)<sub>0-2</sub> clusters, and NCIPlots of the global minima of the (BPL)<sub>2</sub>-(CO<sub>2</sub>)<sub>3</sub> cluster. The upper panel depicts a top view, while the lower panel provides a side view.

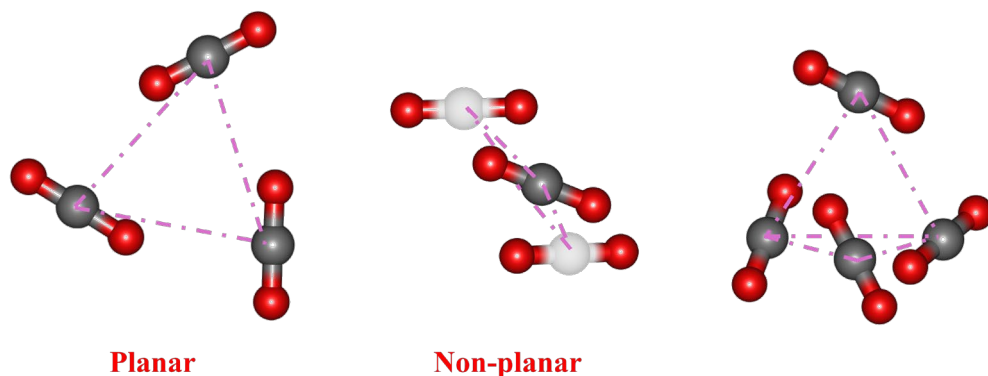


**Figure 5.5.** Molecular structures of the CO<sub>2</sub> trimer,<sup>269</sup> including the planar and non-planar isomers, and the CO<sub>2</sub> tetramer.<sup>270</sup> The drawings were adapted from the cited references.

For the most stable apolar isomer of (BPL)<sub>2</sub> cluster, known as (BPL)<sub>2</sub>-I, the alkyl O atoms in the one of the BPL molecules interact with the electron-deficient C atom of the C=O group in the second BPL molecule through another tetrel bond ( $n \rightarrow \pi^*$  interaction). For the second isomer (BPL)<sub>2</sub>-II, the alkyl O in one of the BPL molecules still prefers to interact with the electron-deficient C atom of the C=O group in the second BPL, while the two C=O groups form two C-H $\cdots$ O hydrogen bonds with the methylene group of the opposite BPL molecule.

The relative molecular position in the (BPL)<sub>2</sub>-(CO<sub>2</sub>)<sub>1-3</sub> cluster is particularly interesting. As shown in Figure 5.6, in (BPL)<sub>2</sub>-CO<sub>2</sub> the two carbonyl groups closely connect with CO<sub>2</sub> through C $\cdots$ O=C tetrel bonds, with a slight change in the relative positions of the two BPL molecules compared to (BPL)<sub>2</sub>-II. The distance between the two carbonyl O atoms in (BPL)<sub>2</sub>-II is approximately 3.82 Å, whereas the one in (BPL)<sub>2</sub>-CO<sub>2</sub> is approximately 3.58 Å. Moreover, the stability of both (BPL)<sub>2</sub>-II and (BPL)<sub>2</sub>-CO<sub>2</sub> is controlled by a tetrel bond ( $n \rightarrow \pi^*$  interaction) and C-H $\cdots$ O hydrogen bonds. In addition, the alkyl O in (BPL)<sub>2</sub>-CO<sub>2</sub> binds with the carbonyl C atom in the second BPL molecule, similarly to (BPL)<sub>2</sub>. After inserting two CO<sub>2</sub> molecules into the BPL dimer, several intriguing characteristics emerge.

First of all, the carbonyl groups of the two BPL molecules arrange in a near antiparallel direction, unlike in (BPL)<sub>2</sub>-CO<sub>2</sub>. Then, the alkyl O of one of the BPL molecules binds with the C atom of each of the two CO<sub>2</sub> molecules, which is the first observation of two bifurcated C $\cdots$ O=C tetrel bonds originated by a single alkyl O in BPL. Simultaneously, two tetrel bonds ( $n \rightarrow \pi^*$  interactions) occur between the alkyl O and the C=O group of the second BPL molecule. Furthermore, each CO<sub>2</sub> molecule connects with the C=O group in one of the two BPL molecules, pushing them apart

(with the distance between the two carbonyl O atoms being approximately 4.63 Å), resulting in a noticeable shift in the relative positions of the two BPL molecules compared to  $(\text{BPL})_2\text{-II}$  and  $(\text{BPL})_2\text{-CO}_2$ . For the global-minimum structure of  $(\text{BPL})_2\text{-(CO}_2)_3$  cluster, the two  $\text{CO}_2$  molecules bind to the  $\text{C=O}$  group of the below BPL molecule through  $\text{C}\cdots\text{O}=\text{C}$  tetrel bonds, and the C atoms of the two  $\text{CO}_2$  molecules form two  $\text{C}\cdots\text{O}_{(\text{C-O})}$  tetrel bonds with the two alkyl O atoms. The three  $\text{CO}_2$  molecules in  $(\text{BPL})_2\text{-(CO}_2)_3$  are not interconnected, which is extremely different from  $\text{BPL-(CO}_2)_3$ . The two BPL molecules are linked through the  $\text{C=O}$  groups, forming a tetrel bond ( $n\rightarrow\pi^*$  interaction), with the distance between the two carbonyl O atoms being approximately 3.26 Å. It is noteworthy that the relative positions of the two BPL molecules show continuous change among  $(\text{BPL})_2\text{-II}$ ,  $(\text{BPL})_2\text{-CO}_2$ ,  $(\text{BPL})_2\text{-(CO}_2)_2$ , and  $(\text{BPL})_2\text{-(CO}_2)_3$ . Additionally, as the number of  $\text{CO}_2$  molecules in  $(\text{BPL})_2$  increases from 0 to 3, the alkyl O atom begins to participate in  $\text{C}\cdots\text{O}=\text{C}$  tetrel bond, which is significantly different from  $\text{BPL-(CO}_2)_{1-3}$ .

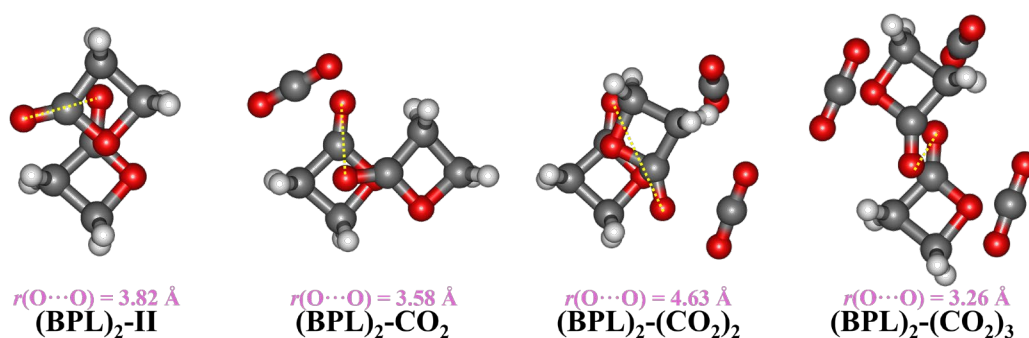


**Figure 5.6.** The theoretical  $\text{O}\cdots\text{O}$  distance between the carbonyl groups for the observed isomers of  $\text{BPL-(CO}_2)_{1-3}$  and  $(\text{BPL})_2\text{-(CO}_2)_{0-2}$  clusters and the theoretical global minimum of  $(\text{BPL})_2\text{-(CO}_2)_3$  cluster, at the B3LYP-D3(BJ)/def2-TZVP level of theory.

## 5.4 Conclusions

With the assistance of theoretical calculations at the B3LYP-D3(BJ)/def2-TZVP level of theory, the rotational spectra of  $\text{BPL-(CO}_2)_{1-3}$  and  $(\text{BPL})_2\text{-(CO}_2)_{1-3}$  clusters were recorded within the 2-8 GHz range using a broadband CP-FTMW spectrometer. Notably, the stability of all the observed isomers is contributed by at least a  $\text{C}\cdots\text{O}$  tetrel bond and a  $\text{C-H}\cdots\text{O}$  hydrogen bond. In the  $\text{CO}_2$  clusters of the  $(\text{BPL})_2$  series, the relative positions of the two BPL molecules show continuous change among  $(\text{BPL})_2\text{-II}$ ,  $(\text{BPL})_2\text{-CO}_2$ ,  $(\text{BPL})_2\text{-(CO}_2)_2$ , and  $(\text{BPL})_2\text{-(CO}_2)_3$ . Particularly, in  $(\text{BPL})_2\text{-(CO}_2)_2$ , the C atom of the two  $\text{CO}_2$  molecules simultaneously links with the alkyl O of one of the BPL molecules, leading to the first observation of two  $\text{C}\cdots\text{O}$  tetrel bonds

provided by the alkyl O of BPL. Besides, another relevant observation in  $(\text{BPL})_2\text{-(CO}_2)_2$  is that two tetrel bonds ( $n \rightarrow \pi^*$  interactions) occur between the alkyl O and the C=O group of the two BPL molecules. Additionally, as the number of  $\text{CO}_2$  in  $(\text{BPL})_2$  increases from 0 to 3, the alkyl O atoms gradually participate more in  $\text{C} \cdots \text{O}$  tetrel bonds ( $n \rightarrow \pi^*$  interactions). However, in the  $\text{BPL} \text{-(CO}_2)_{1-3}$  series, we only observed one case of NCIs involving the alkyl O in  $\text{BPL} \text{-(CO}_2)_3$ . In this way, the aggregation patterns of BPL interacting with  $\text{CO}_2$ , have revealed the interplay between the self-aggregation properties of BPL and that of  $\text{CO}_2$  and the important roles of the tetrel bond. This work provides insights for further studies on the role of NCIs in  $\text{CO}_2$  interaction, which eventually may contribute to the design of capture models and to improve the development of novel carbon fixation materials in the future.



## Chapter 6. The Cyclobutanone - CO<sub>2</sub> Clusters

This chapter continues exploring the aggregation properties and intermolecular interactions between aliphatic ketones and carbon dioxide. In this chapter we will conduct an in-depth analysis of the non-covalent interactions originated by cyclobutanone, including the cyclobutanone-(CO<sub>2</sub>)<sub>1-2</sub> and (cyclobutanone)<sub>2</sub>-(CO<sub>2</sub>)<sub>1-2</sub> clusters. Unlike the previously studied case of  $\beta$ -propiolactone in Chapter 5, cyclobutanone does not contain an oxygen atom in the ring, so its intermolecular interactions are primarily caused by the carbonyl group. We thus expect some relevant differences compared to the  $\beta$ -propiolactone clusters. Our work will provide a detailed description of the aggregation patterns of carbon dioxide and cyclobutanone, which may add fundamental insight into the association of carbon dioxide with organic compounds and its possible applications to carbon dioxide capture processes

### 6.1 Introduction

Carbon dioxide (CO<sub>2</sub>) emissions have long been a pressing concern, as excessive CO<sub>2</sub> atmospheric concentrations contribute to the greenhouse effect and global climate change.<sup>271</sup> To effectively prevent the rise of CO<sub>2</sub> or reduce CO<sub>2</sub> concentration in the atmosphere, understanding how CO<sub>2</sub> interacts and reacts with capture agents is extremely important to improve effective carbon capture and storage technologies. In the CO<sub>2</sub> capture process, NCIs such as hydrogen bond,  $\pi$ - $\pi$  stacking interactions, tetrel bonds, and other van der Waals forces, govern the binding between CO<sub>2</sub> and capture agents.<sup>272,273</sup> In particular, tetrel bonds in which the carbon atom in CO<sub>2</sub> participates through unoccupied orbitals with electron-rich atoms or molecular fragments (such as nitrogen, oxygen, etc.), may significantly enhance the binding properties of CO<sub>2</sub>, indirectly affecting selectivity and capture efficiency of the capture materials.<sup>135,267,273</sup> Besides the dominant tetrel bond, hydrogen bonds normally play a synergic role in the molecular stability of CO<sub>2</sub> systems. For example, recent investigations on monoethanolamine-(CO<sub>2</sub>)<sub>1-4</sub><sup>135</sup> and cyclopentene-(CO<sub>2</sub>)<sub>1-3</sub><sup>144</sup> using rotational spectroscopy have identified the contributions of tetrel and hydrogen bonds to the stability of the clusters.

In recent years, several studies have explored the possibility of using ketones for the development of novel CO<sub>2</sub> capture agents.<sup>274</sup> These studies have been complemented with spectroscopic studies exploring the NCIs formed in the gas phase between carbon dioxide and several ketones. The examples studied to date include formic acid-CO<sub>2</sub>,<sup>264</sup> formamide-CO<sub>2</sub>,<sup>267</sup> acetophenone-CO<sub>2</sub>,<sup>134</sup> and benzaldehyde-CO<sub>2</sub><sup>263</sup> clusters, among others. However, these studies have been normally limited to the formation of clusters with a single carbon dioxide molecule or a single substrate,

which makes the investigation not systematic. In order to progress on the knowledge of these NCIs it is necessary to account for the effects caused by several CO<sub>2</sub> molecules or several substrates, as shown in the previous chapter. This fact highlights the need to extend the investigation on NCIs to cases of multiple aggregation and self-aggregation of potential carbonyl-based capture agents beyond the smaller heterodimers.

This chapter presents rotational spectroscopy experiments combined with quantum chemical calculations of several dimers and trimers formed between cyclobutanone and CO<sub>2</sub>, to better understand the interactions involving carbonyl-based compounds. We will compare these interactions with those observed in the previous chapter with the carboxylic ester of  $\beta$ -propiolactone. These studies may improve our understanding of the interactions of CO<sub>2</sub> and carbonyl groups, which eventually may help the development of carbonyl-based CO<sub>2</sub> capture agents.

## 6.2 Experimental and Theoretical Methods

### 6.2.1 Experimental Methods

Cyclobutanone (CBN, purity >95%, b.p. 96.50 °C) was commercially available and used without further purification. We diluted CO<sub>2</sub> to approximately 1% concentration (total pressure of 10 bar) using a 1:1 mixture of helium and argon as carrier gas. The pressure of the carrier gas containing CO<sub>2</sub> was regulated to 3 Bar before flowing through two heating injectors containing the CBN sample, attached to circular exit nozzles ( $\phi = 1.0$  mm). The injectors were heated to 40°C to vaporize CBN. The pulsed injection inside the expansion chamber created the supersonic jet. The spectra were recorded with a CP-FTMW spectrometer, described in Chapter 1. The molecular FID signal was recorded in the time domain and then Fourier transformed to generate the frequency-domain spectra. In the experiment, the perpendicular expansion of the jet caused shorter decay times, broadening the typical linewidth to approximately 150 kHz (FWHM). The frequency measurements have an accuracy better than 20 kHz.

### 6.2.2 Computational Methods

The conformational landscape of the CBN-(CO<sub>2</sub>)<sub>1-2</sub> and (CBN)<sub>2</sub>-(CO<sub>2</sub>)<sub>0-2</sub> clusters was first explored using CREST.<sup>198</sup> To ensure the accuracy and reliability of the results, we reoptimized the initial structures of all the predicted clusters at the B3LYP-D3(BJ)/def2-TZVP level of theory. The calculation of the harmonic vibrational frequencies assured that the predicted geometries were true minima of the PES. The calculations used Gaussian 16.<sup>202</sup> To visually represent the NCIs within the clusters, we applied the NCI analysis for the observed isomers of the target clusters, using the

reduced electronic density gradient of Johnson and Contreras.<sup>208,224</sup> Furthermore, an SAPT<sup>73,211</sup> energy decomposition analysis was performed to accurately estimate the physical contributions of the binding energy in these clusters, using PSI4<sup>210</sup>. Detailed information on the theoretical results can be found in Tables S6.1-S6.7 in Appendix.

### 6.3 Results and Discussion

The microwave spectrum of the  $(\text{CBN})_{1-2}(\text{CO}_2)_{0-2}$  clusters is presented in Figure 6.1. The spectrum was processed using the BBA software to remove the transitions from the CBN monomer. As expected, the spectrum is dominated by the strong transitions of the CBN-CO<sub>2</sub> heterodimer. Based on the predictions for the transitions of other species, several distinct spectral patterns were later clearly identified. First, the *a*-type transitions of the  $(\text{CBN}-(\text{CO}_2)_2)$  trimer were assigned, followed by the additional *c*-type transitions. Consequently, the spectra of the  $(\text{CBN})_2\text{-CO}_2$  and  $(\text{CBN})_2-(\text{CO}_2)_2$  clusters were easily assigned to the corresponding structures predicted from quantum chemical calculations. Figure 6.1 illustrates some representative transitions of the  $(\text{CBN})_2\text{-CO}_2$  and  $(\text{CBN})_2-(\text{CO}_2)_2$  clusters, showing some characteristic quartets. These spectral features correspond to the transitions of a set composed of four quantum energy levels. For the  $(\text{CBN})_2\text{-CO}_2$  cluster, two of these transitions are *a*-type, while the other two are *b*-type. Regarding the  $(\text{CBN})_2-(\text{CO}_2)_2$  cluster, two *b*-type and two *c*-type transitions are included. Based on these spectral patterns, three rotational constants could be fitted initially, allowing for a more accurate prediction of additional rotational transitions. The most stable CBN dimer has a symmetrical antiparallel structure resulting in zero electric dipole moment components along all three axes, so this isomer could not be detected by rotational spectroscopy. All fitted spectral parameters are listed in Table 6.1, with the experimental parameters showing good agreement with those of theoretical calculations, particularly in the observed isomers of the  $(\text{CBN}-(\text{CO}_2)_{1-2})$  and  $(\text{CBN})_2-(\text{CO}_2)_{1-2}$  clusters. All the measured transitions are listed in Tables S6.8-S6.11 in the Appendix.

The theoretical predictions for the  $(\text{CBN}-(\text{CO}_2)_{1-3})$  and  $(\text{CBN})_2-(\text{CO}_2)_{0-3}$  clusters, conducted at the B3LYP-D3(BJ)/def2-TZVP level of theory, are listed in Tables S6.1-S6.7 in the Appendix. The predicted species included an energy window of 5 kJ mol<sup>-1</sup>. For the  $(\text{CBN}-(\text{CO}_2)_{1-3})$  cluster series, only two isomers are predicted for the heterodimer CBN-CO<sub>2</sub>. Both isomers are stabilized by one C···O=C tetrel bond and two C-H···O hydrogen bonds. However, in the most stable isomer the CO<sub>2</sub> molecule lies coplanar with the heavy atoms of CBN, while in the second most stable isomer, which is 2.1 kJ mol<sup>-1</sup> higher in energy than the global minimum, the CO<sub>2</sub> molecule locates above the plane of the heavy atoms in CBN. For the  $(\text{CBN}-(\text{CO}_2)_2)$  trimer, there are still only two isomers that can be found below 5 kJ mol<sup>-1</sup>. In these isomers, at least one CO<sub>2</sub> molecule is located adjacent to the four-membered ring of CBN. In isomer I,

another CO<sub>2</sub> is positioned directly above the ring, with both CO<sub>2</sub> molecules linking to the CBN molecule through one C···O=C tetrel bond and one C-H···O hydrogen bond. Additionally, the two CO<sub>2</sub> molecules bind to each other also by a C···O tetrel bond, forming a slipped-barrel structure. In isomer II, the two CO<sub>2</sub> molecules are located on opposite sides of the C=O group of the CBN molecule, interacting with CBN molecule through C···O tetrel bonds and C-H···O hydrogen bonds, but there is no C···O tetrel bond between the two CO<sub>2</sub> molecules. When the number of CO<sub>2</sub> increases to 3, eight isomers of the CBN-(CO<sub>2</sub>)<sub>3</sub> cluster are found below 5 kJ mol<sup>-1</sup>. Regarding the structure of the most stable isomer, it can be built upon that of the CBN-(CO<sub>2</sub>)<sub>2</sub> cluster, locating an additional CO<sub>2</sub> molecule coplanar with the heavy atoms of CBN. It is notable that as the number of CO<sub>2</sub> molecules increases, CO<sub>2</sub> gradually surrounds the C=O group of CBN molecule and induces the formation of additional C···O tetrel bonds.

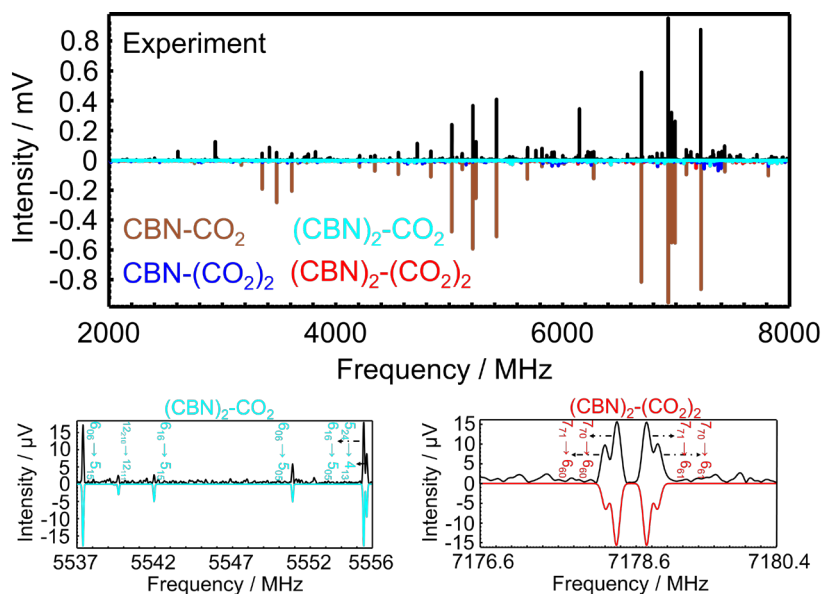


**Figure 6.1** The broadband rotational spectra of the CBN-(CO<sub>2</sub>)<sub>1-2</sub> and (Cbn)<sub>2</sub>-(CO<sub>2</sub>)<sub>1-2</sub> clusters within the 2-8 GHz range. The black trace represents the experimental spectra (1.1 million FID acquisitions) after removing the CBN monomer. The colored traces below correspond to the spectra simulated based on the experimental rotational parameters for the assigned CBN-(CO<sub>2</sub>)<sub>1-2</sub> and (Cbn)<sub>2</sub>-(CO<sub>2</sub>)<sub>1-2</sub> clusters.

Concerning the (Cbn)<sub>2</sub>-(CO<sub>2</sub>)<sub>0-3</sub> cluster series, the homodimer (Cbn)<sub>2</sub> is not detectable by rotational spectroscopy because of its zero electric dipole moment. After the introduction of one CO<sub>2</sub> on (Cbn)<sub>2</sub>, the CO<sub>2</sub> molecule breaks the parallel arrangement between the rings of the homodimer and links to the two CBN molecules through a C···O tetrel bond and a C-H···O hydrogen bond in the most stable isomer.

When two CO<sub>2</sub> molecules are attached to the homodimer the situation is more complicated and fourteen isomers are detected below 5 kJ mol<sup>-1</sup>, but all of them are primarily stabilized by C···O tetrel bonds. In the most stable isomer, the two CBN rings are antiparallel and the two CO<sub>2</sub> molecules are attached laterally, forming again a slipped-barrel structure. Finally, when three CO<sub>2</sub> molecules are introduced into the pure (CBN)<sub>2</sub> cluster, all CO<sub>2</sub> molecules form C···O tetrel bonds, with each CO<sub>2</sub> interacting with at least one C=O group of the CBN molecule.

**Table 6.1** Experimental parameters of the CBN-(CO<sub>2</sub>)<sub>1-2</sub> and (CBN)<sub>2</sub>-(CO<sub>2</sub>)<sub>1-2</sub> clusters.

Parameters <sup>a</sup>	CBN-CO <sub>2</sub>	CBN-(CO <sub>2</sub> ) <sub>2</sub>	(CBN) <sub>2</sub> -CO <sub>2</sub>	(CBN) <sub>2</sub> -(CO <sub>2</sub> ) <sub>2</sub>
<i>A</i> / MHz	5014.3633(44) <sup>c</sup>	1340.3728(23)	901.17223(78)	520.20563(57)
<i>B</i> / MHz	936.08127(91)	743.7725(14)	602.30163(67)	451.96482(75)
<i>C</i> / MHz	804.7317(10)	583.3062(18)	439.24596(63)	361.43137(88)
<i>D<sub>J</sub></i> / kHz	0.5683(95)	0.296(28)	0.1657(65)	0.0872(57)
<i>D<sub>JK</sub></i> / kHz	[0.33] <sup>d</sup>	1.06(10)	0.611(10)	[0.021]
<i>D<sub>K</sub></i> / kHz	10.61(43)	[3.17]	1.155(11)	[-0.077]
<i>d<sub>1</sub></i> / kHz	-0.0791(40)	[-0.081]	-0.0028(11)	[-0.0090]
<i>d<sub>2</sub></i> / Hz	[-0.012]	[-0.016]	-0.00694(37)	[0.0047]
<i> μ </i> / D	$\mu_a > \mu_b$ , no $\mu_c$	$\mu_a > \mu_c$ , no $\mu_b$	$\mu_b > \mu_a$ , no $\mu_c$	$\mu_c > \mu_b$ , no $\mu_a$
<i>N</i>	40	36	138	75
$\sigma$ / kHz <sup>b</sup>	11.3	10.4	8.7	18.2

<sup>a</sup>Rotational constants (*A*, *B*, *C*), Watson's *S*-reduction centrifugal distortion constants (*D<sub>J</sub>*, *D<sub>JK</sub>*, *D<sub>K</sub>*, *d<sub>1</sub>*, *d<sub>2</sub>*), electric dipole moments ( $\mu_\alpha$ ,  $\alpha = a, b, c$ ) and number of transitions (*N*) be used in the fits. <sup>b</sup>Root-mean-square deviation of the fit. <sup>c</sup>Values in parentheses are standard errors in units of the last digit. <sup>d</sup>Values in squared brackets were fixed to their theoretical values.

Figure 6.2 presents the NCIPlots for the most stable isomers of the CBN-(CO<sub>2</sub>)<sub>1-3</sub> and (CBN)<sub>2</sub>-(CO<sub>2</sub>)<sub>0-3</sub> clusters, illustrating the location and strength of their NCIs generally. In this work, the isomers of CBN-(CO<sub>2</sub>)<sub>1-2</sub> and (CBN)<sub>2</sub>-(CO<sub>2</sub>)<sub>1-2</sub> clusters were observed experimentally while the global minimum of (CBN)<sub>2</sub>-(CO<sub>2</sub>)<sub>3</sub> cluster is studied only theoretically. Figure 6.2 provides two different perspectives at the top and side views. In CBN-CO<sub>2</sub>, the CO<sub>2</sub> molecule is positioned sideways to the CBN molecule and forms a C···O=C tetrel bond and two C-H···O hydrogen bonds. As one more CO<sub>2</sub>(2) is added, the NCIs between the two CO<sub>2</sub> molecules cause CO<sub>2</sub>(1) to deviate from the plane of the ring of CBN molecule. CBN-(CO<sub>2</sub>)<sub>2</sub> is stabilized by multiple C···O tetrel bonds and C-H···O hydrogen bonds. The number of NCIs increases in CBN-(CO<sub>2</sub>)<sub>3</sub>, which are dominated by C···O tetrel bonds. Interestingly, the structures of CBN-(CO<sub>2</sub>)<sub>1-2</sub> are quite similar to those of corresponding BPL-(CO<sub>2</sub>)<sub>1-2</sub> complexes discussed in the previous chapter. However, as the number of CO<sub>2</sub> molecules increases to three, the relative positions and types of interactions between the three CO<sub>2</sub> molecules in CBN-(CO<sub>2</sub>)<sub>3</sub> show differences compared to BPL-(CO<sub>2</sub>)<sub>3</sub>. For example, in CBN-(CO<sub>2</sub>)<sub>3</sub>, CO<sub>2</sub>(2) is planar with the CBN molecule and the entire

structure is symmetric, while these features cannot be seen in BPL-(CO<sub>2</sub>)<sub>3</sub> because of the alkyl O, causing CO<sub>2</sub>(2) to not interact with C=O group of BPL molecule. In the CBN-(CO<sub>2</sub>)<sub>1-3</sub> clusters, the C=O group in CBN prefers to connect with CO<sub>2</sub> via a C···O=C tetrel bond rather than a C···O tetrel bond, which is also consistent with that observed in the BPL-(CO<sub>2</sub>)<sub>1-3</sub> clusters.

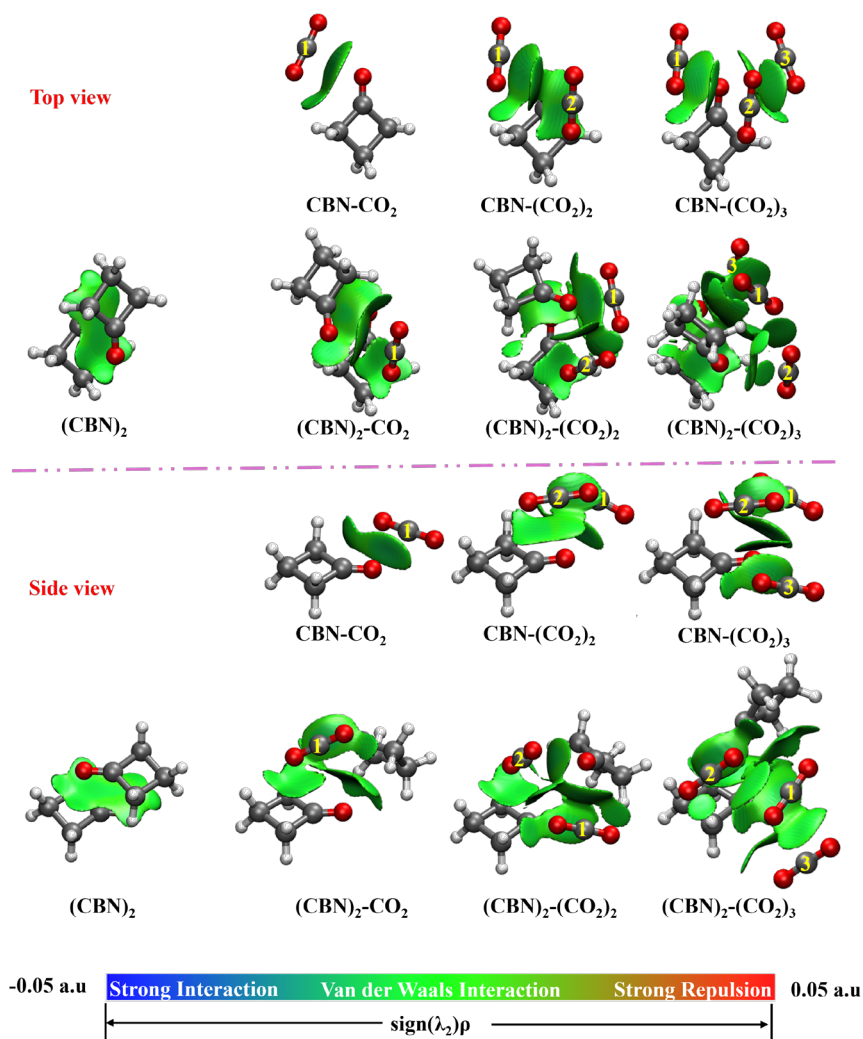


**Figure 6.2** Non-covalent interaction (NCI) plots for all experimentally assigned isomers of CBN-(CO<sub>2</sub>)<sub>1-2</sub> and (CBN)<sub>2</sub>-(CO<sub>2</sub>)<sub>1-2</sub> clusters, as well as for the global minimum of the predicted (CBN)<sub>2</sub> and (CBN)<sub>1-2</sub>-(CO<sub>2</sub>)<sub>3</sub> clusters. The top view is shown in the upper part of the purple dashed line, while the lower part provides a side view. The isosurface cut-off value is set to 0.5. Attractive and repulsive interactions are determined by the product of electron density and the second Hessian eigenvalue [ $\text{sign}(\lambda_2)\rho$ ], ranging from -0.05 to 0.05 a.u. Here,  $\lambda_2$  is the second eigenvalue of the electron density Hessian, and  $\rho$  denotes the electron density. In the accompanying color bar, deep blue indicates strong attractive interactions, green represents weaker van der Waals forces, and red denotes strong repulsive interactions.

In the  $(\text{CBN})_2\text{-(CO}_2\text{)}_{0-3}$  cluster series, it is interesting to note that the absence of an alkyl oxygen significantly influences the structure. One intriguing aspect is that the global minima of both  $(\text{CBN})_2$  and  $(\text{BPL})_2$  exhibit centers of symmetry. However, compared to  $(\text{BPL})_2$ , the difference in  $(\text{CBN})_2$  is that the two  $\text{C}=\text{O}$  groups are staggered, forming tetrel bonds ( $n\rightarrow\pi^*$  interactions), and leading to different relative distance between the  $\text{C}=\text{O}$  groups. After introducing one  $\text{CO}_2$  into  $(\text{CBN})_2$ , the  $\text{CO}_2$  molecule inserts into the two  $\text{CBN}$  molecules and pushes the  $\text{CBN}$  molecules apart while connecting the two  $\text{CBN}$  monomers through two  $\text{C}\cdots\text{O}=\text{C}$  tetrel bonds. In  $(\text{CBN})_2\text{-(CO}_2\text{)}_2$ , two  $\text{CO}_2$  molecules are also inserted in between the two rings of the  $\text{CBN}$  molecules, and each  $\text{CO}_2$  links the two  $\text{CBN}$  molecules through a  $\text{C}\cdots\text{O}=\text{C}$  tetrel bond and  $\text{C-H}\cdots\text{O}$  hydrogen bonds.  $\text{CO}_2(1)$  in  $(\text{CBN})_2\text{-(CO}_2\text{)}_3$ , maintains a similar interaction as observed in  $\text{CBN}-(\text{CO}_2)_2$ . Additionally, in  $(\text{CBN})_2\text{-(CO}_2\text{)}_3$ , it is particularly interesting that the interaction patterns between  $\text{CO}_2(1)$  and  $\text{CO}_2(2)$  are similar to that of in  $\text{CBN}-(\text{CO}_2)_3$ . As introducing an additional  $\text{CBN}$  into  $\text{CBN}-(\text{CO}_2)_3$ , the newly added  $\text{CBN}$  appears to replace  $\text{CO}_2(3)$  from its position, pushing it away from the other two  $\text{CBN}$  molecules, while there is a tetrel bond ( $n\rightarrow\pi^*$  interaction) between the two  $\text{CBN}$  molecules.  $\text{CO}_2(3)$  forms a  $\text{C}\cdots\text{OC}$  tetrel bond with the newly introduced  $\text{CBN}$  and a  $\text{C}(2)\cdots\text{O}(3)$  tetrel bond with  $\text{CO}_2(2)$ . Similarly,  $\text{CO}_2(1)$  interacts with the original  $\text{CBN}$  and  $\text{CO}_2(2)$  molecules through  $\text{C}\cdots\text{O}=\text{C}$  and  $\text{C}\cdots\text{O}(1)$  tetrel bonds, respectively. However,  $\text{CO}_2(2)$  connects with the other three molecules by forming two  $\text{C}\cdots\text{O}=\text{C}$  tetrel bonds, a  $\text{C}\cdots\text{O}(1)$  tetrel bond, and a  $\text{C}\cdots\text{O}(3)$  tetrel bond. Notably, the features of these interactions are significantly different from those in the  $(\text{BPL})_2\text{-(CO}_2\text{)}_{1-3}$  clusters, indicating that the absence of alkyl oxygen can lead to structural variations.

## 6.4 Conclusions

In this chapter, we successfully assigned the rotational spectrum corresponding to the  $\text{CBN}-(\text{CO}_2)_{1-2}$  and  $(\text{CBN})_2\text{-(CO}_2)_{1-2}$  clusters, which was recorded using broadband CP-FTMW spectrometer in the 2-8 GHz frequency range. The experimental results were analyzed assisted by quantum chemical calculations at the B3LYP-D3(BJ)/def2-TZVP level of theory, which adequately reproduce the experimental parameters. Additionally, we applied an NCI analysis to the lowest-energy isomers of the  $\text{CBN}-(\text{CO}_2)_{1-3}$  and  $(\text{CBN})_2\text{-(CO}_2)_{0-3}$  clusters, clearly showing the positions and strengths of the weak bonds. In the  $\text{CO}_2$  clusters of the  $\text{CBN}$  monomer series, we observed that at least one  $\text{CO}_2$  molecule maintains the interaction patterns observed in smaller clusters. However, in the  $\text{CO}_2$  clusters of the  $\text{CBN}$  dimer series, the relative position of  $\text{CO}_2$  significantly changed. For example, for  $(\text{CBN})_2\text{-CO}_2$ , the introduction of  $\text{CO}_2$  completely disrupts the original structure of the  $(\text{CBN})_2$  cluster. As the number of  $\text{CO}_2$  molecules increases from one to three, the  $(\text{CBN})_2$  structure is adjusted stepwise, displaying notably different behavior compared to the  $(\text{BPL})_2$  dimer series. These differences indicate that even with similar shape of

molecular skeleton, the absence of alkyl oxygen can still substantially impact cluster structure. This chapter's results, along with their comparison to the BPL series, represent a first description of the CO<sub>2</sub> clusters with four-membered cyclic ketones. These works will be extended to larger systems including other functional groups.

## Chapter 7. Conclusions

This Thesis has examined the formation of weakly-bound intermolecular aggregates generated in jet-cooled supersonic expansions, with the triple objective of discerning their electronic, structural and aggregation properties.

The methodology used in the Thesis combined high-resolution broadband microwave spectroscopy and quantum mechanical calculations, showing that this complementary rotational-computational approach has two great benefits for the study of intermolecular clusters in the gas phase. First, the use of chirped pulse Fourier transform microwave spectroscopy provides a highly sensitive technique for the detection of weak polar species up to the range of trimers or tetramers, unambiguously discriminating between isomers and isotopologues. Second, the use of quantum mechanical methods, in particular density-functional theory, provides efficient molecular orbital methods which permit the rationalization of the observed rotational spectra. Other computational techniques, like energy decomposition or the analysis of the electronic density function were performed for the experimentally assigned structures.

For each molecular system specific conclusions have been presented within each chapter. Moreover, several general conclusions can also be drawn from this work:

- The Thesis has extended the range of target molecular systems to molecular adducts containing two different chemical classes: 1) Heteroaggregates containing mono and biarenes functionalized with thiols and alcohols, and 2) Heteroaggregates containing four-membered cyclic ketones and carbon dioxide.
- The Thesis provides information on different intermolecular interactions scarcely explored before, including: 1) For the aggregates between thiols and alcohols the thesis has examined the competition between alcohol-to-alcohol (O-H $\cdots$ O), alcohol-to-thiol (O-H $\cdots$ S) and thiol-to-thiol (S-H $\cdots$ S) hydrogen bonds and those directed to the  $\pi$  systems. 2) For the aggregates containing aromatic systems the Thesis has explored the formation of weak  $\pi$ - $\pi$  interactions and its competition with the hydrogen bond. 3) For the aggregates of ketones and carbon dioxide the Thesis studied the formation of tetrel bonds and secondary hydrogen bonds involving aliphatic donors.

- In thiol and alcohol heterodimers, we observed that all the detected structural conformations are stabilized by the synergic effect of the O-H $\cdots$ S hydrogen bond and  $\pi$ - $\pi$  stacking, unlike their corresponding pure thiol dimers and alcohol dimers. Notably, in PN-TPN, dispersion contributions are nearly 30% higher than those in H<sub>2</sub>S-H<sub>2</sub>O. Besides, replacing an O atom with an S atom in the transition from the PN-PN to PN-TPN leads to significant shifts in both electrostatic and dispersion contributions: the electrostatic contribution decreases by about 15%, while the dispersion contribution increases by nearly 10%. Dispersion contributions dominate the interactions in both PN-TPN and TPN-TPN clusters. In 1NA-1NT, the contribution of dispersion is 11.8% higher than in PN-TPN, while the electrostatic contribution decreases by 4.1%, indicating that the introduction of a phenyl group enhances dispersion-type non-covalent interactions. Additionally, the total binding energy and attractive contributions of 2NA-2NT are similar to those of 1NA-1NT, suggesting that changes in substituent position have little effect on the attractive contributions or total binding energy in structures stabilized by the synergistic effect of O-H $\cdots$ S hydrogen bond and  $\pi$ - $\pi$  stacking.
- In the study of non-covalent interactions involving cyclic ketones or lactones and CO<sub>2</sub>, we find for the (BPL)<sub>2</sub>-(CO<sub>2</sub>)<sub>1-3</sub> series that the relative position of the two BPL molecules changes progressively among (BPL)<sub>2</sub>-II, (BPL)<sub>2</sub>-CO<sub>2</sub>, (BPL)<sub>2</sub>-(CO<sub>2</sub>)<sub>2</sub>, and (BPL)<sub>2</sub>-(CO<sub>2</sub>)<sub>3</sub>. Furthermore, as the number of CO<sub>2</sub> molecules in (BPL)<sub>2</sub> increases from one to three, the alkyl O atoms progressively engage more in C $\cdots$ O=C tetrel bonds using n $\rightarrow$  $\pi^*$  interactions. However, in the BPL-(CO<sub>2</sub>)<sub>1-3</sub> series, only BPL-(CO<sub>2</sub>)<sub>3</sub> exhibits a C $\cdots$ O=C tetrel bond involving the alkyl O atom. In the CBN-(CO<sub>2</sub>)<sub>1-3</sub> series, we observed that at least one CO<sub>2</sub> retains the interaction patterns typical of smaller clusters, whereas in the (CBN)<sub>2</sub>-(CO<sub>2</sub>)<sub>1-3</sub> series, the relative position of CO<sub>2</sub> shifts notably. For instance, in (CBN)<sub>2</sub>-CO<sub>2</sub>, the introduction of CO<sub>2</sub> disrupts the structure of the original (CBN)<sub>2</sub> entirely. The (CBN)<sub>2</sub> is continuously adjusted with the increase of the number of CO<sub>2</sub> from one to three, showing significantly different behavior from that seen in the (BPL)<sub>2</sub>-(CO<sub>2</sub>)<sub>0-3</sub> series.

## References

- (1) Janiak, C. A Critical Account on  $\pi$ - $\pi$  Stacking in Metal Complexes with Aromatic Nitrogen-Containing Ligands. *J. Chem. Soc., Dalton Trans.* **2000**, 32(21), 3885–3896. <https://doi.org/10.1039/b003010o>.
- (2) Yamauchi, O. Noncovalent Interactions in Biocomplexes. *Phys. Rev. Lett.* **2019**, 1(4), 20160001. <https://doi.org/10.1515/psr-2016-0001>.
- (3) Burley, S. K.; Petsko, G. A. Weakly Polar Interactions In Proteins. *Adv Protein Chem* **1988**, 39(C), 125–189. [https://doi.org/10.1016/S0065-3233\(08\)60376-9](https://doi.org/10.1016/S0065-3233(08)60376-9).
- (4) Nishio, M. CH $\cdots\pi$  Hydrogen Bonds in Organic Reactions. *Tetrahedron.* **2005**, 61(29), 6923–6950. <https://doi.org/10.1016/j.tet.2005.04.041>.
- (5) Schneider, H. J. Non-covalent Interactions: A Brief Account of a Long History. *J. Phys. Org. Chem.* **2022**, 25, e4340. <https://doi.org/10.1002/poc.4340>.
- (6) Yamada, S.; Tokugawa, Y. Cation- $\pi$  controlled Solid-State Photodimerization of 4-Azachalcones. *J. Am. Chem. Soc.* **2009**, 131(6), 2098–2099. <https://doi.org/10.1021/ja809906c>.
- (7) Yamada, S. Cation- $\pi$  Interactions in Organic Synthesis. *Chem. Rev.* **2018**, 118(23), 11353–11432. <https://doi.org/10.1021/acs.chemrev.8b00377>.
- (8) Zhu, W.; Deng, M.; Chen, D.; Chen, D.; Xi, H.; Chang, J.; Zhang, J.; Zhang, C.; Hao, Y. Sacrificial Additive-Assisted Film Growth Endows Self-Powered CsPbBr<sub>3</sub> Photodetectors with Ultra-Low Dark Current and High Sensitivity. *J. Mater Chem. C. Mater* **2019**, 8(1), 209–218. <https://doi.org/10.1039/c9tc05403k>.
- (9) Huang, X.; Sun, C.; Feng, X. Crystallinity and Stability of Covalent Organic Frameworks. *Sci. China: Chem.* **2020**, 63, 1367–1390. <https://doi.org/10.1007/s11426-020-9836-x>.
- (10) Montero-Campillo, M. M.; Brea, O.; M $\acute{o}$ , O.; Alkorta, I.; Elguero, J.; Y $\acute{a}$ ñez, M. Modulating the Intrinsic Reactivity of Molecules through Non-Covalent Interactions. *Phys. Chem. Chem. Phys.* **2019**, 21(5), 2222–2233. <https://doi.org/10.1039/c8cp06908e>.
- (11) Chand, A.; Sahoo, D. K.; Rana, A.; Jena, S.; Biswal, H. S. The Prodigious Hydrogen Bonds with Sulfur and Selenium in Molecular Assemblies, Structural Biology, and Functional Materials. *Acc. Chem. Res.* **2020**, 53(8), 1580–1592. <https://doi.org/10.1021/acs.accounts.0c00289>.
- (12) Newberry, R. W.; Raines, R. T. Secondary Forces in Protein Folding. *ACS Chem Biol* **2019**, 14(8), 1677–1686. <https://doi.org/10.1021/acscchembio.9b00339>.
- (13) Mundlapati, V. R.; Gautam, S.; Sahoo, D. K.; Ghosh, A.; Biswal, H. S. Thioamide, a Hydrogen Bond Acceptor in Proteins and Nucleic Acids. *J. Phys.*

- Chem. Lett.* **2017**, *8*(18), 4573–4579. <https://doi.org/10.1021/acs.jpcllett.7b01810>.
- (14) Zhou, P.; Tian, F.; Lv, F.; Shang, Z. Geometric Characteristics of Hydrogen Bonds Involving Sulfur Atoms in Proteins. *Proteins: Struct., Funct., Bioinf.* **2009**, *76*(1), 151–163. <https://doi.org/10.1002/prot.22327>.
- (15) Benz, S.; López-Andarias, J.; Mareda, J.; Sakai, N.; Matile, S. Catalysis with Chalcogen Bonds. *Angew. Chem. Int. Ed.* **2017**, *56*(3), 812–815. <https://doi.org/10.1002/anie.201611019>.
- (16) Mahmudov, K. T.; Aliyeva, V. A.; Guedes da Silva, M. F. C.; Pombeiro, A. J. L. The Chalcogen Bond in Solution: Synthesis, Catalysis and Molecular Recognition. *Halogen Bonding in Solution*; 2021; pp 363–382. <https://doi.org/10.1002/9783527825738.ch11>.
- (17) Olivella, M.; Caltabiano, G.; Cordoní, A. The Role of Cysteine 6.47 in Class A GPCRs. *BMC Struct. Biol.* **2013**, *13*(1), 1–11. <https://doi.org/10.1186/1472-6807-13-3>.
- (18) Biswal, H. S. Hydrogen Bonds Involving Sulfur: New Insights from Ab Initio Calculations and Gas Phase Laser Spectroscopy. *Challenges Adv. Comput. Chem. Phys.* **2015**, *19*, 15–45. [https://doi.org/10.1007/978-3-319-14163-3\\_2](https://doi.org/10.1007/978-3-319-14163-3_2).
- (19) Zhou, Y. J.; Zhang, M. M.; Wang, X. S. The N-H···X Hydrogen Bonds in the Crystal Structures of (Thio)Isochromene Derivatives. *J. Chem. Crystallogr.* **2013**, *43*(1), 26–30. <https://doi.org/10.1007/s10870-012-0380-z>.
- (20) Aldamen, M. A.; Sinnokrot, M. Crystallographic and Theoretical Studies of 1-(1-Naphthyl)-2-Thiourea with Intermolecular N-H···S Heteroatom Interaction and N-H··· $\pi$  Interaction. *J. Struct. Chem.* **2014**, *55*(1), 53–60. <https://doi.org/10.1134/S0022476614010089>.
- (21) Saragi, R. T.; Juanes, M.; Pinacho, R.; Rubio, J. E.; Fernández, J. A.; Lesarri, A. Molecular Recognition, Transient Chirality and Sulfur Hydrogen Bonding in the Benzyl Mercaptan Dimer. *Symmetry* **2021**, *13*(11), 2022. <https://doi.org/10.3390/sym13112022>.
- (22) Daeffler, K. N. M.; Lester, H. A.; Dougherty, D. A. Functionally Important Aromatic-Aromatic and Sulfur- $\pi$  Interactions in the D2 Dopamine Receptor. *J. Am. Chem. Soc.* **2012**, *134*(36), 14890–14896. <https://doi.org/10.1021/ja304560x>.
- (23) Hathwar, V. R.; Manivel, P.; Nawaz Khan, F.; Guru Row, T. N. Evaluation of Intermolecular Interactions in Thioisocoumarin Derivatives: The Role of the Sulfur Atom in Generating Packing Motifs. *Cryst. Eng. Comm.* **2009**, *11*(2), 284–291. <https://doi.org/10.1039/b807896c>.
- (24) Kojasoy, V.; Tantillo, D. J. Impacts of Noncovalent Interactions Involving Sulfur Atoms on Protein Stability, Structure, Folding, and Bioactivity. *Org. Biomol. Chem.* **2022**, *21*(1), 11–23. <https://doi.org/10.1039/d2ob01602h>.
- (25) Kutí, M.; Rábai, J.; Kapovits, I.; Jalsovszky, I.; Argay, G.; Kálmán, A.; Párkányi, L. Transannular Sulfur-Nitrogen Interaction in 1,5-Thiazocine

- Derivatives: An X-Ray Study. *J. Mol. Struct.* **1996**, 382(1), 1–11. [https://doi.org/10.1016/0022-2860\(96\)09237-X](https://doi.org/10.1016/0022-2860(96)09237-X).
- (26) Jin, Y.; Li, W.; Saragi, R. T.; Juanes, M.; Pérez, C.; Lesarri, A.; Feng, G. Sulfur-Arene Interactions: The S $\cdots\pi$  and S-H $\cdots\pi$  Interactions in the Dimers of Benzofuran $\cdots$ sulfur Dioxide and Benzofuran $\cdots$ hydrogen Sulfide. *Phys. Chem. Chem. Phys.* **2023**, 25(17), 12174–12181. <https://doi.org/10.1039/d3cp01146a>.
- (27) Juanes, M.; Saragi, R. T.; Pinacho, R.; Rubio, J. E.; Lesarri, A. Sulfur Hydrogen Bonding and Internal Dynamics in the Monohydrates of Thenyl Mercaptan and Thenyl Alcohol. *Phys. Chem. Chem. Phys.* **2020**, 22(22), 12412–12421. <https://doi.org/10.1039/d0cp01706j>.
- (28) Juanes, M.; Lesarri, A.; Pinacho, R.; Charro, E.; Rubio, J. E.; Enríquez, L.; Jaraíz, M. Sulfur Hydrogen Bonding in Isolated Monohydrates: Furfuryl Mercaptan versus Furfuryl Alcohol. *Chem. -Eur. J.* **2018**, 24(25), 6564–6571. <https://doi.org/10.1002/chem.201705727>.
- (29) Saragi, R. T.; Juanes, M.; Abad, J. L.; Lesarri, A.; Pinacho, R.; Rubio, J. E. Rotational Spectroscopy of Organophosphorous Chemical Agents: Cresyl and Phenyl Saligenin Phosphates. *Phys. Chem. Chem. Phys.* **2019**, 21(30), 16418–16422. <https://doi.org/10.1039/c9cp03093j>.
- (30) Juanes, M.; Saragi, R. T.; Caminati, W.; Lesarri, A. The Hydrogen Bond and Beyond: Perspectives for Rotational Investigations of Non-Covalent Interactions. *Chem. -Eur. J.* **2019**, 25, 11402–11411. <https://doi.org/10.1002/chem.201901113>.
- (31) Dian, B. C.; Brown, G. G.; Douglass, K. O.; Pate, B. H. Measuring Picosecond Isomerization Kinetics via Broadband Microwave Spectroscopy. *Science* **2008**, 320(5878), 924–928. <https://doi.org/10.1126/science.1155736>.
- (32) Tang, J.; Xu, Y.; McKellar, A. R. W.; Jäger, W. Quantum Solvation of Carbonyl Sulfide with Helium Atoms. *Science* **2002**, 297(5589), 2030–2033. <https://doi.org/10.1126/science.1073718>.
- (33) Saragi, R. T.; Juanes, M.; Pérez, C.; Pinacho, P.; Tikhonov, D. S.; Caminati, W.; Schnell, M.; Lesarri, A. Switching Hydrogen Bonding to  $\pi$ -Stacking: The Thiophenol Dimer and Trimer. *J. Phys. Chem. Lett.* **2021**, 12(5), 1367–1373. <https://doi.org/10.1021/acs.jpcllett.0c03797>.
- (34) Xu, L. H.; Liu, Q.; Suenram, R. D.; Lovas, F. J.; Walker, A. R. H.; Jensen, J. O.; Samuels, A. C. Rotational Spectra, Conformational Structures, and Dipole Moments of Thiodiglycol by Jet-Cooled FTMW and Ab Initio Calculations. *J. Mol. Spectrosc.* **2004**, 228 (2 SPEC. ISS.), 243–250. <https://doi.org/10.1016/j.jms.2004.04.004>.
- (35) Cole, G. C.; Møllendal, H.; Guillemin, J. C. Microwave Spectrum of 3-Butyne-1-Thiol: Evidence for Intramolecular S-H $\cdots\pi$  Hydrogen Bonding. *J. Phys. Chem. A* **2006**, 110(30), 9370–9376. <https://doi.org/10.1021/jp062093y>.
- (36) Juanes, M.; Saragi, R. T.; Jin, Y.; Zingsheim, O.; Schlemmer, S.; Lesarri, A. Rotational Spectrum and Intramolecular Hydrogen Bonding in 1,2-

- Butanedithiol. *J. Mol. Struct.* **2020**, *1211*, 128080. <https://doi.org/10.1016/j.molstruc.2020.128080>.
- (37) Sanz, M. E.; López, J. C.; Alonso, J. L.; Maris, A.; Favero, P. G.; Caminati, W. Conformation and Stability of Adducts of Sulfurated Cyclic Compounds with Water: Rotational Spectrum of Tetrahydrothiophene-Water. *J. Phys. Chem. A* **1999**, *103*(27), 5285–5290. <https://doi.org/10.1021/jp991002c>.
- (38) Cooke, S. A.; Corlett, G. K.; Legon, A. C. Comparisons of the Interactions of Benzene, Furan and Thiophene with Lewis Acids: The Rotational Spectrum of Thiophene···HF. *Chem. Phys. Lett.* **1998**, *291*(3–4), 269–276. [https://doi.org/10.1016/S0009-2614\(98\)00587-9](https://doi.org/10.1016/S0009-2614(98)00587-9).
- (39) Cocinero, E. J.; Sánchez, R.; Blanco, S.; Lesarri, A.; López, J. C.; Alonso, J. L. Weak Hydrogen Bonds C-H···S and C-H···F-C in the Thiirane-Trifluoromethane Dimer. *Chem. Phys. Lett.* **2005**, *402*(1–3), 4–10. <https://doi.org/10.1016/j.cplett.2004.11.073>.
- (40) Das, A.; Mandal, P. K.; Lovas, F. J.; Medcraft, C.; Walker, N. R.; Arunan, E. The H<sub>2</sub>S Dimer Is Hydrogen-Bonded: Direct Confirmation from Microwave Spectroscopy. *Angew. Chem. Int. Ed.* **2018**, *57*(46), 15199–15203. <https://doi.org/10.1002/anie.201808162>.
- (41) Tubergen, M. J.; Flad, J. E.; Del Bene, J. E. Microwave Spectroscopic and Ab Initio Studies of the Hydrogen-Bonded Trimethylamine-Hydrogen Sulfide Complex. *J. Chem. Phys.* **1997**, *107*(7), 2227–2231. <https://doi.org/10.1063/1.474619>.
- (42) Saragi, R. T.; Calabrese, C.; Juanes, M.; Pinacho, R.; Rubio, J. E.; Pérez, C.; Lesarri, A.  $\pi$ -Stacking Isomerism in Polycyclic Aromatic Hydrocarbons: The 2-Naphthalenethiol Dimer. *J. Phys. Chem. Lett.* **2023**, *14*(1), 207–213. <https://doi.org/10.1021/acs.jpcclett.2c03299>.
- (43) Arunan, E.; Emilsson, T.; Gutowsky, H. S.; Fraser, G. T.; De Oliveira, G.; Dykstra, C. E. Rotational Spectrum of the Weakly Bonded C<sub>6</sub>H<sub>6</sub>-H<sub>2</sub>S Dimer and Comparisons to C<sub>6</sub>H<sub>6</sub>-H<sub>2</sub>O Dimer. *J. Chem. Phys.* **2002**, *117*(21), 9766–9776. <https://doi.org/10.1063/1.1518999>.
- (44) Goswami, M.; Arunan, E. Microwave Spectrum and Structure of C<sub>6</sub>H<sub>5</sub>CCH···H<sub>2</sub>S Complex. *J. Mol. Spectrosc.* **2011**, *268*(1–2), 147–156. <https://doi.org/10.1016/j.jms.2011.04.011>.
- (45) Goswami, M.; Neill, J. L.; Muckle, M.; Pate, B. H.; Arunan, E. Microwave, Infrared-Microwave Double Resonance, and Theoretical Studies of C<sub>2</sub>H<sub>4</sub>···H<sub>2</sub>S Complex. *J. Chem. Phys.* **2013**, *139*(10), 104303. <https://doi.org/10.1063/1.4819787>.
- (46) Vila, A.; Mosquera, R. A. Are the Hydrogen Bonds Involving Sulfur Bases Inverse or Anomalous? *Int. J. Quantum. Chem.* **2006**, *106*(4), 928–934. <https://doi.org/10.1002/qua.20853>.
- (47) Crittenden, D. L. A Systematic CCSD(T) Study of Long-Range and Noncovalent Interactions between Benzene and a Series of First- and Second-

- Row Hydrides and Rare Gas Atoms. *J. Phys. Chem. A* **2009**, *113*(8), 1663–1669. <https://doi.org/10.1021/jp809106b>.
- (48) Kaur, D.; Aulakh, D.; Khanna, S.; Singh, H. Theoretical Study on the Nature of S···H and O···H Hydrogen Bonds. *J. Sulfur Chem.* **2014**, *35*(3), 290–303. <https://doi.org/10.1080/17415993.2013.874425>.
- (49) Wennmohs, F.; Staemmler, V.; Schindler, M. Theoretical Investigation of Weak Hydrogen Bonds to Sulfur. *J. Chem. Phys.* **2003**, *119*(6), 3208–3218. <https://doi.org/10.1063/1.1588291>.
- (50) Tauer, T. P.; Derrick, M. E.; Sherrill, C. D. Estimates of the Ab Initio Limit for Sulfur- $\pi$  Interactions: The H<sub>2</sub>S-Benzene Dimer. *J. Phys. Chem. A* **2005**, *109*(1), 191–196. <https://doi.org/10.1021/jp046778e>.
- (51) Saragi, R. T.; Juanes, M.; Caminati, W.; Lesarri, A.; Enríquez, L.; Jaraíz, M. Rotational Spectrum, Tunneling Motions, and Intramolecular Potential Barriers in Benzyl Mercaptan. *J. Phys. Chem. A* **2019**, *123*(39), 8435–8440. <https://doi.org/10.1021/acs.jpca.9b06921>.
- (52) Tama Saragi, R.; Li, W.; Juanes, M.; Enríquez, L.; Pinacho, R.; Rubio, J. E.; Lesarri, A. Rotational Spectroscopy and Conformational Flexibility of 2-Phenylethanethiol: The Dominant S–H··· $\pi$  Intramolecular Hydrogen Bond. *ChemPhysChem* **2024**, *25*(5), e202300799(1 of 8). <https://doi.org/10.1002/cphc.202300799>.
- (53) Salonen, L. M.; Ellermann, M.; Diederich, F. Aromatic Rings in Chemical and Biological Recognition: Energetics and Structures. *Angew. Chem. Int. Ed.* **2011**, *50*(21), 4808–4842. <https://doi.org/10.1002/anie.201007560>.
- (54) Zacharias, N.; Dougherty, D. A. Cation- $\pi$  Interactions in Ligand Recognition and Catalysis. *Trends Pharmacol. Sci.* **2002**, *23*, 281–287. [https://doi.org/10.1016/S0165-6147\(02\)02027-8](https://doi.org/10.1016/S0165-6147(02)02027-8).
- (55) Hudson, K. L.; Bartlett, G. J.; Diehl, R. C.; Agirre, J.; Gallagher, T.; Kiessling, L. L.; Woolfson, D. N. Carbohydrate-Aromatic Interactions in Proteins. *J. Am. Chem. Soc.* **2015**, *137*(48), 15152–15160. <https://doi.org/10.1021/jacs.5b08424>.
- (56) Zhao, Y.; Cotellet, Y.; Liu, L.; López-Andarias, J.; Bornhof, A. B.; Akamatsu, M.; Sakai, N.; Matile, S. The Emergence of Anion- $\pi$  Catalysis. *Acc. Chem. Res.* **2018**, *51*(9), 2255–2263. <https://doi.org/10.1021/acs.accounts.8b00223>.
- (57) Tiekink, E. R. T.; Zukerman-Schpector, J. *The Importance of Pi-Interactions in Crystal Engineering: Frontiers in Crystal Engineering*; 2012. <https://doi.org/10.1002/9781119945888>.
- (58) Zhuang, W. R.; Wang, Y.; Cui, P. F.; Xing, L.; Lee, J.; Kim, D.; Jiang, H. L.; Oh, Y. K. Applications of  $\pi$ - $\pi$  Stacking Interactions in the Design of Drug-Delivery Systems. *J. Controlled Release* **2019**, *294*, 311–326. <https://doi.org/10.1016/j.jconrel.2018.12.014>.

- (59) Kool, E. T. Hydrogen Bonding, Base Stacking, and Steric Effects in DNA Replication. *Annu. Rev. Biophys. Biomol. Struct.* **2001**, *30*, 1–22. <https://doi.org/10.1146/annurev.biophys.30.1.1>.
- (60) Georgiou, C. D. Functional Properties of Amino Acid Side Chains as Biomarkers of Extraterrestrial Life. *Astrobiology* **2018**, *18*(11), 1479–1496. <https://doi.org/10.1089/ast.2018.1868>.
- (61) Adhav, V. A.; Saikrishnan, K. The Realm of Unconventional Noncovalent Interactions in Proteins: Their Significance in Structure and Function. *ACS Omega* **2023**, *8*(25), 22268–22284. <https://doi.org/10.1021/acsomega.3c00205>.
- (62) Sticke, D. F.; Presta, L. G.; Dill, K. A.; Rose, G. D. Hydrogen Bonding in Globular Proteins. *J. Mol. Biol.* **1992**, *226*(4), 1143–1159. [https://doi.org/10.1016/0022-2836\(92\)91058-W](https://doi.org/10.1016/0022-2836(92)91058-W).
- (63) Jena, S.; Dutta, J.; Tulsiyan, K. D.; Sahu, A. K.; Choudhury, S. S.; Biswal, H. S. Noncovalent Interactions in Proteins and Nucleic Acids: Beyond Hydrogen Bonding and  $\pi$ -Stacking. *Chem. Soc. Rev.* **2022**, *51*, 4261–4286. <https://doi.org/10.1039/d2cs00133k>.
- (64) Zaky, M.; Youssef, Y.; Megahed, M. Impact of Surface Design and Coating on The Efficacy of Nano-Carriers as Drug Delivery Systems: A Review. *ERU Res. J.* **2023**, *2*(3), 415–446. <https://doi.org/10.21608/erurj.2023.219322.1045>.
- (65) Quinn, J. F.; Whittaker, M. R.; Davis, T. P. Glutathione Responsive Polymers and Their Application in Drug Delivery Systems. *Polym. Chem.* **2017**, *8*, 97–126. <https://doi.org/10.1039/c6py01365a>.
- (66) Seifert, N. A.; Hazrah, A. S.; Jäger, W. The 1-Naphthol Dimer and Its Surprising Preference for  $\pi$ - $\pi$  Stacking over Hydrogen Bonding. *J. Phys. Chem. Lett.* **2019**, *10*(11), 2836–2841. <https://doi.org/10.1021/acs.jpclett.9b00646>.
- (67) Seifert, N. A.; Steber, A. L.; Neill, J. L.; Pérez, C.; Zaleski, D. P.; Pate, B. H.; Lesarri, A. The Interplay of Hydrogen Bonding and Dispersion in Phenol Dimer and Trimer: Structures from Broadband Rotational Spectroscopy. *Phys. Chem. Chem. Phys.* **2013**, *15*(27), 11468–11477. <https://doi.org/10.1039/c3cp51725j>.
- (68) Mulliken, R. S. The Nature of the Chemical Bond. By Linus Pauling. *J. Phys. Chem.* **1940**, *44*(6), 827–828. <https://doi.org/10.1021/j150402a016>.
- (69) Huggins, M. L. The Hydrogen Bond (Pimentel, George C.; McClellan, Aubrey L.). *J. Chem. Educ.* **1960**, *37*(11), A754. <https://doi.org/10.1021/ed037pa754>.
- (70) Vinogradov, S.N.; Linnell, R. H. *Hydrogen Bonding*, Van Nostrand Reinhold, New York, 1971, pp 319.
- (71) Arunan, E.; Desiraju, G. R.; Klein, R. A.; Sadlej, J.; Scheiner, S.; Alkorta, I.; Clary, D. C.; Crabtree, R. H.; Dannenber, J. J.; Hobza, P.; Kjaergaard, H. G.; Legon, A. C.; Mennucci, B.; Nesbitt, D. J. Definition of the Hydrogen Bond (IUPAC Recommendations 2011). *Pure Appl. Chem.* **2011**, *83*(8), 1637–1641. <https://doi.org/10.1351/PAC-REC-10-01-02>.

- (72) Gili, G.; Gili, P. “*The nature of the hydrogen bond*”, Oxford University Press, 2009. <https://doi.org/10.1093/acprof:oso/9780199558964.001.0001>.
- (73) Scheiner, S. *Hydrogen Bonding: A Theoretical Perspective*; 1997; Vol. 120. <https://doi.org/10.1093/oso/9780195090116.001.0001>.
- (74) Desiraju, G.; Steiner, T. “*The Weak Hydrogen Bond: In Structural Chemistry and Biology*”, Oxford University Press, 2001. <https://doi.org/10.1093/acprof:oso/9780198509707.001.0001>.
- (75) Biswal, H. S.; Shirhatti, P. R.; Wategaonkar, S. O-H $\cdots$ O versus O-H $\cdots$ S Hydrogen Bonding i: Experimental and Computational Studies on the p-Cresol $\cdots$ H<sub>2</sub>O and p-Cresol $\cdots$ H<sub>2</sub>S Complexes. *J. Phys. Chem. A* **2009**, *113*(19), 5633–5643. <https://doi.org/10.1021/jp9009355>.
- (76) Goebel, J. R.; Ault, B. S.; Del Bene, J. E. Matrix Isolation and Ab Initio Study of 1:1 Hydrogen-Bonded Complexes of H<sub>2</sub>O<sub>2</sub> with Phosphorus and Sulfur Bases. *J. Phys. Chem. A* **2001**, *105*(50), 11365–11370. <https://doi.org/10.1021/jp013262b>.
- (77) Wierzejewska, M. Infrared Matrix Isolation Studies of Complexes Formed between Dimethylsulfide, Dimethyldisulfide and Nitrous Acid. *J. Mol. Struct.* **2000**, *520*(1–3), 199–214. [https://doi.org/10.1016/S0022-2860\(99\)00342-7](https://doi.org/10.1016/S0022-2860(99)00342-7).
- (78) Biswal, H. S.; Wategaonkar, S. OH $\cdots$ X (X = O, S) Hydrogen Bonding in Tetrahydrofuran and Tetrahydrothiophene. *J. Chem. Phys.* **2011**, *135*(13), 134306. <https://doi.org/10.1063/1.3645107>.
- (79) Bhattacharjee, A.; Matsuda, Y.; Fujii, A.; Wategaonkar, S. The Intermolecular S-H $\cdots$ Y (Y=S,O) Hydrogen Bond in the H<sub>2</sub>S Dimer and the H<sub>2</sub>S-MeOH Complex. *ChemPhysChem* **2013**, *14*(5), 905–914. <https://doi.org/10.1002/cphc.201201012>.
- (80) Bhattacharyya, S.; Bhattacharjee, A.; Shirhatti, P. R.; Wategaonkar, S. O-H $\cdots$ S Hydrogen Bonds Conform to the Acid-Base Formalism. *J. Phys. Chem. A* **2013**, *117*, 8238–8250. <https://doi.org/10.1021/jp405414h>.
- (81) Wategaonkar, S.; Bhattacharjee, A. N-H $\cdots$ S Interaction Continues to Be an Enigma: Experimental and Computational Investigations of Hydrogen-Bonded Complexes of Benzimidazole with Thioethers. *J. Phys. Chem. A* **2018**, *122*(17), 4313–4321. <https://doi.org/10.1021/acs.jpca.8b01943>.
- (82) Lobo, I. A.; Robertson, P. A.; Villani, L.; Wilson, D. J. D.; Robertson, E. G. Thiols as Hydrogen Bond Acceptors and Donors: Spectroscopy of 2-Phenylethanethiol Complexes. *J. Phys. Chem. A* **2018**, *122*(36), 7171–7180. <https://doi.org/10.1021/acs.jpca.8b06649>.
- (83) Martin, D. E.; Robertson, E. G.; Thompson, C. D.; Morrison, R. J. S. Resonant 2-Photon Ionization Study of the Conformation and the Binding of Water Molecules to 2-Phenylethanethiol (PhCH<sub>2</sub>CH<sub>2</sub>SH). *J. Chem. Phys.* **2008**, *128*(16), 164301. <https://doi.org/10.1063/1.2903477>.
- (84) Mishra, K. K.; Borish, K.; Singh, G.; Panwaria, P.; Metya, S.; Madhusudhan, M. S.; Das, A. Observation of an Unusually Large IR Red-Shift in an

- Unconventional S-H $\cdots$ S Hydrogen-Bond. *J. Phys. Chem. Lett.* **2021**, *12*(4), 1228–1235. <https://doi.org/10.1021/acs.jpcllett.0c03183>.
- (85) Bhattacharyya, S.; Wategaonkar, S. ZEKE Photoelectron Spectroscopy of P-Fluorophenol $\cdots$ H<sub>2</sub>S/H<sub>2</sub>O Complexes and Dissociation Energy Measurement Using the Birge-Sponer Extrapolation Method. *J. Phys. Chem. A* **2014**, *118*(40), 9386–9396. <https://doi.org/10.1021/jp505393p>.
- (86) Bhattacharjee, A.; Matsuda, Y.; Fujii, A.; Wategaonkar, S. Acid-Base Formalism in Dispersion-Stabilized S-H $\cdots$ Y (Y=O, S) Hydrogen-Bonding Interactions. *J. Phys. Chem. A* **2015**, *119*(7), 1117–1126. <https://doi.org/10.1021/jp511904a>.
- (87) Juanes, M.; Saragi, R. T.; Pérez, C.; Enríquez, L.; Jaraíz, M.; Lesarri, A. Torsional Chirality and Molecular Recognition: The Homo and Heterochiral Dimers of Thenyl and Furfuryl Alcohol. *Phys. Chem. Chem. Phys.* **2022**, *24*(15), 8999–9006. <https://doi.org/10.1039/d2cp00479h>.
- (88) Ghosh, S.; Bhattacharyya, S.; Wategaonkar, S. Dissociation Energies of Sulfur-Centered Hydrogen-Bonded Complexes. *J. Phys. Chem. A* **2015**, *119*(44), 10863–10870. <https://doi.org/10.1021/acs.jpca.5b08185>.
- (89) Biswal, H. S.; Shirhatti, P. R.; Wategaonkar, S. O-H $\cdots$ O versus O-H $\cdots$ S Hydrogen Bonding. 2. Alcohols and Thiols as Hydrogen Bond Acceptors. *J. Phys. Chem. A* **2010**, *114*(26), 6944–6955. <https://doi.org/10.1021/jp102346n>.
- (90) Biswal, H. S.; Chakraborty, S.; Wategaonkar, S. Experimental Evidence of O-H-S Hydrogen Bonding in Supersonic Jet. *J. Chem. Phys.* **2008**, *129*(18). <https://doi.org/10.1063/1.3012569>.
- (91) Wang, D.; Chopra, P.; Wategaonkar, S.; Fujii, A. Electronic and Infrared Spectroscopy of Benzene-(H<sub>2</sub>S)<sub>n</sub> (n = 1 and 2): The Prototype of the SH- $\pi$  Interaction. *J. Phys. Chem. A* **2019**, *123*(33), 7255–7260. <https://doi.org/10.1021/acs.jpca.9b02199>.
- (92) Grimme, S. Do Special Noncovalent  $\pi$ - $\pi$  Stacking Interactions Really Exist? *Angew. Chem. Int. Ed.* **2008**, *47*(18), 3430–3434. <https://doi.org/10.1002/anie.200705157>.
- (93) Martinez, C. R.; Iverson, B. L. Rethinking the Term “Pi-Stacking.” *Chem. Sci.* **2012**, *3*, 2191–2201. <https://doi.org/10.1039/c2sc20045g>.
- (94) Schlosser, F.; Moos, M.; Lambert, C.; Würthner, F. Redox-Switchable Intramolecular  $\pi$ - $\pi$ -Stacking of Perylene Bisimide Dyes in a Cyclophane. *Adv. Mater.* **2013**, *25*(3), 410–414. <https://doi.org/10.1002/adma.201201266>.
- (95) Maharramov, A. M.; Mahmudov, K. T.; Kopylovich, M. N.; Pombeiro, A. J. L. *Non-Covalent Interactions in the Synthesis and Design of New Compounds*; 2016. <https://doi.org/10.1002/9781119113874>.
- (96) Stornaiuolo, M.; De Kloe, G. E.; Rucktooa, P.; Fish, A.; Van Elk, R.; Edink, E. S.; Bertrand, D.; Smit, A. B.; De Esch, I. J. P.; Sixma, T. K. Assembly of a  $\pi$ - $\pi$  Stack of Ligands in the Binding Site of an Acetylcholine-Binding Protein. *Nat. Commun.* **2013**, *4*, 1875. <https://doi.org/10.1038/ncomms2900>.

- (97) Ma, S.; Zhao, W.; Zhou, J.; Wang, J.; Chu, S.; Liu, Z.; Xiang, G. A New Type of Noncovalent Surface- $\pi$  Stacking Interaction Occurring on Peroxide-Modified Titania Nanosheets Driven by Vertical  $\pi$ -State Polarization. *Chem Sci* **2021**, *12*(12), 4411–4417. <https://doi.org/10.1039/d0sc06601j>.
- (98) Knowles, R. R.; Jacobsen, E. N. Attractive Noncovalent Interactions in Asymmetric Catalysis: Links between Enzymes and Small Molecule Catalysts. *Proc. Natl. Acad. Sci. USA* **2010**, *107*(48), 20678–20685. <https://doi.org/10.1073/pnas.1006402107>.
- (99) Krenske, E. H.; Houk, K. N. Aromatic Interactions as Control Elements in Stereoselective Organic Reactions. *Acc. Chem. Res.* **2013**, *46*(4), 979–989. <https://doi.org/10.1021/ar3000794>.
- (100) Burley, S. K.; Petsko, G. A. Aromatic-Aromatic Interaction: A Mechanism of Protein Structure Stabilization. *Science* **1985**, *229* (4708), 23–28. <https://doi.org/10.1126/science.3892686>.
- (101) McGaughey, G. B.; Gagné, M.; Rappé, A. K.  $\pi$ -Stacking Interactions. Alive and Well in Proteins. *Journal of Biological Chemistry* **1998**, *273*(25), 15458–15463. <https://doi.org/10.1074/jbc.273.25.15458>.
- (102) Hunter, C. a; Sanders, J. K. M. The Nature of Pi-Pi Interactions. *J. Am. Chem. Soc.* **1990**, *112*(2), 5525–5534.
- (103) Sinnokrot, M. O.; Sherrill, C. D. High-Accuracy Quantum Mechanical Studies of  $\pi$ - $\pi$  Interactions in Benzene Dimers. *J. Phys. Chem. A* **2006**, *110*(37), 10656–10668. <https://doi.org/10.1021/jp0610416>.
- (104) Wheeler, S. E.; Houk, K. N. Substituent Effects in the Benzene Dimer Are Due to Direct Interactions of the Substituents with the Unsubstituted Benzene. *J. Am. Chem. Soc.* **2008**, *130* (33), 10854–10855. <https://doi.org/10.1021/ja802849j>.
- (105) Riwar, L. J.; Trapp, N.; Kuhn, B.; Diederich, F. Substituent Effects in Parallel-Displaced  $\pi$ - $\pi$  Stacking Interactions: Distance Matters. *Angew. Chem. Int. Ed.* **2017**, *56*(37), 11252–11257. <https://doi.org/10.1002/anie.201703744>.
- (106) Watt, M.; Hardebeck, L. K. E.; Kirkpatrick, C. C.; Lewis, M. Face-to-Face Arene-Arene Binding Energies: Dominated by Dispersion but Predicted by Electrostatic and Dispersion/Polarizability Substituent Constants. *J. Am. Chem. Soc.* **2011**, *133*(11), 3854–3862. <https://doi.org/10.1021/ja105975a>.
- (107) Mondal, S. I.; Sen, S.; Hazra, A.; Patwari, G. N.  $\pi$ -Stacked Dimers of Fluorophenylacetylenes: Role of Dipole Moment. *J. Phys. Chem. A* **2017**, *121*(18), 3383–3391. <https://doi.org/10.1021/acs.jpca.7b00209>.
- (108) Kundu, A.; Sen, S.; Patwari, G. N. The Propargylbenzene Dimer: C-H $\cdots$  $\pi$  Assisted  $\pi$ - $\pi$  Stacking. *Phys. Chem. Chem. Phys.* **2015**, *17*(14), 9090–9097. <https://doi.org/10.1039/c5cp00162e>.
- (109) Maity, S.; Patwari, G. N.; Sedlak, R.; Hobza, P. A  $\pi$ -Stacked Phenylacetylene Dimer. *Phys. Chem. Chem. Phys.* **2011**, *13*(37), 16706–16712. <https://doi.org/10.1039/c1cp20677j>.

- (110) Pietraperzia, G.; Pasquini, M.; Schiccheri, N.; Piani, G.; Becucci, M.; Castellucci, E.; Biczysko, M.; Bloino, J.; Barone, V. The Gas Phase Anisole Dimer: A Combined High-Resolution Spectroscopy and Computational Study of a Stacked Molecular System. *J. Phys. Chem. A* **2009**, *113*(52), 14343–14351. <https://doi.org/10.1021/jp903236z>.
- (111) Busker, M.; Svartsov, Y. N.; Häber, T.; Kleinermanns, K. IR-UV Double Resonance Spectra of Pyrazine Dimers: Competition between  $\text{CH}\cdots\pi$ ,  $\pi\cdots\pi$  and  $\text{CH}\cdots\pi$  Interactions. *Chem. Phys. Lett.* **2009**, *467*(4–6), 255–259. <https://doi.org/10.1016/j.cplett.2008.10.091>.
- (112) Crisp, D.; Atlas, R. M.; Breon, F. M.; Brown, L. R.; Burrows, J. P.; Ciais, P.; Connor, B. J.; Doney, S. C.; Fung, I. Y.; Jacob, D. J.; Miller, C. E.; O'Brien, D.; Pawson, S.; Randerson, J. T.; Rayner, P.; Salawitch, R. J.; Sander, S. P.; Sen, B.; Stephens, G. L.; Tans, P. P.; Toon, G. C.; Wennberg, P. O.; Wofsy, S. C.; Yung, Y. L.; Kuang, Z.; Chudasama, B.; Sprague, G.; Weiss, B.; Pollock, R.; Kenyon, D.; Schroll, S. The Orbiting Carbon Observatory (OCO) Mission. *Adv. Space Res.* **2004**, *34*, 700–709. <https://doi.org/10.1016/j.asr.2003.08.062>.
- (113) Beerling, D. J.; Royer, D. L. Convergent Cenozoic  $\text{CO}_2$  History. *Nat. Geosci.* **2011**, *4*, 418–420. <https://doi.org/10.1038/ngeo1186>.
- (114) Kartika, W. Studi Pemanfaatan Limbah  $\text{CO}_2$  Menjadi  $\text{CO}_2$  Cair Dengan Teknologi  $\text{CO}_2$  Purification Di Industri Baja. *Jurnal Jaring Sain Tek* **2021**, *3*(2), 51–58. <https://doi.org/10.31599/jaringsaintek.v3i2.738>.
- (115) Deepan Kumar, M.; Jaccob, M. Revealing the Non-Covalent Interactions Existing between  $\text{CO}_2$  and Succinimide-Based Ionic Liquid: A DFT Exploration. *J. Mol. Liq.* **2024**, *399*, 124325. <https://doi.org/10.1016/j.molliq.2024.124325>.
- (116) Anila, S.; Suresh, C. H.; Schaefer, H. F. Demarcating Noncovalent and Covalent Bond Territories: Imine- $\text{CO}_2$  Complexes and Cooperative  $\text{CO}_2$  Capture. *J. Phys. Chem. A* **2022**, *126* (30), 4952–4961. <https://doi.org/10.1021/acs.jpca.2c03221>.
- (117) Zhang, X.; Zhao, H.; Yang, Q.; Yao, M.; Wu, Y. nan; Gu, Y. Direct Air Capture of  $\text{CO}_2$  in Designed Metal-Organic Frameworks at Lab and Pilot Scale. *Carbon Capture Sci. Technol.* **2023**, *9*, 100145. <https://doi.org/10.1016/j.ccst.2023.100145>.
- (118) Pawłędzio, S.; Wang, X. Crystal Engineering of Hydrogen Bonding for Direct Air Capture of  $\text{CO}_2$ : A Quantum Crystallography Perspective. *Crystals*. **2024**, *14*(1), 77. <https://doi.org/10.3390/cryst14010077>.
- (119) Li, W.; Maris, A.; Melandri, S.; Lesarri, A.; Evangelisti, L. The Structure of 2,6-Di-Tert-Butylphenol–Argon by Rotational Spectroscopy. *Molecules* **2023**, *28*(24), 8111. <https://doi.org/10.3390/molecules28248111>.
- (120) Li, W.; Maris, A.; Melandri, S.; Lesarri, A.; Evangelisti, L. Molecular Structure and Internal Dynamics of the Antioxidant 2,6-Di-Tert-Butylphenol. *J. Mol. Struct.* **2024**, *1296*, 136910. <https://doi.org/10.1016/j.molstruc.2023.136910>.

- (121) Li, W.; Saragi, R. T.; Juanes, M.; Demaison, J.; Vogt, N.; Fernández-Ramos, A.; Lesarri, A. Equilibrium Structures of Selenium Compounds: The Torsionally Flexible Molecule of Selenophenol. *J. Chem. Phys.* **2023**, *159*(2), 024303. <https://doi.org/10.1063/5.0156413>.
- (122) Li, W.; Xu, Y.; Jin, Y.; Li, X.; Caminati, W.; Feng, G. Three Non-Bonding Interaction Topologies of the Thiazole-Formaldehyde Complex Observed by Rotational Spectroscopy. *Phys. Chem. Chem. Phys.* **2023**, *25*(8), 6491–6497. <https://doi.org/10.1039/d2cp05711e>.
- (123) Li, W.; Chen, J.; Xu, Y.; Lu, T.; Gou, Q.; Feng, G. Unveiling the Structural and Energetic Properties of Thiazole-Water Complex by Microwave Spectroscopy and Theoretical Calculations. *Spectrochim. Acta, Part A* **2020**, *242*, 118720. <https://doi.org/10.1016/j.saa.2020.118720>.
- (124) Li, W.; Li, M.; Jin, Y.; Gou, Q.; Grabow, J. U.; Feng, G. Molecular Structure and Non-Covalent Interaction of 2-Thiophenecarboxaldehyde and Its Monohydrated Complex. *J. Chem. Phys.* **2019**, *151*(16), 164307. <https://doi.org/10.1063/1.5126126>.
- (125) Mäder, H.; Heineking, N.; Stahl, W.; Jäger, W.; Xu, Y. Rotational Spectrum of the Isotopically Substituted van Der Waals Complex Ar-CO<sub>2</sub> Investigated with a Molecular Beam Fourier Transform Microwave Spectrometer. *J. Chem. Soc., Faraday Trans.* **1996**, *92*(6), 901–905. <https://doi.org/10.1039/FT9969200901>.
- (126) Peterson, K. I.; Suenram, R. D.; Lovas, F. J. The Structure of the CO<sub>2</sub>-CO<sub>2</sub>-H<sub>2</sub>O van Der Waals Complex Determined by Microwave Spectroscopy. *J. Chem. Phys.* **1989**, *90*(11), 5964–5970. <https://doi.org/10.1063/1.456362>.
- (127) Peterson, K. I.; Klemperer, W. Structure and Internal Rotation of H<sub>2</sub>O-CO<sub>2</sub>, HDO-CO<sub>2</sub>, and D<sub>2</sub>O-CO<sub>2</sub> van Der Waals Complexes. *J. Chem. Phys.* **1983**, *80*(6), 2439–2445. <https://doi.org/10.1063/1.446993>.
- (128) Moazzen-Ahmadi, N.; McKellar, A. R. W. Spectroscopy of Dimers, Trimers and Larger Clusters of Linear Molecules. *Int. Rev. Phys. Chem.* **2013**, *32*(4), 611–650. <https://doi.org/10.1080/0144235X.2013.813799>.
- (129) Christenholz, C. L.; Dorris, R. E.; Peebles, R. A.; Peebles, S. A. Characterization of Two Isomers of the Vinyl Fluoride···carbon Dioxide Dimer by Rotational Spectroscopy. *J. Phys. Chem. A* **2014**, *118*(38), 8765–8772. <https://doi.org/10.1021/jp507869y>.
- (130) Serafin, M. M.; Peebles, R. A.; Peebles, S. A. Internal Rotation Effects in the Pulsed Jet Rotational Spectrum of the Trifluoromethane-Carbon Dioxide Dimer. *J. Mol. Spectrosc.* **2008**, *250*(1), 1–7. <https://doi.org/10.1016/j.jms.2008.03.019>.
- (131) Anderton, A. M.; Peebles, R. A.; Peebles, S. A. Rotational Spectrum and Structure of the 1,1-Difluoroethylene···Carbon Dioxide Complex. *J. Phys. Chem. A* **2016**, *120*(2), 247–253. <https://doi.org/10.1021/acs.jpca.5b11345>.
- (132) Dorris, R. E.; Trendell, W. C.; Peebles, R. A.; Peebles, S. A. Rotational Spectrum, Structure, and Interaction Energy of the Trifluoroethylene···Carbon

- Dioxide Complex. *J. Phys. Chem. A* **2016**, *120*(40), 7865–7872. <https://doi.org/10.1021/acs.jpca.6b08286>.
- (133) Orita, Y.; Kawashima, Y.; Hirota, E. Fourier Transform Microwave Spectrum of the CO<sub>2</sub>-Propylene Oxide Complex. *J. Mol. Spectrosc.* **2011**, *268*(1–2), 78–84. <https://doi.org/10.1016/j.jms.2011.03.021>.
- (134) Li, M.; Lei, J.; Feng, G.; Grabow, J. U.; Gou, Q. The Rotational Spectrum of Acetophenone-CO<sub>2</sub>: Preferred Non-Covalent Interactions. *Spectrochim. Acta, Part A* **2020**, *238*, 118424. <https://doi.org/10.1016/j.saa.2020.118424>.
- (135) Xie, F.; Sun, W.; Pinacho, P.; Schnell, M. CO<sub>2</sub> Aggregation on Monoethanolamine: Observations from Rotational Spectroscopy. *Angew. Chem. Int. Ed.* **2023**, *62*(14), e202218539(2 of 7). <https://doi.org/10.1002/anie.202218539>.
- (136) Varadwaj, P. R.; Varadwaj, A.; Marques, H. M.; Yamashita, K. Definition of the Tetrel Bond. *CrystEngComm* **2023**, *25*(9), 1411–1423. <https://doi.org/10.1039/d2ce01621d>.
- (137) Legon, A. C. Tetrel, Pnictogen and Chalcogen Bonds Identified in the Gas Phase before They Had Names: A Systematic Look at Non-Covalent Interactions. *Phys. Chem. Chem. Phys.* **2017**, *19*, 14884–14896. <https://doi.org/10.1039/c7cp02518a>.
- (138) Zeng, Y. P.; Sharpe, S. W.; Shin, S. K.; Wittig, C.; Beaudet, R. A. Infrared Spectroscopy of CO<sub>2</sub>-D(H)Br: Molecular Structure and Its Reliability. *J. Chem. Phys.* **1992**, *97*(8), 5392–5402. <https://doi.org/10.1063/1.463799>.
- (139) Prichard, D. G.; Nandi, R. N.; Muentner, J. S.; Howard, B. J. Vibration-Rotation Spectrum of the Carbon Dioxide-Acetylene van Der Waals Complex in the 3 $\mu$  Region. *J. Chem. Phys.* **1988**, *89*(3), 1245–1250. <https://doi.org/10.1063/1.455175>.
- (140) Gnanasekar, S. P.; Arunan, E. Rotational Spectroscopic Studies of the Tetrel Bonded CH<sub>3</sub>CN-CO<sub>2</sub> Complex. *J. Mol. Spectrosc.* **2022**, *388*, 111671. <https://doi.org/10.1016/j.jms.2022.111671>.
- (141) Doran, J. L.; Hon, B.; Leopold, K. R. Rotational Spectrum and Structure of the Pyridine-CO<sub>2</sub> van Der Waals Complex. *J. Mol. Struct.* **2012**, *1019*, 191–195. <https://doi.org/10.1016/j.molstruc.2012.03.039>.
- (142) Newby, J. J.; Peebles, R. A.; Peebles, S. A. Structure of the Dimethyl Ether-CO<sub>2</sub> van Der Waals Complex from Microwave Spectroscopy. *J. Phys. Chem. A* **2004**, *108*(51), 11234–11240. <https://doi.org/10.1021/jp0464573>.
- (143) Gao, S.; Obenchain, D. A.; Lei, J.; Feng, G.; Herbers, S.; Gou, Q.; Grabow, J. U. Tetrel Bonds and Conformational Equilibria in the Formamide-CO<sub>2</sub> Complex: A Rotational Study. *Phys. Chem. Chem. Phys.* **2019**, *21*(13), 7016–7020. <https://doi.org/10.1039/c9cp00055k>.
- (144) Lei, J.; Tian, X.; Wang, J.; Herbers, S.; Li, M.; Gao, T.; Zou, S.; Grabow, J., Gou, Q. How Nonpolar CO<sub>2</sub> Aggregates on Cycloalkenes: A Case Study with

- Cyclopentene-(CO<sub>2</sub>)<sub>1-3</sub> Clusters, *J. Phys. Chem. Lett.* **2024**, *15*(30), 7597-7602. 10.1021/acs.jpcllett.4c01737.
- (145) Wang, H.; Caminati, W.; Li, M.; Chen, J.; Tian, X.; Grabow, J. U.; Gou, Q. n→π\* Interaction Enabling Transient Inversion of Chirality. *J. Phys. Chem. Lett.* **2023**, *14*(39), 8874–8879. <https://doi.org/10.1021/acs.jpcllett.3c02264>.
- (146) Konarev, D. V., Neretin, I. S., Slovokhotov, Y. L., Yudanova, E. I., Drichko, N. Y. V., Shulga, Y. M., Tarasov, B. P., Gumanov, L. L.; Batsanov, A. S.; Howard JA, Lyubovskaya RN. New molecular complexes of fullerenes C60 and C70 with tetraphenylporphyrins [M(tp)], in which M=H2, Mn, Co, Cu, Zn, and FeCl. *Chem.* **2001**, *7*(12), 2605–2616.
- (147) Steiner, T. The Whole Palette of Hydrogen Bonds. *Angew. Chem. Int. Ed.* **2002**, *41*, 48.
- (148) Kornreich, M.; Avinery, R.; Beck, R. Modern X-Ray Scattering Studies of Complex Biological Systems. *Curr. Opin. Biotechnol.* **2013**, *24*(4), 716–723. <https://doi.org/10.1016/j.copbio.2013.01.005>.
- (149) Barnes, A. J. Molecular Complexes of the Hydrogen Halides Studied by Matrix Isolation Infrared Spectroscopy. *J. Mol. Struct.* **1983**, *100*(C), 259–280. [https://doi.org/10.1016/0022-2860\(83\)90096-0](https://doi.org/10.1016/0022-2860(83)90096-0).
- (150) Sarkar, S.; Ramanathan, N.; Sundararajan, K. Effect of Methyl Substitution on the N-H···O Interaction in Complexes of Pyrrole with Water, Methanol, and Dimethyl Ether: Matrix Isolation Infrared Spectroscopy and Ab Initio Computational Studies. *J. Phys. Chem. A* **2018**, *122*(9), 2445–2460. <https://doi.org/10.1021/acs.jpca.8b00023>.
- (151) Chandra, S.; Suryaprasad, B.; Ramanathan, N.; Sundararajan, K. Dominance of Unique P···π Phosphorus Bonding with π Donors: Evidence Using Matrix Isolation Infrared Spectroscopy and Computational Methodology. *Phys. Chem. Chem. Phys.* **2020**, *22*(36), 20771–20791. <https://doi.org/10.1039/d0cp02880k>.
- (152) Geboes, Y.; De Vleeschouwer, F.; De Proft, F.; Herrebout, W. A. Exploiting the σ-Hole Concept: An Infrared and Raman-Based Characterization of the S···O Chalcogen Bond between 2,2,4,4-Tetrafluoro-1,3-Dithiethane and Dimethyl Ether. *Chem. -Eur. J.* **2017**, *23*(68), 17384–17392. <https://doi.org/10.1002/chem.201704406>.
- (153) Geboes, Y.; De Vos, E.; Herrebout, W. A. S···S and S···P Chalcogen Bonding in Solution: A Cryospectroscopic Study of the Complexes of 2,2,4,4-Tetrafluoro-1,3-Dithietane with Dimethyl Sulfide and Trimethylphosphine. *New J. Chem.* **2018**, *42*(13), 10563–10571. <https://doi.org/10.1039/c8nj01648h>.
- (154) Ahokas, J. M. E.; Kosendiak, I.; Krupa, J.; Wierzejewska, M.; Lundell, J. Raman Spectroscopy of Glycolic Acid Complexes with N<sub>2</sub>. *J. Mol. Struct.* **2019**, *1183*, 367–372. <https://doi.org/10.1016/j.molstruc.2019.01.080>.
- (155) Suzuki, S.; Green, P. G.; Bumgarner, R. E.; Dasgupta, S.; Goddard, W. A.; Blake, G. A. Benzene Forms Hydrogen Bonds with Water. *Science* **1992**, *257*(5072), 942–945. <https://doi.org/10.1126/science.257.5072.942>.

- (156) Zwier, T. S. Laser Spectroscopy of Jet-Cooled Biomolecules and Their Water-Containing Clusters: Water Bridges and Molecular Conformation. *J. Phys. Chem. A* **2001**, *105*(39), 8827–8839. <https://doi.org/10.1021/jp011659+>.
- (157) Zhao, Y.; Li, Z.; Liu, J.; Hu, C.; Zhang, H.; Qin, B.; Wu, Y. Intermolecular Vibrational Modes and H-Bond Interactions in Crystalline Urea Investigated by Terahertz Spectroscopy and Theoretical Calculation. *Spectrochim. Acta, Part A* **2018**, *189*, 528–534. <https://doi.org/10.1016/j.saa.2017.08.041>.
- (158) Andersen, J.; Heimdal, J.; Nelander, B.; Wugt Larsen, R. Competition between Weak OH $\cdot\pi$  and CH $\cdot$ O Hydrogen Bonds: THz Spectroscopy of the C<sub>2</sub>H<sub>2</sub>-H<sub>2</sub>O and C<sub>2</sub>H<sub>4</sub>-H<sub>2</sub>O Complexes. *J. Chem. Phys.* **2017**, *146*(19), 194302. <https://doi.org/10.1063/1.4983293>.
- (159) Cuniasse, P.; Tavares, P.; Orlova, E. V.; Zinn-Justin, S. Structures of Biomolecular Complexes by Combination of NMR and CryoEM Methods. *Curr. Opin. Struct. Biol.* **2017**, *43*, 104–113. <https://doi.org/10.1016/j.sbi.2016.12.008>.
- (160) Platzner, G.; Mayer, M.; Beier, A.; Brüscheiler, S.; Fuchs, J. E.; Engelhardt, H.; Geist, L.; Bader, G.; Schörghuber, J.; Lichtenecker, R.; Wolkerstorfer, B.; Kessler, D.; McConnell, D. B.; Konrat, R. PI by NMR: Probing CH $\pi$  Interactions in Protein–Ligand Complexes by NMR Spectroscopy. *Angew. Chem. Int. Ed.* **2020**, *59*(35), 14861–14868. <https://doi.org/10.1002/anie.202003732>.
- (161) Wang, X. Bin. Cluster Model Studies of Anion and Molecular Specificities via Electrospray Ionization Photoelectron Spectroscopy. *J. Phys. Chem. A* **2017**, *121*(7), 1389–1401. <https://doi.org/10.1021/acs.jpca.6b09784>.
- (162) Zhang, X.; Liu, G.; Ciborowski, S.; Wang, W.; Gong, C.; Yao, Y.; Bowen, K. Spectroscopic Measurement of a Halogen Bond Energy. *Angew. Chem. Int. Ed.* **2019**, *58*(33), 11400–11403. <https://doi.org/10.1002/anie.201906279>.
- (163) Dean, J. C.; Buchanan, E. G.; Zwier, T. S. Mixed 14/16 Helices in the Gas Phase: Conformation-Specific Spectroscopy of Z-(Gly)<sub>n</sub>, n = 1,3,5. *J. Am. Chem. Soc.* **2012**, *134*(41), 17186–17201. <https://doi.org/10.1021/ja306652c>.
- (164) Zhang, B.; Yu, Y.; Zhang, Y. Y.; Jiang, S.; Li, Q.; Hu, H. S.; Li, G.; Zhao, Z.; Wang, C.; Xie, H.; Zhang, W.; Dai, D.; Wu, G.; Zhang, D. H.; Jiang, L.; Li, J.; Yang, X. Infrared Spectroscopy of Neutral Water Clusters at Finite Temperature: Evidence for a Noncyclic Pentamer. *Proc. Natl. Acad. Sci. USA* **2020**, *117*(27), 15423–15428. <https://doi.org/10.1073/pnas.2000601117>.
- (165) Zhang, B.; Yang, S.; Huang, Q. R.; Jiang, S.; Chen, R.; Yang, X.; Zhang, D. H.; Zhang, Z.; Kuo, J. L.; Jiang, L. Deconstructing Vibrational Motions on the Potential Energy Surfaces of Hydrogen-Bonded Complexes. *CCS Chem.* **2021**, *3*(1), 829–835. <https://doi.org/10.31635/ccschem.020.202000230>.
- (166) Li, G.; Zhang, Y. Y.; Li, Q.; Wang, C.; Yu, Y.; Zhang, B.; Hu, H. S.; Zhang, W.; Dai, D.; Wu, G.; Zhang, D. H.; Li, J.; Yang, X.; Jiang, L. Infrared Spectroscopic Study of Hydrogen Bonding Topologies in the Smallest Ice

- Cube. *Nat. Commun.* **2020**, *11*(1), 5449. <https://doi.org/10.1038/s41467-020-19226-6>.
- (167) Chatterjee, K.; Dopfer, O. Protonation of Naphthalene-(Water)<sub>n</sub> Nanoclusters: Intracluster Proton Transfer to Hydration Shell Revealed by Infrared Photodissociation Spectroscopy. *J. Phys. Chem. A* **2020**, *124*(6), 1134–1151. <https://doi.org/10.1021/acs.jpca.9b11779>.
- (168) Straka, M.; Andris, E.; Vícha, J.; Růžička, A.; Roithová, J.; Rulíšek, L. Spectroscopic and Computational Evidence of Intramolecular Au I···H + –N Hydrogen Bonding. *Angew. Chem. Int. Ed.* **2019**, *58*(7), 2011–2016. <https://doi.org/10.1002/anie.201811982>.
- (169) Xie, M.; Shen, Z.; Wang, D.; Fujii, A.; Lee, Y. P. Spectral Characterization of Three-Electron Two-Center (3e-2c) Bonds of Gaseous CH<sub>3</sub>S-S(H)CH<sub>3</sub> and (CH<sub>3</sub>SH)<sub>2</sub><sup>+</sup> and Enhancement of the 3e-2c Bond upon Protonation. *J. Phys. Chem. Lett.* **2018**, *9*(13), 3725–3730. <https://doi.org/10.1021/acs.jpcllett.8b01491>.
- (170) Richardson, J. O.; Pérez, C.; Lobsiger, S.; Reid, A. A.; Temelso, B.; Shields, G. C.; Kisiel, Z.; Wales, D. J.; Pate, B. H.; Althorpe, S. C. Concerted Hydrogen-Bond Breaking by Quantum Tunneling in the Water Hexamer Prism. *Science* **2016**, *351*(6279), 1310–1313. <https://doi.org/10.1126/science.aae0012>.
- (171) Pérez, C.; Muckle, M. T.; Zaleski, D. P.; Seifert, N. A.; Temelso, B.; Shields, G. C.; Kisiel, Z.; Pate, B. H. Structures of Cage, Prism, and Book Isomers of Water Hexamer from Broadband Rotational Spectroscopy. *Science* **2012**, *336*(6083), 897–901. <https://doi.org/10.1126/science.1220574>.
- (172) Becucci, M.; Melandri, S. High-Resolution Spectroscopic Studies of Complexes Formed by Medium-Size Organic Molecules. *Chem. Rev.* **2016**, *116*(9), 5014–5037. <https://doi.org/10.1021/acs.chemrev.5b00512>.
- (173) Xie, F.; Seifert, N. A.; Jäger, W.; Xu, Y. Conformational Panorama and Chirality Controlled Structure–Energy Relationship in a Chiral Carboxylic Acid Dimer. *Angew. Chem. Int. Ed.* **2020**, *59*(36), 15703–15710. <https://doi.org/10.1002/anie.202005685>.
- (174) Li, X.; Lu, T.; Obenchain, D. A.; Zhang, J.; Herbers, S.; Grabow, J. U.; Feng, G. The Characteristics of Disulfide-Centered Hydrogen Bonds. *Angew. Chem. Int. Ed.* **2021**, *60*(11), 5838–5842. <https://doi.org/10.1002/anie.202014364>.
- (175) Xie, F.; Fusè, M.; Hazrah, A. S.; Jäger, W.; Barone, V.; Xu, Y. Discovering the Elusive Global Minimum in a Ternary Chiral Cluster: Rotational Spectra of Propylene Oxide Trimer. *Angew. Chem. Int. Ed.* **2020**, *59*(50), 22427–22430. <https://doi.org/10.1002/anie.202010055>.
- (176) Grabow, J. U.; Stahl, W. A Pulsed ‘Molecular Beam Microwave Fourier Transform Spectrometer with Parallel Molecular Beam and Resonator Axes. *Z. Naturforsch., A: Phys. Sci.* **1990**, *45a*, 1043–1044. <https://doi.org/10.1515/zna-1990-0817>.

- (177) Grabow, J. U.; Stahl, W.; Dreizler, H. A Multioctave Coaxially Oriented Beam-Resonator Arrangement Fourier-Transform Microwave Spectrometer. *Rev. Sci. Instrum.* **1996**, *67*(12), 4072–4084. <https://doi.org/10.1063/1.1147553>.
- (178) Grabow, J. U.; Mata, S.; Alonso, J. L.; Peña, I.; Blanco, S.; López, J. C.; Cabezas, C. Rapid Probe of the Nicotine Spectra by High-Resolution Rotational Spectroscopy. *Phys. Chem. Chem. Phys.* **2011**, *13*(47), 21063–21069. <https://doi.org/10.1039/c1cp22197c>.
- (179) Brown, G. G.; Dian, B. C.; Douglass, K. O.; Geyer, S. M.; Pate, B. H. The Rotational Spectrum of Epifluorohydrin Measured by Chirped-Pulse Fourier Transform Microwave Spectroscopy. *J. Mol. Spectrosc.* **2006**, *238*(2), 200–212. <https://doi.org/10.1016/j.jms.2006.05.003>.
- (180) Laane, J. Molecular spectroscopy. *Front. Mol. Spectrosc.* 2008. <https://doi.org/10.1016/B978-0-444-53175-9.X0001-3>.
- (181) Laane, J. Molecular spectroscopy. *Front. Adv. Mol. Spectrosc.* 2017. <https://doi.org/10.1016/C2016-0-01052-5>.
- (182) Microwave Molecular Spectra. *J. Mol. Struct.* **1972**, *11*(2), 332–333. [https://doi.org/10.1016/0022-2860\(72\)80039-5](https://doi.org/10.1016/0022-2860(72)80039-5).
- (183) *Handbook of High-resolution Spectroscopy*; 2011. <https://doi.org/10.1002/9780470749593>.
- (184) Born, M.; Oppenheimer, R. Zur Quantentheorie Der Molekeln. *Ann. Phys.* **1927**, *389*(20), 457–484. <https://doi.org/10.1002/andp.19273892002>.
- (185) Buszek, R. J.; Francisco, J. S.; Anglada, J. M. Water Effects on Atmospheric Reactions. *Int. Rev. Phys. Chem.* **2011**, *30*(3), 335–369. <https://doi.org/10.1080/0144235X.2011.634128>.
- (186) Watson, J. K. G. *Aspects of Quartic and Sextic Centrifugal Effects on Rotational Energy Levels*; 1977.
- (187) Dicke, R. H.; Romer, R. H. Pulse Techniques in Microwave Spectroscopy. *Rev. Sci. Instrum.* **1955**, *26*(10), 915–928. <https://doi.org/10.1063/1.1715156>.
- (188) Steckelmacher, W. Atomic and Molecular Beam Methods, Vol 1. *Vacuum* **1991**, *42*(7), 505–506. [https://doi.org/10.1016/0042-207x\(91\)90027-g](https://doi.org/10.1016/0042-207x(91)90027-g).
- (189) Demaison, J. Accurate Structures of Non-Rigid Molecules by Microwave Spectroscopy. *Structures and Conformations of Non-Rigid Molecules*, 1993; pp 239–256. [https://doi.org/10.1007/978-94-011-2074-6\\_12](https://doi.org/10.1007/978-94-011-2074-6_12).
- (190) Ruoff, R. S.; Klots, T. D.; Emilsson, T.; Gutowsky, H. S. Relaxation of Conformers and Isomers in Seeded Supersonic Jets of Inert Gases. *J. Chem. Phys.* **1990**, *93*(5), 3142–3150. <https://doi.org/10.1063/1.458848>.
- (191) Legon, A. C. Isolation and Characterisation of Some Transient Complexes of Chemical Interest Using Pulsed-Nozzle, Fourier-Transform Microwave Spectroscopy. *J. Mol. Struct.* **1992**, *266*(C), 21–37. [https://doi.org/10.1016/0022-2860\(92\)80047-L](https://doi.org/10.1016/0022-2860(92)80047-L).

- (192) Balle, T. J.; Flygare, W. H. Fabry-Perot Cavity Pulsed Fourier Transform Microwave Spectrometer with a Pulsed Nozzle Particle Source. *Rev. Sci. Instrum.* **1981**, *52*(1), 33–45. <https://doi.org/10.1063/1.1136443>.
- (193) Grabow, J. U.; Heineking, N.; Stahl, W. The Microwave Spectrum of Tert-Butyl Isocyanate. *J. Mol. Spectrosc.* **1992**, *154*(1), 129–136. [https://doi.org/10.1016/0022-2852\(92\)90034-L](https://doi.org/10.1016/0022-2852(92)90034-L).
- (194) Grabow, J. Chemische Bindung und interne Dynamik in großen isolieren Molekülen: Rotationsspektroskopische Untersuchung. (2004).
- (195) Neill, J. L.; Shipman, S. T.; Alvarez-Valtierra, L.; Lesarri, A.; Kisiel, Z.; Pate, B. H. Rotational Spectroscopy of Iodobenzene and Iodobenzene-Neon with a Direct Digital 2-8 GHz Chirped-Pulse Fourier Transform Microwave Spectrometer. *J. Mol. Spectrosc.* **2011**, *269*(1), 21–29. <https://doi.org/10.1016/j.jms.2011.04.016>.
- (196) Brown, G. G.; Dian, B. C.; Douglass, K. O.; Geyer, S. M.; Shipman, S. T.; Pate, B. H. A Broadband Fourier Transform Microwave Spectrometer Based on Chirped Pulse Excitation. *Rev. Sci. Instrum.* **2008**, *79*(5), 053103. <https://doi.org/10.1063/1.2919120>.
- (197) Pracht, P.; Bohle, F.; Grimme, S. Automated Exploration of the Low-Energy Chemical Space with Fast Quantum Chemical Methods. *Phys. Chem. Chem. Phys.* **2020**, *22*(14), 7169–7192. <https://doi.org/10.1039/c9cp06869d>.
- (198) Grimme, S. Exploration of Chemical Compound, Conformer, and Reaction Space with Meta-Dynamics Simulations Based on Tight-Binding Quantum Chemical Calculations. *J. Chem. Theory. Comput.* **2019**, *15*(5), 2847–2862. <https://doi.org/10.1021/acs.jctc.9b00143>.
- (199) Grimme, S.; Bannwarth, C.; Shushkov, P. A Robust and Accurate Tight-Binding Quantum Chemical Method for Structures, Vibrational Frequencies, and Noncovalent Interactions of Large Molecular Systems Parametrized for All Spd-Block Elements ( $Z = 1-86$ ). *J. Chem. Theory. Comput.* **2017**, *13*(5), 1989–2009. <https://doi.org/10.1021/acs.jctc.7b00118>.
- (200) Bannwarth, C.; Ehlert, S.; Grimme, S. GFN2-XTB - An Accurate and Broadly Parametrized Self-Consistent Tight-Binding Quantum Chemical Method with Multipole Electrostatics and Density-Dependent Dispersion Contributions. *J. Chem. Theory. Comput.* **2019**, *15*(3), 1652–1671. <https://doi.org/10.1021/acs.jctc.8b01176>.
- (201) Bursch, M.; Neugebauer, H.; Grimme, S. Structure Optimisation of Large Transition-Metal Complexes with Extended Tight-Binding Methods. *Angew. Chem. Int. Ed.* **2019**, *58*(32), 11078–11087. <https://doi.org/10.1002/anie.201904021>.
- (202) Frisch, M. J.; Trucks, G. W.; Schlegel, H. B.; Scuseria, G. E.; Robb, M. A.; Cheeseman, J. R.; Scalmani, G.; Barone, V.; Petersson, G. A.; Nakatsuji, H.; Caricato, M.; Marenich, A. V.; Bloino, J.; Janesko, B. G.; Gomperts, R.; Mennucci, B.; Hratchian, H. P.; Ortiz, J. V.; Izmaylov, A. F.; Sonnenberg, J.

- L.; Williams-Young, D.; Hing, F.; Lipparini, F.; Egidi, F.; Goings, J.; Peng, B.; Petrone, A.; Henderson, T.; Ranasinghe, D.; Zakrzewski, V. G.; Gao, J.; Rega, N.; Zheng, G.; Liang, W.; Hada, M.; Ehara, M.; Toyota, K.; Fukuda, R.; Hasegawa, J.; Ishida, M.; Nakajima, T.; Honda, Y.; Kitao, O.; Nakai, H.; Vreven, T.; Throssell, K.; Montgomery, J. A. Jr.; Peralta, J. E.; Ogliaro, F.; Bearpark, M. J.; Heyd, J. J.; Brothers, E. N.; Kudin, K. N.; Staroverov, V. N.; Keith, T. A.; Kobayashi, R.; Normand, J.; Raghavachari, K.; Rendell, A. P.; Burant, J. C.; Iyengar, S. S.; Tomasi, J.; Cossi, M.; Millam, J. M.; Klene, M.; Adamo, C.; Cammi, R.; Ochterski, J. W.; Martin, R. L.; Morokuma, K.; Farkas, O.; Foresman, J. B.; Fox, D. J. Gaussian 16, Revision A.03; Gaussian, Inc.: Wallingford CT. 2016.
- (203) Neese, F. Software Update: The ORCA Program System—Version 5.0. *Wiley Interdiscip. Rev.: Comput. Mol. Sci.* 2022. <https://doi.org/10.1002/wcms.1606>.
- (204) Glendening, E. D.; Landis, C. R.; Weinhold, F. Natural Bond Orbital Methods. *Wiley Interdiscip. Rev.: Comput. Mol. Sci.* **2012**, *2*, 1–42. <https://doi.org/10.1002/wcms.51>.
- (205) Glendening, E. D.; Streitwieser, A. Natural Energy Decomposition Analysis: An Energy Partitioning Procedure for Molecular Interactions with Application to Weak Hydrogen Bonding, Strong Ionic, and Moderate Donor-Acceptor Interactions. *J. Chem. Phys.* **1994**, *100*(4), 2900–2909. <https://doi.org/10.1063/1.466432>.
- (206) Lu, T.; Chen, F. Multiwfn: A Multifunctional Wavefunction Analyzer. *J. Comput. Chem.* **2012**, *33*(5), 580–592. <https://doi.org/10.1002/jcc.22885>.
- (207) Humphrey, W.; Dalke, A.; Schulten, K. VMD: Visual Molecular Dynamics. *J Mol Graph* **1996**, *14*(1), 33–38. [https://doi.org/10.1016/0263-7855\(96\)00018-5](https://doi.org/10.1016/0263-7855(96)00018-5).
- (208) Bader, R. F. W. A Quantum Theory of Molecular Structure and Its Applications. *Chem. Rev.* **1991**, *91*(5), 893–928. <https://doi.org/10.1021/cr00005a013>.
- (209) Johnson, E. R.; Keinan, S.; Mori-Sánchez, P.; Contreras-García, J.; Cohen, A. J.; Yang, W. Revealing Noncovalent Interactions. *J. Am. Chem. Soc.* **2010**, *132*(18), 6498–6506. <https://doi.org/10.1021/ja100936w>.
- (210) Lefebvre, C.; Khartabil, H.; Boisson, J. C.; Contreras-García, J.; Piquemal, J. P.; Hénon, E. The Independent Gradient Model: A New Approach for Probing Strong and Weak Interactions in Molecules from Wave Function Calculations. *ChemPhysChem* **2018**, *19*(6), 724–735. <https://doi.org/10.1002/cphc.201701325>.
- (211) Parrish, R. M.; Burns, L. A.; Smith, D. G. A.; Simmonett, A. C.; DePrince, A. E.; Hohenstein, E. G.; Bozkaya, U.; Sokolov, A. Y.; Di Remigio, R.; Richard, R. M.; Gonthier, J. F.; James, A. M.; McAlexander, H. R.; Kumar, A.; Saitow, M.; Wang, X.; Pritchard, B. P.; Verma, P.; Schaefer, H. F.; Patkowski, K.; King, R. A.; Valeev, E. F.; Evangelista, F. A.; Turney, J. M.; Crawford, T. D.; Sherrill, C. D. Psi4 1.1: An Open-Source Electronic Structure Program Emphasizing

- Automation, Advanced Libraries, and Interoperability. *J. Chem. Theory. Comput.* **2017**, *13*(7), 3185–3197. <https://doi.org/10.1021/acs.jctc.7b00174>.
- (212) Jeziorski, B.; Moszynski, R.; Szalewicz, K. Perturbation Theory Approach to Intermolecular Potential Energy Surfaces of van Der Waals Complexes. *Chem. Rev.* **1994**, *94*(7), 1887–1930. <https://doi.org/10.1021/cr00031a008>.
- (213) Parker, T. M.; Burns, L. A.; Parrish, R. M.; Ryno, A. G.; Sherrill, C. D. Levels of Symmetry Adapted Perturbation Theory (SAPT). I. Efficiency and Performance for Interaction Energies. *J. Chem. Phys.* **2014**, *140* (9), 094106. <https://doi.org/10.1063/1.4867135>.
- (214) Sham, L. J. Density Functional Theory. *Phys. Today* **1982**, *35*(2), 36–43. <https://doi.org/10.1063/1.2914933>.
- (215) Ochi, M.; Tsuneyuki, S. Second-Order Møller-Plesset Perturbation Theory for the Transcorrelated Hamiltonian Applied to Solid-State Calculations. *Chem. Phys. Lett.* **2015**, *621*, 177–183. <https://doi.org/10.1016/j.cplett.2015.01.009>.
- (216) Arul Anitha, A.; Stephen, A.; Arockiam, L. A Hybrid Method for Smart Irrigation System. *Int. J. Recent Technol. Eng.* **2019**, *8*(3), 2995–2998. <https://doi.org/10.35940/ijrte.C4826.098319>.
- (217) Becke, A. D. A New Mixing of Hartree-Fock and Local Density-Functional Theories. *J. Chem. Phys.* **1993**, *98*(2), 1372–1377. <https://doi.org/10.1063/1.464304>.
- (218) Perdew, J. P.; Burke, K. Generalized Gradient Approximation for the Exchange-Correlation Hole of a Many-Electron System. *Phys Rev B Condens Matter Mater Phys.* **1996**, *54*(23), 16533–16539. <https://doi.org/10.1103/PhysRevB.54.16533>.
- (219) Weigend, F.; Ahlrichs, R. Balanced Basis Sets of Split Valence, Triple Zeta Valence and Quadruple Zeta Valence Quality for H to Rn: Design and Assessment of Accuracy. *Phys. Chem. Chem. Phys.* **2005**, *7*(18), 3297–3305. <https://doi.org/10.1039/b508541a>.
- (220) Weigend, F. Accurate Coulomb-Fitting Basis Sets for H to Rn. *Phys. Chem. Chem. Phys.* **2006**, *8*(9), 1057–1065. <https://doi.org/10.1039/b515623h>.
- (221) Grimme, S.; Ehrlich, S.; Goerigk, L. Effect of the Damping Function in Dispersion Corrected Density Functional Theory. *J. Comput. Chem.* **2011**, *32*(7), 1456–1465. <https://doi.org/10.1002/jcc.21759>.
- (222) Grimme, S.; Antony, J.; Ehrlich, S.; Krieg, H. A Consistent and Accurate Ab Initio Parametrization of Density Functional Dispersion Correction (DFT-D) for the 94 Elements H-Pu. *J. Chem. Phys.* **2010**, *132*(15), 154104. <https://doi.org/10.1063/1.3382344>.
- (223) Boys, S. F.; Bernardi, F. The Calculation of Small Molecular Interactions by the Differences of Separate Total Energies. Some Procedures with Reduced Errors. *Mol. Phys.* **1970**, *19*(4), 553–566. <https://doi.org/10.1080/00268977000101561>.

- (224) Contreras-García, J.; Johnson, E. R.; Keinan, S.; Chaudret, R.; Piquemal, J. P.; Beratan, D. N.; Yang, W. NCIPLLOT: A Program for Plotting Noncovalent Interaction Regions. *J. Chem. Theory Comput.* **2011**, *7*(3), 625–632. <https://doi.org/10.1021/ct100641a>.
- (225) Laplaza, R.; Peccati, F.; A. Boto, R.; Quan, C.; Carbone, A.; Piquemal, J. P.; Maday, Y.; Contreras-García, J. NCIPLLOT and the Analysis of Noncovalent Interactions Using the Reduced Density Gradient. *Wiley Interdiscip. Rev.: Comput. Mol. Sci.* **2021**, *11*, e1497. <https://doi.org/10.1002/wcms.1497>.
- (226) Weinhold, F.; Landis, C. R. Natural Bond Orbitals and Extensions of Localized Bonding Concepts. *Chem. Educ. Res. Pract.* **2001**, *2*(2), 91–104. <https://doi.org/10.1039/b1rp90011k>.
- (227) Weinhold, F.; Landis, C. R. *Discovering Chemistry with Natural Bond Orbitals*; 2012. <https://doi.org/10.1002/9781118229101>.
- (228) Pickett, H. M. The Fitting and Prediction of Vibration-Rotation Spectra with Spin Interactions. *J. Mol. Spectrosc.* **1991**, *148*(2), 371–377. [https://doi.org/10.1016/0022-2852\(91\)90393-O](https://doi.org/10.1016/0022-2852(91)90393-O).
- (229) Hartwig, H.; Dreizler, H. The Microwave Spectrum of Trans-2,3-Dimethyloxirane in Torsional Excited States. *Z. Naturforsch., A:Phys. Sci.* **1996**, *51*(8), 923–932. <https://doi.org/10.1515/zna-1996-0807>.
- (230) Kisiel, Z.; Pszczółkowski, L.; Medvedev, I. R.; Winnewisser, M.; De Lucia, F. C.; Herbst, E. Rotational Spectrum of Trans-Trans Diethyl Ether in the Ground and Three Excited Vibrational States. *J. Mol. Spectrosc.* **2005**, *233*(2), 231–243. <https://doi.org/10.1016/j.jms.2005.07.006>.
- (231) Kisiel, Z.; Pszczółkowski, L.; Drouin, B. J.; Brauer, C. S.; Yu, S.; Pearson, J. C.; Medvedev, I. R.; Fortman, S.; Neese, C. Broadband Rotational Spectroscopy of Acrylonitrile: Vibrational Energies from Perturbations. *J. Mol. Spectrosc.* **2012**, *280*(1), 134–144. <https://doi.org/10.1016/j.jms.2012.06.013>.
- (232) Western, C. M. PGOPHER: A Program for Simulating Rotational, Vibrational and Electronic Spectra. *J. Quant. Spectrosc. Radiat. Transf.* **2017**, *186*, 221–242. <https://doi.org/10.1016/j.jqsrt.2016.04.010>.
- (233) Seifert, N. A.; Finneran, I. A.; Perez, C.; Zaleski, D. P.; Neill, J. L.; Steber, A. L.; Suenram, R. D.; Lesarri, A.; Shipman, S. T.; Pate, B. H. AUTOFIT, an Automated Fitting Tool for Broadband Rotational Spectra, and Applications to 1-Hexanal. *J. Mol. Spectrosc.* **2015**, *312*, 13–21. <https://doi.org/10.1016/j.jms.2015.02.003>.
- (234) Haque, A.; Alenezi, K. M.; Khan, M. S.; Wong, W. Y.; Raithby, P. R. Non-Covalent Interactions (NCIs) in  $\pi$ -Conjugated Functional Materials: Advances and Perspectives. *Chem. Soc. Rev.* **2023**, *52*, 454–472. <https://doi.org/10.1039/d2cs00262k>.
- (235) Basha, A. A.; Kubaib, A.; Azam, M. Exploring the Antiviral Potency of  $\gamma$ -FP and PA Compounds: Electronic Characterization, Non-Covalent Interaction Analysis and Docking Profiling with Emphasis on QTAIM Aspects. *Comput.*

- Theor. Chem.* **2024**, *1231*, 114412. <https://doi.org/10.1016/j.comptc.2023.114412>.
- (236) Neel, A. J.; Hilton, M. J.; Sigman, M. S.; Toste, F. D. Exploiting Non-Covalent  $\pi$  Interactions for Catalyst Design. *Nature* **2017**, *543*, 637–646. <https://doi.org/10.1038/nature21701>.
- (237) Medel, R.; Camiruaga, A.; Saragi, R. T.; Pinacho, P.; Pérez, C.; Schnell, M.; Lesarri, A.; Suhm, M. A.; Fernández, J. A. Rovibronic Signatures of Molecular Aggregation in the Gas Phase: Subtle Homochirality Trends in the Dimer, Trimer and Tetramer of Benzyl Alcohol. *Phys. Chem. Chem. Phys.* **2021**, *23*(41), 23610–23624. <https://doi.org/10.1039/d1cp03508h>.
- (238) Camiruaga, A.; Saragi, R. T.; Torres-Hernández, F.; Juanes, M.; Usabiaga, I.; Lesarri, A.; Fernández, J. A. The Evolution towards Cyclic Structures in the Aggregation of Aromatic Alcohols: The Dimer, Trimer and Tetramer of 2-Phenylethanol. *Phys. Chem. Chem. Phys.* **2022**, *24*(40), 24800–24809. <https://doi.org/10.1039/d2cp03485a>.
- (239) Schnell, M.; Erlekam, U.; Bunker, P. R.; Von Helden, G.; Grabow, J. U.; Meijer, G.; Van Der Avoird, A. Unraveling the Internal Dynamics of the Benzene Dimer: A Combined Theoretical and Microwave Spectroscopy Study. *Phys. Chem. Chem. Phys.* **2013**, *15*(25), 10207–10223. <https://doi.org/10.1039/c3cp51181b>.
- (240) Sung, E. M.; Harmony, M. The Microwave Spectrum, Structure, and Dipole Moment of 2-Mercaptoethanol; Evidence for an Intramolecular OH $\cdots$ S Hydrogen Bond. *J. Am. Chem. Soc.* **1977**, *99*(17), 5603–5608. <https://doi.org/10.1021/ja00459a012>.
- (241) Howard, D. L.; Kjaergaard, H. G. Hydrogen Bonding to Divalent Sulfur. *Phys. Chem. Chem. Phys.* **2008**, *10*(28), 4113–4118. <https://doi.org/10.1039/b806165c>.
- (242) Biswal, H. S.; Wategaonkar, S. O-H $\cdots$ O versus O-H $\cdots$ S Hydrogen Bonding. 3. IR-UV Double Resonance Study of Hydrogen Bonded Complexes of p-Cresol with Diethyl Ether and Its Sulfur Analog. *J. Phys. Chem. A* **2010**, *114*(19), 5947–5957. <https://doi.org/10.1021/jp100439w>.
- (243) Hermann, J.; Alfè, D.; Tkatchenko, A. Nanoscale  $\pi$ - $\pi$  Stacked Molecules Are Bound by Collective Charge Fluctuations. *Nat. Commun.* **2017**, *8*, 14052. <https://doi.org/10.1038/ncomms14052>.
- (244) Juanes, M.; Saragi, R. T.; Caminati, W.; Lesarri, A. The Hydrogen Bond and Beyond: Perspectives for Rotational Investigations of Non-Covalent Interactions. *Chem. -Eur. J.* **2019**, *25*, 11402–11411. <https://doi.org/10.1002/chem.201901113>.
- (245) Chen, D.; Oezguen, N.; Urvil, P.; Ferguson, C.; Dann, S. M.; Savidge, T. C. Regulation of Protein-Ligand Binding Affinity by Hydrogen Bond Pairing. *Sci. Adv.* **2016**, *2*(3), e1501240. <https://doi.org/10.1126/sciadv.1501240>.

- (246) Shi, X.; Bao, W. Hydrogen-Bonded Conjugated Materials and Their Application in Organic Field-Effect Transistors. *Front. Chem.* **2021**, *9*, 723718. <https://doi.org/10.3389/fchem.2021.723718>.
- (247) Caminati, W.; Grabow, J. U. Advancements in Microwave Spectroscopy. *Front. Adv. Mol. Spectrosc.* 2017; pp 569–598. <https://doi.org/10.1016/B978-0-12-811220-5.00018-6>.
- (248) Dubinets, N. O.; Safonov, A. A; Bagaturyants, A. A. Structures and Binding Energies of the Naphthalene Dimer in Its Ground and Excited States. *J. Phys. Chem. A* **2016**, *120*(17), 2779–2782. <https://doi.org/10.1021/acs.jpca.6b03761>.
- (249) Saeki, M.; Akagi, H.; Fujii, M. Theoretical Study on the Structure and the Frequency of Isomers of the Naphthalene Dimer. *J. Chem. Theory Comput.* **2006**, *2*(4), 1176–1183. <https://doi.org/10.1021/ct050278n>.
- (250) Wilson, A. K.; Van Mourik, T.; Dunning, T. H. Gaussian Basis Sets for Use in Correlated Molecular Calculations. VI. Sextuple Zeta Correlation Consistent Basis Sets for Boron through Neon. *J. Mol. Struct.: THEOCHEM* **1996**, *388*(1–3), 339–349. [https://doi.org/10.1016/s0166-1280\(96\)80048-0](https://doi.org/10.1016/s0166-1280(96)80048-0).
- (251) Hohenstein, E. G.; Sherrill, C. D. Density Fitting of Intramonomer Correlation Effects in Symmetry-Adapted Perturbation Theory. *J. Chem. Phys.* **2010**, *133*(1), 014101. <https://doi.org/10.1063/1.3451077>.
- (252) Nair, K. P. R.; Herbers, S.; Nguyen, H. V. L.; Grabow, J. U. The Structure and Low-Barrier Methyl Torsion of 3-Fluorotoluene. *Spectrochim Acta A Mol Biomol Spectrosc* **2020**, *242*(5), 118709. <https://doi.org/10.1016/j.saa.2020.118709>.
- (253) Nguyen, H. V. L.; Caminati, W.; Grabow, J. U. The LAM of the Rings: Large Amplitude Motions in Aromatic Molecules Studied by Microwave Spectroscopy. *Molecules* **2022**, *27*(12), 3948. <https://doi.org/10.3390/molecules27123948>.
- (254) Hansen, J.; Kharecha, P.; Sato, M.; Masson-Delmotte, V.; Ackerman, F.; Beerling, D. J.; Hearty, P. J.; Hoegh-Guldberg, O.; Hsu, S. L.; Parmesan, C.; Rockstrom, J.; Rohling, E. J.; Sachs, J.; Smith, P.; Steffen, K.; Van Susteren, L.; Von Schuckmann, K.; Zachos, J. C. Assessing “Dangerous Climate Change”: Required Reduction of Carbon Emissions to Protect Young People, Future Generations and Nature. *PLoS One* **2013**, *8*(12), e81648. <https://doi.org/10.1371/journal.pone.0081648>.
- (255) Meinshausen, M.; Smith, S. J.; Calvin, K.; Daniel, J. S.; Kainuma, M. L. T.; Lamarque, J.; Matsumoto, K.; Montzka, S. A.; Raper, S. C. B.; Riahi, K.; Thomson, A.; Velders, G. J. M.; van Vuuren, D. P. P. The RCP Greenhouse Gas Concentrations and Their Extensions from 1765 to 2300. *Clim. Change* **2011**, *109*(1), 213–241. <https://doi.org/10.1007/s10584-011-0156-z>.
- (256) Dziejarski, B.; Serafin, J.; Andersson, K.; Krzyżyńska, R. CO<sub>2</sub> Capture Materials: A Review of Current Trends and Future Challenges. *Mater. Today*

- Sustainability*. **2023**, *24*, 100483. <https://doi.org/10.1016/j.mtsust.2023.100483>.
- (257) Shi, Y.; Ni, R.; Zhao, Y. Review on Multidimensional Adsorbents for CO<sub>2</sub> Capture from Ambient Air: Recent Advances and Future Perspectives. *Energy and Fuels* **2023**, *37*(9), 6365–6381. <https://doi.org/10.1021/acs.energyfuels.3c00381>.
- (258) Liu, H.; Lu, H.; Hu, H. CO<sub>2</sub> Capture and Mineral Storage: State of the Art and Future Challenges. *Renewable Sustainable Energy Rev.* **2024**, *189*, 113908. <https://doi.org/10.1016/j.rser.2023.113908>.
- (259) Grabowski, S. J. Pnictogen and Tetrel Bonds—Tetrahedral Lewis Acid Centres. *Struct. Chem.* **2019**, *30*(4), 1141–1152. <https://doi.org/10.1007/s11224-019-01358-1>.
- (260) Desiraju, G. R.; Shing Ho, P.; Kloo, L.; Legon, A. C.; Marquardt, R.; Metrangolo, P.; Politzer, P.; Resnati, G.; Rissanen, K. Definition of the Halogen Bond (IUPAC Recommendations 2013). *Pure Appl. Chem.* **2013**, *85*(8), 1711–1713. <https://doi.org/10.1351/PAC-REC-12-05-10>.
- (261) Resnati, G.; Bryce, D. L.; Desiraju, G. R.; Frontera, A.; Krossing, I.; Legon, A. C.; Metrangolo, P.; Nicotra, F.; Rissanen, K.; Scheiner, S.; Terraneo, G. Definition of the Pnictogen Bond (IUPAC Recommendations 2023). *Pure Appl. Chem.* **2024**, *96*(1), 135–145. <https://doi.org/10.1515/pac-2020-1002>.
- (262) Lu, T.; Zhang, J.; Gou, Q.; Feng, G. Structure and C···N Tetrel-Bonding of the Isopropylamine-CO<sub>2</sub> complex Studied by Microwave Spectroscopy and Theoretical Calculations. *Phys. Chem. Chem. Phys.* **2020**, *22*(16), 8467–8475. <https://doi.org/10.1039/d0cp00925c>.
- (263) Wang, H.; Wang, X.; Tian, X.; Cheng, W.; Zheng, Y.; Obenchain, D. A.; Xu, X.; Gou, Q. Competitive Tetrel Bond and Hydrogen Bond in Benzaldehyde-CO<sub>2</sub>: Characterization: Via Rotational Spectroscopy. *Phys. Chem. Chem. Phys.* **2021**, *23*(45), 25784–25788. <https://doi.org/10.1039/d1cp03608d>.
- (264) Vigorito, A.; Gou, Q.; Calabrese, C.; Melandri, S.; Maris, A.; Caminati, W. How CO<sub>2</sub> Interacts with Carboxylic Acids: A Rotational Study of Formic Acid-CO<sub>2</sub>. *ChemPhysChem* **2015**, *16*(14), 2961–2967. <https://doi.org/10.1002/cphc.201500531>.
- (265) Wang, H.; Chen, J.; Zheng, Y.; Obenchain, D. A.; Xu, X.; Gou, Q.; Grabow, J. U.; Caminati, W. Interaction Types in C<sub>6</sub>H<sub>5</sub>(CH<sub>2</sub>)NOH-CO<sub>2</sub>(<sub>n=0-4</sub>) Determined by the Length of the Side Alkyl Chain. *J. Phys. Chem. Lett.* **2022**, *13*(1), 149–155. <https://doi.org/10.1021/acs.jpcllett.1c03740>.
- (266) Wang, H.; Chen, J.; Cheng, W.; Zheng, Y.; Zou, S.; Du, W.; Xu, X.; Gou, Q. Rotational Spectrum of Anisole-CO<sub>2</sub>: Cooperative C···O Tetrel Bond and C–H···O Hydrogen Bond. *Spectrochim. Acta, Part A* **2022**, *282*(5), 121677. <https://doi.org/10.1016/j.saa.2022.121677>.
- (267) Gao, S.; Obenchain, D. A.; Lei, J.; Feng, G.; Herbers, S.; Gou, Q.; Grabow, J. U. Tetrel Bonds and Conformational Equilibria in the Formamide-CO<sub>2</sub>

- Complex: A Rotational Study. *Phys. Chem. Chem. Phys.* **2019**, *21*(13), 7016–7020. <https://doi.org/10.1039/c9cp00055k>.
- (268) Machat, M. R.; Marbach, J.; Schumacher, H.; Raju, S.; Lansing, M.; Over, L. C.; Adler, L.; Langanke, J.; Wolf, A.; Leitner, W.; Gürtler, C. Turning CO/CO<sub>2</sub>-Containing Industrial Process Gas into Valuable Building Blocks for the Polyurethane Industry. *React. Chem. Eng.* **2022**, *7*(3), 580–589. <https://doi.org/10.1039/d1re00508a>.
- (269) Weida, M. J.; Nesbitt, D. J. Geometric Isomerism in Clusters: High Resolution Infrared Spectroscopy of a Noncyclic CO<sub>2</sub> Trimer. *J. Chem. Phys.* **1996**, *105*(23), 10210–10223. <https://doi.org/10.1063/1.472930>.
- (270) Takeuchi, H. Geometry Optimization of Carbon Dioxide Clusters (CO<sub>2</sub>)<sub>n</sub> for 4 ≤ n ≤ 40. *J. Phys. Chem. A* **2008**, *112*(33), 7492–7497. <https://doi.org/10.1021/jp802872p>.
- (271) Kabir, M.; Habiba, U. E.; Khan, W.; Shah, A.; Rahim, S.; Rios-Escalante, P. R. D. los; Farooqi, Z. U. R.; Ali, L. Climate Change Due to Increasing Concentration of Carbon Dioxide and Its Impacts on Environment in 21st Century; a Mini Review. *J. King Saud Univ., Sci.* **2023**, *35*(5), 102693. <https://doi.org/10.1016/j.jksus.2023.102693>.
- (272) Yin, J.; Fu, W.; Zhang, J.; Ran, H.; Lv, N.; Chao, Y.; Li, H.; Zhu, W.; Liu, H.; Li, H. Unraveling the Mechanism of CO<sub>2</sub> capture and Separation by Porous Liquids. *RSC Adv.* **2020**, *10*(70), 42706–42717. <https://doi.org/10.1039/d0ra08039j>.
- (273) Vidal-Vidal, Á.; Faza, O. N.; Silva López, C. CO<sub>2</sub> Complexes with Five-Membered Heterocycles: Structure, Topology, and Spectroscopic Characterization. *J. Phys. Chem. A* **2017**, *121*(47), 9118–9130. <https://doi.org/10.1021/acs.jpca.7b09394>.
- (274) Assaf, K. I.; Qaroush, A. K.; Okashah, I. K.; Al-Qaisi, F. M.; Alsoubani, F.; Eftaiha, A. F. Activation of β-Diketones for CO<sub>2</sub> capture and Utilization. *React. Chem. Eng.* **2021**, *6*(12), 2364–2375. <https://doi.org/10.1039/d1re00278c>.

# **Gas-Phase Rotational Analysis of Non-Covalent Interactions in Thiol and Carbon Dioxide Aggregates**

## **Appendixes**

## Contents of Appendixes

<b>Table S2.1.</b> Observed rotational transitions and residuals (in MHz) for phenol and thiophenol (dimer-I).....	S1
<b>Table S2.2.</b> Observed rotational transitions and residuals (in MHz) for phenol and thiophenol (dimer-II).....	S6
<b>Table S2.3</b> Theoretical spectroscopic parameters at B3LYP-D3(BJ)/def2-TZVP for phenol and thiophenol cluster in less than 5 kJ mol <sup>-1</sup> of the relative zero-point corrected energy. ....	S8
<b>Table S3.1</b> Theoretical spectroscopic parameters at B3LYP-D3(BJ)/def2-TZVP for the first eleven isomers of 1-naphthol and 1-naphthalenethiol complex in less than 5 kJ mol <sup>-1</sup> of the relative zero-point corrected energy.....	S9
<b>Table S3.2.</b> Observed rotational transitions and residuals (in MHz) for 1-naphthol and 1-naphthalenethiol.....	S10
<b>Table S4.1</b> Theoretical spectroscopic parameters at B3LYP-D3(BJ)/def2-TZVP for the first ten isomers of 2-naphthol and 2-naphthalenethiol complex in less than 5 kJ mol <sup>-1</sup> of the relative zero-point corrected energy.....	S14
<b>Table S4.2.</b> Observed rotational transitions and residuals (in MHz) for 2-naphthol and 2-naphthalenethiol.....	S15
<b>Table S5.1.</b> Calculated geometries and spectroscopic parameters of the plausible isomers of BPL-CO <sub>2</sub> at the B3LYP-D3(BJ)/def2-TZVP level of theory.....	S19
<b>Table S5.2.</b> Calculated geometries and spectroscopic parameters of the plausible isomers of BPL-(CO <sub>2</sub> ) <sub>2</sub> at the B3LYP-D3(BJ)/def2-TZVP level of theory.....	S20
<b>Table S5.3.</b> Calculated geometries and spectroscopic parameters of the plausible isomers of BPL-(CO <sub>2</sub> ) <sub>3</sub> at the B3LYP-D3(BJ)/def2-TZVP level of theory.....	S21
<b>Table S5.4.</b> Calculated geometries and spectroscopic parameters of the plausible isomers of (BPL) <sub>2</sub> at the B3LYP-D3(BJ)/def2-TZVP level of theory.....	S24
<b>Table S5.5.</b> Calculated geometries and spectroscopic parameters of the plausible isomers of (BPL) <sub>2</sub> -CO <sub>2</sub> at the B3LYP-D3(BJ)/def2-TZVP level of theory.....	S25
<b>Table S5.6.</b> Calculated geometries and spectroscopic parameters of the plausible isomers of (BPL) <sub>2</sub> -(CO <sub>2</sub> ) <sub>2</sub> at the B3LYP-D3(BJ)/def2-TZVP level of theory.....	S26
<b>Table S5.7.</b> Calculated geometries and spectroscopic parameters of the plausible isomers of (BPL) <sub>2</sub> -(CO <sub>2</sub> ) <sub>3</sub> at the B3LYP-D3(BJ)/def2-TZVP level of theory.....	S29
<b>Table S5.8.</b> Observed rotational transitions and residuals (in MHz) for BPL-CO <sub>2</sub> .....	S33
<b>Table S5.9.</b> Observed rotational transitions and residuals (in MHz) for BPL-(CO <sub>2</sub> ) <sub>2</sub> .....	S34
<b>Table S5.10.</b> Observed rotational transitions and residuals (in MHz) for BPL-(CO <sub>2</sub> ) <sub>3</sub> .....	S36
<b>Table S5.11.</b> Observed rotational transitions and residuals (in MHz) for (BPL) <sub>2</sub> .....	S38
<b>Table S5.12.</b> Observed rotational transitions and residuals (in MHz) for (BPL) <sub>2</sub> -CO <sub>2</sub> .....	S41
<b>Table S5.13.</b> Observed rotational transitions and residuals (in MHz) for (BPL) <sub>2</sub> -(CO <sub>2</sub> ) <sub>2</sub> .....	S44

<b>Table S6.1.</b> Calculated geometries and spectroscopic parameters of the plausible isomers of CBN-CO <sub>2</sub> at the B3LYP-D3(BJ)/def2-TZVP level of theory.....	S46
<b>Table S6.2.</b> Calculated geometries and spectroscopic parameters of the plausible isomers of CBN-(CO <sub>2</sub> ) <sub>2</sub> at the B3LYP-D3(BJ)/def2-TZVP level of theory.....	S47
<b>Table S6.3.</b> Calculated geometries and spectroscopic parameters of the plausible isomers of CBN-(CO <sub>2</sub> ) <sub>3</sub> at the B3LYP-D3(BJ)/def2-TZVP level of theory.....	S48
<b>Table S6.4.</b> Calculated geometries and spectroscopic parameters of the plausible isomers of (CBN) <sub>2</sub> at the B3LYP-D3(BJ)/def2-TZVP level of theory.....	S49
<b>Table S6.5.</b> Calculated geometries and spectroscopic parameters of the plausible isomers of (CBN) <sub>2</sub> -CO <sub>2</sub> at the B3LYP-D3(BJ)/def2-TZVP level of theory.....	S50
<b>Table S6.6.</b> Calculated geometries and spectroscopic parameters of the plausible isomers of (CBN) <sub>2</sub> -(CO <sub>2</sub> ) <sub>2</sub> at the B3LYP-D3(BJ)/def2-TZVP level of theory.....	S51
<b>Table S6.7.</b> Calculated geometries and spectroscopic parameters of the plausible isomers of (CBN) <sub>2</sub> -(CO <sub>2</sub> ) <sub>3</sub> at the B3LYP-D3(BJ)/def2-TZVP level of theory.....	S53
<b>Table S6.8.</b> Observed rotational transitions and residuals (in MHz) for CBN-CO <sub>2</sub> .....	S57
<b>Table S6.9.</b> Observed rotational transitions and residuals (in MHz) for CBN-(CO <sub>2</sub> ) <sub>2</sub> .....	S58
<b>Table S6.10.</b> Observed rotational transitions and residuals (in MHz) for (CBN) <sub>2</sub> -CO <sub>2</sub> .....	S59
<b>Table S6.11.</b> Observed rotational transitions and residuals (in MHz) for (CBN) <sub>2</sub> -(CO <sub>2</sub> ) <sub>2</sub> .....	S62

**Table S2.1.** Observed rotational transitions and residuals (in MHz) for phenol and thiophenol (dimer-I).

$J'$	$K_a'$	$K_c'$	$J''$	$K_a''$	$K_c''$	Obs.	Obs.-Cal.
3	1	3	2	1	2	2444.3507	-0.0099
3	0	3	2	0	2	2542.3408	0.0027
3	2	2	2	2	1	2627.4919	0.0134
3	2	1	2	2	0	2712.6193	0.0059
3	1	2	2	1	1	2781.7607	0.0039
4	1	4	3	1	3	3238.5349	0.0070
4	0	4	3	0	3	3316.3905	0.0074
4	2	3	3	2	2	3485.5008	0.0032
4	3	2	3	3	1	3541.1596	-0.0011
4	3	1	3	3	0	3558.0158	-0.0062
4	2	2	3	2	1	3672.0753	0.0057
4	1	3	3	1	2	3675.3654	-0.0002
5	1	5	4	1	4	4021.5015	-0.0056
5	0	5	4	0	4	4070.3535	-0.0078
5	2	4	4	2	3	4328.9304	0.0021
5	4	2	4	4	1	4429.1496	0.0022
5	3	3	4	3	2	4431.4146	-0.0035
5	4	1	4	4	0	4431.5457	0.0022
5	3	2	4	3	1	4486.9184	0.0133
5	1	4	4	1	3	4533.0882	-0.0018
5	2	3	4	2	2	4635.1910	0.0055
6	1	6	5	1	5	4795.8255	0.0024
6	0	6	5	0	5	4821.8966	-0.0086
6	2	5	5	2	4	5155.6706	-0.0069
6	5	2	5	5	1	5312.2759	-0.0007
6	3	4	5	3	3	5315.9356	-0.0091
6	4	3	5	4	2	5328.5122	-0.0008
6	4	2	5	4	1	5338.9549	0.0071
6	1	5	5	1	4	5344.4624	0.0017
6	3	3	5	3	2	5447.5069	0.0041
7	1	7	6	1	6	5564.4155	-0.0057
7	0	7	6	0	6	5576.9920	-0.0122
6	2	4	5	2	3	5578.0649	0.0005
7	2	6	6	2	5	5965.3759	0.0033
7	1	6	6	1	5	6112.4682	0.0169
7	3	5	6	3	4	6189.1437	-0.0019
7	6	2	6	6	1	6194.9968	0.0129
7	6	1	6	6	0	6194.9968	-0.0178
7	5	3	6	5	2	6211.7100	-0.0157
7	5	2	6	5	1	6213.2716	0.0054
7	4	4	6	4	3	6231.0100	-0.0032
7	4	3	6	4	2	6263.8760	0.0019
8	1	8	7	1	7	6329.7033	-0.0077
8	0	8	7	0	7	6335.4135	0.0093
7	3	4	6	3	3	6433.4273	0.0071
7	2	5	6	2	4	6485.8675	-0.0053
8	2	7	7	2	6	6759.5959	-0.0003
8	1	7	7	1	6	6856.5130	0.0045

8	3	6	7	3	5	7046.4492	-0.0043
8	7	2	7	7	1	7077.7893	-0.0070
8	7	1	7	7	0	7077.7893	-0.0101
8	6	3	7	6	2	7093.0481	0.0079
9	1	9	8	1	8	7093.2746	0.0028
9	0	9	8	0	8	7095.7303	-0.0084
8	5	4	7	5	3	7116.7827	-0.0015
8	5	3	7	5	2	7122.7312	-0.0017
8	4	5	7	4	4	7132.7329	0.0035
8	4	4	7	4	3	7214.9396	0.0056
8	2	6	7	2	5	7347.7983	0.0008
8	3	5	7	3	4	7420.8856	-0.0037
9	2	8	8	2	7	7541.4538	0.0125
9	1	8	8	1	7	7597.1961	-0.0072
10	1	10	9	1	9	7855.9995	0.0091
10	0	10	9	0	9	7857.0366	0.0098
9	3	7	8	3	6	7885.0985	0.0038
2	1	2	1	0	1	2002.2869	-0.0024
3	3	0	3	2	1	2011.9548	-0.0096
5	2	4	5	1	5	2169.9786	-0.0011
4	3	2	4	2	3	2172.5178	0.0159
6	1	5	6	0	6	2197.2299	-0.0082
8	2	6	8	1	7	2242.7797	0.0054
10	3	7	10	2	8	2251.4701	-0.0001
3	0	3	2	1	2	2269.0773	-0.0040
5	3	3	5	2	4	2275.0020	0.0102
8	4	4	8	3	5	2353.4656	0.0092
6	3	4	6	2	5	2435.2670	0.0080
6	2	5	6	1	6	2529.8357	0.0014
7	4	3	7	3	4	2559.4234	0.0116
7	3	5	7	2	6	2659.0347	0.0027
3	1	3	2	0	2	2717.6142	-0.0031
6	4	2	6	3	3	2728.9629	0.0050
7	1	6	7	0	7	2732.6941	0.0088
4	1	3	3	2	2	2737.4744	0.0054
9	2	7	9	1	8	2802.3362	0.0028
5	4	1	5	3	2	2837.5149	0.0021
4	4	0	4	3	1	2892.8757	0.0012
5	4	2	5	3	3	2910.0537	0.0037
4	4	1	4	3	2	2912.3187	-0.0020
6	4	3	6	3	4	2922.6184	0.0002
7	2	6	7	1	7	2930.7842	-0.0013
8	3	6	8	2	7	2945.8880	-0.0012
2	2	1	1	1	0	2957.2725	0.0031
7	4	4	7	3	5	2964.4847	-0.0010
8	4	5	8	3	6	3050.7684	0.0068
2	2	0	1	1	1	3093.3380	0.0062
4	0	4	3	1	3	3141.1052	0.0014
9	4	6	9	3	7	3193.9507	0.0023
10	5	5	10	4	6	3196.9786	0.0138
8	1	7	8	0	8	3253.7937	0.0041
9	3	7	9	2	8	3289.5327	-0.0099
8	2	7	8	1	8	3360.6768	0.0059

10	2	8	10	1	9	3376.4482	-0.0001
10	4	7	10	3	8	3401.4463	0.0081
4	1	4	3	0	3	3413.8083	0.0012
9	5	4	9	4	5	3415.9064	0.0066
8	5	3	8	4	4	3568.7804	0.0000
7	5	2	7	4	3	3660.9769	-0.0044
11	4	8	11	3	9	3674.2568	0.0079
10	3	8	10	2	9	3679.4424	-0.0034
9	5	5	9	4	6	3687.5606	-0.0041
8	5	4	8	4	5	3689.1818	0.0049
10	5	6	10	4	7	3714.7403	0.0049
7	3	4	6	4	3	3717.6013	0.0032
3	2	2	2	1	1	3719.6517	-0.0018
6	5	2	6	4	3	3724.4081	-0.0013
5	5	0	5	4	1	3737.9742	0.0003
5	5	1	5	4	2	3740.6325	-0.0133
9	1	8	9	0	9	3755.2595	0.0053
5	1	4	4	2	3	3785.0618	0.0004
9	2	8	9	1	9	3808.8441	0.0038
6	2	4	5	3	3	3903.6632	-0.0026
11	2	9	11	1	10	3931.4985	0.0084
5	0	5	4	1	4	3972.9357	-0.0015
11	3	9	11	2	10	4103.3149	0.0011
5	1	5	4	0	4	4118.9313	0.0001
3	2	1	2	1	2	4167.7117	-0.0019
10	1	9	10	0	10	4241.9076	-0.0056
10	2	9	10	1	10	4267.3945	-0.0015
11	6	5	11	5	6	4274.5709	-0.0072
10	6	4	10	5	5	4400.7063	-0.0076
12	6	7	12	5	8	4423.1176	0.0111
4	2	3	3	1	2	4423.3918	-0.0025
13	6	8	13	5	9	4435.9088	0.0023
11	6	6	11	5	7	4439.2586	-0.0005
10	6	5	10	5	6	4469.8954	-0.0028
9	6	3	9	5	4	4478.8361	-0.0093
9	6	4	9	5	5	4503.8581	0.0018
8	6	2	8	5	3	4526.6509	-0.0032
7	6	1	7	5	2	4556.1433	-0.0069
7	6	2	7	5	3	4557.9553	-0.0175
6	6	0	6	5	1	4574.4181	0.0162
6	6	1	6	5	2	4574.7161	0.0014
11	1	10	11	0	11	4719.5911	-0.0013
3	3	1	2	2	0	4721.6892	0.0012
3	3	0	2	2	1	4747.2000	-0.0070
6	0	6	5	1	5	4773.3426	0.0072
6	1	5	5	2	4	4800.5939	0.0000
6	1	6	5	0	5	4844.3913	-0.0016
7	2	5	6	3	4	5073.5950	0.0010
5	2	4	4	1	3	5076.9687	0.0117
11	7	4	11	6	5	5291.9030	-0.0111
11	7	5	11	6	6	5305.4571	-0.0071
10	7	3	10	6	4	5338.8000	-0.0039
10	7	4	10	6	5	5343.0080	-0.0073

8	7	1	8	6	2	5393.7554	-0.0072
8	7	2	8	6	3	5393.9939	0.0045
4	2	2	3	1	3	5395.4244	0.0018
7	7	0	7	6	1	5409.1930	-0.0070
7	7	1	7	6	2	5409.2407	0.0075
4	3	2	3	2	1	5550.2295	-0.0058
7	0	7	6	1	6	5554.5211	0.0045
7	1	7	6	0	6	5586.9102	0.0012
6	2	5	5	1	4	5699.5511	0.0066
7	1	6	6	2	5	5757.3557	-0.0118
9	3	6	8	4	5	6158.0539	0.0008
10	8	2	10	7	3	6210.2437	-0.0178
10	8	3	10	7	4	6210.3987	-0.0047
8	2	6	7	3	5	6232.2378	-0.0078
5	3	3	4	2	2	6309.5808	-0.0031
7	2	6	6	1	5	6320.4527	-0.0036
8	0	8	7	1	7	6325.5072	0.0077
8	1	8	7	0	7	6339.6096	-0.0061
4	4	1	3	3	0	6450.5935	0.0018
4	4	0	3	3	1	6453.7883	0.0020
8	1	7	7	2	6	6648.5047	0.0013
5	3	2	4	2	3	6679.1654	0.0073
5	2	3	4	1	4	6792.0685	-0.0116
8	2	7	7	1	6	6967.6042	0.0029
6	3	4	5	2	3	6990.3493	0.0060
11	9	2	11	8	3	7047.4148	0.0210
11	9	3	11	8	4	7047.4148	0.0041
9	9	1	9	8	1	7077.7893	0.0167
9	9	0	9	8	1	7077.7893	0.0167
9	9	1	9	8	2	7077.7893	0.0164
9	9	0	9	8	2	7077.7893	0.0164
11	4	7	10	5	6	7089.9487	-0.0134
9	0	9	8	1	8	7091.5341	0.0069
9	1	9	8	0	8	7097.4946	0.0113
5	4	2	4	3	1	7321.7154	-0.0015
9	2	7	8	3	6	7342.5651	0.0105
5	4	1	4	3	2	7344.1744	0.0054
10	3	7	9	4	6	7432.7826	0.0000
9	1	8	8	2	7	7486.1050	-0.0055
7	3	5	6	2	4	7601.4280	0.0034
9	2	8	8	1	7	7652.5331	-0.0009
6	3	3	5	2	4	7797.7300	-0.0025
10	0	10	9	1	9	7855.2723	-0.0098
10	1	10	9	0	9	7857.7280	-0.0069
3	2	1	2	1	1	3827.4288	0.0111
3	2	2	2	1	2	4059.9346	-0.0148
6	6	1	6	5	1	4574.4181	0.0188
6	6	0	6	5	2	4574.7161	-0.0011
4	2	2	3	1	2	4717.7434	0.0130
3	3	0	2	2	0	4724.5741	-0.0036
3	3	1	2	2	1	4744.3032	-0.0140
4	2	3	3	1	3	5101.0728	-0.0136
8	7	2	8	6	2	5393.7554	-0.0039

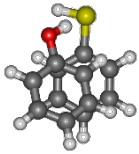
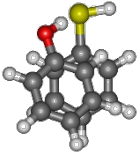
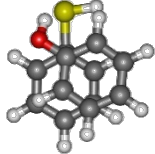
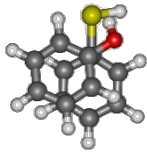
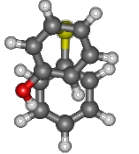
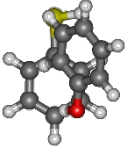
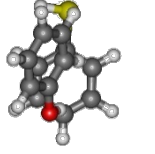
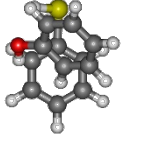
8	7	1	8	6	3	5393.9939	0.0012
7	7	1	7	6	1	5409.1930	-0.0067
7	7	0	7	6	2	5409.2407	0.0073
10	8	3	10	7	3	6210.2437	-0.0150
10	8	2	10	7	4	6210.3987	-0.0075
4	4	0	3	3	0	6450.8796	-0.0168
4	4	1	3	3	1	6453.4783	-0.0031
5	3	3	4	2	3	6603.9085	-0.0115
6	2	4	5	1	4	6722.5218	-0.0026
11	9	3	11	8	3	7047.4148	0.0212
11	9	2	11	8	4	7047.4148	0.0038

**Table S2.2.** Observed rotational transitions and residuals (in MHz) for phenol and thiophenol (dimer-II).

$J'$	$K_a'$	$K_c'$	$J''$	$K_a''$	$K_c''$	Obs.	Obs.-Cal.
3	0	3	2	0	2	2555.7041	-0.00447
3	1	3	2	0	2	2720.6182	-0.00964
8	3	6	8	2	7	2906.5847	0.01665
2	2	1	1	1	0	2931.9882	0.00313
2	2	0	1	1	1	3069.5319	-0.00580
4	0	4	3	1	3	3167.9869	-0.00255
4	0	4	3	0	3	3332.9010	-0.00772
3	1	2	2	0	2	3401.7205	0.00918
4	1	4	3	0	3	3422.7967	-0.00664
4	1	3	3	1	2	3695.8814	-0.00227
4	2	2	3	2	1	3698.4563	0.00610
3	2	2	2	1	1	3699.2073	-0.01357
5	0	5	4	1	4	4001.1764	-0.00365
3	2	2	2	1	2	4041.3022	-0.02011
5	1	5	4	1	4	4045.0931	0.00370
5	0	5	4	0	4	4091.0721	-0.00257
5	1	5	4	0	4	4134.9769	-0.00712
3	2	1	2	1	2	4152.9655	-0.00975
5	2	4	4	2	3	4354.2623	0.00978
4	2	3	3	1	2	4407.5012	0.00399
5	3	2	4	3	1	4519.3315	0.00665
4	1	3	3	0	3	4541.8859	-0.00051
5	1	4	4	1	3	4555.8572	0.00358
5	2	3	4	2	2	4666.7933	-0.02120
3	3	1	2	2	0	4677.8083	-0.00670
3	3	0	2	2	0	4680.9316	0.00674
3	3	1	2	2	1	4701.3283	-0.00446
3	3	0	2	2	1	4704.4396	-0.00301
4	2	2	3	1	2	4710.9842	-0.00639
6	0	6	5	1	5	4803.7648	0.00729
6	1	6	5	1	5	4823.6847	0.00579
6	0	6	5	0	5	4847.6696	0.00274
6	1	5	5	2	4	4858.0050	-0.00374
6	1	6	5	0	5	4867.5895	0.00124
5	2	4	4	1	3	5065.8703	0.00424
4	2	3	3	1	3	5088.5797	-0.00099
6	2	5	5	2	4	5184.7219	0.01427
6	3	4	5	3	3	5349.4334	0.00189
6	4	3	5	4	2	5363.9293	0.02478
6	1	5	5	1	4	5368.0181	-0.00309
4	2	2	3	1	3	5392.0627	-0.01137
6	3	3	5	3	2	5488.8725	0.01556
4	3	2	3	2	1	5510.0799	0.00202
4	3	1	3	2	1	5531.2991	0.00332
7	0	7	6	1	6	5588.0904	-0.01000
7	1	7	6	1	6	5596.6854	-0.01543
7	0	7	6	0	6	5608.0103	-0.01150
6	2	4	5	2	3	5612.9098	-0.02351
7	1	7	6	0	6	5616.6291	0.00687

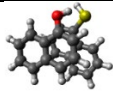
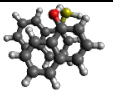
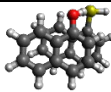
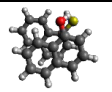
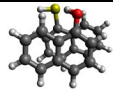
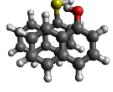
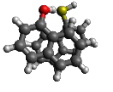
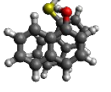
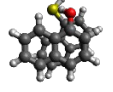
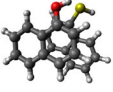
4	3	1	3	2	2	5642.9386	-0.01012
5	2	3	4	1	3	5681.9200	-0.00143
7	1	6	6	2	5	5810.5469	0.01118
7	2	6	6	2	5	5997.7770	0.00411
7	1	6	6	1	5	6137.2519	0.01729
5	2	4	4	1	4	6184.9475	-0.00164
7	3	5	6	3	4	6226.7303	0.00377
7	5	3	6	5	2	6253.1233	0.01479
5	3	3	4	2	2	6271.6365	-0.00306
7	4	4	6	4	3	6272.3756	0.01720
7	4	3	6	4	2	6308.6867	0.01696
7	2	6	6	1	5	6324.4700	-0.00178
5	3	2	4	2	2	6352.1624	-0.00803
8	0	8	7	1	7	6362.9866	-0.00221
8	1	8	7	1	7	6366.5748	0.00093
8	0	8	7	0	7	6371.5935	0.00427
8	1	8	7	0	7	6375.1817	0.00740
4	4	1	3	3	0	6388.6642	-0.00159
4	4	0	3	3	0	6389.0100	0.00460
4	4	1	3	3	1	6391.7756	-0.00004
4	4	0	3	3	1	6392.1094	-0.00585
7	3	4	6	3	3	6482.4820	-0.00417
7	2	5	6	2	4	6522.0118	0.00243
5	3	3	4	2	3	6575.1314	-0.00154
5	3	2	4	2	3	6655.6692	0.00539
8	1	7	7	2	6	6697.5117	-0.00231
6	2	4	5	1	4	6738.9965	-0.00462
8	2	7	7	2	6	6795.2991	-0.00423
8	1	7	7	1	6	6884.7418	-0.00938
6	3	4	5	2	3	6954.2646	0.00803
8	2	7	7	1	6	6982.5411	0.00060
9	0	9	8	1	8	7133.3766	-0.00652
9	1	9	8	1	8	7134.8429	0.00379
9	0	9	8	0	8	7136.9648	-0.00338
9	1	9	8	0	8	7138.4311	0.00693
8	5	4	7	5	3	7164.6333	-0.01384
6	3	3	5	2	3	7174.2177	0.00483
5	4	2	4	3	1	7264.6856	0.00995
5	4	1	4	3	1	7267.6897	0.00838
8	4	4	7	4	3	7269.5732	0.01070
5	4	2	4	3	2	7285.8930	-0.00056
5	4	1	4	3	2	7288.9090	0.00978
6	2	5	5	1	5	7324.5764	0.00903
8	2	6	7	2	5	7383.0247	-0.01225
8	3	5	7	3	4	7474.2913	-0.02728
9	1	8	8	2	7	7532.9781	-0.01618
6	3	4	5	2	4	7570.3025	-0.00944
9	1	8	8	1	7	7630.7893	0.00570
9	2	8	8	1	7	7678.4492	0.00842
6	3	3	5	2	4	7790.2675	-0.00074
10	0	10	9	1	9	7901.7639	0.00513
10	1	10	9	1	9	7902.3361	-0.00218
10	1	10	9	0	9	7903.7905	-0.00377

**Table S2.3** Theoretical spectroscopic parameters at B3LYP-D3(BJ)/def2-TZVP for phenol and thiophenol cluster in less than 5 kJ mol<sup>-1</sup> of the relative zero-point corrected energy.

Parameters	I	II	III	IV
				
<i>A</i> / MHz	862.3	856.8	802.7	808.5
<i>B</i> / MHz	516.4	517.4	573.1	568.9
<i>C</i> / MHz	394.2	395.3	455.8	454.7
<i>D<sub>J</sub></i> / kHz	0.183	0.199	0.143	0.163
<i>D<sub>K</sub></i> / kHz	0.0717	-0.00722	-0.0583	0.0771
<i>D<sub>JK</sub></i> / kHz	0.0429	0.108	0.0974	-0.0100
<i>d<sub>1</sub></i> / kHz	-0.0459	-0.0526	-0.0329	-0.0407
<i>d<sub>2</sub></i> / kHz	-0.0104	-0.0122	-0.00776	-0.00693
$ \mu_a $ / D	0.9	1.3	0.2	1.0
$ \mu_b $ / D	1.5	1.8	0.5	0.7
$ \mu_c $ / D	0.3	1.1	1.6	0.5
$\Delta E$ / kJ mol <sup>-1</sup>	0.0	1.3	1.6	1.6
$\Delta E_0$ / kJ mol <sup>-1</sup>	0.0	1.1	1.0	1.2
<i>E<sub>c</sub></i> / kJ mol <sup>-1</sup>	-35.65	-35.69	-34.14	-35.90
<i>E<sub>c</sub>-BSSE</i> / kJ mol <sup>-1</sup>	-32.68	-32.43	-31.21	-32.84
Parameters	V	VI	VII	VIII
				
<i>A</i> / MHz	925.4	867.6	881.0	918.8
<i>B</i> / MHz	468.7	436.8	415.4	420.7
<i>C</i> / MHz	403.2	327.1	315.1	378.6
<i>D<sub>J</sub></i> / kHz	0.160	0.320	0.776	0.288
<i>D<sub>K</sub></i> / kHz	0.853	-0.904	-1.056	0.821
<i>D<sub>JK</sub></i> / kHz	-0.452	0.918	0.599	-0.404
<i>d<sub>1</sub></i> / kHz	-0.0161	-0.0888	-0.209	-0.0441
<i>d<sub>2</sub></i> / kHz	-0.00640	-0.0213	-0.0243	-0.00678
$ \mu_a $ / D	1.1	1.2	1.4	1.3
$ \mu_b $ / D	0.7	0.0	0.1	1.5
$ \mu_c $ / D	1.1	0.3	0.5	0.2
$\Delta E$ / kJ mol <sup>-1</sup>	4.5	4.6	4.8	5.2
$\Delta E_0$ / kJ mol <sup>-1</sup>	3.9	3.9	3.9	4.8
<i>E<sub>c</sub></i> / kJ mol <sup>-1</sup>	-32.93	-30.38	-29.96	-30.63
<i>E<sub>c</sub>-BSSE</i> / kJ mol <sup>-1</sup>	-29.66	-27.53	-27.15	-27.41

*E<sub>c</sub>*: Binding energy; *E<sub>c</sub>-BSSE*: BSSE-corrected binding energy.

**Table S3.1** Theoretical spectroscopic parameters at B3LYP-D3(BJ)/def2-TZVP for the first eleven isomers of 1-naphthol and 1-naphthalenethiol complex in less than 5 kJ mol<sup>-1</sup> of the relative zero-point corrected energy.

Parameters	I	II	III	IV	V	
						
<i>A</i> / MHz	381.7	359.0	441.1	351.2	381.6	
<i>B</i> / MHz	288.7	318.4	247.0	326.8	290.9	
<i>C</i> / MHz	245.3	238.2	239.0	245.4	259.0	
<i>D</i> <sub>J</sub> / kHz	0.0216	0.0303	0.0159	0.0274	0.0178	
<i>D</i> <sub>K</sub> / kHz	0.0304	0.0268	0.0268	0.0267	0.00762	
<i>D</i> <sub>JK</sub> / kHz	-0.0268	-0.0311	-0.00303	-0.0312	0.00466	
<i>d</i> <sub>1</sub> / kHz	-0.00147	0.00309	0.00116	0.00217	-0.000485	
<i>d</i> <sub>2</sub> / kHz	0.000119	-0.00296	0.000796	-0.000081	-0.00238	
<i>μ</i> <sub>a</sub>   / D	0.8	0.0	1.4	1.0	0.4	
<i>μ</i> <sub>b</sub>   / D	0.4	0.5	1.3	0.3	0.2	
<i>μ</i> <sub>c</sub>   / D	0.7	1.4	0.2	1.1	2.0	
$\Delta E$ / kJ mol <sup>-1</sup>	0.0	0.7	0.4	0.9	1.2	
$\Delta E_0$ / kJ mol <sup>-1</sup>	0.0	0.3	0.5	1.0	1.3	
<i>E</i> <sub>c</sub> / kJ mol <sup>-1</sup>	-52.80	-52.72	-51.21	-54.14	-55.40	
<i>E</i> <sub>c-BSSE</sub> / kJ mol <sup>-1</sup>	-49.04	-48.87	-47.49	-50.54	-51.76	
Parameters	VI	VI	VII	IX	X	XI
						
<i>A</i> / MHz	386.1	381.3	364.6	439.3	378.4	374.1
<i>B</i> / MHz	291.9	288.7	293.3	248.3	296.0	291.6
<i>C</i> / MHz	232.6	251.1	274.0	237.1	248.8	248.3
<i>D</i> <sub>J</sub> / kHz	0.0273	0.0140	0.0174	0.0173	0.0183	0.181
<i>D</i> <sub>K</sub> / kHz	0.0206	-0.0172	0.0259	0.0233	0.00264	0.0135
<i>D</i> <sub>JK</sub> / kHz	-0.0309	0.0234	-0.0161	0.00493	0.00878	-0.00860
<i>d</i> <sub>1</sub> / kHz	-0.00178	-0.000578	-0.000875	-0.000022	0.000239	-0.000976
<i>d</i> <sub>2</sub> / kHz	0.000421	0.000432	-0.000367	0.000084	-0.00229	0.0000600
<i>μ</i> <sub>a</sub>   / D	1.2	2.0	0.7	0.8	0.6	1.2
<i>μ</i> <sub>b</sub>   / D	0.9	1.7	1.1	1.6	2.1	1.2
<i>μ</i> <sub>c</sub>   / D	1.0	0.2	0.8	0.7	0.0	0.0
$\Delta E$ / kJ mol <sup>-1</sup>	1.2	1.3	1.4	1.2	1.6	2.5
$\Delta E_0$ / kJ mol <sup>-1</sup>	1.4	1.6	1.6	1.8	2.1	2.9
<i>E</i> <sub>c</sub> / kJ mol <sup>-1</sup>	-53.97	-54.73	-55.02	-53.60	-49.12	-48.62
<i>E</i> <sub>c-BSSE</sub> / kJ mol <sup>-1</sup>	-50.33	-51.30	-51.42	-49.92	-45.06	-44.77

**Table S3.2.** Observed rotational transitions and residuals (in MHz) for 1-naphthol and 1-naphthalenethiol.

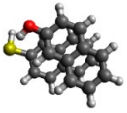
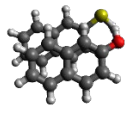
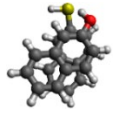
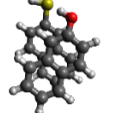
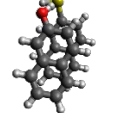
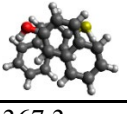
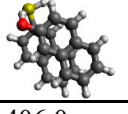
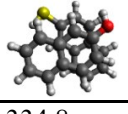
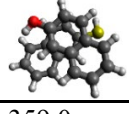
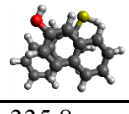
$J'$	$K_a'$	$K_c'$	$J''$	$K_a''$	$K_c''$	Obs.	Obs.-Cal.
8	0	8	7	0	7	3945.5118	0.00340
8	1	8	7	1	7	3944.8708	0.00375
7	0	7	6	0	6	3462.2428	-0.00797
7	1	7	6	1	6	3460.5446	-0.00919
9	0	9	8	0	8	4429.1320	0.01187
9	1	9	8	1	8	4428.8859	-0.00122
6	0	6	5	0	5	2979.7819	-0.00325
6	1	6	5	1	5	2975.5479	0.00179
6	1	5	5	1	4	3149.0778	0.00562
7	1	6	6	1	5	3627.0343	0.00028
8	1	7	7	1	6	4103.4633	0.00533
9	1	8	8	1	7	4582.3559	0.00860
10	1	9	9	1	8	5063.5591	-0.00198
4	4	1	3	3	1	2900.5330	-0.00797
4	4	0	3	3	0	2898.9980	-0.00520
6	5	2	5	4	2	4181.3212	0.00945
6	5	1	5	4	1	4179.4746	0.00858
7	5	3	6	4	3	4710.4090	-0.00133
7	5	2	6	4	2	4701.9785	-0.00249
8	5	3	7	4	3	5215.4660	0.00312
8	6	2	7	5	2	5459.7314	-0.00483
8	6	3	7	5	3	5461.3734	-0.00029
8	7	2	7	6	2	5687.0341	-0.01609
8	7	1	7	6	1	5687.0341	0.02509
9	5	5	8	4	5	5780.7148	0.00667
9	5	4	8	4	4	5715.2407	0.00821
9	6	3	8	5	3	5982.2384	0.01200
9	6	4	8	5	4	5988.7158	-0.00779
10	5	5	9	4	5	6204.3242	0.01603
10	1	9	9	0	9	6280.2934	0.00866
9	7	3	8	6	3	6214.3873	-0.00396
9	7	2	8	6	2	6214.1097	-0.00733
9	8	2	8	7	2	6440.2014	-0.00129
9	8	1	8	7	1	6440.2014	0.00414
9	9	1	8	8	1	6665.3998	0.00880
9	9	0	8	8	0	6665.3998	0.00884
10	9	2	9	8	2	7193.3196	-0.01331
10	9	1	9	8	1	7193.3196	-0.01263
10	10	1	9	9	1	7418.4722	0.00016
10	10	0	9	9	0	7418.4722	0.00017
5	2	3	4	2	2	2720.5975	-0.00468
5	2	3	4	1	3	3014.7193	0.00006
6	2	5	5	2	4	3101.3381	-0.00789
5	3	2	4	2	2	3162.9595	-0.00981
6	3	4	5	3	3	3169.1264	-0.00362
6	4	3	5	4	2	3180.1820	0.01078
6	4	2	5	4	1	3188.3955	0.01881
6	3	3	5	3	2	3238.6899	-0.01776
5	3	3	4	2	3	3246.6214	0.00526

6	2	4	5	2	3	3260.1050	0.01242
5	4	2	4	3	2	3431.4968	-0.00153
5	4	1	4	3	1	3421.7017	0.00964
7	2	6	6	2	5	3597.1576	0.00500
6	2	4	5	1	4	3614.9131	0.01081
5	5	0	4	4	0	3652.8432	-0.00399
5	5	1	4	4	1	3653.0578	-0.00741
6	3	3	5	2	3	3681.0710	-0.00379
7	3	5	6	3	4	3688.0326	0.02297
7	6	1	6	6	0	3701.7107	-0.02007
7	6	2	6	6	1	3701.7107	0.02359
7	5	3	6	5	2	3709.2963	0.02650
7	4	3	6	4	2	3739.3442	0.00228
6	2	5	5	1	5	3771.4220	-0.04665
7	2	5	6	2	4	3781.4686	0.01516
7	3	4	6	3	3	3803.8716	-0.01339
6	3	4	5	2	4	3816.7624	-0.00558
6	4	2	5	3	2	3934.2021	0.00601
6	4	3	5	3	3	3967.7718	0.00773
8	7	1	7	7	0	4229.5386	-0.00166
8	7	2	7	7	1	4229.5386	0.00411
7	2	5	6	1	5	4247.2913	0.00775
8	4	5	7	4	4	4246.8410	0.01121
8	5	4	7	5	3	4246.7244	-0.01233
8	5	3	7	5	2	4252.8348	0.01099
8	2	6	7	2	5	4281.2513	0.00810
8	4	4	7	4	3	4303.2637	-0.00074
8	3	5	7	3	4	4359.0101	-0.00450
7	1	6	6	0	6	4367.8071	0.00941
6	6	1	5	5	1	4406.0976	-0.00536
6	6	0	5	5	0	4406.0976	0.02234
7	2	6	6	1	6	4393.0648	-0.01033
7	3	5	6	2	5	4403.4444	0.01278
9	2	8	8	2	7	4575.0900	-0.02449
7	4	3	6	3	3	4434.8250	-0.00536
7	4	4	6	3	4	4513.3710	-0.01249
9	3	7	8	3	6	4702.3326	-0.00527
9	8	1	8	8	0	4757.4190	-0.01780
9	8	2	8	8	1	4757.4190	-0.01707
9	2	7	8	2	6	4762.3462	-0.00497
9	4	6	8	4	5	4773.6975	-0.00432
9	6	3	8	6	2	4775.2872	-0.02678
8	3	5	7	2	5	4802.4523	0.02394
9	5	4	8	5	3	4803.0519	0.01786
9	4	5	8	4	4	4876.1841	0.00021
9	3	6	8	3	5	4896.0511	-0.00166
8	2	6	7	1	6	4901.5036	0.01087
10	0	10	9	0	9	4912.8413	-0.03364
10	1	10	9	1	9	4912.8413	0.04860
7	6	1	6	5	1	4933.6346	-0.00937
7	6	2	6	5	2	4933.9343	-0.00053
8	4	4	7	3	4	4934.2045	-0.00530
8	3	6	7	2	6	5005.4380	0.00533

10	2	9	9	2	8	5060.4497	-0.02051
8	1	7	7	0	7	5009.0010	-0.00388
7	7	1	6	6	1	5159.2031	0.00029
7	7	0	6	6	0	5159.2031	0.00358
10	3	8	9	3	7	5198.4599	-0.01128
10	2	8	9	2	7	5235.0445	0.01105
10	5	6	9	5	5	5322.4691	0.02025
11	0	11	10	0	10	5396.6658	-0.01781
11	1	11	10	1	10	5396.6658	0.01058
10	3	7	9	3	6	5410.3533	0.00180
10	4	6	9	4	5	5445.9307	-0.01680
9	3	7	8	2	7	5619.9334	-0.00556
9	4	6	8	3	6	5646.7422	-0.00962
8	8	1	7	7	1	5912.2996	-0.00151
8	8	0	7	7	0	5912.2996	-0.00113
10	4	6	9	3	6	6001.2747	0.00087
12	2	11	11	2	10	6028.8513	-0.00658
12	1	11	11	1	10	6029.3455	0.00179
10	3	7	9	2	7	6065.2614	0.02315
10	4	7	9	3	7	6237.5866	-0.02876
10	3	8	9	2	8	6243.2722	-0.02345
12	4	9	11	4	8	6306.8720	0.01717
10	5	6	9	4	6	6329.4502	-0.00497
13	0	13	12	0	12	6364.3172	-0.02330
13	1	13	12	1	12	6364.3172	-0.02008
12	7	6	11	7	5	6380.8405	0.00483
12	7	5	11	7	4	6383.7797	-0.01059
13	2	12	12	2	11	6512.7015	0.01954
13	1	12	12	1	11	6512.8703	0.00532
10	7	4	9	6	4	6740.9709	-0.00338
14	1	14	13	1	13	6848.1684	0.00121
12	5	7	11	4	7	7218.5705	0.02472
12	4	8	11	3	8	7222.1536	0.00333
11	7	4	10	6	4	7262.1147	-0.02830
11	7	5	10	6	5	7266.8566	-0.00022
14	4	11	13	4	10	7292.4806	0.01489
14	3	11	13	3	10	7313.7164	-0.01758
12	3	9	11	2	9	7397.0971	0.02039
12	1	11	11	0	11	7546.1763	-0.01646
12	2	11	11	1	11	7546.4470	-0.01897
12	6	7	11	5	7	7589.8446	0.00057
11	9	3	10	8	3	7720.9711	0.01084
11	9	2	10	8	2	7720.9711	0.01673
5	5	0	4	4	1	3653.0733	-0.02332
5	5	1	6	4	0	3652.8349	0.01912
7	2	6	5	1	5	3655.0082	0.00033
6	6	0	5	5	1	4406.0976	-0.00907
6	6	1	3	5	0	4406.0976	0.02605
4	4	1	3	3	0	2898.7400	-0.01377
4	4	0	5	3	1	2900.7702	-0.02020
6	0	6	4	1	5	2972.8602	0.01049
5	3	3	4	2	2	3119.0037	-0.00820
5	4	2	4	3	1	3419.5122	0.00410

5	4	1	6	3	2	3433.6823	0.00001
7	0	7	6	1	6	3459.5391	-0.01527
7	1	6	7	2	5	3569.1867	0.00796
8	0	8	5	1	7	3944.4979	-0.01108
6	4	2	7	3	3	3978.1480	-0.00550
8	1	7	5	2	6	4075.4924	0.00829
6	5	1	5	4	2	4181.6518	0.00182
6	5	2	6	4	1	4179.1409	0.01311
7	4	4	5	3	3	4399.8615	0.01306
6	6	0	5	5	1	4406.0976	-0.00907
6	6	1	8	5	0	4406.0976	0.02605
9	0	9	8	1	8	4428.7336	-0.02845
9	1	9	8	0	8	4429.2350	-0.01019
9	2	8	8	1	7	4587.4596	-0.00235
9	2	7	6	3	6	4630.4345	-0.00288
7	5	3	6	4	2	4700.0217	0.00080
7	5	2	8	4	3	4712.3589	-0.01153
9	3	7	7	2	6	4834.2588	0.00714
8	4	5	6	3	4	4842.8118	0.01856
7	6	2	6	5	1	4933.6195	0.02290
7	6	1	9	5	2	4933.9533	-0.02890
10	1	9	9	2	8	5058.4549	0.00847
10	2	9	6	1	8	5065.5726	-0.01227
7	7	0	6	6	1	5159.2031	-0.00013
7	7	1	7	6	0	5159.2031	0.00400
8	5	4	4	4	3	5207.4613	0.04560
12	0	12	11	1	11	5880.5058	0.00998
8	8	0	7	7	1	5912.3008	-0.00035
8	8	1	7	7	0	5912.3008	0.00011
9	6	4	8	5	3	5980.6817	0.00529
9	6	3	8	5	4	5990.2478	-0.02578
12	1	11	11	2	10	6028.5783	0.00807
9	7	3	8	6	2	6214.0531	-0.01552
9	7	2	8	6	3	6214.4428	0.00313
13	1	13	12	0	12	6364.3219	-0.02018
13	0	13	12	1	12	6364.3219	-0.01380
9	8	1	8	7	2	6440.2014	-0.00206
9	8	2	8	7	1	6440.2014	0.00491
12	4	9	11	3	8	6454.4084	-0.00248
10	6	5	9	5	4	6491.3505	-0.00101
9	9	0	8	8	1	6665.3999	0.00889
9	9	1	8	8	0	6665.3999	0.00894
10	7	4	9	6	3	6739.4268	0.00251
13	4	10	12	3	9	6882.3320	0.01196
10	9	1	9	8	2	7193.3196	-0.01340
10	9	2	9	8	1	7193.3196	-0.01254
11	7	4	10	6	5	7267.9962	-0.00447
10	10	0	9	9	1	7418.4722	0.00016
10	10	1	9	9	0	7418.4722	0.00017
12	6	7	11	5	6	7436.9284	0.02025

**Table S4.1** Theoretical spectroscopic parameters at B3LYP-D3(BJ)/def2-TZVP for the first ten isomers of 2-naphthol and 2-naphthalenethiol complex in less than 5 kJ mol<sup>-1</sup> of the relative zero-point corrected energy.

Parameters	I	II	III	IV	V
					
$A$ / MHz	413.8	363.0	403.9	408.1	443.0
$B$ / MHz	250.9	292.7	258.2	252.6	247.7
$C$ / MHz	221.0	196.7	220.2	223.8	193.7
$D_J$ / kHz	0.0176	0.0951	0.0182	0.0189	0.0108
$D_K$ / kHz	0.112	0.0754	0.141	0.124	0.0951
$D_{JK}$ / kHz	-0.0283	-0.164	-0.0352	-0.0337	-0.00803
$d_1$ / kHz	0.000657	-0.0149	-0.00440	0.000305	-0.00341
$d_2$ / kHz	0.000239	0.0284	-0.000203	0.000718	-0.000751
$ \mu_a $ / D	0.5	1.2	0.7	0.4	0.1
$ \mu_b $ / D	1.1	0.9	0.7	1.4	1.5
$ \mu_c $ / D	0.1	0.7	1.1	1.3	0.2
$\Delta E$ / kJ mol <sup>-1</sup>	0.0	1.3	1.3	1.5	1.3
$\Delta E_0$ / kJ mol <sup>-1</sup>	0.0	1.2	1.3	1.3	1.3
$E_c$ / kJ mol <sup>-1</sup>	-52.05	-52.05	-51.34	-51.04	-53.22
$E_{c\text{-BSSE}}$ / kJ mol <sup>-1</sup>	-48.33	-48.62	-47.45	-47.40	-49.41
Parameters	VI	VI	VII	IX	X
					
$A$ / MHz	367.3	406.0	334.8	359.0	335.8
$B$ / MHz	262.5	269.8	290.9	267.9	272.4
$C$ / MHz	236.7	205.6	232.7	239.2	255.6
$D_J$ / kHz	0.0249	0.0151	0.0349	0.0290	0.0336
$D_K$ / kHz	0.0785	0.0640	0.00822	0.0711	-0.0246
$D_{JK}$ / kHz	-0.0422	0.0363	-0.0263	-0.0315	0.0486
$d_1$ / kHz	-0.00447	-0.00674	-0.00741	-0.00467	0.000438
$d_2$ / kHz	-0.000916	-0.00205	-0.00337	-0.00139	-0.00443
$ \mu_a $ / D	0.8	0.4	0.1	1.3	0.6
$ \mu_b $ / D	1.1	0.4	0.1	0.1	-0.4
$ \mu_c $ / D	0.7	1.6	0.2	0.3	-0.4
$\Delta E$ / kJ mol <sup>-1</sup>	1.7	3.4	3.5	4.7	5.4
$\Delta E_0$ / kJ mol <sup>-1</sup>	1.5	3.0	3.0	4.1	4.2
$E_c$ / kJ mol <sup>-1</sup>	-50.67	-51.97	-46.99	-47.36	-50.83
$E_{c\text{-BSSE}}$ / kJ mol <sup>-1</sup>	-46.86	-48.16	-43.51	-43.89	-50.06

**Table S4.2.** Observed rotational transitions and residuals (in MHz) for 2-naphthol and 2-naphthalenethiol.

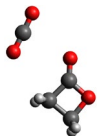
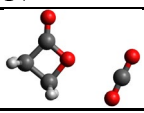
$J'$	$K_a'$	$K_c'$	$J''$	$K_a''$	$K_c''$	Obs.	Obs.-Cal.
10	0	10	9	1	9	4396.2248	0.00410
10	1	10	9	0	9	4400.9798	-0.00161
9	1	9	8	0	8	3971.3524	0.00498
9	0	9	8	1	8	3961.8664	0.00252
8	1	8	7	0	7	3543.8517	0.00517
8	0	8	7	1	7	3525.4387	0.00817
11	0	11	10	1	10	4829.4548	0.00238
11	1	11	10	0	10	4831.7992	0.00364
13	1	13	12	0	12	5694.9927	0.00785
12	1	12	11	0	11	5263.2281	-0.00371
12	0	12	11	1	11	5262.1010	0.00441
14	0	14	13	1	13	6126.6558	0.01831
5	1	8	4	0	4	2288.6864	0.00271
6	1	8	5	0	5	2701.2535	0.00426
6	0	7	5	1	4	2639.3427	0.00619
5	0	7	4	1	5	2184.6550	0.00457
3	3	8	2	2	5	2251.6690	0.00661
3	3	8	2	2	4	2256.3303	-0.00012
4	3	7	3	2	0	2706.2407	0.00449
4	3	7	3	2	1	2729.7832	-0.00162
7	1	8	6	0	1	3119.9256	0.00669
7	0	8	6	1	2	3085.3560	0.00162
5	3	7	4	2	6	3145.6815	0.00118
5	3	7	4	2	6	3215.5774	0.00099
6	3	8	5	2	2	3564.7375	0.00131
6	3	8	5	2	3	3722.4562	0.00374
7	3	7	6	2	3	3962.1845	-0.00066
7	3	7	6	2	4	4261.1251	-0.00143
8	3	8	7	2	4	4340.2732	0.00972
8	3	8	7	2	5	4841.9428	0.00367
9	3	7	8	2	5	4703.2260	-0.00256
10	3	7	9	2	6	5056.8207	0.00499
9	3	8	8	2	6	5471.5458	0.00768
15	1	15	14	0	14	6558.8856	0.00717
15	0	15	14	1	14	6558.7554	-0.00258
5	0	5	4	0	4	2249.2272	0.00877
6	0	6	5	0	5	2678.8036	0.00184
6	1	6	5	1	5	2661.7737	-0.01029
5	2	4	4	2	3	2308.7961	0.01180
5	1	4	4	1	3	2374.3263	-0.00114
5	2	3	4	2	2	2377.6798	0.00498
6	2	5	5	2	4	2762.8850	-0.00059
6	3	4	5	3	3	2796.7361	0.00541
6	3	3	5	3	2	2815.6754	0.01504
6	1	5	5	1	4	2832.0637	0.00212
6	2	4	5	2	3	2865.1335	0.00223
7	1	7	6	1	6	3097.4792	0.00777
7	0	7	6	0	6	3107.8074	0.00554
7	2	6	6	2	5	3213.2142	-0.01374

7	3	5	6	3	4	3262.5780	-0.00223
7	4	4	6	4	3	3265.9112	0.00209
7	4	3	6	4	2	3268.9144	-0.01742
7	1	6	6	1	5	3279.1668	0.00485
7	3	4	6	3	3	3301.5624	0.00274
7	2	5	6	2	4	3348.0345	0.00006
8	1	8	7	1	7	3531.7384	0.00892
8	0	8	7	0	7	3537.5529	0.00532
8	2	7	7	2	6	3659.6966	-0.00191
8	1	7	7	1	6	3715.7216	-0.01750
8	3	6	7	3	5	3726.1149	0.00214
8	5	4	7	5	3	3730.3955	0.00034
8	5	3	7	5	2	3730.7680	0.01024
8	4	5	7	4	4	3736.3285	-0.00479
8	4	4	7	4	3	3744.3346	0.00780
8	3	5	7	3	4	3794.0314	-0.00914
8	2	6	7	2	5	3823.4424	0.00858
9	1	9	8	1	8	3965.0548	0.00633
9	0	9	8	0	8	3968.1656	0.00278
9	2	8	8	2	7	4102.4830	-0.00543
9	1	8	8	1	7	4144.8387	0.00270
9	3	7	8	3	6	4186.3978	-0.00110
9	5	5	8	5	4	4201.0586	-0.00540
9	4	6	8	4	5	4206.9377	-0.01245
9	2	7	8	2	6	4289.1536	-0.01054
9	3	6	8	3	5	4289.3037	0.00620
10	1	10	9	1	9	4397.7998	0.00298
10	2	9	9	2	8	4542.0613	-0.00138
10	1	9	9	1	8	4570.8625	0.00068
10	5	5	9	5	4	4676.0709	-0.00851
10	4	7	9	4	6	4676.8541	-0.00298
10	4	6	9	4	5	4712.5581	-0.00511
10	2	8	9	2	7	4743.3961	0.00346
10	3	7	9	3	6	4781.9409	0.00087
11	1	11	10	1	10	4830.2136	-0.00584
11	0	11	10	0	10	4831.0359	0.00736
11	2	10	10	2	9	4979.0664	0.00710
11	1	10	10	1	9	4997.0666	-0.00541
11	2	9	10	2	8	5185.3344	-0.00086
13	0	13	12	0	12	5694.8154	0.00530
13	1	13	12	1	12	5694.6362	0.01954
12	1	12	11	1	11	5262.4634	-0.00139
4	2	3	3	1	2	2277.0506	-0.00089
6	1	5	5	2	4	2528.5015	0.00561
5	2	4	4	1	3	2677.8947	0.00157
4	4	1	3	3	0	3062.5269	-0.00087
4	4	0	3	3	1	3062.9263	0.00193
6	2	5	5	1	4	3066.4507	-0.00058
5	2	3	4	1	4	3119.4526	0.00128
7	2	6	6	1	5	3447.6241	0.00646
5	4	2	4	3	1	3525.9391	0.00136
5	4	1	4	3	2	3528.7353	-0.00218
8	1	7	7	2	6	3547.2885	0.00508

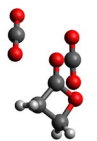
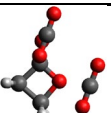
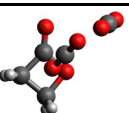
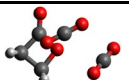
11	4	8	10	5	5	3620.8334	-0.00433
15	2	13	14	5	10	3673.0284	-0.00872
9	2	7	8	3	6	3772.3173	-0.01718
12	5	7	11	6	6	3793.1903	0.00597
16	2	15	15	3	12	3809.9327	0.00192
8	2	7	7	1	6	3828.1549	0.00071
5	5	0	4	4	1	3871.3706	-0.01911
5	5	1	4	4	0	3871.3706	0.00899
12	3	9	12	0	12	3919.7916	0.00832
6	4	3	5	3	2	3985.1516	-0.00334
6	4	2	5	3	3	3996.3548	-0.00224
9	1	8	8	2	7	4032.4231	0.00219
9	2	8	8	1	7	4214.9062	0.00268
10	2	8	9	3	7	4329.3307	0.00248
6	5	2	5	4	1	4336.1104	-0.00112
6	5	1	5	4	2	4336.3663	0.00023
7	4	4	6	3	3	4435.4028	-0.00089
15	7	8	14	8	7	4479.7355	0.00562
10	1	9	9	2	8	4500.7901	-0.00420
10	2	9	9	1	8	4612.1289	-0.00130
6	6	0	5	5	1	4679.9914	-0.00197
6	6	1	5	5	0	4679.9914	-0.00017
7	5	3	6	4	2	4799.8753	-0.00196
7	5	2	6	4	3	4801.1504	-0.00277
8	4	5	7	3	4	4870.1738	-0.00352
11	2	9	10	3	8	4871.9061	-0.00608
8	4	4	7	3	5	4950.3035	-0.00124
11	1	10	10	2	9	4955.7967	-0.00693
12	3	9	11	4	8	4976.3565	0.00366
11	2	10	10	1	9	5020.3187	-0.00898
7	6	1	6	5	2	5144.9497	-0.01477
7	6	2	6	5	1	5144.9497	0.00517
8	5	4	7	4	3	5261.3382	-0.00240
8	5	3	7	4	4	5266.0024	0.00059
9	4	5	8	3	6	5449.2007	0.00115
7	7	0	6	6	1	5488.5852	-0.00065
7	7	1	6	6	0	5488.5852	-0.00054
8	6	3	7	5	2	5609.5113	0.00049
8	6	2	7	5	3	5609.6343	0.00355
15	7	9	15	4	12	5621.4041	0.01186
8	7	1	8	4	4	5624.1807	0.00608
10	4	7	9	3	6	5670.6514	0.00489
9	5	5	8	4	4	5718.0762	-0.00159
9	5	4	8	4	5	5731.8909	0.00674
13	1	12	12	2	11	5841.2280	-0.01526
8	7	1	7	6	4	5953.5985	0.00119
8	7	2	7	6	6	5953.5985	0.00261
10	4	6	9	3	4	5975.3514	-0.01246
9	6	4	8	5	5	6073.2630	-0.02411
9	6	3	8	5	4	6073.8043	-0.00190
14	1	14	13	0	13	6126.8846	-0.00979
13	3	11	12	2	10	6134.9210	-0.00723
10	5	7	9	4	5	6166.0298	0.00015

10	5	7	9	4	6	6201.0143	0.00087
8	8	9	7	7	1	6297.1573	0.00130
8	8	8	7	7	0	6297.1573	0.00130
14	2	12	13	3	11	6369.9272	0.00373
12	4	9	11	3	3	6376.6016	-0.00466
9	7	2	8	6	2	6418.3789	-0.00426
9	7	3	8	6	4	6418.3789	0.00570
10	6	5	9	5	5	6535.6017	0.00338
10	6	4	9	5	6	6537.4017	-0.00223
11	5	7	10	4	2	6599.2923	-0.01264
9	8	1	8	7	1	6762.1964	0.00193
9	8	2	8	7	4	6762.1964	0.00203
10	7	3	9	6	3	6882.7152	-0.05303
10	7	4	9	6	3	6882.7152	-0.00325
15	3	13	14	2	12	6919.9019	0.00051
11	6	6	10	5	5	6995.2681	0.00281
11	6	5	10	5	6	7000.6114	-0.00165
9	9	0	8	8	1	7105.7073	0.00607
9	9	1	8	8	0	7105.7073	0.00607
16	1	15	15	2	14	7144.7864	0.00197
10	8	2	9	7	3	7227.0717	0.00231
10	8	3	9	7	2	7227.0717	0.00307
16	2	14	15	3	13	7280.5632	-0.02075
11	7	5	10	6	4	7346.3578	-0.00335
11	7	4	10	6	5	7346.5513	-0.00823
17	0	17	16	1	16	7422.9135	0.01406
11	8	3	10	7	4	7691.6549	0.00260
11	8	4	10	7	3	7691.6549	0.00689
14	5	10	13	4	9	7751.3468	0.00674
12	7	6	11	6	5	7808.8990	-0.01011
10	10	0	9	9	1	7914.2229	0.00400
10	10	1	9	9	0	7914.2229	0.00400

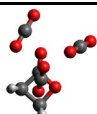
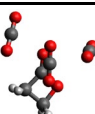
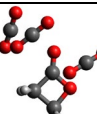
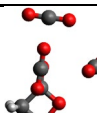
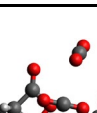
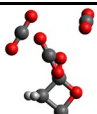
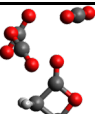
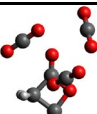
**Table S5.1.** Calculated geometries and spectroscopic parameters of the plausible isomers of BPL-CO<sub>2</sub> at the B3LYP-D3(BJ)/def2-TZVP level of theory.

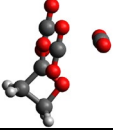
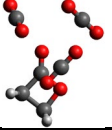
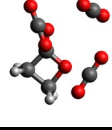
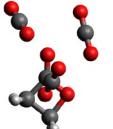
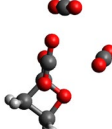
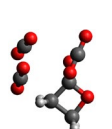
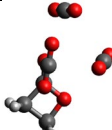
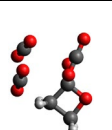
Parameters	I	II	III
			
<i>A</i> /MHz	5337	3394	4258
<i>B</i> /MHz	972	1324	1086
<i>C</i> /MHz	831	1185	1028
$\mu_a, \mu_b, \mu_c$ /D	2.3, -3.6, 0.0	-2.3, 3.4, 0.7	4.4, 1.6, 0.0
<i>D<sub>J</sub></i> /kHz	0.47	2.15	1.33
<i>D<sub>JK</sub></i> /kHz	-0.50	23.21	20.63
<i>D<sub>K</sub></i> /kHz	12.35	-2.54	-6.96
<i>d<sub>1</sub></i> /kHz	-0.08	-0.30	-0.14
<i>d<sub>2</sub></i> /kHz	-0.01	-0.11	0.05
$\Delta E_0$ /kJ mol <sup>-1</sup>	0	0.9	1.64
<i>E<sub>c</sub></i> /kJ mol <sup>-1</sup>	-15.40	-14.14	-13.10
<i>E<sub>c-BSSSE</sub></i> /kJ mol <sup>-1</sup>	-14.23	-13.14	-12.01
Parameters	IV		
			
<i>A</i> /MHz	3777		
<i>B</i> /MHz	1078		
<i>C</i> /MHz	847		
$\mu_a, \mu_b, \mu_c$ /D	0.9, -4.1, 0.0		
<i>D<sub>J</sub></i> /kHz	0.86		
<i>D<sub>JK</sub></i> /kHz	1.34		
<i>D<sub>K</sub></i> /kHz	1.21		
<i>d<sub>1</sub></i> /kHz	-0.22		
<i>d<sub>2</sub></i> /kHz	-0.03		
$\Delta E_0$ /kJ mol <sup>-1</sup>	2.9		
<i>E<sub>c</sub></i> /kJ mol <sup>-1</sup>	-11.80		
<i>E<sub>c-BSSSE</sub></i> /kJ mol <sup>-1</sup>	-10.67		

**Table S5.2.** Calculated geometries and spectroscopic parameters of the plausible isomers of BPL-(CO<sub>2</sub>)<sub>2</sub> at the B3LYP-D3(BJ)/def2-TZVP level of theory.

Parameters	I	II	III
			
<i>A</i> / MHz	1371	1116	1206
<i>B</i> / MHz	753	911	868
<i>C</i> / MHz	595	599	602
$\mu_a, \mu_b, \mu_c$ / D	-2.6, 0.4, 3.3	-3.7, 1.9, -1.6	3.2, 1.8, -2.2
<i>D<sub>J</sub></i> / kHz	0.28	4.97	2.95
<i>D<sub>JK</sub></i> / kHz	2.05	-7.17	-4.10
<i>D<sub>K</sub></i> / kHz	0.84	2.89	1.78
<i>d<sub>1</sub></i> / kHz	-0.08	-0.17	-0.58
<i>d<sub>2</sub></i> / kHz	-0.03	-0.70	0.02
$\Delta E_0$ / kJ mol <sup>-1</sup>	0	0.3	0.3
<i>E<sub>c</sub></i> / kJ mol <sup>-1</sup>	-32.72	-32.05	-31.92
<i>E<sub>c</sub>-BSSE</i> / kJ mol <sup>-1</sup>	-30.33	-29.75	-29.62
Parameters	IV	V	VI
			
<i>A</i> / MHz	1103	1124	1045
<i>B</i> / MHz	925	947	893
<i>C</i> / MHz	602	621	560
$\mu_a, \mu_b, \mu_c$ / D	-3.8, 1.8, 1.5	3.1, -0.9, -2.6	1.3, -3.8, -1.6
<i>D<sub>J</sub></i> / kHz	1.54	1.37	33.30
<i>D<sub>JK</sub></i> / kHz	-2.06	-1.98	139.01
<i>D<sub>K</sub></i> / kHz	0.84	0.94	-146.30
<i>d<sub>1</sub></i> / kHz	-0.04	-0.17	12.12
<i>d<sub>2</sub></i> / kHz	-0.08	0.01	3.87
$\Delta E_0$ / kJ mol <sup>-1</sup>	0.3	1.3	2.0
<i>E<sub>c</sub></i> / kJ mol <sup>-1</sup>	-32.09	-31.05	-30.42
<i>E<sub>c</sub>-BSSE</i> / kJ mol <sup>-1</sup>	-29.75	-28.70	-28.20
Parameters	VII	VIII	
			
<i>A</i> / MHz	1268	1574	
<i>B</i> / MHz	807	614	
<i>C</i> / MHz	668	512	
$\mu_a, \mu_b, \mu_c$ / D	-1.4, -1.3, 3.6	0.0, 3.6, 1.9	
<i>D<sub>J</sub></i> / kHz	0.48	0.87	
<i>D<sub>JK</sub></i> / kHz	0.35	-0.31	
<i>D<sub>K</sub></i> / kHz	0.82	11.50	
<i>d<sub>1</sub></i> / kHz	-0.11	-0.23	
<i>d<sub>2</sub></i> / kHz	-0.01	0.00	
$\Delta E_0$ / kJ mol <sup>-1</sup>	2.2	3.6	
<i>E<sub>c</sub></i> / kJ mol <sup>-1</sup>	-29.83	-28.03	
<i>E<sub>c</sub>-BSSE</i> / kJ mol <sup>-1</sup>	-27.45	-25.94	

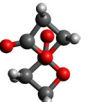
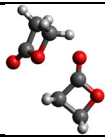
**Table S5.3.** Calculated geometries and spectroscopic parameters of the plausible isomers of BPL-(CO<sub>2</sub>)<sub>3</sub> at the B3LYP-D3(BJ)/def2-TZVP level of theory.

Parameters	I	II	III
			
<i>A</i> / MHz	635	680	754
<i>B</i> / MHz	564	514	530
<i>C</i> / MHz	469	437	380
$\mu_a, \mu_b, \mu_c$ / D	-2.6, -3.4, -0.4	-0.2, -4.2, 1.5	0.4, 2.9, 3.0
<i>D<sub>J</sub></i> / kHz	0.32	0.19	0.50
<i>D<sub>JK</sub></i> / kHz	-0.34	-0.25	-0.61
<i>D<sub>K</sub></i> / kHz	0.17	0.68	0.18
<i>d<sub>1</sub></i> / kHz	-0.02	-0.03	-0.23
<i>d<sub>2</sub></i> / kHz	0.05	0.00	-0.16
$\Delta E_0$ / kJ mol <sup>-1</sup>	0	0.4	0.4
<i>E<sub>c</sub></i> / kJ mol <sup>-1</sup>	-51.84	-51.34	-51.00
<i>E<sub>c</sub>-BSSE</i> / kJ mol <sup>-1</sup>	-48.12	-47.57	-47.32
Parameters	VII	VIII	IX
			
<i>A</i> / MHz	741	919	635
<i>B</i> / MHz	500	447	590
<i>C</i> / MHz	438	357	495
$\mu_a, \mu_b, \mu_c$ / D	4.5, -1.8, -0.3	1.1, 2.7, 3.0	3.9, 2.0, -0.4
<i>D<sub>J</sub></i> / kHz	0.08	0.10	0.22
<i>D<sub>JK</sub></i> / kHz	0.22	0.21	0.02
<i>D<sub>K</sub></i> / kHz	0.00	0.26	-0.13
<i>d<sub>1</sub></i> / kHz	-0.01	-0.02	0.00
<i>d<sub>2</sub></i> / kHz	0.00	0.00	0.02
$\Delta E_0$ / kJ mol <sup>-1</sup>	1.9	2.0	2.0
<i>E<sub>c</sub></i> / kJ mol <sup>-1</sup>	-49.41	-49.45	-49.08
<i>E<sub>c</sub>-BSSE</i> / kJ mol <sup>-1</sup>	-45.77	-45.69	-45.15
Parameters	X	XI	XII
			
<i>A</i> / MHz	686	687	642
<i>B</i> / MHz	493	469	507
<i>C</i> / MHz	446	444	490
$\mu_a, \mu_b, \mu_c$ / D	-4.1, -1.9, -0.1	-4.2, -1.9, -0.1	-3.7, 2.4, 0.5
<i>D<sub>J</sub></i> / kHz	0.44	0.42	1.4
<i>D<sub>JK</sub></i> / kHz	-0.95	0.83	3.4
<i>D<sub>K</sub></i> / kHz	1.87	-0.87	0.18
<i>d<sub>1</sub></i> / kHz	-0.09	-0.17	-0.13
<i>d<sub>2</sub></i> / kHz	0.07	-0.02	0.45
$\Delta E_0$ / kJ mol <sup>-1</sup>	2.2	2.4	2.5
<i>E<sub>c</sub></i> / kJ mol <sup>-1</sup>	-48.91	-48.74	-49.12
<i>E<sub>c</sub>-BSSE</i> / kJ mol <sup>-1</sup>	-45.27	-45.15	-45.48

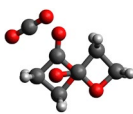
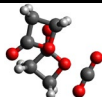
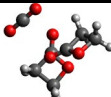
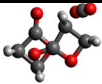
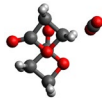
	XIII	XIV	XV
Parameters			
$A$ / MHz	751	716	652
$B$ / MHz	488	502	533
$C$ / MHz	389	457	493
$\mu_a, \mu_b, \mu_c$ / D	0.0, 4.4, 0.8	4.3, -1.7, 0.5	4.3, -1.4, 0.7
$D_J$ / kHz	0.16	0.19	0.23
$D_{JK}$ / kHz	0.06	1.15	-0.22
$D_K$ / kHz	0.65	-1.02	0.39
$d_1$ / kHz	-0.02	0.01	-0.04
$d_2$ / kHz	-0.01	0.00	0.00
$\Delta E_0$ / kJ mol <sup>-1</sup>	2.5	2.5	2.7
$E_c$ / kJ mol <sup>-1</sup>	-48.62	-48.91	-48.62
$E_{c\text{-BSSE}}$ / kJ mol <sup>-1</sup>	-45.02	-45.19	-44.81
	XVI	XVII	XVIII
Parameters			
$A$ / MHz	667	693	709
$B$ / MHz	523	504	476
$C$ / MHz	442	433	438
$\mu_a, \mu_b, \mu_c$ / D	-3.8, -0.6, -2.2	-4.6, 1.1, 0.6	1.3, 2.5, 3.1
$D_J$ / kHz	0.15	0.25	0.25
$D_{JK}$ / kHz	0.05	2.04	0.46
$D_K$ / kHz	0.19	-1.71	0.07
$d_1$ / kHz	-0.03	-0.03	-0.01
$d_2$ / kHz	0.00	-0.06	0.00
$\Delta E_0$ / kJ mol <sup>-1</sup>	2.8	3.3	3.5
$E_c$ / kJ mol <sup>-1</sup>	-48.79	-47.66	-47.78
$E_{c\text{-BSSE}}$ / kJ mol <sup>-1</sup>	-45.19	-44.02	-44.31
	XVI	XVII	XVIII
Parameters			
$A$ / MHz	667	693	709
$B$ / MHz	523	504	476
$C$ / MHz	442	433	438
$\mu_a, \mu_b, \mu_c$ / D	-3.8, -0.6, -2.2	-4.6, 1.1, 0.6	1.3, 2.5, 3.1
$D_J$ / kHz	0.15	0.25	0.25
$D_{JK}$ / kHz	0.05	2.04	0.46
$D_K$ / kHz	0.19	-1.71	0.07
$d_1$ / kHz	-0.03	-0.03	-0.01
$d_2$ / kHz	0.00	-0.06	0.00
$\Delta E_0$ / kJ mol <sup>-1</sup>	2.8	3.3	3.5
$E_c$ / kJ mol <sup>-1</sup>	-48.79	-47.66	-47.78
$E_{c\text{-BSSE}}$ / kJ mol <sup>-1</sup>	-45.19	-44.02	-44.31

Parameters	XIX
$A$ / MHz	895
$B$ / MHz	462
$C$ / MHz	353
$\mu_a, \mu_b, \mu_c$ / D	-0.5, 4.1, 1.4
$D_J$ / kHz	0.12
$D_{JK}$ / kHz	0.16
$D_K$ / kHz	0.58
$d_1$ / kHz	-0.03
$d_2$ / kHz	-0.01
$\Delta E_0$ / kJ mol <sup>-1</sup>	4.1
$E_c$ / kJ mol <sup>-1</sup>	-46.57
$E_{c\text{-BSSE}}$ / kJ mol <sup>-1</sup>	-42.89

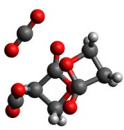
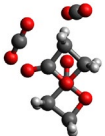
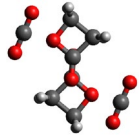
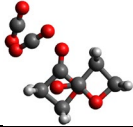
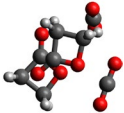
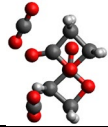
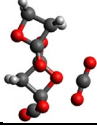
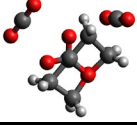
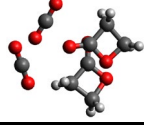
**Table S5.4.** Calculated geometries and spectroscopic parameters of the plausible isomers of (BPL)<sub>2</sub> at the B3LYP-D3(BJ)/def2-TZVP level of theory.

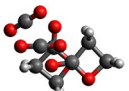
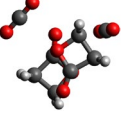
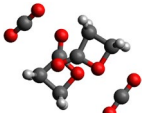
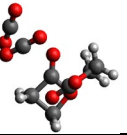
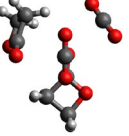
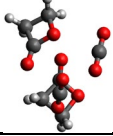
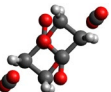
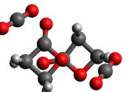
Parameters	I	II	III
			
<i>A</i> / MHz	2026	2157	2559
<i>B</i> / MHz	1063	959	775
<i>C</i> / MHz	845	886	687
$\mu_a, \mu_b, \mu_c$ / D	0.0, 0.0, 0.0	0.3, -0.5, -1.6	0.1, 0.1, 0.7
<i>D<sub>J</sub></i> / kHz	0.30	0.53	0.31
<i>D<sub>JK</sub></i> / kHz	3.11	-0.05	0.68
<i>D<sub>K</sub></i> / kHz	-2.94	1.46	3.71
<i>d<sub>1</sub></i> / kHz	-0.06	0.04	-0.01
<i>d<sub>2</sub></i> / kHz	-0.04	0.00	0.00
$\Delta E_0$ / kJ mol <sup>-1</sup>	0	0.5	2.8
<i>E<sub>c</sub></i> / kJ mol <sup>-1</sup>	-36.23	-36.11	-32.84
<i>E<sub>c</sub></i> -BSSE / kJ mol <sup>-1</sup>	-34.06	-34.10	-30.96

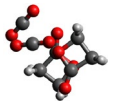
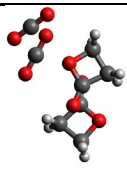
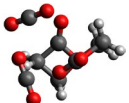
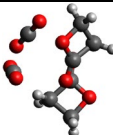
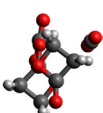
**Table S5.5.** Calculated geometries and spectroscopic parameters of the plausible isomers of (BPL)<sub>2</sub>-CO<sub>2</sub> at the B3LYP-D3(BJ)/def2-TZVP level of theory.

Parameters	I	II	III
			
<i>A</i> / MHz	891	914	937
<i>B</i> / MHz	728	699	630
<i>C</i> / MHz	514	511	477
$\mu_a, \mu_b, \mu_c$ / D	-2.3, -1.0, -0.1	1.4, 0.8, 0.4	-0.7, 0.1, -0.4
<i>D<sub>J</sub></i> / kHz	0.32	0.44	0.17
<i>D<sub>JK</sub></i> / kHz	-0.40	-0.59	0.07
<i>D<sub>K</sub></i> / kHz	0.15	0.24	0.34
<i>d<sub>1</sub></i> / kHz	-0.05	-0.10	-0.04
<i>d<sub>2</sub></i> / kHz	0.01	-0.01	0.00
$\Delta E_0$ / kJ mol <sup>-1</sup>	0	0.8	2.8
<i>E<sub>c</sub></i> / kJ mol <sup>-1</sup>	-59.66	-58.99	-56.15
<i>E<sub>c</sub></i> -BSSE / kJ mol <sup>-1</sup>	-55.86	-55.23	-52.63
Parameters	IV	V	VI
			
<i>A</i> / MHz	844	858	932
<i>B</i> / MHz	712	668	649
<i>C</i> / MHz	520	470	460
$\mu_a, \mu_b, \mu_c$ / D	0.1, -0.4, 0.2	-0.4, 2.0, -0.2	0.1, -0.2, -1.2
<i>D<sub>J</sub></i> / kHz	0.51	0.40	0.51
<i>D<sub>JK</sub></i> / kHz	-0.71	-0.57	-0.67
<i>D<sub>K</sub></i> / kHz	0.30	0.22	0.24
<i>d<sub>1</sub></i> / kHz	-0.08	-0.05	-0.14
<i>d<sub>2</sub></i> / kHz	-0.01	0.05	-0.03
$\Delta E_0$ / kJ mol <sup>-1</sup>	3.3	3.4	3.7
<i>E<sub>c</sub></i> / kJ mol <sup>-1</sup>	-55.56	-55.40	-55.31
<i>E<sub>c</sub></i> -BSSE / kJ mol <sup>-1</sup>	-51.97	-51.92	-51.97
Parameters	VII		
			
<i>A</i> / MHz	1035		
<i>B</i> / MHz	565		
<i>C</i> / MHz	434		
$\mu_a, \mu_b, \mu_c$ / D	0.0, -0.2, 1.8		
<i>D<sub>J</sub></i> / kHz	0.18		
<i>D<sub>JK</sub></i> / kHz	-0.12		
<i>D<sub>K</sub></i> / kHz	1.50		
<i>d<sub>1</sub></i> / kHz	-0.05		
<i>d<sub>2</sub></i> / kHz	0.00		
$\Delta E_0$ / kJ mol <sup>-1</sup>	4.9		
<i>E<sub>c</sub></i> / kJ mol <sup>-1</sup>	-54.06		
<i>E<sub>c</sub></i> -BSSE / kJ mol <sup>-1</sup>	-50.75		

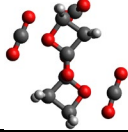
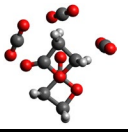
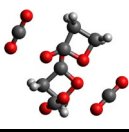
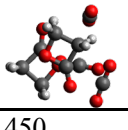
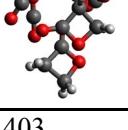
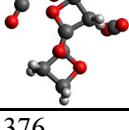
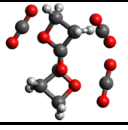
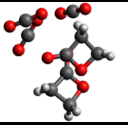
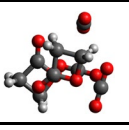
**Table S5.6.** Calculated geometries and spectroscopic parameters of the plausible isomers of (BPL)<sub>2</sub>-(CO)<sub>2</sub> at the B3LYP-D3(BJ)/def2-TZVP level of theory.

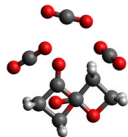
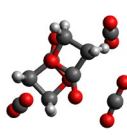
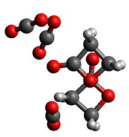
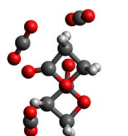
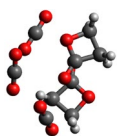
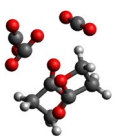
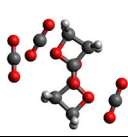
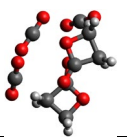
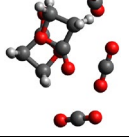
Parameters	I	II	III
			
<i>A</i> / MHz	508	563	700
<i>B</i> / MHz	465	410	395
<i>C</i> / MHz	452	388	294
$\mu_a, \mu_b, \mu_c$ / D	-1.8, -1.1, -0.1	-2.2, 0.3, 1.4	0.0, 0.0, 0.0
<i>D<sub>J</sub></i> / kHz	0.07	0.05	0.04
<i>D<sub>JK</sub></i> / kHz	0.00	0.02	0.21
<i>D<sub>K</sub></i> / kHz	0.01	0.10	0.06
<i>d<sub>1</sub></i> / kHz	0.01	0.00	-0.02
<i>d<sub>2</sub></i> / kHz	0.00	0.00	-0.01
$\Delta E_0$ / kJ mol <sup>-1</sup>	0	0.6	0.6
<i>E<sub>c</sub></i> / kJ mol <sup>-1</sup>	-79.96	-79.66	-79.58
<i>E<sub>c</sub></i> -BSSE / kJ mol <sup>-1</sup>	-74.48	-74.56	-74.18
Parameters	IV	V	VI
			
<i>A</i> / MHz	760	502	557
<i>B</i> / MHz	368	480	413
<i>C</i> / MHz	299	424	358
$\mu_a, \mu_b, \mu_c$ / D	2.2, -1.6, -0.5	-0.9, 0.0, -0.5	1.3, 1.2, -1.3
<i>D<sub>J</sub></i> / kHz	0.04	0.09	0.07
<i>D<sub>JK</sub></i> / kHz	-0.03	0.01	-0.12
<i>D<sub>K</sub></i> / kHz	0.34	-0.03	0.25
<i>d<sub>1</sub></i> / kHz	-0.01	0.01	0.00
<i>d<sub>2</sub></i> / kHz	0.00	0.00	0.00
$\Delta E_0$ / kJ mol <sup>-1</sup>	0.6	1.0	1.3
<i>E<sub>c</sub></i> / kJ mol <sup>-1</sup>	-79.62	-78.74	-78.66
<i>E<sub>c</sub></i> -BSSE / kJ mol <sup>-1</sup>	-74.39	-73.60	-73.51
Parameters	VII	VIII	IX
			
<i>A</i> / MHz	549	555	599
<i>B</i> / MHz	428	385	397
<i>C</i> / MHz	368	371	357
$\mu_a, \mu_b, \mu_c$ / D	-1.2, 0.1, -1.0	1.2, 1.8, 1.4	-2.4, 0.5, -1.4
<i>D<sub>J</sub></i> / kHz	0.04	0.19	0.04
<i>D<sub>JK</sub></i> / kHz	0.17	-0.68	0.03
<i>D<sub>K</sub></i> / kHz	-0.07	1.20	0.10
<i>d<sub>1</sub></i> / kHz	0.00	0.06	0.00
<i>d<sub>2</sub></i> / kHz	0.00	-0.01	0.00
$\Delta E_0$ / kJ mol <sup>-1</sup>	1.3	1.9	1.9
<i>E<sub>c</sub></i> / kJ mol <sup>-1</sup>	-79.04	-77.99	-77.86
<i>E<sub>c</sub></i> -BSSE / kJ mol <sup>-1</sup>	-74.06	-72.89	-72.84

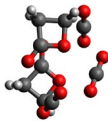
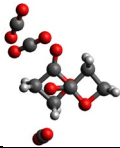
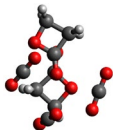
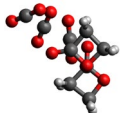
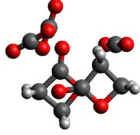
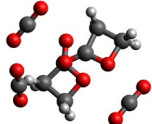
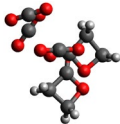
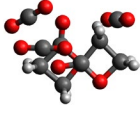
Parameters	X	XI	XII
			
$A$ / MHz	644	530	719
$B$ / MHz	427	403	382
$C$ / MHz	319	381	299
$\mu_a, \mu_b, \mu_c$ / D	-1.8, 1.8, -0.5	0.6, 1.1, 0.2	1.2, 1.0, 0.7
$D_J$ / kHz	0.13	0.08	0.05
$D_{JK}$ / kHz	-0.15	-0.07	-0.09
$D_K$ / kHz	0.05	0.20	0.33
$d_1$ / kHz	-0.03	0.00	-0.01
$d_2$ / kHz	-0.01	0.00	0.00
$\Delta E_0$ / kJ mol <sup>-1</sup>	2.1	2.3	2.7
$E_c$ / kJ mol <sup>-1</sup>	-77.91	-77.36	-76.82
$E_{c\text{-BSSE}}$ / kJ mol <sup>-1</sup>	-72.80	-72.17	-71.63
Parameters	XIII	XIV	XV
			
$A$ / MHz	716	677	509
$B$ / MHz	384	382	478
$C$ / MHz	295	293	368
$\mu_a, \mu_b, \mu_c$ / D	0.8, -0.1, -0.1	-1.2, 2.0, -0.7	1.6, 1.0, -1.5
$D_J$ / kHz	0.06	0.06	0.12
$D_{JK}$ / kHz	-0.09	-0.11	-0.09
$D_K$ / kHz	0.42	0.33	0.01
$d_1$ / kHz	-0.02	-0.02	-0.03
$d_2$ / kHz	0.00	0.00	-0.01
$\Delta E_0$ / kJ mol <sup>-1</sup>	2.9	3.4	3.5
$E_c$ / kJ mol <sup>-1</sup>	-76.65	-76.48	-76.40
$E_{c\text{-BSSE}}$ / kJ mol <sup>-1</sup>	-71.46	-71.55	-71.42
Parameters	XVI	XVII	XVIII
			
$A$ / MHz	530	834	704
$B$ / MHz	449	321	359
$C$ / MHz	401	267	289
$\mu_a, \mu_b, \mu_c$ / D	-0.3, -1.7, -2.5	0.0, 0.0, 0.0	-1.8, 0.3, 0.5
$D_J$ / kHz	0.11	0.04	0.06
$D_{JK}$ / kHz	-0.12	-0.03	1.60
$D_K$ / kHz	0.25	0.27	-0.73
$d_1$ / kHz	-0.02	-0.01	-0.01
$d_2$ / kHz	0.00	0.00	-0.01
$\Delta E_0$ / kJ mol <sup>-1</sup>	3.7	3.8	3.8
$E_c$ / kJ mol <sup>-1</sup>	-76.32	-75.65	-75.77
$E_{c\text{-BSSE}}$ / kJ mol <sup>-1</sup>	-71.25	-70.71	-70.67

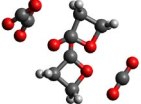
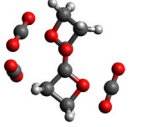
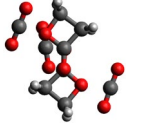
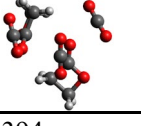
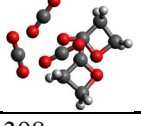
	XIX	XX	XXI
Parameters			
$A$ / MHz	648	772	607
$B$ / MHz	420	354	378
$C$ / MHz	328	300	355
$\mu_a, \mu_b, \mu_c$ / D	1.3, -1.0, 0.1	1.6, -0.9, 0.0	1.1, 1.7, 0.9
$D_J$ / kHz	0.10	0.08	0.07
$D_{JK}$ / kHz	-0.14	-0.35	-0.16
$D_K$ / kHz	0.50	1.23	0.47
$d_1$ / kHz	-0.03	-0.02	0.00
$d_2$ / kHz	0.00	0.00	0.00
$\Delta E_0$ / kJ mol <sup>-1</sup>	4.3	4.3	4.7
$E_c$ / kJ mol <sup>-1</sup>	-74.73	-75.40	-74.98
$E_{c\text{-BSSE}}$ / kJ mol <sup>-1</sup>	-69.45	-70.25	-70.00
	XXII	XXIII	
Parameters			
$A$ / MHz	542	777	
$B$ / MHz	400	336	
$C$ / MHz	388	283	
$\mu_a, \mu_b, \mu_c$ / D	-0.2, -0.9, 0.2	0.6, -0.1, 0.2	
$D_J$ / kHz	0.08	0.03	
$D_{JK}$ / kHz	-0.07	0.08	
$D_K$ / kHz	0.18	0.20	
$d_1$ / kHz	0.00	0.00	
$d_2$ / kHz	0.00	0.00	
$\Delta E_0$ / kJ mol <sup>-1</sup>	4.9	5.0	
$E_c$ / kJ mol <sup>-1</sup>	-75.10	-74.43	
$E_{c\text{-BSSE}}$ / kJ mol <sup>-1</sup>	-70.25	-69.66	

**Table S5.7.** Calculated geometries and spectroscopic parameters of the plausible isomers of (BPL)<sub>2</sub>-(CO<sub>2</sub>)<sub>3</sub> at the B3LYP-D3(BJ)/def2-TZVP level of theory.

Parameters	I	II	III
			
<i>A</i> / MHz	446	379	436
<i>B</i> / MHz	270	339	288
<i>C</i> / MHz	251	279	277
$\mu_a, \mu_b, \mu_c$ / D	0.3, 0.1, 0.5	-0.8, 2.6, -0.1	-0.4, -0.7, 1.0
<i>D<sub>J</sub></i> / kHz	0.03	0.04	0.04
<i>D<sub>JK</sub></i> / kHz	-0.02	-0.04	-0.01
<i>D<sub>K</sub></i> / kHz	0.10	0.01	0.07
<i>d<sub>1</sub></i> / kHz	0.00	0.00	-0.01
<i>d<sub>2</sub></i> / kHz	0.00	0.00	0.00
$\Delta E_0$ / kJ mol <sup>-1</sup>	0	0.2	0.5
<i>E<sub>c</sub></i> / kJ mol <sup>-1</sup>	-100.88	-100.00	-99.75
<i>E<sub>c</sub>-BSSE</i> / kJ mol <sup>-1</sup>	-94.14	-93.39	-92.88
Parameters	IV	V	VI
			
<i>A</i> / MHz	450	403	376
<i>B</i> / MHz	305	307	334
<i>C</i> / MHz	298	291	284
$\mu_a, \mu_b, \mu_c$ / D	-1.8, -0.2, 1.3	-1.5, 1.7, 1.5	-0.7, 1.3, -0.1
<i>D<sub>J</sub></i> / kHz	0.03	0.06	0.06
<i>D<sub>JK</sub></i> / kHz	0.04	0.00	-0.03
<i>D<sub>K</sub></i> / kHz	0.02	0.00	0.00
<i>d<sub>1</sub></i> / kHz	0.00	0.00	-0.01
<i>d<sub>2</sub></i> / kHz	0.00	0.00	-0.01
$\Delta E_0$ / kJ mol <sup>-1</sup>	0.6	0.6	0.6
<i>E<sub>c</sub></i> / kJ mol <sup>-1</sup>	-99.16	-99.83	-99.83
<i>E<sub>c</sub>-BSSE</i> / kJ mol <sup>-1</sup>	-92.13	-93.18	-93.22
Parameters	VII	VIII	IX
			
<i>A</i> / MHz	413	391	450
<i>B</i> / MHz	304	297	309
<i>C</i> / MHz	283	254	288
$\mu_a, \mu_b, \mu_c$ / D	0.5, -0.2, 2.1	-2.0, -1.9, -1.1	1.0, -0.6, 0.3
<i>D<sub>J</sub></i> / kHz	0.03	0.02	0.02
<i>D<sub>JK</sub></i> / kHz	0.05	0.06	0.05
<i>D<sub>K</sub></i> / kHz	-0.01	-0.02	-0.02
<i>d<sub>1</sub></i> / kHz	0.00	0.00	0.00
<i>d<sub>2</sub></i> / kHz	0.00	0.00	0.00
$\Delta E_0$ / kJ mol <sup>-1</sup>	0.7	1.0	1.1
<i>E<sub>c</sub></i> / kJ mol <sup>-1</sup>	-100.37	-99.66	-98.78
<i>E<sub>c</sub>-BSSE</i> / kJ mol <sup>-1</sup>	-93.39	-93.14	-92.05

	X	XI	XII
Parameters			
$A$ / MHz	373	486	401
$B$ / MHz	335	260	303
$C$ / MHz	277	257	242
$\mu_a, \mu_b, \mu_c$ / D	1.7, 1.7, -0.1	1.3, -0.7, -0.9	-2.2, -0.7, -1.0
$D_J$ / kHz	0.07	0.02	0.07
$D_{JK}$ / kHz	-0.09	0.04	-0.08
$D_K$ / kHz	0.06	0.00	0.03
$d_1$ / kHz	-0.01	0.00	-0.01
$d_2$ / kHz	-0.01	0.00	0.01
$\Delta E_0$ / kJ mol <sup>-1</sup>	1.3	1.4	1.6
$E_c$ / kJ mol <sup>-1</sup>	-98.70	-98.49	-98.83
$E_{c-B SSE}$ / kJ mol <sup>-1</sup>	-92.13	-91.71	-92.22
	XIII	XIV	XV
Parameters			
$A$ / MHz	502	411	411
$B$ / MHz	246	309	318
$C$ / MHz	231	261	268
$\mu_a, \mu_b, \mu_c$ / D	-1.4, -0.7, 1.7	0.1, 2.0, 0.8	1.2, -1.0, -1.3
$D_J$ / kHz	0.02	0.02	0.03
$D_{JK}$ / kHz	0.00	0.01	0.04
$D_K$ / kHz	0.07	0.03	-0.02
$d_1$ / kHz	0.00	0.00	0.00
$d_2$ / kHz	0.00	0.00	-0.01
$\Delta E_0$ / kJ mol <sup>-1</sup>	1.7	1.8	1.9
$E_c$ / kJ mol <sup>-1</sup>	-98.49	-98.95	-98.62
$E_{c-B SSE}$ / kJ mol <sup>-1</sup>	-92.09	-92.42	-92.13
	XVI	XVII	XVIII
Parameters			
$A$ / MHz	513	435	459
$B$ / MHz	253	279	268
$C$ / MHz	232	253	258
$\mu_a, \mu_b, \mu_c$ / D	0.5, 0.2, -0.2	0.1, 1.8, -1.3	-0.3, -2.1, 0.4
$D_J$ / kHz	0.02	0.02	0.02
$D_{JK}$ / kHz	0.05	0.00	0.00
$D_K$ / kHz	0.03	0.05	0.03
$d_1$ / kHz	0.00	0.00	0.00
$d_2$ / kHz	0.00	0.00	0.00
$\Delta E_0$ / kJ mol <sup>-1</sup>	2.0	2.1	2.1
$E_c$ / kJ mol <sup>-1</sup>	-98.28	-98.62	-97.74
$E_{c-B SSE}$ / kJ mol <sup>-1</sup>	-91.46	-92.09	-91.13

	XIX	XX	XXI
Parameters			
$A$ / MHz	465	504	401
$B$ / MHz	289	229	319
$C$ / MHz	259	221	256
$\mu_a, \mu_b, \mu_c$ / D	-0.2, 0.1, 1.4	1.7, -1.0, -2.0	0.2, 1.2, -0.9
$D_J$ / kHz	0.03	0.06	0.05
$D_{JK}$ / kHz	-0.02	-0.36	-0.03
$D_K$ / kHz	0.05	0.97	0.00
$d_1$ / kHz	0.00	0.01	-0.01
$d_2$ / kHz	0.00	0.00	0.00
$\Delta E_0$ / kJ mol <sup>-1</sup>	2.3	2.4	2.6
$E_c$ / kJ mol <sup>-1</sup>	-97.78	-97.91	-97.49
$E_{c-BSE}$ / kJ mol <sup>-1</sup>	-91.13	-91.38	-91.13
	XXII	XXIII	XXIV
Parameters			
$A$ / MHz	434	424	426
$B$ / MHz	292	284	284
$C$ / MHz	210	276	236
$\mu_a, \mu_b, \mu_c$ / D	0.8, 2.8, 0.1	-0.5, -1.0, 0.3	0.6, 1.9, -1.1
$D_J$ / kHz	0.05	0.02	0.03
$D_{JK}$ / kHz	-0.07	0.03	0.08
$D_K$ / kHz	0.03	0.00	-0.05
$d_1$ / kHz	-0.01	0.00	0.00
$d_2$ / kHz	0.00	0.00	0.00
$\Delta E_0$ / kJ mol <sup>-1</sup>	2.6	2.7	3.0
$E_c$ / kJ mol <sup>-1</sup>	-97.78	-97.07	-97.15
$E_{c-BSE}$ / kJ mol <sup>-1</sup>	-91.29	-90.67	-90.75
	XXV	XXVI	XXVII
Parameters			
$A$ / MHz	446	481	504
$B$ / MHz	268	272	250
$C$ / MHz	250	214	221
$\mu_a, \mu_b, \mu_c$ / D	-1.1, 0.1, -0.2	-1.4, 2.3, -0.2	1.3, -1.3, -1.4
$D_J$ / kHz	0.05	0.02	0.02
$D_{JK}$ / kHz	-0.14	0.00	-0.02
$D_K$ / kHz	0.26	0.11	0.14
$d_1$ / kHz	0.00	0.00	0.00
$d_2$ / kHz	0.00	0.00	0.00
$\Delta E_0$ / kJ mol <sup>-1</sup>	3.0	3.1	3.2
$E_c$ / kJ mol <sup>-1</sup>	-97.03	-97.24	-96.82
$E_{c-BSE}$ / kJ mol <sup>-1</sup>	-90.50	-90.75	-90.42

	XXVIII	XXIX	XXX
Parameters			
$A$ / MHz	531	396	463
$B$ / MHz	243	296	274
$C$ / MHz	200	257	205
$\mu_a, \mu_b, \mu_c$ / D	-1.1, 0.0, 0.0	-0.3, -0.1, 0.2	0.0, 0.4, -0.1
$D_J$ / kHz	0.02	0.03	0.04
$D_{JK}$ / kHz	0.03	0.02	-0.10
$D_K$ / kHz	0.15	0.01	0.28
$d_1$ / kHz	0.00	0.00	-0.01
$d_2$ / kHz	0.00	0.00	0.00
$\Delta E_0$ / kJ mol <sup>-1</sup>	3.5	3.7	3.8
$E_c$ / kJ mol <sup>-1</sup>	-96.61	-96.69	-96.52
$E_{c-BSE}$ / kJ mol <sup>-1</sup>	-89.96	-90.12	-89.96
	XXXI	XXXII	
Parameters			
$A$ / MHz	394	398	
$B$ / MHz	280	293	
$C$ / MHz	266	252	
$\mu_a, \mu_b, \mu_c$ / D	-0.9, -2.2, 1.1	1.3, 2.2, 1.3	
$D_J$ / kHz	0.03	0.04	
$D_{JK}$ / kHz	0.02	-0.04	
$D_K$ / kHz	0.01	0.08	
$d_1$ / kHz	0.00	0.00	
$d_2$ / kHz	0.00	0.00	
$\Delta E_0$ / kJ mol <sup>-1</sup>	3.9	4.6	
$E_c$ / kJ mol <sup>-1</sup>	-96.36	-95.02	
$E_{c-BSE}$ / kJ mol <sup>-1</sup>	-90.00	-88.74	

**Table S5.8.** Observed rotational transitions and residuals (in MHz) for BPL-CO<sub>2</sub>.

$J'$	$K_a'$	$K_c'$	$J''$	$K_a''$	$K_c''$	Obs.	Obs.-Cal.
2	1	2	1	1	1	3461.3728	-0.0036
2	0	2	1	0	1	3597.1045	-0.0044
2	1	1	1	1	0	3739.4047	-0.0060
3	1	3	2	1	2	5190.0029	-0.0052
3	0	3	2	0	2	5387.4373	0.0012
3	2	2	2	2	1	5400.5623	-0.0041
3	2	1	2	2	0	5413.6753	-0.0080
3	1	2	2	1	1	5606.9970	-0.0045
4	1	4	3	1	3	6916.2369	-0.0024
4	0	4	3	0	3	7167.9592	-0.0034
4	2	3	3	2	2	7198.1430	0.0030
4	2	2	3	2	1	7230.8660	0.0153
4	1	3	3	1	2	7471.9906	0.0037
6	2	4	7	1	7	2879.1547	-0.0165
4	0	4	3	1	3	3155.9229	-0.0007
4	2	3	5	1	4	3221.7741	-0.0044
8	1	7	7	2	6	3539.1808	-0.0023
5	2	3	6	1	6	4054.4152	0.0059
1	1	0	1	0	1	4484.2243	0.0056
2	1	1	2	0	2	4626.5244	0.0040
3	1	2	3	0	3	4846.0841	-0.0017
4	1	3	4	0	4	5150.1155	0.0055
5	0	5	4	1	4	5175.3402	0.0064
4	2	2	5	1	5	5354.6905	0.0050
3	2	2	4	1	3	5357.0151	-0.0073
5	1	4	5	0	5	5547.8573	0.0130
9	1	8	8	2	7	5898.1180	-0.0065
6	1	5	6	0	6	6050.1218	0.0192
1	1	1	0	0	0	6145.3938	-0.0082
7	1	6	7	0	7	6668.4484	0.0041
3	2	1	4	1	4	6763.2198	0.0037
7	3	5	8	2	6	7156.4198	0.0008
6	0	6	5	1	5	7223.8088	0.0039
8	1	7	8	0	8	7413.9953	-0.0115
2	2	1	3	1	2	7428.4434	0.0005
2	1	2	1	0	1	7806.5634	-0.0126

**Table S5.9.** Observed rotational transitions and residuals (in MHz) for BPL-(CO<sub>2</sub>)<sub>2</sub>.

$J'$	$K_a'$	$K_c'$	$J''$	$K_a''$	$K_c''$	Obs.	Obs.-Cal.
2	1	2	1	1	1	2537.7512	0.0113
2	0	2	1	0	1	2669.7636	-0.0017
2	1	1	1	1	0	2855.0148	-0.0055
3	1	3	2	1	2	3791.1415	-0.0077
3	0	3	2	0	2	3942.6923	0.0041
3	2	2	2	2	1	4044.5209	0.0041
3	2	1	2	2	0	4146.3971	0.0113
3	1	2	2	1	1	4264.2117	-0.0083
4	1	4	3	1	3	5029.6426	-0.0021
4	0	4	3	0	3	5162.0603	-0.0031
4	2	3	3	2	2	5371.8090	0.0033
4	3	1	3	3	0	5455.0648	-0.0031
4	2	2	3	2	1	5602.1929	0.0017
4	1	3	3	1	2	5647.4566	-0.0041
5	1	5	4	1	4	6253.2902	0.0017
5	0	5	4	0	4	6346.3569	0.0033
5	2	4	4	2	3	6681.7522	-0.0011
5	4	2	4	4	1	6799.5191	-0.0012
5	4	1	4	4	0	6801.4979	-0.0020
5	3	3	4	3	2	6806.3378	-0.0044
5	3	2	4	3	1	6862.4139	-0.0034
5	1	4	4	1	3	6990.3254	0.0022
5	2	3	4	2	2	7074.2249	0.0001
6	1	6	5	1	5	7464.4327	0.0001
6	0	6	5	0	5	7520.1392	-0.0017
6	2	5	5	2	4	7971.3464	-0.0037
2	2	0	2	1	2	2371.5377	-0.0032
6	3	4	6	2	4	2605.2952	-0.0091
5	3	3	5	2	3	2966.7139	0.0000
4	3	2	4	2	2	3234.5891	-0.0072
3	3	0	3	2	2	3529.7751	0.0132
4	3	1	4	2	3	3613.0309	0.0067
2	1	1	1	0	1	3636.6820	0.0077
5	3	2	5	2	4	3793.6807	-0.0074
4	1	3	3	2	1	3869.6766	-0.0003
8	4	5	8	3	5	4069.9959	0.0004
6	3	3	6	2	5	4130.1966	-0.0106
7	4	4	7	3	4	4427.0277	-0.0042
5	0	5	4	1	3	4572.5226	0.0072
6	4	3	6	3	3	4661.5005	0.0014
7	3	4	7	2	6	4684.1860	0.0002
2	2	0	1	1	0	4750.6332	-0.0053
7	1	7	6	2	5	4790.6518	0.0171
5	4	2	5	3	2	4793.0121	0.0030
4	4	1	4	3	1	4855.9070	0.0009
5	4	1	5	3	3	4870.8677	0.0015
4	4	0	4	3	2	4875.7076	-0.0008
2	2	1	1	1	1	4882.6575	-0.0018
6	4	2	6	3	4	4885.9835	-0.0004
7	4	3	7	3	5	4950.0465	0.0000

6	0	6	5	1	4	5102.3364	0.0032
8	4	4	8	3	6	5107.2836	0.0031
7	3	4	6	4	2	5120.7185	0.0022
6	2	4	6	1	6	5187.2015	0.0129
3	1	2	2	0	2	5231.1301	0.0010
5	1	4	4	2	2	5257.8092	0.0002
7	2	6	6	3	4	5322.5160	0.0015
9	4	5	9	3	7	5416.6079	0.0027
6	2	4	5	3	2	5489.0156	-0.0045
8	3	5	8	2	7	5498.4927	0.0013
7	0	7	6	1	5	5520.7372	-0.0001
10	5	6	10	4	6	5614.1496	0.0010
8	0	8	7	1	6	5893.3258	-0.0029
9	5	5	9	4	5	5901.6943	0.0072
10	4	6	10	3	8	5943.1314	-0.0044
8	3	6	7	4	4	5946.8865	-0.0050
9	1	9	8	2	7	5983.5553	0.0034
3	2	1	2	1	1	6042.0036	-0.0002
8	5	4	8	4	4	6078.1121	0.0004
7	5	3	7	4	3	6178.7248	0.0023
9	5	4	9	4	6	6188.1065	0.0019
8	5	3	8	4	5	6194.6154	-0.0028
7	5	2	7	4	4	6218.8864	-0.0034
10	5	5	10	4	7	6227.5171	0.0034
6	5	2	6	4	2	6233.7399	0.0003
6	5	1	6	4	3	6244.8978	0.0002
5	5	1	5	4	1	6263.1607	-0.0020
5	5	0	5	4	2	6265.4138	0.0009
9	0	9	8	1	7	6270.7543	-0.0053
8	2	7	7	3	5	6285.8105	-0.0053
3	2	2	2	1	2	6389.4391	0.0028
6	1	5	5	2	3	6461.6084	-0.0034
4	1	3	3	0	3	6935.8945	-0.0071
7	2	5	6	3	3	7132.8044	-0.0016
9	2	8	8	3	6	7141.7928	-0.0030
9	3	7	8	4	5	7175.5886	0.0080
4	2	2	3	1	2	7379.9729	-0.0020
7	1	6	6	2	4	7435.3218	0.0009
11	6	5	11	5	7	7482.1711	0.0019
10	6	4	10	5	6	7527.6017	-0.0042
3	3	0	2	2	0	7547.6527	-0.0043
9	6	4	9	5	4	7553.9708	-0.0104
3	3	1	2	2	1	7571.4469	0.0079
9	6	3	9	5	5	7573.2231	0.0074
8	6	2	8	5	4	7611.6681	0.0001
4	2	3	3	1	3	7970.0947	0.0021

**Table S5.10.** Observed rotational transitions and residuals (in MHz) for BPL-(CO<sub>2</sub>)<sub>3</sub>.

$J'$	$K_a'$	$K_c'$	$J''$	$K_a''$	$K_c''$	Obs.	Obs.-Cal.
3	1	3	2	1	2	2910.5186	0.0023
3	2	1	2	2	0	3211.0095	-0.0113
4	1	4	3	1	3	3851.4614	-0.0036
4	0	4	3	0	3	3858.8166	0.0234
4	2	3	3	2	2	4057.9796	0.0021
4	1	3	3	1	2	4136.9915	-0.0066
4	3	1	3	3	0	4239.3327	-0.0106
4	2	2	3	2	1	4290.5092	0.0007
5	1	5	4	1	4	4786.4318	-0.0091
5	0	5	4	0	4	4788.2557	-0.0015
5	2	4	4	2	3	5019.7124	-0.0039
5	1	4	4	1	3	5059.9098	-0.0080
5	3	3	4	3	2	5176.8303	-0.0060
5	4	2	4	4	1	5221.4503	-0.0112
5	4	1	4	4	0	5256.9032	-0.0131
5	2	3	4	2	2	5316.6270	0.0085
5	3	2	4	3	1	5360.2099	-0.0182
6	1	6	5	1	5	5719.4710	0.0145
6	0	6	5	0	5	5719.8524	-0.0029
6	2	5	5	2	4	5964.5653	0.0046
6	1	5	5	1	4	5978.5485	0.0027
6	3	4	5	3	3	6168.2343	-0.0113
6	4	3	5	4	2	6266.9158	0.0092
6	2	4	5	2	3	6273.8776	0.0167
6	5	1	5	5	0	6283.8197	-0.0061
6	4	2	5	4	1	6382.0839	0.0129
6	3	3	5	3	2	6446.5284	0.0069
7	1	7	6	1	6	6651.9380	-0.0163
7	0	7	6	0	6	6652.0452	0.0093
7	2	6	6	2	5	6900.9423	-0.0098
7	1	6	6	1	5	6904.8524	-0.0098
7	3	5	6	3	4	7133.3528	-0.0125
7	2	5	6	2	4	7186.9850	0.0155
7	4	4	6	4	3	7290.0772	0.0053
7	6	2	6	6	1	7314.8966	-0.0158
7	6	1	6	6	0	7318.8305	0.0050
7	5	3	6	5	2	7333.3502	0.0038
7	5	2	6	5	1	7388.8183	0.0177
7	3	4	6	3	3	7466.4831	0.0017
7	4	3	6	4	2	7516.8371	0.0201
8	1	8	7	1	7	7584.3215	0.0002
8	0	8	7	0	7	7584.3215	-0.0156
8	2	7	7	2	6	7834.2319	-0.0098
8	1	7	7	1	6	7835.2094	0.0025
3	0	3	2	1	2	2900.8746	0.0028
3	1	3	2	0	2	2943.4442	0.0047
3	3	1	2	2	0	3669.9533	-0.0059
3	3	0	2	2	1	3733.5873	-0.0109
4	0	4	3	1	3	3849.1607	0.0120
4	1	4	3	0	3	3861.1174	0.0078

4	1	3	3	2	2	3998.6372	0.0008
4	2	3	3	1	2	4196.3458	0.0066
4	3	2	3	2	1	4617.1784	-0.0057
5	0	5	4	1	4	4785.9430	0.0021
5	1	5	4	0	4	4788.7683	0.0110
4	3	1	3	2	2	4900.5270	-0.0097
4	4	1	3	3	0	4960.9542	-0.0030
4	4	0	3	3	1	4983.3059	-0.0046
5	2	3	4	3	2	4989.9340	-0.0087
5	1	4	4	2	3	5000.5674	-0.0093
5	2	4	4	1	3	5079.0668	0.0093
5	3	3	4	2	2	5503.5114	-0.0005
6	0	6	5	1	5	5719.3637	0.0083
6	1	6	5	0	5	5719.9597	0.0032
5	4	2	4	3	1	5943.0838	0.0083
6	1	5	5	2	4	5959.3916	-0.0145
6	3	4	5	2	3	6355.1426	0.0033
6	2	5	5	1	4	5983.6984	-0.0019
5	4	1	4	3	2	6081.9745	-0.0066
5	5	1	4	4	0	6240.9163	-0.0082
5	5	0	4	4	1	6247.5324	-0.0031
7	0	7	6	1	6	6651.9380	0.0031
7	1	7	6	0	6	6652.0452	-0.0102
6	4	3	5	3	2	6849.7658	0.0119
7	1	6	6	2	5	6899.7145	0.0068
7	2	6	6	1	5	6906.1160	0.0092
7	2	5	6	3	4	7105.6962	0.0051
7	3	5	6	2	4	7214.6416	-0.0020
6	5	2	5	4	1	7255.2800	0.0068
6	5	1	5	4	2	7309.9017	0.0018
6	6	1	5	5	0	7515.3470	-0.0026
6	6	0	5	5	1	7517.1232	0.0027
8	0	8	7	1	7	7584.3215	0.0038
8	1	8	7	0	7	7584.3215	-0.0193
6	3	3	5	2	4	7629.5972	0.0047
7	4	4	6	3	3	7693.3026	-0.0016
8	1	7	7	2	6	7833.9577	-0.0047
8	2	7	7	1	6	7835.4836	-0.0026

**Table S5.11.** Observed rotational transitions and residuals (in MHz) for (BPL)<sub>2</sub>.

$J'$	$K_a'$	$K_c'$	$J''$	$K_a''$	$K_c''$	Obs.	Obs.-Cal.
6	1	5	6	0	6	2097.0583	-0.0007
9	2	8	9	1	8	2313.7093	-0.0024
7	1	6	7	0	7	2436.4233	0.0144
2	0	2	1	1	0	2446.8899	0.0009
8	2	7	8	1	7	2571.9523	0.0045
7	2	6	7	1	6	2812.6121	-0.0041
6	2	5	6	1	5	3030.7889	-0.0019
1	1	1	0	0	0	3067.8749	-0.0082
5	2	4	4	3	2	3093.4572	-0.0065
8	2	6	8	1	7	3105.6881	-0.0104
1	1	0	0	0	0	3135.8004	-0.0050
7	2	5	7	1	6	3143.9066	-0.0180
5	2	3	4	3	1	3188.8723	-0.0079
6	2	4	6	1	5	3219.4614	-0.0075
5	2	4	5	1	4	3222.7516	-0.0030
5	2	3	5	1	4	3318.6674	-0.0046
4	1	4	3	2	2	3380.4655	-0.0173
4	2	3	4	1	3	3385.7942	-0.0085
4	2	2	4	1	3	3427.3267	0.0038
3	2	2	3	1	2	3518.0330	0.0030
3	2	1	3	1	2	3531.9328	-0.0097
2	2	1	2	1	1	3618.1450	0.0051
2	2	0	2	1	1	3620.9345	0.0059
2	1	2	1	1	1	3655.7078	-0.0195
2	0	2	1	0	1	3720.8676	0.0051
2	1	1	1	1	0	3791.5587	-0.0141
2	2	1	2	1	2	3821.9094	0.0018
2	2	0	2	1	2	3824.6989	0.0026
3	2	2	3	1	3	3925.5023	0.0055
3	2	1	3	1	3	3939.4021	-0.0072
4	1	3	3	2	1	4045.3076	0.0010
4	1	3	3	2	2	4059.2194	0.0002
4	2	3	4	1	4	4064.5361	-0.0029
4	2	2	4	1	4	4106.0567	-0.0025
3	0	3	2	1	1	4229.6290	-0.0077
5	2	4	5	1	5	4239.6069	-0.0157
5	2	3	5	1	5	4335.5346	-0.0055
7	3	5	6	4	3	4382.5984	0.0008
7	3	4	6	4	2	4397.3923	-0.0151
3	0	3	2	1	2	4433.3935	-0.0109
6	2	5	6	1	6	4451.2391	-0.0061
6	2	4	6	1	6	4639.9236	0.0002
7	2	6	7	1	7	4699.6832	-0.0001
2	1	2	1	0	1	4861.7601	-0.0184
6	2	5	5	3	2	4931.7241	-0.0016
6	2	5	5	3	3	4933.7268	0.0008
8	2	7	8	1	8	4984.8676	0.0008
5	1	5	4	2	2	5021.5483	-0.0064
7	2	5	7	1	7	5030.9896	-0.0021
5	1	5	4	2	3	5063.0808	0.0058

2	1	1	1	0	1	5065.5484	0.0021
6	2	4	5	3	2	5120.4085	0.0045
6	2	4	5	3	3	5122.3993	-0.0048
9	2	8	9	1	9	5306.2677	-0.0048
10	3	8	10	2	8	5393.9819	0.0013
3	1	3	2	1	2	5481.8392	-0.0100
10	3	7	10	2	8	5511.4150	0.0034
8	2	6	8	1	8	5518.6152	-0.0023
3	0	3	2	0	2	5574.2979	-0.0227
3	2	2	2	2	1	5585.4201	-0.0183
3	2	1	2	2	0	5596.5424	-0.0199
9	3	7	9	2	7	5627.5129	0.0030
3	1	2	2	1	1	5685.5321	-0.0162
9	3	6	9	2	7	5691.7548	0.0076
8	3	6	8	2	6	5815.8517	0.0046
8	3	5	8	2	6	5848.3243	-0.0038
7	3	5	7	2	5	5959.3916	0.0096
4	0	4	3	1	2	5963.6593	-0.0191
7	3	4	7	2	5	5974.2570	-0.0034
5	1	4	4	2	2	6038.4274	0.0045
6	3	4	6	2	4	6061.5182	0.0028
6	3	3	6	2	4	6067.5025	0.0054
5	1	4	4	2	3	6079.9479	0.0048
9	2	7	9	1	9	6109.4880	-0.0002
5	3	3	5	2	3	6128.3588	0.0049
5	3	2	5	2	3	6130.3616	0.0075
4	3	2	4	2	2	6167.7217	0.0080
4	3	1	4	2	2	6168.2343	0.0196
3	3	1	3	2	1	6187.7966	0.0027
3	3	0	3	2	1	6187.8800	0.0145
3	3	1	3	2	2	6201.7322	0.0258
3	3	0	3	2	2	6201.7918	0.0137
4	3	2	4	2	3	6209.2423	0.0084
4	3	1	4	2	3	6209.7430	0.0082
5	3	3	5	2	4	6224.2746	0.0032
5	3	2	5	2	4	6226.2773	0.0057
6	3	4	6	2	5	6250.2027	0.0091
8	3	6	7	4	3	6255.0783	0.0193
8	3	6	7	4	4	6255.3287	0.0187
6	3	3	6	2	5	6256.1870	0.0117
8	3	5	7	4	3	6287.5628	0.0227
7	3	5	7	2	6	6290.6981	0.0077
7	3	4	7	2	6	6305.5754	0.0065
8	3	6	8	2	7	6349.6113	0.0134
4	0	4	3	1	3	6371.1643	0.0190
8	3	5	8	2	7	6382.0720	-0.0069
9	3	7	9	2	8	6430.7213	-0.0042
9	3	6	9	2	8	6494.9632	0.0003
10	3	8	10	2	9	6537.6997	0.0086
6	1	6	5	2	3	6610.8584	0.0237
3	1	3	2	0	2	6622.7436	-0.0217
10	3	7	10	2	9	6655.1328	0.0106
6	1	6	5	2	4	6706.7623	0.0101

7	2	6	6	3	3	6754.3149	0.0250
7	2	6	6	3	4	6760.2873	0.0157
3	1	2	2	0	2	7030.2248	-0.0073
7	2	5	6	3	3	7085.6214	0.0231
7	2	5	6	3	4	7091.5818	0.0018
4	1	4	3	1	3	7305.9678	-0.0117
2	2	1	1	1	0	7409.7037	-0.0089
2	2	0	1	1	0	7412.4813	-0.0200
4	0	4	3	0	3	7419.5743	-0.0157
4	2	3	3	2	2	7445.0135	-0.0083
4	3	2	3	3	1	7452.5356	-0.0137
4	3	1	3	3	0	7452.9648	-0.0138
4	2	2	3	2	1	7472.6105	-0.0189
2	2	1	1	1	1	7477.6292	-0.0057
2	2	0	1	1	1	7480.4187	-0.0049
4	1	3	3	1	2	7577.2405	-0.0085
5	0	5	4	1	3	7640.9221	-0.0001

**Table S5.12.** Observed rotational transitions and residuals (in MHz) for (BPL)<sub>2</sub>-CO<sub>2</sub>.

$J'$	$K_a'$	$K_c'$	$J''$	$K_a''$	$K_c''$	Obs.	Obs.-Cal.
4	2	3	4	0	4	2020.0729	-0.0069
5	3	3	5	1	4	2100.7776	0.0235
7	3	4	7	3	5	2102.7923	0.0162
2	1	2	1	1	1	2264.7262	0.0069
2	0	2	1	0	1	2366.7216	0.0028
6	2	4	6	2	5	2377.8081	0.0060
2	1	2	1	0	1	2436.7213	-0.0099
5	2	4	5	0	5	2556.5267	0.0103
2	1	1	1	1	0	2691.6027	-0.0097
7	2	5	7	2	6	3027.1888	0.0130
7	2	5	7	1	6	3029.4180	-0.0098
8	4	5	8	3	6	3046.7272	0.0027
8	4	5	8	2	6	3061.2946	-0.0184
7	3	5	7	2	6	3079.9150	-0.0014
7	3	5	7	1	6	3082.1800	0.0113
6	1	5	6	1	6	3111.0048	-0.0008
6	2	5	6	0	6	3120.9230	0.0095
2	2	1	1	1	0	3207.6478	-0.0016
3	0	3	2	1	2	3319.0608	-0.0099
3	1	3	2	1	2	3338.7423	0.0074
3	0	3	2	0	2	3389.0843	0.0010
3	1	3	2	0	2	3408.7539	0.0066
2	2	0	1	1	1	3532.5289	-0.0157
10	5	6	10	3	7	3558.8980	-0.0062
9	4	6	9	2	7	3594.1482	-0.0026
8	2	6	8	2	7	3632.3190	0.0011
8	3	6	8	1	7	3647.3751	-0.0165
7	1	6	7	1	7	3691.4587	-0.0075
7	2	6	7	0	7	3693.7475	-0.0046
2	2	0	1	0	1	3704.5598	0.0031
3	2	2	2	2	1	3717.2437	0.0068
3	1	2	2	1	1	3936.3503	-0.0009
3	2	1	2	2	0	4045.3911	-0.0016
10	3	7	10	3	8	4142.9639	0.0117
10	4	7	10	2	8	4162.5977	0.0023
9	2	7	9	2	8	4218.8525	0.0030
9	3	7	9	1	8	4222.5838	-0.0040
3	2	2	2	1	1	4233.2649	-0.0089
8	1	7	8	1	8	4267.9191	-0.0055
8	1	7	8	0	8	4267.9191	-0.0116
8	2	7	8	1	8	4268.4197	0.0097
8	2	7	8	0	8	4268.4197	0.0036
4	0	4	3	1	3	4378.3545	0.0236
4	1	4	3	1	3	4382.8607	0.0003
4	0	4	3	0	3	4398.0002	0.0052
4	1	4	3	0	3	4402.5302	0.0058
11	3	8	11	3	9	4736.3996	-0.0103
4	1	3	3	2	2	4741.2872	0.0052
11	4	8	11	2	9	4741.5376	-0.0068
10	2	8	10	2	9	4798.7938	-0.0031

10	2	8	10	1	9	4798.7938	-0.0226
10	3	8	10	2	9	4799.6521	0.0109
10	3	8	10	1	9	4799.6521	-0.0086
9	1	8	9	1	9	4843.0800	-0.0058
9	1	8	9	0	9	4843.0800	-0.0068
9	2	8	9	1	9	4843.1873	0.0022
9	2	8	9	0	9	4843.1873	0.0011
4	2	3	3	2	2	4863.5364	0.0056
4	1	3	3	1	2	5038.2018	-0.0027
3	3	1	2	2	0	5057.8117	0.0059
4	3	2	3	3	1	5102.8490	0.0011
4	2	3	3	1	2	5160.4509	-0.0024
3	3	0	2	2	1	5211.9732	0.0024
4	3	1	3	3	0	5301.2729	0.0013
3	2	1	2	1	2	5313.2057	-0.0124
11	2	9	11	2	10	5376.2794	0.0053
11	2	9	11	1	10	5376.2794	0.0015
11	3	9	11	2	10	5376.4701	0.0105
11	3	9	11	1	10	5376.4701	0.0068
3	2	1	2	0	2	5383.2293	-0.0013
4	2	2	3	2	1	5408.3824	0.0051
5	0	5	4	1	4	5412.8408	0.0155
5	1	5	4	1	4	5413.7468	-0.0167
5	0	5	4	0	4	5417.3589	0.0041
10	1	9	10	1	10	5417.7403	0.0124
10	1	9	10	0	10	5417.7403	0.0122
10	2	9	10	1	10	5417.7403	-0.0071
10	2	9	10	0	10	5417.7403	-0.0072
5	1	5	4	0	4	5418.2887	-0.0043
3	3	0	2	1	1	5728.0064	-0.0014
5	1	4	4	2	3	5916.0709	-0.0182
5	2	3	4	3	2	5934.3934	-0.0073
5	2	4	4	2	3	5953.7888	-0.0024
11	1	10	11	1	11	5992.1026	0.0067
11	1	10	11	0	11	5992.1026	0.0067
11	2	10	11	1	11	5992.1026	0.0030
11	2	10	11	0	11	5992.1026	0.0030
5	1	4	4	1	3	6038.3201	-0.0178
5	2	4	4	1	3	6076.0260	-0.0139
4	3	2	3	2	1	6115.2458	-0.0150
5	3	3	4	3	2	6325.5072	-0.0025
3	3	1	2	1	2	6325.6383	0.0071
5	4	2	4	4	1	6436.8844	0.0059
6	0	6	5	1	5	6440.3653	-0.0032
6	1	6	5	1	5	6440.5560	0.0053
6	0	6	5	0	5	6441.3071	0.0002
6	1	6	5	0	5	6441.4859	-0.0030
5	4	1	4	4	0	6527.3762	0.0009
5	2	3	4	2	2	6641.2806	-0.0037
5	3	2	4	3	1	6764.3404	0.0105
4	3	1	3	2	2	6796.0024	-0.0030
4	4	1	3	3	0	6899.1780	0.0203
4	4	0	3	3	1	6955.3614	0.0276

6	1	5	5	2	4	6995.9760	-0.0023
6	2	5	5	2	4	7005.7034	-0.0005
5	3	3	4	2	2	7032.3944	0.0010
6	1	5	5	1	4	7033.6819	0.0015
6	2	5	5	1	4	7043.3974	-0.0086
4	3	1	3	1	2	7092.9289	0.0007
6	2	4	5	3	3	7320.4517	-0.0023
4	2	2	3	0	3	7402.5035	-0.0211
7	0	7	6	1	6	7466.3401	0.0390
7	1	7	6	1	6	7466.3401	0.0051
7	0	7	6	0	6	7466.4831	-0.0001
7	1	7	6	0	6	7466.4831	-0.0339
6	3	4	5	3	3	7482.8744	-0.0037
6	2	4	5	2	3	7711.5536	-0.0095
6	4	3	5	4	2	7723.1884	0.0024
6	5	2	5	5	1	7739.3532	0.0191
6	5	1	5	5	0	7772.7795	0.0087

**Table S5.13.** Observed rotational transitions and residuals (in MHz) for (BPL)<sub>2</sub>-(CO<sub>2</sub>)<sub>2</sub>.

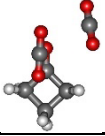
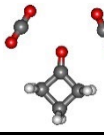
$J'$	$K_a'$	$K_c'$	$J''$	$K_a''$	$K_c''$	Obs.	Obs.-Cal.
3	1	3	2	1	2	2714.7889	-0.0063
3	0	3	2	0	2	2727.0675	0.0032
3	1	2	2	1	1	2760.7799	0.0124
4	0	4	3	1	3	3607.0704	0.0100
4	1	4	3	1	3	3616.6191	-0.0144
4	0	4	3	0	3	3625.6433	0.0063
4	1	4	3	0	3	3635.2038	-0.0063
4	2	3	3	2	2	3650.5938	-0.0047
4	3	2	3	3	1	3659.0815	-0.0038
4	1	3	3	1	2	3675.6635	-0.0013
4	2	2	3	2	1	3678.2384	-0.0142
5	0	5	4	1	4	4512.4769	-0.0153
5	1	5	4	1	4	4516.9115	0.0076
5	0	5	4	0	4	4522.0613	-0.0040
5	1	5	4	0	4	4526.4721	-0.0049
5	2	4	4	2	3	4558.9328	-0.0045
5	3	3	4	3	2	4574.3704	0.0121
5	4	2	4	4	1	4574.4061	-0.0111
5	4	1	4	4	0	4574.9068	0.0114
5	3	2	4	3	1	4583.8833	0.0170
5	1	4	4	1	3	4584.8727	0.0102
5	2	3	4	2	2	4603.0641	-0.0033
5	4	2	4	3	1	4920.1131	0.0014
5	4	1	4	3	2	4924.1185	0.0133
6	0	6	5	1	5	5414.1521	0.0032
6	1	6	5	1	5	5416.0357	-0.0025
6	0	6	5	0	5	5418.5748	0.0142
6	1	6	5	0	5	5420.4583	0.0083
6	2	5	5	2	4	5464.7684	-0.0105
6	1	5	5	1	4	5487.1559	-0.0188
6	3	4	5	3	3	5488.5268	0.0034
6	4	3	5	4	2	5491.2567	-0.0062
6	4	2	5	4	1	5493.3190	-0.0050
6	3	3	5	3	2	5510.2944	0.0013
6	2	5	5	1	4	5521.5597	-0.0051
6	2	4	5	2	3	5524.1466	0.0059
6	4	3	5	3	2	5827.4865	-0.0218
6	4	2	5	3	3	5843.0791	0.0081
6	5	2	5	4	1	5936.5392	0.0145
6	5	1	5	4	2	5937.1471	0.0114
6	6	1	5	5	0	6037.0326	0.0055
6	6	0	5	5	1	6037.0326	-0.0017
7	0	7	6	1	6	6313.7174	0.0116
7	1	7	6	1	6	6314.4803	0.0039
7	0	7	6	0	6	6315.6009	0.0056
7	1	7	6	0	6	6316.3757	0.0099
7	2	6	6	2	5	6368.1722	0.0013
7	1	6	6	1	5	6384.0508	-0.0032
7	3	5	6	3	4	6400.7401	-0.0045
7	2	6	6	1	5	6402.5521	-0.0087

7	6	2	6	6	1	6403.3031	-0.0168
7	6	1	6	6	0	6403.3031	-0.0248
7	5	3	6	5	2	6405.8781	-0.0071
7	5	2	6	5	1	6406.2238	-0.0094
7	4	4	6	4	3	6408.3695	-0.0124
7	4	3	6	4	2	6414.7472	-0.0054
7	3	4	6	3	3	6439.2924	0.0021
7	2	5	6	2	4	6439.4832	0.0050
7	3	5	6	2	4	6555.7122	-0.0059
7	4	3	6	3	4	6769.3114	0.0111
7	7	1	6	6	0	7051.5156	0.0059
7	7	0	6	6	1	7051.5156	0.0051
8	0	8	7	1	7	7212.2574	0.0225
8	1	8	7	1	7	7212.5554	0.0169
8	0	8	7	0	7	7213.0203	0.0148
8	1	8	7	0	7	7213.3303	0.0213
8	1	7	7	2	6	7260.4060	0.0082
8	2	7	7	2	6	7269.4659	-0.0041
8	1	7	7	1	6	7278.9073	0.0027
8	2	7	7	1	6	7287.9672	-0.0096
8	7	2	7	7	1	7317.6980	-0.0243
8	7	1	7	7	0	7317.6980	-0.0252
8	6	3	7	6	2	7320.0822	-0.0108
8	6	2	7	6	1	7320.1299	-0.0137
8	5	4	7	5	3	7323.6346	-0.0058
8	5	3	7	5	2	7324.9698	-0.0002
8	4	5	7	4	4	7325.0532	0.0006
8	4	4	7	4	3	7340.4908	0.0190
8	2	6	7	2	5	7347.5599	0.0021
8	3	5	7	3	4	7366.7049	0.0143
8	3	6	7	2	5	7426.6195	-0.0339
8	7	2	7	6	1	7965.8985	-0.0056
8	7	1	7	6	2	7965.8985	-0.0152

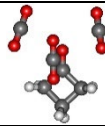
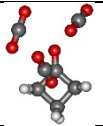
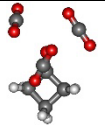
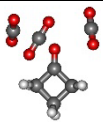
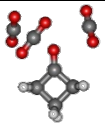
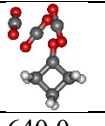
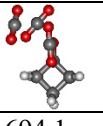
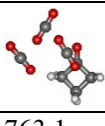
**Table S6.1.** Calculated geometries and spectroscopic parameters of the plausible isomers of CBN-CO<sub>2</sub> at the B3LYP-D3(BJ)/def2-TZVP level of theory.

Parameters	I	II
		
$A$ / MHz	5052.3	3840.0
$B$ / MHz	943.1	1119.1
$C$ / MHz	806.7	1010.2
$\mu_a, \mu_b, \mu_c$ / D	2.9, 1.5, 0.0	-1.9, 0.0, 1.7
$D_J$ / kHz	0.475	2.428
$D_{JK}$ / kHz	0.326	-8.639
$D_K$ / kHz	7.999	35.562
$d_1$ / kHz	-0.0732	-0.469
$d_2$ / kHz	0.0121	0.0193
$\Delta E_0$ / kJ mol <sup>-1</sup>	0.0	2.1
$E_c$ / kJ mol <sup>-1</sup>	-15.27	-13.43
$E_{c-BSE}$ / kJ mol <sup>-1</sup>	-13.85	-12.55

**Table S6.2.** Calculated geometries and spectroscopic parameters of the plausible isomers of CBN-(CO<sub>2</sub>)<sub>2</sub> at the B3LYP-D3(BJ)/def2-TZVP level of theory.

Parameters	I	II
		
$A$ / MHz	1329.5	885.4
$B$ / MHz	755.7	818.5
$C$ / MHz	589.3	440.1
$\mu_a, \mu_b, \mu_c$ / D	-2.9, 0.0, -1.3	0.1, -3.4, 0.0
$D_J$ / kHz	0.288	2.718
$D_{JK}$ / kHz	0.367	-4.624
$D_K$ / kHz	3.171	2.106
$d_1$ / kHz	-0.0813	0.257
$d_2$ / kHz	-0.0161	0.653
$\Delta E_0$ / kJ mol <sup>-1</sup>	0.0	1.7
$E_c$ / kJ mol <sup>-1</sup>	-33.18	-30.38
$E_{c-BSE}$ / kJ mol <sup>-1</sup>	-30.67	-27.61

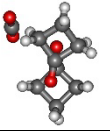
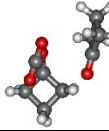
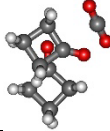
**Table S6.3.** Calculated geometries and spectroscopic parameters of the plausible isomers of CBN-(CO<sub>2</sub>)<sub>3</sub> at the B3LYP-D3(BJ)/def2-TZVP level of theory.

Parameters	I	II	III
			
<i>A</i> / MHz	625.8	666.6	611.9
<i>B</i> / MHz	569.1	517.5	547.1
<i>C</i> / MHz	443.6	442.0	408.3
$\mu_a, \mu_b, \mu_c$ / D	-3.3, 0.0, -0.3	3.2, -0.6, 0.4	-1.8, 2.7, 0.9
<i>D<sub>J</sub></i> / kHz	0.406	0.130	1.080
<i>D<sub>JK</sub></i> / kHz	-0.308	0.0548	0.544
<i>D<sub>K</sub></i> / kHz	-0.0143	0.217	-0.0881
<i>d<sub>1</sub></i> / kHz	-0.176	-0.0200	-0.0482
<i>d<sub>2</sub></i> / kHz	-0.0908	0.00529	-0.113
$\Delta E_0$ / kJ mol <sup>-1</sup>	0.0	0.9	1.1
<i>E<sub>c</sub></i> / kJ mol <sup>-1</sup>	-52.76	-51.55	-50.92
<i>E<sub>c</sub>-BSSE</i> / kJ mol <sup>-1</sup>	-48.66	-47.70	-46.90
Parameters	IV	V	VI
			
<i>A</i> / MHz	696.9	608.2	584.9
<i>B</i> / MHz	501.1	549.5	557.3
<i>C</i> / MHz	455.0	406.2	406.1
$\mu_a, \mu_b, \mu_c$ / D	-3.4, 0.0, 0.3	-1.8, 2.7, -0.9	-2.7, -2.1, 0.7
<i>D<sub>J</sub></i> / kHz	0.305	0.571	0.520
<i>D<sub>JK</sub></i> / kHz	-0.186	0.118	-0.159
<i>D<sub>K</sub></i> / kHz	0.394	0.0178	0.00447
<i>d<sub>1</sub></i> / kHz	-0.0750	-0.0269	0.00120
<i>d<sub>2</sub></i> / kHz	0.0428	-0.0479	0.0979
$\Delta E_0$ / kJ mol <sup>-1</sup>	1.1	1.1	1.2
<i>E<sub>c</sub></i> / kJ mol <sup>-1</sup>	-51.42	-50.92	-50.71
<i>E<sub>c</sub>-BSSE</i> / kJ mol <sup>-1</sup>	-47.49	-46.90	-46.65
Parameters	VII	VIII	IX
			
<i>A</i> / MHz	640.0	694.1	763.1
<i>B</i> / MHz	542.9	524.2	462.4
<i>C</i> / MHz	381.4	373.8	402.6
$\mu_a, \mu_b, \mu_c$ / D	1.5, -2.6, 1.1	-1.6, -2.5, -1.2	1.9, 2.0, 1.4
<i>D<sub>J</sub></i> / kHz	0.490	0.422	0.118
<i>D<sub>JK</sub></i> / kHz	-0.525	-0.555	0.0344
<i>D<sub>K</sub></i> / kHz	0.122	0.214	0.551
<i>d<sub>1</sub></i> / kHz	-0.143	-0.0829	-0.00921
<i>d<sub>2</sub></i> / kHz	-0.0186	-0.00818	-0.000298
$\Delta E_0$ / kJ mol <sup>-1</sup>	2.5	2.7	5.0
<i>E<sub>c</sub></i> / kJ mol <sup>-1</sup>	-49.16	-49.37	-47.28
<i>E<sub>c</sub>-BSSE</i> / kJ mol <sup>-1</sup>	-45.48	-45.65	-43.64

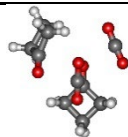
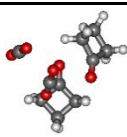
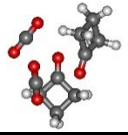
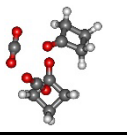
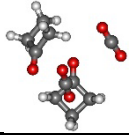
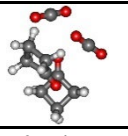
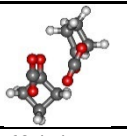
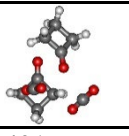
**Table S6.4.** Calculated geometries and spectroscopic parameters of the plausible isomers of (CBN)<sub>2</sub> at the B3LYP-D3(BJ)/def2-TZVP level of theory.

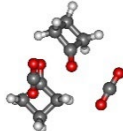
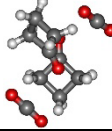
Parameters	I
	
<i>A</i> / MHz	2350.3
<i>B</i> / MHz	831.4
<i>C</i> / MHz	769.3
$\mu_a, \mu_b, \mu_c$ / D	0.0, 0.0, 0.0
<i>D<sub>J</sub></i> / kHz	0.458
<i>D<sub>JK</sub></i> / kHz	4.575
<i>D<sub>K</sub></i> / kHz	-1.377
<i>d<sub>1</sub></i> / kHz	-0.0721
<i>d<sub>2</sub></i> / Hz	0.205
$\Delta E_0$ / kJ mol <sup>-1</sup>	0.0
<i>E<sub>c</sub></i> / kJ mol <sup>-1</sup>	-30.08
<i>E<sub>c</sub>-BSSE</i> / kJ mol <sup>-1</sup>	-28.28

**Table S6.5.** Calculated geometries and spectroscopic parameters of the plausible isomers of (CBN)<sub>2</sub>-CO<sub>2</sub> at the B3LYP-D3(BJ)/def2-TZVP level of theory.

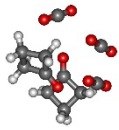
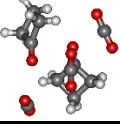
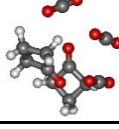
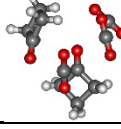
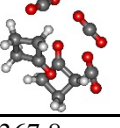
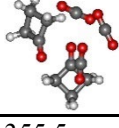
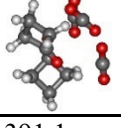
Parameters	I	II	III
			
<i>A</i> / MHz	904.3	745.9	786.7
<i>B</i> / MHz	607.6	695.6	673.3
<i>C</i> / MHz	442.6	422.6	443.5
$\mu_a, \mu_b, \mu_c$ / D	0.7, 1.6, -0.1	-0.4, 0.2, -0.1	-0.3, 0.1, 0.2
<i>D<sub>J</sub></i> / kHz	0.748	0.560	0.419
<i>D<sub>JK</sub></i> / kHz	-0.697	-0.876	-0.525
<i>D<sub>K</sub></i> / kHz	0.107	0.383	0.188
<i>d<sub>1</sub></i> / kHz	-0.387	-0.0183	-0.0689
<i>d<sub>2</sub></i> / kHz	-0.0954	0.0437	0.0105
$\Delta E_0$ / kJ mol <sup>-1</sup>	0.0	0.6	1.1
<i>E<sub>c</sub></i> / kJ mol <sup>-1</sup>	-49.83	-48.74	-48.37
<i>E<sub>c</sub></i> -BSSE / kJ mol <sup>-1</sup>	-46.23	-45.40	-44.98
Parameters	IV	V	VI
			
<i>A</i> / MHz	785.0	1165.1	800.0
<i>B</i> / MHz	619.8	478.0	698.5
<i>C</i> / MHz	403.4	429.5	469.1
$\mu_a, \mu_b, \mu_c$ / D	0.5, 0.5, 0.4	0.0, 1.2, 0.0	2.9, 2.1, 0.2
<i>D<sub>J</sub></i> / kHz	0.545	0.0920	0.316
<i>D<sub>JK</sub></i> / kHz	-0.807	0.0736	-0.416
<i>D<sub>K</sub></i> / kHz	0.328	1.179	0.171
<i>d<sub>1</sub></i> / kHz	-0.0531	-0.0154	-0.00311
<i>d<sub>2</sub></i> / kHz	-0.00888	-0.00169	0.0107
$\Delta E_0$ / kJ mol <sup>-1</sup>	2.0	4.3	4.6
<i>E<sub>c</sub></i> / kJ mol <sup>-1</sup>	-47.57	-45.27	-45.56
<i>E<sub>c</sub></i> -BSSE / kJ mol <sup>-1</sup>	-44.31	-41.97	-42.13

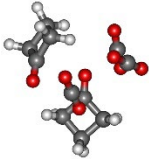
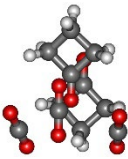
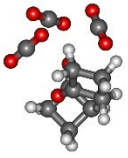
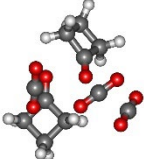
**Table S6.6.** Calculated geometries and spectroscopic parameters of the plausible isomers of (CBN)<sub>2</sub>-(CO<sub>2</sub>)<sub>2</sub> at the B3LYP-D3(BJ)/def2-TZVP level of theory.

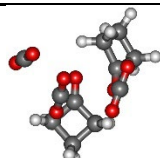
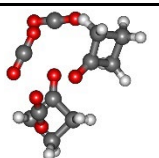
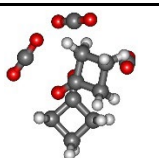
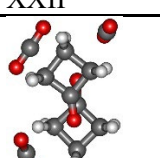
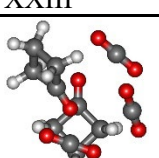
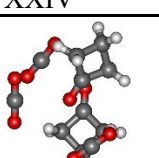
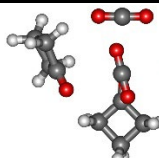
Parameters	I	II	III
			
<i>A</i> / MHz	524.7	512.3	513.4
<i>B</i> / MHz	456.0	416.2	403.4
<i>C</i> / MHz	365.9	366.0	353.8
$\mu_a, \mu_b, \mu_c$ / D	0.3, 1.4, 1.7	0.5, -1.5, 1.1	-0.7, 0.0, -0.3
<i>D<sub>J</sub></i> / kHz	0.0909	0.0767	0.0710
<i>D<sub>JK</sub></i> / kHz	-0.0758	-0.00837	-0.00440
<i>D<sub>K</sub></i> / kHz	0.0205	0.0412	0.0735
<i>d<sub>1</sub></i> / kHz	-0.00888	-0.00499	-0.00186
<i>d<sub>2</sub></i> / kHz	0.00474	-0.00741	0.00783
$\Delta E_0$ / kJ mol <sup>-1</sup>	0.0	1.6	1.9
<i>E<sub>c</sub></i> / kJ mol <sup>-1</sup>	-71.92	-69.91	-68.70
<i>E<sub>c</sub></i> -BSSE / kJ mol <sup>-1</sup>	-66.69	-64.68	-63.81
Parameters	IV	V	VI
			
<i>A</i> / MHz	567.1	509.1	460.5
<i>B</i> / MHz	404.3	431.3	422.2
<i>C</i> / MHz	367.3	372.4	341.8
$\mu_a, \mu_b, \mu_c$ / D	0.0, -1.2, 0.0	1.7, 3.2, 0.8	0.9, 0.0, 1.3
<i>D<sub>J</sub></i> / kHz	0.117	0.0865	0.303
<i>D<sub>JK</sub></i> / kHz	-0.363	-0.0700	0.298
<i>D<sub>K</sub></i> / kHz	0.743	0.0427	-0.223
<i>d<sub>1</sub></i> / kHz	-0.0283	-0.00741	-0.0663
<i>d<sub>2</sub></i> / kHz	0.00858	0.00321	0.0118
$\Delta E_0$ / kJ mol <sup>-1</sup>	1.9	2.1	2.3
<i>E<sub>c</sub></i> / kJ mol <sup>-1</sup>	-68.62	-69.58	-68.91
<i>E<sub>c</sub></i> -BSSE / kJ mol <sup>-1</sup>	-63.55	-64.48	-63.72
Parameters	VII	VIII	IX
			
<i>A</i> / MHz	505.4	624.4	491.7
<i>B</i> / MHz	437.3	382.8	423.1
<i>C</i> / MHz	346.2	288.2	312.3
$\mu_a, \mu_b, \mu_c$ / D	-0.9, 1.7, -1.1	-2.1, 1.2, -0.5	-1.5, -0.4, -0.4
<i>D<sub>J</sub></i> / kHz	0.0815	0.0490	0.126
<i>D<sub>JK</sub></i> / kHz	-0.00442	-0.0217	-0.0145
<i>D<sub>K</sub></i> / kHz	-0.0351	0.165	-0.0628
<i>d<sub>1</sub></i> / kHz	-0.0176	-0.0140	-0.0221
<i>d<sub>2</sub></i> / kHz	-0.00334	-0.00170	0.00215
$\Delta E_0$ / kJ mol <sup>-1</sup>	2.3	2.4	3.2
<i>E<sub>c</sub></i> / kJ mol <sup>-1</sup>	-69.04	-68.99	-68.03
<i>E<sub>c</sub></i> -BSSE / kJ mol <sup>-1</sup>	-64.14	-64.02	-63.22

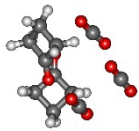
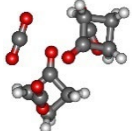
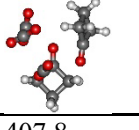
Parameters	X	XI	XII
			
$A$ / MHz	470.7	686.3	539.5
$B$ / MHz	387.7	328.1	398.9
$C$ / MHz	342.3	244.3	365.4
$\mu_a, \mu_b, \mu_c$ / D	0.8, 0.0, -1.3	0.0, 0.0, 0.0	0.0, -1.1, 0.0
$D_J$ / kHz	0.111	0.0471	0.207
$D_{JK}$ / kHz	-0.0421	-0.0230	-0.524
$D_K$ / kHz	0.142	0.357	-1.255
$d_1$ / kHz	-0.0115	-0.0160	-0.0845
$d_2$ / kHz	-0.00506	-0.00248	-0.0142
$\Delta E_0$ / kJ mol <sup>-1</sup>	3.2	3.7	4.2
$E_c$ / kJ mol <sup>-1</sup>	-67.57	-67.03	-66.78
$E_{c-BSE}$ / kJ mol <sup>-1</sup>	-62.55	-62.26	-61.67
Parameters	XIII	XIV	
			
$A$ / MHz	576.5	541.6	
$B$ / MHz	385.2	413.1	
$C$ / MHz	259.1	281.6	
$\mu_a, \mu_b, \mu_c$ / D	-0.7, 0.5, -0.3	-1.1, 0.9, -0.3	
$D_J$ / kHz	0.225	0.879	
$D_{JK}$ / kHz	-0.311	-1.455	
$D_K$ / kHz	0.133	0.811	
$d_1$ / kHz	-0.0170	-0.0606	
$d_2$ / kHz	-0.0457	0.0332	
$\Delta E_0$ / kJ mol <sup>-1</sup>	4.6	4.9	
$E_c$ / kJ mol <sup>-1</sup>	-65.98	-65.61	
$E_{c-BSE}$ / kJ mol <sup>-1</sup>	-61.30	-60.88	

**Table S6.7.** Calculated geometries and spectroscopic parameters of the plausible isomers of (CBN)<sub>2</sub>-(CO<sub>2</sub>)<sub>3</sub> at the B3LYP-D3(BJ)/def2-TZVP level of theory.

Parameters	I	II	III
			
<i>A</i> / MHz	394.3	333.8	375.9
<i>B</i> / MHz	273.3	313.3	294.5
<i>C</i> / MHz	266.8	293.1	270.8
$\mu_a, \mu_b, \mu_c$ / D	-1.8, -0.8, 1.7	-0.1, 0.7, 2.2	-0.1, -0.1, 2.3
<i>D<sub>J</sub></i> / kHz	0.0252	0.0331	0.0241
<i>D<sub>JK</sub></i> / kHz	0.0108	-0.0138	0.0141
<i>D<sub>K</sub></i> / kHz	0.00644	0.0239	0.0130
<i>d<sub>1</sub></i> / kHz	-0.00160	-0.00318	0.00330
<i>d<sub>2</sub></i> / kHz	0.000429	0.00423	-0.00237
$\Delta E_0$ / kJ mol <sup>-1</sup>	0.0	0.1	0.1
<i>E<sub>c</sub></i> / kJ mol <sup>-1</sup>	-91.59	-91.84	-90.96
<i>E<sub>c</sub>-BSSE</i> / kJ mol <sup>-1</sup>	-84.94	-85.19	-84.35
Parameters	IV	V	VI
			
<i>A</i> / MHz	386.8	334.1	360.4
<i>B</i> / MHz	296.2	313.0	325.9
<i>C</i> / MHz	263.4	292.8	284.2
$\mu_a, \mu_b, \mu_c$ / D	-0.3, -0.1, -2.4	-0.1, 0.7, 2.2	0.7, -0.2, 2.0
<i>D<sub>J</sub></i> / kHz	0.0228	0.0325	0.0399
<i>D<sub>JK</sub></i> / kHz	0.0164	-0.0124	-0.0137
<i>D<sub>K</sub></i> / kHz	0.0113	0.0227	-0.00491
<i>d<sub>1</sub></i> / kHz	0.00166	-0.00305	0.00112
<i>d<sub>2</sub></i> / kHz	-0.00113	0.00378	0.00187
$\Delta E_0$ / kJ mol <sup>-1</sup>	0.1	0.1	0.2
<i>E<sub>c</sub></i> / kJ mol <sup>-1</sup>	-91.42	-91.84	-90.79
<i>E<sub>c</sub>-BSSE</i> / kJ mol <sup>-1</sup>	-84.85	-85.19	-84.10
Parameters	VII	VIII	IX
			
<i>A</i> / MHz	367.8	355.5	391.1
<i>B</i> / MHz	294.1	329.2	269.4
<i>C</i> / MHz	281.4	279.7	262.1
$\mu_a, \mu_b, \mu_c$ / D	-0.2, 0.4, 2.2	-0.2, -0.5, -1.8	1.6, 1.3, 1.5
<i>D<sub>J</sub></i> / kHz	0.0243	0.0449	0.0259
<i>D<sub>JK</sub></i> / kHz	0.00954	-0.0210	0.0207
<i>D<sub>K</sub></i> / kHz	0.00564	-0.00328	-0.00493
<i>d<sub>1</sub></i> / kHz	0.00332	-0.00318	-0.00170
<i>d<sub>2</sub></i> / kHz	-0.00169	-0.00460	0.00147
$\Delta E_0$ / kJ mol <sup>-1</sup>	0.2	0.3	0.7
<i>E<sub>c</sub></i> / kJ mol <sup>-1</sup>	-91.59	-91.29	-90.29
<i>E<sub>c</sub>-BSSE</i> / kJ mol <sup>-1</sup>	-84.94	-84.56	-83.72

Parameters	X	XI	XII
			
$A$ / MHz	381.8	398.4	405.4
$B$ / MHz	298.0	288.1	298.4
$C$ / MHz	272.4	273.3	254.2
$\mu_a, \mu_b, \mu_c$ / D	-1.1, -0.1, 1.3	0.5, -0.3, 0.1	-2.2, 0.5, -1.3
$D_J$ / kHz	0.0372	0.0410	0.0375
$D_{JK}$ / kHz	-0.00994	0.0286	-0.0167
$D_K$ / kHz	0.0215	-0.0274	0.0242
$d_1$ / kHz	-0.00156	-0.00785	-0.0121
$d_2$ / kHz	-0.00221	-0.00104	-0.00279
$\Delta E_0$ / kJ mol <sup>-1</sup>	1.0	1.1	1.2
$E_c$ / kJ mol <sup>-1</sup>	-89.96	-89.54	-89.70
$E_{c\text{-BSSE}}$ / kJ mol <sup>-1</sup>	-83.30	-83.18	-83.14
Parameters	XIII	XIV	XV
			
$A$ / MHz	438.2	406.0	355.7
$B$ / MHz	281.0	307.9	307.2
$C$ / MHz	241.8	254.2	268.2
$\mu_a, \mu_b, \mu_c$ / D	3.7, -1.1, -1.1	0.4, -0.5, 0.2	-1.5, 0.3, 0.4
$D_J$ / kHz	0.0209	0.0240	0.0441
$D_{JK}$ / kHz	-0.00429	0.0542	-0.0596
$D_K$ / kHz	0.0609	-0.0416	0.0490
$d_1$ / kHz	-0.00504	-0.00410	0.00159
$d_2$ / kHz	-0.000468	-0.000142	-0.00233
$\Delta E_0$ / kJ mol <sup>-1</sup>	1.6	1.7	1.8
$E_c$ / kJ mol <sup>-1</sup>	-89.41	-89.12	-88.62
$E_{c\text{-BSSE}}$ / kJ mol <sup>-1</sup>	-82.84	-82.89	-82.13
Parameters	XVI	XVII	XVIII
			
$A$ / MHz	432.1	363.8	410.8
$B$ / MHz	272.9	285.5	281.6
$C$ / MHz	225.4	275.4	238.3
$\mu_a, \mu_b, \mu_c$ / D	0.0, -0.7, -2.1	-1.7, 0.6, -0.6	-1.6, 0.6, -0.3
$D_J$ / kHz	0.0251	0.0323	0.0282
$D_{JK}$ / kHz	-0.00992	0.0850	0.0174
$D_K$ / kHz	0.0478	-0.0394	-0.00486
$d_1$ / kHz	-0.00383	0.000135	-0.00454
$d_2$ / kHz	-0.000428	0.000331	0.000778
$\Delta E_0$ / kJ mol <sup>-1</sup>	1.9	2.1	2.2
$E_c$ / kJ mol <sup>-1</sup>	-89.24	-88.41	-88.28
$E_{c\text{-BSSE}}$ / kJ mol <sup>-1</sup>	-82.68	-81.76	-82.01

Parameters	XIX	XX	XXI
			
$A$ / MHz	430.4	394.3	328.8
$B$ / MHz	248.3	282.3	318.2
$C$ / MHz	243.0	252.2	302.5
$\mu_a, \mu_b, \mu_c$ / D	1.5, -0.7, -1.4	0.0, 0.0, 2.3	-2.7, 1.0, 0.8
$D_J$ / kHz	0.0246	0.0158	0.0316
$D_{JK}$ / kHz	0.00183	0.0214	-0.0172
$D_K$ / kHz	0.0410	0.000744	0.0128
$d_1$ / kHz	-0.00104	0.00119	-0.00260
$d_2$ / kHz	-0.000671	-0.00128	-0.000683
$\Delta E_0$ / kJ mol <sup>-1</sup>	2.3	2.5	2.6
$E_c$ / kJ mol <sup>-1</sup>	-88.70	-88.62	-88.03
$E_{c-BSE}$ / kJ mol <sup>-1</sup>	-82.17	-82.17	-81.50
Parameters	XXII	XXIII	XXIV
			
$A$ / MHz	462.6	365.0	364.0
$B$ / MHz	234.7	292.5	308.3
$C$ / MHz	215.0	276.1	287.0
$\mu_a, \mu_b, \mu_c$ / D	0.4, -0.2, -0.1	-0.6, -0.4, 1.8	1.1, 1.5, -0.6
$D_J$ / kHz	0.0316	0.0377	0.0382
$D_{JK}$ / kHz	-0.0219	-0.0498	0.0633
$D_K$ / kHz	0.116	0.0741	-0.0343
$d_1$ / kHz	-0.00284	-0.00143	0.00328
$d_2$ / kHz	0.000733	-0.000647	-0.00343
$\Delta E_0$ / kJ mol <sup>-1</sup>	2.9	3.0	3.0
$E_c$ / kJ mol <sup>-1</sup>	-87.40	-87.19	-87.78
$E_{c-BSE}$ / kJ mol <sup>-1</sup>	-81.00	-80.75	-81.21
Parameters	XXV	XXVI	XXVII
			
$A$ / MHz	323.7	424.1	418.6
$B$ / MHz	317.3	297.9	260.5
$C$ / MHz	286.3	237.3	229.1
$\mu_a, \mu_b, \mu_c$ / D	0.9, -0.4, 1.2	1.1, 1.3, -1.7	0.2, -0.9, 1.6
$D_J$ / kHz	0.0474	0.0246	0.0659
$D_{JK}$ / kHz	0.0562	-0.0292	-0.102
$D_K$ / kHz	-0.0680	0.0807	0.203
$d_1$ / kHz	-0.00122	-0.00370	-0.00708
$d_2$ / kHz	0.00413	0.00122	0.00451
$\Delta E_0$ / kJ mol <sup>-1</sup>	3.3	3.3	3.4
$E_c$ / kJ mol <sup>-1</sup>	-88.12	-87.36	-87.40
$E_{c-BSE}$ / kJ mol <sup>-1</sup>	-81.80	-80.79	-80.79

	XXVIII	XXIX	XXX
Parameters			
$A$ / MHz	327.1	464.3	426.6
$B$ / MHz	317.6	234.9	277.9
$C$ / MHz	288.6	198.6	233.3
$\mu_a, \mu_b, \mu_c$ / D	-0.4, 1.0, 0.6	-0.4, -0.1, 0.3	-1.2, -1.2, -1.6
$D_J$ / kHz	0.0473	0.0232	0.0249
$D_{JK}$ / kHz	0.00192	0.0324	0.0465
$D_K$ / kHz	-0.0123	0.0730	-0.157
$d_1$ / kHz	-0.00590	-0.00313	-0.000585
$d_2$ / kHz	0.000059	-0.000997	-0.00118
$\Delta E_0$ / kJ mol <sup>-1</sup>	3.7	3.9	4.1
$E_c$ / kJ mol <sup>-1</sup>	-86.82	-86.99	-87.19
$E_{c\text{-BSSE}}$ / kJ mol <sup>-1</sup>	-80.33	-80.75	-80.96
Parameters	XXXI		
			
$A$ / MHz	407.8		
$B$ / MHz	273.0		
$C$ / MHz	241.4		
$\mu_a, \mu_b, \mu_c$ / D	-0.3, 0.2, -0.9		
$D_J$ / kHz	0.0540		
$D_{JK}$ / kHz	-0.102		
$D_K$ / kHz	0.151		
$d_1$ / kHz	-0.00432		
$d_2$ / kHz	-0.00167		
$\Delta E_0$ / kJ mol <sup>-1</sup>	4.3		
$E_c$ / kJ mol <sup>-1</sup>	-86.61		
$E_{c\text{-BSSE}}$ / kJ mol <sup>-1</sup>	-80.08		

**Table S6.8.** Observed rotational transitions and residuals (in MHz) for CBN-CO<sub>2</sub>.

$J'$	$K_a'$	$K_c'$	$J''$	$K_a''$	$K_c''$	Obs.	Obs.-Cal.
2	1	2	1	1	1	3350.2459	-0.0135
2	0	2	1	0	1	3478.4794	-0.0065
2	1	1	1	1	0	3612.9475	-0.0060
3	1	3	2	1	2	5023.4318	0.0004
3	0	3	2	0	2	5209.8989	-0.0034
3	2	2	2	2	1	5222.3682	-0.0027
3	2	1	2	2	0	5234.8495	0.0056
3	1	2	2	1	1	5417.4066	-0.0099
4	1	4	3	1	3	6694.3169	-0.0015
4	0	4	3	0	3	6931.9963	-0.0001
4	2	3	3	2	2	6960.6781	0.0075
4	3	2	3	3	1	6969.2135	0.0239
4	3	1	3	3	0	6969.4996	0.0320
4	2	2	3	2	1	6991.7798	0.0056
4	1	3	3	1	2	7219.3980	-0.0001
4	2	3	5	1	4	2762.9495	0.0004
4	0	4	3	1	3	3168.4160	-0.0068
5	2	3	6	1	6	3510.4632	-0.0055
8	1	7	7	2	6	3744.0777	-0.0150
1	1	0	1	0	1	4209.6138	-0.0061
2	1	1	2	0	2	4344.0819	-0.0056
3	1	2	3	0	3	4551.6014	-0.0004
4	2	2	5	1	5	4778.4567	0.0053
3	2	2	4	1	3	4820.2395	-0.0008
4	1	3	4	0	4	4839.0031	-0.0005
5	0	5	4	1	4	5115.9739	-0.0106
5	1	4	5	0	5	5215.0846	-0.0006
6	1	5	6	0	6	5690.1216	0.0057
1	1	1	0	0	0	5819.0703	-0.0114
9	1	8	8	2	7	6012.3205	0.0073
3	2	1	4	1	4	6148.9344	-0.0081
7	1	6	7	0	7	6275.0578	0.0013
7	3	5	8	2	6	6303.2746	-0.0308
2	2	1	3	1	2	6817.2693	0.0017
7	3	4	8	2	7	6946.3491	0.0293
8	1	7	8	0	8	6980.4430	0.0028
6	0	6	5	1	5	7090.7593	-0.0053
2	1	2	1	0	1	7428.5150	-0.0154
2	2	0	3	1	3	7608.4256	0.0085
9	1	8	9	0	9	7814.9915	-0.0076

**Table S6.9.** Observed rotational transitions and residuals (in MHz) for CBN-(CO<sub>2</sub>)<sub>2</sub>.

$J'$	$K_a'$	$K_c'$	$J''$	$K_a''$	$K_c''$	Obs.	Obs.-Cal.
2	1	2	1	1	1	2493.6676	-0.0124
2	0	2	1	0	1	2625.9184	0.0089
2	1	1	1	1	0	2814.6028	-0.0046
3	1	3	2	1	2	3724.1816	0.0066
3	0	3	2	0	2	3873.5986	0.0025
3	2	2	2	2	1	3981.1730	-0.0072
3	2	1	2	2	0	4088.7952	0.0098
3	1	2	2	1	1	4202.3897	-0.0023
4	1	4	3	1	3	4939.0912	0.0032
4	0	4	3	0	3	5066.5259	0.0072
4	2	3	3	2	2	5286.0856	0.0096
4	3	2	3	3	1	5356.3952	0.0017
4	3	1	3	3	0	5374.9681	-0.0097
4	2	2	3	2	1	5527.4963	0.0009
4	1	3	3	1	2	5562.3293	0.0021
5	1	5	4	1	4	6138.7300	-0.0018
5	0	5	4	0	4	6225.6694	-0.0066
5	2	4	4	2	3	6572.6280	0.0013
5	4	2	4	4	1	6697.6547	-0.0049
5	4	1	4	4	0	6699.9674	-0.0062
5	3	3	4	3	2	6703.6867	-0.0021
5	3	2	4	3	1	6765.7709	0.0121
5	1	4	4	1	3	6878.8886	0.0010
5	2	3	4	2	2	6979.8827	0.0162
6	1	6	5	1	5	7325.7923	-0.0068
6	0	6	5	0	5	7376.2774	-0.0086
6	2	5	5	2	4	7837.7962	0.0121
2	2	0	1	1	0	4632.5684	-0.0144
2	2	1	1	1	1	4764.8072	-0.0034
3	2	1	2	1	1	5906.7488	-0.0119
3	2	2	2	1	2	6252.3007	-0.0101
4	1	3	3	0	3	6836.8793	-0.0027
4	2	2	3	1	2	7231.8673	0.0032
3	3	0	2	2	0	7356.3576	0.0230
3	3	1	2	2	1	7381.4273	0.0192
4	2	3	3	1	3	7814.1809	-0.0309

**Table S6.10.** Observed rotational transitions and residuals (in MHz) for (CBN)<sub>2</sub>-CO<sub>2</sub>.

$J'$	$K_a'$	$K_c'$	$J''$	$K_a''$	$K_c''$	Obs.	Obs.-Cal.
3	1	3	2	1	2	2852.0107	-0.0227
3	0	3	2	0	2	2947.3901	-0.0095
4	1	4	3	1	3	3762.4121	0.0154
4	2	3	3	2	2	4125.7143	0.0009
4	1	3	3	1	2	4356.3843	-0.0016
5	0	5	4	0	4	4680.3951	0.0141
5	2	4	4	2	3	5095.8514	0.0011
5	1	4	4	1	3	5298.8172	-0.0076
5	3	3	4	3	2	5301.2371	0.0060
5	4	2	4	4	1	5319.3569	0.0158
5	3	2	4	3	1	5474.1621	-0.0075
6	1	6	5	1	5	5541.9445	-0.0079
6	0	6	5	0	5	5550.8614	-0.0049
5	2	3	4	2	2	5609.5839	0.0044
6	2	5	5	2	4	6034.7438	-0.0087
6	1	5	5	1	4	6170.3801	-0.0008
6	3	4	5	3	3	6335.4135	-0.0133
6	4	3	5	4	2	6405.0555	0.0166
7	1	7	6	1	6	6422.8535	-0.0013
7	0	7	6	0	6	6425.9410	-0.0045
6	4	2	5	4	1	6460.7024	0.0068
7	2	6	6	2	5	6947.6843	0.0004
7	1	6	6	1	5	7018.5065	0.0014
8	1	8	7	1	7	7302.0220	-0.0056
8	0	8	7	0	7	7303.0353	-0.0076
7	3	5	6	3	4	7337.1291	-0.0013
7	4	4	6	4	3	7484.8413	0.0147
7	4	3	6	4	2	7641.9711	0.0142
7	2	5	6	2	4	7654.7384	-0.0041
8	2	7	7	2	6	7842.9461	-0.0114
7	3	4	6	3	3	7869.2913	-0.0088
8	1	7	7	1	6	7874.1193	0.0105
6	3	4	6	2	5	2553.9637	-0.0018
6	4	3	6	3	4	2684.9985	-0.0012
9	3	6	9	2	7	2697.7539	0.0301
3	0	3	2	1	2	2760.8752	0.0151
8	5	3	8	4	4	2822.9117	0.0004
7	4	4	7	3	5	2832.6988	0.0029
7	3	5	7	2	6	2943.3966	-0.0154
6	2	5	6	1	6	2953.5413	0.0051
3	1	3	2	0	2	3038.5733	0.0001
7	5	2	7	4	3	3073.2870	-0.0133
8	4	5	8	3	6	3075.0394	0.0001
2	2	1	1	1	0	3142.7145	-0.0122
8	2	6	8	1	7	3157.0435	0.0003
6	5	1	6	4	2	3227.9253	0.0021
7	5	3	7	4	4	3284.9789	0.0245
6	5	2	6	4	3	3296.0176	0.0142
8	5	4	8	4	5	3312.9334	-0.0184
2	2	0	1	1	1	3356.5044	-0.0071

8	3	6	8	2	7	3403.4610	-0.0005
10	3	7	10	2	8	3405.1418	0.0004
9	5	5	9	4	6	3408.6943	0.0058
9	4	6	9	3	7	3413.9276	-0.0014
7	1	6	7	0	7	3429.4963	0.0072
7	2	6	7	1	7	3478.3602	-0.0050
10	6	4	10	5	5	3500.1516	-0.0022
10	5	6	10	4	7	3594.8634	0.0031
4	1	3	3	2	2	3665.9479	0.0122
4	0	4	3	1	3	3725.2903	-0.0022
9	6	3	9	5	4	3761.3273	-0.0007
9	2	7	9	1	8	3795.4688	-0.0047
4	1	4	3	0	3	3853.5714	0.0012
11	5	7	11	4	8	3881.2160	-0.0090
9	3	7	9	2	8	3911.1733	0.0006
8	6	2	8	5	3	3921.2942	0.0071
10	6	5	10	5	6	3939.2948	0.0024
9	6	4	9	5	5	3947.3653	0.0077
8	6	3	8	5	4	3983.5691	-0.0053
11	6	6	11	5	7	3987.9680	0.0225
8	1	7	8	0	8	4000.5565	0.0017
7	6	1	7	5	2	4009.4972	0.0010
8	2	7	8	1	8	4019.2842	-0.0108
3	2	2	2	1	1	4021.1916	-0.0030
7	6	2	7	5	3	4025.4474	-0.0007
11	3	8	11	2	9	4099.0233	0.0017
10	3	8	10	2	9	4446.0654	-0.0034
11	7	4	11	6	5	4449.9278	-0.0005
9	1	8	9	0	9	4560.2918	-0.0004
9	2	8	9	1	9	4567.0509	-0.0020
13	7	7	13	6	8	4574.1320	-0.0054
7	3	5	6	4	2	4581.1653	0.0019
11	7	5	11	6	6	4606.8549	-0.0019
10	7	3	10	6	4	4610.7650	-0.0071
5	0	5	4	1	4	4643.2734	-0.0034
5	1	5	4	0	4	4693.8658	0.0028
9	7	2	9	6	3	4706.7642	-0.0039
13	5	9	13	4	10	4720.3779	-0.0066
9	7	3	9	6	4	4721.7250	0.0089
3	2	1	2	1	2	4738.3070	-0.0073
12	3	9	12	2	10	4745.2688	-0.0096
8	7	1	8	6	2	4765.6894	0.0131
8	7	2	8	6	3	4768.8961	-0.0050
4	2	3	3	1	2	4816.1745	0.0107
12	4	9	12	3	10	4848.5875	0.0021
11	2	9	11	1	10	4974.6633	-0.0066
11	3	9	11	2	10	4993.9632	0.0018
3	3	1	2	2	0	5003.7742	0.0082
3	3	0	2	2	1	5064.9405	-0.0100
10	1	9	10	0	10	5114.8415	-0.0035
10	2	9	10	1	10	5117.1780	-0.0002
13	4	10	13	3	11	5395.5317	-0.0076
11	8	3	11	7	4	5398.6430	0.0079

11	8	4	11	7	5	5411.7322	0.0000
10	8	2	10	7	3	5466.7115	0.0021
10	8	3	10	7	4	5469.8586	-0.0061
6	2	4	5	3	3	5513.6085	-0.0100
6	0	6	5	1	5	5537.3788	-0.0056
12	2	10	12	1	11	5539.6557	0.0008
6	1	6	5	0	5	5555.4390	0.0045
5	2	4	4	1	3	5555.6297	0.0017
11	1	10	11	0	11	5667.0785	0.0080
11	2	10	11	1	11	5667.8534	0.0045
6	1	5	5	2	4	5913.5795	0.0016
4	3	2	3	2	1	5945.6706	-0.0002
13	2	11	13	1	12	6098.4492	0.0024
13	3	11	13	2	12	6101.0361	0.0000
12	9	3	12	8	4	6162.0593	-0.0033
12	9	4	12	8	5	6164.9084	-0.0053
4	3	1	3	2	2	6242.3110	-0.0002
6	2	5	5	1	4	6291.5564	0.0006
4	2	2	3	1	3	6359.8633	-0.0371
7	0	7	6	1	6	6421.3753	-0.0021
7	1	7	6	0	6	6427.4192	-0.0037
5	3	3	4	2	2	6773.2811	-0.0013
4	4	1	3	3	0	6830.5612	-0.0006
4	4	0	3	3	1	6842.7920	0.0022
7	1	6	6	2	5	6897.3303	0.0000
7	2	6	6	1	5	7068.8605	0.0018
8	3	5	7	4	4	7274.5323	0.0081
8	0	8	7	1	7	7301.5690	0.0034
8	1	8	7	0	7	7303.5002	-0.0048
6	3	4	5	2	3	7499.1345	0.0047
5	3	2	4	2	3	7590.7826	0.0150
8	1	7	7	2	6	7823.7534	-0.0017
5	4	2	4	3	1	7847.9290	-0.0023
8	2	7	7	1	6	7893.3120	0.0008
5	4	1	4	3	2	7931.9358	0.0064

**Table S6.11.** Observed rotational transitions and residuals (in MHz) for (CBN)<sub>2</sub>-(CO<sub>2</sub>)<sub>2</sub>.

$J'$	$K_a'$	$K_c'$	$J''$	$K_a''$	$K_c''$	Obs.	Obs.-Cal.
4	1	3	3	2	2	3168.0107	-0.0249
5	0	5	4	1	4	3733.4323	-0.0279
5	1	4	4	2	3	3948.1163	-0.0087
5	2	4	4	1	3	4005.7778	-0.0177
5	3	3	4	2	2	4395.8783	0.0348
6	1	5	5	2	4	4690.7067	-0.0197
6	2	5	5	1	4	4706.9430	-0.0100
5	5	1	4	4	0	5093.3242	0.0162
5	5	0	4	4	1	5101.7165	0.0375
7	1	6	6	2	5	5418.8728	-0.0045
7	2	6	6	1	5	5422.7471	-0.0232
6	4	3	5	3	2	5501.8544	0.0158
7	2	5	6	3	4	5630.0402	0.0141
7	3	5	6	2	4	5704.5698	-0.0008
6	5	2	5	4	1	5892.7178	0.0104
7	4	4	6	3	3	6135.8213	0.0112
6	6	1	5	5	0	6136.8585	0.0053
6	6	0	5	5	1	6139.2903	0.0022
8	1	7	7	2	6	6142.7832	-0.0088
8	2	7	7	1	6	6143.6295	-0.0084
8	2	6	7	3	5	6376.2665	0.0141
8	3	6	7	2	5	6398.3321	0.0049
8	3	5	7	4	4	6522.0594	0.0190
7	5	3	6	4	2	6622.7555	-0.0123
8	4	5	7	3	4	6753.8857	0.0082
9	1	8	8	2	7	6865.7041	0.0043
7	6	2	6	5	1	6955.5402	-0.0088
7	6	1	6	5	2	6980.1807	-0.0166
9	2	7	8	3	6	7105.4220	0.0065
9	3	7	8	2	6	7111.1083	0.0233
7	7	1	6	6	0	7178.1993	-0.0279
7	7	0	6	6	1	7178.8907	-0.0021
8	5	4	7	4	3	7270.5626	-0.0254
9	3	6	8	4	5	7316.1006	0.0186
9	4	6	8	3	5	7401.9790	0.0196
3	3	1	2	2	1	3033.2446	0.0193
4	2	2	3	1	2	3749.9785	-0.0031
4	3	1	3	2	1	3828.0964	0.0127
4	3	2	3	2	2	3910.1362	-0.0137
4	4	0	3	3	0	4050.4098	0.0224
4	4	1	3	3	1	4063.5467	0.0289
5	3	2	4	2	2	4696.2142	-0.0116
5	2	3	4	1	3	4718.3275	-0.0119
5	4	1	4	3	1	4859.6501	0.0002
5	4	2	4	3	2	4919.1594	0.0197
5	5	0	4	4	0	5095.2554	0.0391
5	5	1	4	4	1	5099.7853	0.0146
6	3	3	5	2	3	5623.1856	-0.0172
6	4	2	5	3	2	5681.5028	-0.0031
6	2	4	5	1	4	5711.4959	0.0121

6	3	4	5	2	4	5755.4841	-0.0176
6	1	5	5	0	5	5759.7995	0.0364
6	2	5	5	1	5	5762.6843	0.0363
6	4	3	5	3	3	5802.2141	-0.0069
6	5	1	5	4	1	5911.1953	0.0037
6	5	2	5	4	2	5941.8440	0.0003
6	6	0	5	5	0	6137.3830	0.0031
7	4	3	6	3	3	6556.0341	-0.0218
7	3	4	6	2	4	6606.5192	-0.0087
7	2	5	6	1	5	6694.8056	0.0042
7	3	5	6	2	5	6709.1107	0.0093
7	5	2	6	4	2	6710.9346	-0.0109
7	4	4	6	3	4	6716.0368	-0.0182
7	5	3	6	4	3	6802.4158	-0.0194
7	6	1	6	5	1	6961.7033	-0.0098
7	6	2	6	5	2	6974.0057	-0.0274
7	7	0	6	6	0	7178.3543	-0.0118
7	7	1	6	6	1	7178.7357	-0.0182
8	4	4	7	3	4	7497.3822	-0.0108
8	5	3	7	4	3	7532.6443	-0.0301
8	3	5	7	2	5	7608.0799	0.0105
8	4	5	7	3	5	7655.8352	0.0004
8	2	6	7	1	6	7666.5044	0.0280
8	3	6	7	2	6	7670.3787	0.0205
8	5	4	7	4	4	7690.7992	-0.0347